# Identification of extracellular miRNAs as biomarkers of liver fibrosis in a human 3D-culture system

**Inauguraldissertation**

zur

Erlangung der Würde eines Doktors der Philosophie

vorgelegt der

Philosophisch-Naturwissenschaftlichen Fakultät

der Universität Basel

von

**Catherine Messner**

Basel, 2021

Genehmigt von der Philosophisch-Naturwissenschaftlichen Fakultät auf Antrag von Prof. Dr. Laura Suter-Dick (First Supervisor), Prof. Dr. Stephan Krähenbühl (Second Supervisor), und Prof. Dr. Christopher Goldring (External expert)

Basel, 17.11.2020

Prof. Dr. Martin Spiess
Dekan der Philosophisch-Naturwissenschaftlichen Fakultät

# Table of Contents

*Table of Contents* ..... 3

*Table of Figures* ..... 5

*1 Summary* ..... 6

*2 Aims* ..... 8

*3 Introduction* ..... 10

**3.1 Liver composition and specific cell function** ..... 10

**3.2 Detoxification of xenobiotics** ..... 16

**3.3 Liver fibrosis** ..... 18

**3.4 Liver fibrosis biomarkers and detection methods** ..... 21

**3.5 Investigating liver toxicity *in vitro*** ..... 24

**3.6 miRNA biosynthesis and function** ..... 27

**3.7 Extracellular/circulating miRNA: release mechanisms** ..... 30

*4 Project 1: Biomarkers of liver fibrosis* ..... 33

**4.1 Aims** ..... 33

**4.2 Introduction** ..... 34

4.2.1 MiRNAs as biomarkers of liver injury, disease and fibrosis ..... 34

4.2.2 Methotrexate, structure, metabolism and liver injury ..... 38

4.2.3 Acetaminophen structure, metabolism and toxicity ..... 41

**4.3 Paper 1: Exosomal miRNAs release as a sensitive marker for drug-induced liver injury *in vitro*** ..... 44

**4.4 Paper 2: Identification of miR-199a-5p, miR-214-3p and miR-99b-5p as extracellular biomarkers of fibrosis and promoters of HSC activation.** ..... 56

**4.5 Conclusion** ..... 95

*5 Project 2: Investigating hepatotoxicity and pro-fibrotic potential of additional compounds* ..... 97

**5.1 Aims** ..... 97

**5.2 Introduction** ..... 98

5.2.1 Bile biogenesis and cholestatic injury ..... 98

5.2.2 Cholestatic liver injury ..... 102

5.2.3 Link between cholestasis and fibrosis ..... 104

**5.3 Paper 3: Bile salts regulate CYP7A1 expression and elicit a fibrotic response and abnormal lipid production in 3D liver microtissues** ..... 106

**5.4 Introduction** ..... 118

5.4.1 Environmental Pollutants: dioxins and dioxin-like compounds. ..... 118

5.4.2 Toxicity mechanism of dioxins and dioxin-like compounds. ..... 119

5.4.3 Hepatotoxicity of dioxins and dioxin-like compounds. ..... 121

**5.5 Paper 4 Assessment of fibrotic pathways induced by environmental cheicals using 3D-human liver microtissue model.** ..... 123

**5.6 Conclusion** ..... 133

*6 Project 3: Incorporation of endothelial cells to the multicellular MT model 135*

**6.1 Aims ..... 135**

**6.2 Introduction ..... 136**

6.2.1 LSECs in healthy and fibrotic liver ..... 136

6.2.2 Current *in vitro* liver models containing endothelial cells ..... 138

**6.3 Materials and Methods ..... 141**

6.3.1 Cell culture ..... 141

6.3.2 Human liver microtissue generation ..... 141

6.3.3 CellTracker™ staining ..... 142

6.3.4 Cell treatments ..... 142

6.3.5 Cell viability assay ..... 143

6.3.6 Gene expression analysis ..... 143

6.3.7 Immunohistochemistry ..... 144

6.3.8 Statistical Analysis ..... 145

**6.4 Results ..... 146**

**6.5 Discussion ..... 152**

**6.6 Conclusion ..... 153**

*7 Scientific impact, limitations and future perspectives ..... 154*

*8 Acknowledgements ..... 156*

*9 Abbreviations ..... 157*

*10 References ..... 160*

*11 Curriculum vitae ..... 180*

## Table of Figures


***Figure 1. Illustration of project aims.*** 9

***Figure 2. Schematic representation of liver structure.*** 11

***Figure 3. Hepatocyte Structure.*** 12

***Figure 4. HSC activation.*** 14

***Figure 5. KC activation to M1 and M2.*** 15

***Figure 6. Liver fibrosis progression.*** 18

***Figure 7. Graphic representation of AOP.*** 20

***Figure 8. miRNA biogenesis and gene silencing.*** 29

***Figure 9. Extracellular miRNA release.*** 32

***Figure 10. Structure of methotrexate and folic acid.*** 38

***Figure 11. Pathways of methotrexate metabolism.*** 39

***Figure 12. Structure of acetaminophen.*** 41

***Figure 13. APAP metabolism in the liver.*** 43

***Figure 14. Enterohepatic circulation with bile salt concentrations.*** 98

***Figure 15. Bile salt production.*** 100

***Figure 16. Bile salt transporters.*** 101

***Figure 17. PCDD and PCDF structure.*** 119

***Figure 18. Structure of TCDD, PCB126, B[a]P.*** 120

***Figure 19. Role of LSECs in liver fibrosis & cirrhosis.*** 138

***Figure 20. Long-term culture of four cell HLMTs.*** 147

***Figure 21. Immunostaining confirmation of four cell HLMTs.*** 148

***Figure 22. vWF and vimentin staining of HLMTs.*** 149

***Figure 23. Exposure of HLMTs to pro-fibrotic compounds.*** 150

***Figure 24. Pro-fibrotic compounds result in increased quantities of αSMA.*** 151

# 1 Summary

Liver fibrosis is a common consequence of chronic liver injury caused by chemicals, diseases or diet. Currently, effective methods for early diagnosis and therapy are lacking. Enhancing our understanding of liver fibrosis mechanisms and identification of early non-invasive biomarkers is crucial to combat the clinical burden the disease causes. Using human 3D cell models, we aimed to investigate fibrosis and identify extracellular miRNAs as potential translational biomarkers of fibrosis.

This thesis is divided into three projects, which assess miRNAs as biomarkers using 3D human liver microtissues (MT) (1), the MT response to several compounds i.e. bile salts and environmental pollutants (2) and increasing MT complexity through the addition of a fourth cell type *i.e.* endothelial cells (3). The research goal of project 1 focussed on assessing the suitability of miRNAs as biomarkers of liver toxicity *in vitro*, with a specific focus on early detection of hepatic fibrosis and potential extracellular miRNAs specific to fibrosis. Moreover, the functional involvement of selected miRNAs in the HSC activation was also investigated. Project 2 assessed the effects of several compounds, including bile salts and environmental toxins (dioxin and dioxin-like compounds, on the 3D human liver MTs to investigate the potential adverse outcomes they may cause. Finally, project 3 aimed to increase the complexity of the multicellular MTs through the addition of an endothelial cell type to further improve the models physiological relevance.

We demonstrated that 3D-HepaRG and 3D multicellular MTs are useful tools for investigating miRNA markers of hepatotoxicity and fibrosis, respectively. We show that methotrexate (MTX, pro-fibrotic) and acetaminophen (APAP, acute injury) elicited compound-specific responses in the MTs. Furthermore, were able to identify four extracellular miRNAs (miR-199a-5p, miR-214-3p, miR-99b-5p and miR-125a-5p) that could contribute towards a non-invasive method to detect liver fibrosis. Three of the miRNAs show direct links to HSC activation. We also identified that the MTs are able to display the expected phenotypic response through exposure to several compounds. Taken together, these results highlight the versatility of the MTs as an *in vitro* tool for understanding the biological response to different compounds. Finally, the incorporation of HUVECs into the MTs was successful and did not affect their ability to recapitulate the final sequence of events leading to fibrosis upon exposure to TGF-β1, MTX and thioacetamide: HSC activation and increased collagen expression. This suggests that the cell-line based model is a suitable and cost-effective alternative for investigating liver fibrosis *in vitro*.

In conclusion, the compound-specific responses of the MTs to a range of compounds demonstrates the suitability and versatility of this *in vitro* model as a tool to assessing biological

and toxicological responses. We were able to identify released miRNAs and determine their phenotypic relevance to liver fibrosis. These miRNAs could contribute towards a panel of potentially translational biomarkers of liver fibrosis. We also enhanced the MTs complexity through the addition of a fourth cell type (endothelial cells) to improve the physiological relevance of the *in vitro* model.

# 2 Aims

Liver fibrosis is a common consequence of chronic liver injury caused by various aetiologies and poses a high burden to society. Understanding the underlying cellular mechanisms and promoting early detection using non-invasive biomarkers is crucial to guide and improve clinical interventions and outcomes. Here, using human 3D cell models we aimed to investigate fibrosis and identify extracellular miRNAs as potential translational biomarkers of fibrosis.

The specific aims of this thesis can be divided into 3 sections (Figure 1):

1. Identification and characterisation of liver fibrosis biomarkers in a 3D liver model
    a. Assess the usefulness of extracellular miRNAs, specifically those released via exosomes, as fibrosis biomarkers.
    b. Use an adapted version of the 3D liver model (MT) developed in our group to challenge it with MTX and identify fibrosis-specific extracellular miRNAs.
2. Assessment of the fibrotic potential of hepatotoxic compounds using the 3D human liver model.
    a. Recapitulate bile salt-induced hepatotoxicity and ensuing fibrosis.
    b. Evaluate environmental pollutants such as dioxins and dioxin-like compounds in terms of their pro-fibrotic potential.
3. Optimisation the MTs to increase physiological relevance through the addition of an endothelial cell type.
    a. Add a fourth cell type (HUVECs) as a surrogate for LSECs.
    b. Assess the ability of the 4-cell MTs to recapitulate liver fibrosis.

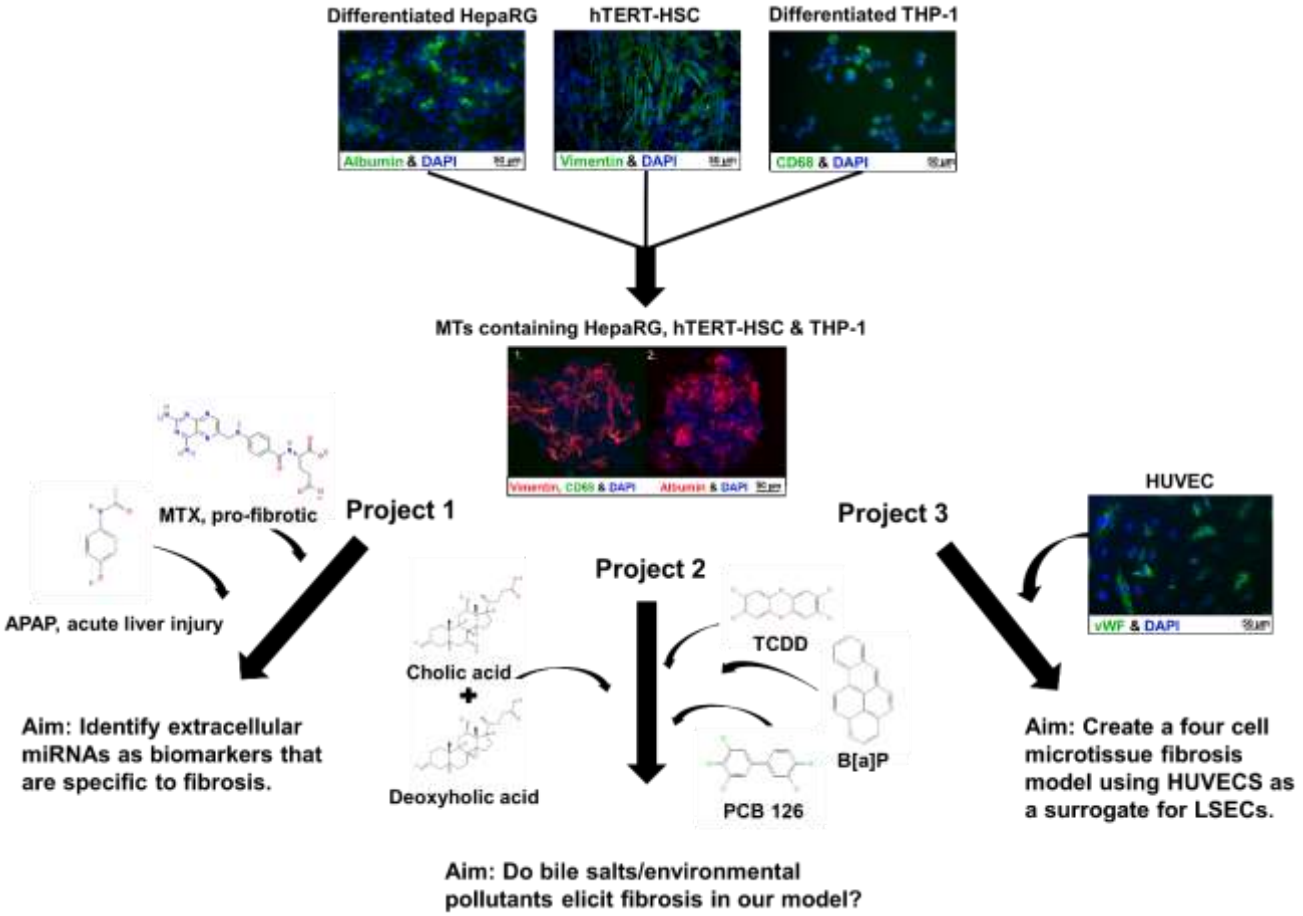


***Figure 1. Illustration of project aims.***

Immunostaining shows HepaRG positive for albumin, hTERT-HSC positive for vimentin and THP-1 positive for CD68 and/or vimentin. The project aims are briefly summarised to show the 3 projects: Assess miRNAs as biomarkers using 3D human liver microtissues (MT) (1), the MT response to several compounds i.e. bile salts and environmental pollutants (2) and increasing MT complexity through the addition of a fourth cell type *i.e.* endothelial cells (3) . Compound images were taken from PubChem.

# 3 Introduction

## 3.1 Liver composition and specific cell function

The liver is the largest internal organ in the human body and is composed of two major left and right lobes, with two smaller inferior lobes. The main role of the liver in the digestion process is the production of bile which is required for emulsification, hydrolysis and uptake of fats in the duodenum [1]. It also acts as the interface between the blood and the digestive system, *i.e.* the small intestine in which nutrients are absorbed, transforms and detoxifies metabolites. A variety of plasma proteins including albumin are produced by the liver [2]. The blood is supplied by two major blood vessels known as the portal vein, which provides 80% of the total blood supply which is nutrient-rich and deoxygenated, and the hepatic artery which supplies oxygenated blood [1].

The functional subunits of the liver are known as lobules, which are polygonal in shape and separated by connective tissue (Figure 2A). The main cell types in the lobules are hepatocytes, cholangiocytes, hepatic stellate cells (HSCs), Kupffer cells (KCs) and liver sinusoidal endothelial cells (LSECs) [1]. Hepatocytes, *i.e.* parenchymal cells, comprise the bulk of the liver occupying up to 80% of the total liver volume and perform the majority of liver functions, such as metabolism, detoxification, storage and bile production [3]. These functions make hepatocytes highly susceptible to damage from excessive exposure to fat, alcohol, drugs, and other toxins as well as a host of pathogens, in particular hepatitis viruses [3,4]. Hepatocytes are packed with membranous secretory organelles and mitochondria and the extensive endoplasmic reticulum and Golgi network reflect their large secretory capacity [4]. The basolateral side of the hepatocytes is closely associated with both arterial and venous blood due to the highly fenestrated vessels found throughout the liver, which enable the bidirectional cell-to-plasma exchange of components (Figure 2C & 3). The main functions of the liver including the production of blood plasma proteins and concomitant endocytic uptake of lipids, growth factors and other trophic agents are facilitated by this bidirectional exchange [4]. The apical plasma membrane is where hepatocytes excrete lipids, salts and degraded proteins into small channels known as canaliculi (~ 1 µm in diameter), where bile flows through a ductile system and is drained from the liver into the gall bladder (Figure 3) [4–6]. The sinusoidal domain of the hepatocytes contains a variety of different receptors such as epidermal growth factor (EGF) receptor, key lipid- and iron-scavenging receptors (e.g low-density lipoprotein receptor, LDLR and transferrin receptor, TfR) and bile acid uptake transporters [7]. In the canalicular domain the predominant receptors include ATP-binding cassette (ABC) transporters and bile acid efflux transporters [4,6].

Situated around the perimeter of the lobule are branches of the hepatic artery, hepatic portal vein and bile duct, which cluster together to form what is known as the portal triad (Figure 2B) [8]. The bile duct is is lined by cholangiocytes [9]. Lymphatics and nerves are also located at the periphery of the lobule. The central vein is located at the centre of the lobule and is an oxygen poor zone with high metabolic activity including phase 1 enzymes [8]. The hepatocytes form an epithelial-like structure and are in close contact with vascular channels called sinusoids, of which the LSECs create a fenestrated endothelium to enable easy communication between the sinusoidal lumen and the space of Disse (Figure 2C) [10]. Blood flows through the sinusoidal lumen where LSECs act as an adhesion platform for liver-resident immune cell populations including innate lymphoid cells, liver dendritic cells and KCs. The space of Disse is located between the endothelium and hepatocytes and collects lymph for delivery to the lymphatic capillaries. It also hosts HSCs, dendritic cells and other immune cells which are in direct communication with LSECs and hepatocytes (Figure 2C) [11]. The space of Disse also contains extracellular matrix (ECM) components such as collagen I and pro-collagen III, non-collagen glycoproteins, proteoglycans and matrix-bound growth factors that are involved in the regulation of cell function in the healthy and fibrotic liver [11].

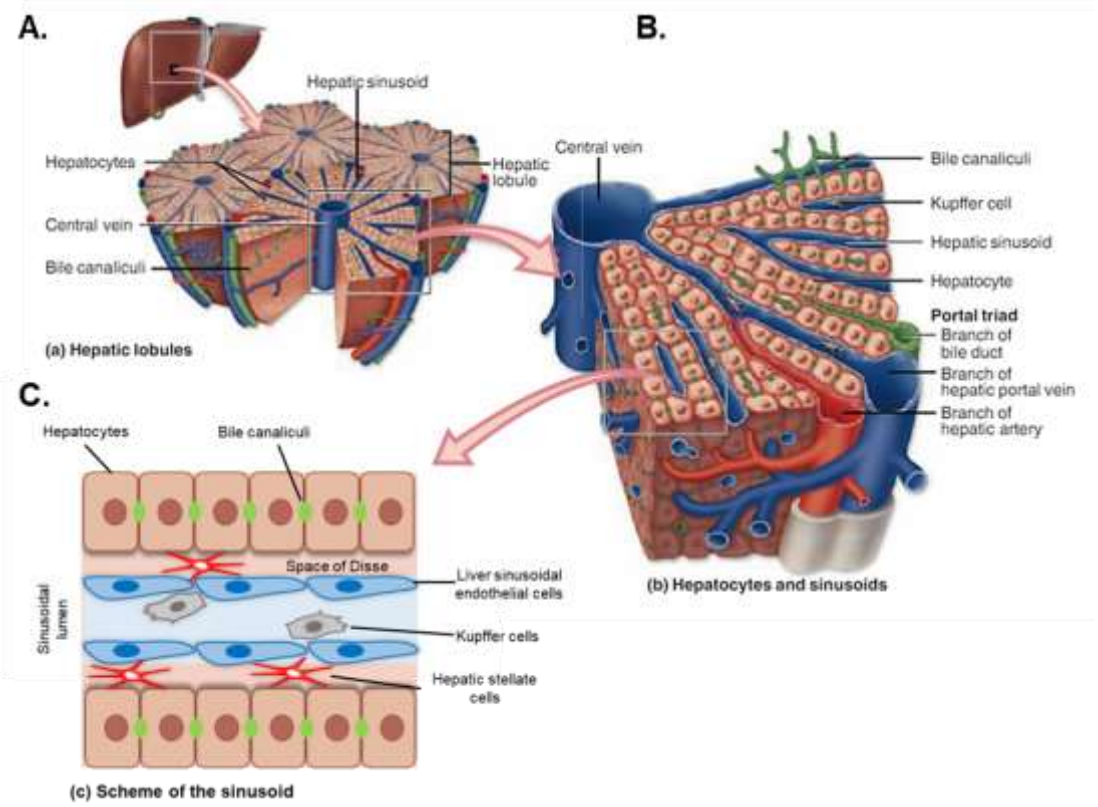


***Figure 2. Schematic representation of liver structure.***

*Schematic drawing of liver lobules (A), detailed visualisation of the lobule highlighting the portal triad (B) and visualisation of the sinusoids, including the Space of Disse (C). Adapted from Mescher et al.* [1]

As mentioned above hepatocytes secrete a variety of key proteins into circulation including α-fetoprotein, albumin, transferrin, plasminogen, fibrinogen and clotting factors. Hepatocytes are the only source of albumin synthesis and secretion and this protein is one of the most highly secreted proteins of any cells [12]. Hepatocytes also produce bile, which is mainly composed of cholesterol, phospholipids, electrolytes, bilirubin and bile acids. Bile is released into the canaliculi and excreted into the gall bladder where it is concentrated or delivered directly into the intestinal lumen [4]. When bile is released into the intestinal lumen, it aids emulsification, digestion and adsorption of dietary fats. It also plays a role in the removal of xenobiotics and endogenous waste products. Hepatocytes also play a principal role in cholesterol homeostasis which is vital for proper cellular and systemic functions [13]. Cholesterol is synthesised via 3-hydroxy-3-methylglutaryl coenzyme A reductase and taken up through LDLR in the hepatocytes [14]. Hepatocytes also play an important role in xenobiotic metabolism (*e.g.* drug metabolism) to result in safe elimination of metabolites through a detoxification pathway. Xenobiotic metabolism may be separated into two phases, which will be discussed in section 3.2 [15].

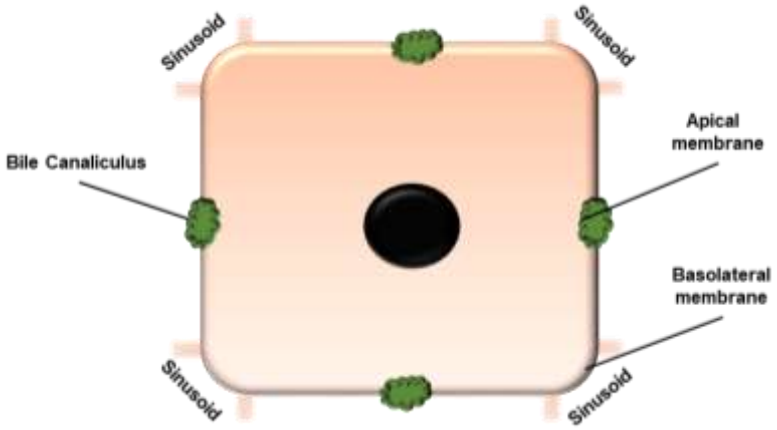


***Figure 3. Hepatocyte Structure.***

*Simple schematic representation of the hepatocyte to highlight the location of the basolateral membrane and the apical membrane. The basolateral membrane is in communication with the sinusoids (i.e. associated with arterial and venous blood), therefore, allowing bidirectional cell-to-plasma exchange of components. These components include blood plasma proteins, lipids, growth factors and other trophic agents. The apical membrane is where lipids, salts and degraded proteins are secreted into small channels known as canaliculi, which then collect in the gallbladder.*

Non-parenchymal cells such as cholangiocytes, HSCs, KCs and LSECs make up 20% of the liver volume. Cholangiocytes comprise approximately 3-4% of the total liver mass and are epithelial cells that line the intra- and extrahepatic ducts of the biliary tree and the main role is in mediation of hepatocyte-derived bile as it travels through the bile ducts [9,16]. Cholangiocytes possess an apical and a basolateral plasma membrane and are joined by tight junctions, which play a role in epithelial cell polarity. Cholangiocytes acquire a greater degree of differentiation along the biliary tree (i.e. small to large ducts) in terms of cell polarity, receptor and transporter expression and response to hormones [17]. Another characteristic of cholangiocytes is the primary cilium which protrudes into the bile duct lumen [18]. Bile is extensively modified by cholangiocytes through reabsorptive and secretory processes such as secretion of chloride anions ($Cl^-$), bicarbonate ($HCO3^-$) and water, and reabsorption of bile salts, amino acids and glucose via a variety of transporters (*e.g.* Na+-independent Cl−/HCO3− exchanger) [9,18]. This is an essential step in bile production as it regulates flow, composition and pH of the primary bile salts produced by the hepatocytes [17].

Of the non-parenchymal cells, LSECs make up approximately 3% of the total liver volume and 15-20 % of total liver cells and play an important role in the sinusoid [19]. The LSEC structure differs from other endothelia as they lack an organised basal lamina and contain many open pores (fenestrae) to allow the flow of small or soluble substrates to the hepatocytes, while excluding larger circulating particles such as blood cells and platelets [20,21]. LSECs have a high capacity for clathrin-mediated endocytic activity, which is reflected by the fact that LSECs contain twice as many clathrin-coated pits per membrane unit in comparison with KCs and hepatocytes [22]. They also contain 45% and 17% of the liver's total mass of pinocytic vesicles and lysosomes [22]. LSECs play a central role in the clearance of blood-borne waste through the expression of a variety of endocytosis receptors that mediate extremely rapid internalisation of waste molecules [22,23]. LSECs will be covered in more detail below (section 6.2).

Another non-parenchymal cell type is the HSC, which is a liver-specific mesenchymal cell that plays a vital role in liver physiology and wound repair. HSCs are located in the space of Disse and account for approximately 1.5% liver volume and 5-8% of the cells in the liver [24,25]. HSCs in the healthy liver are maintained in a quiescent state and contain numerous vitamin A lipid droplets making up the largest reservoir of vitamin A in the body [26]. HSCs also are important sources of paracrine, autocrine, juxtacrine and chemoattractant factors. These characteristics make them critical in maintenance of homeostasis of the hepatic sinusoid microenvironment [27]. HSCs are also able to interact with immune cells, and modulate their activity or promote their differentiation by releasing cytokines or directly acting as antigen presenting cells. HSCs also contribute to angiogenesis, hepatocyte regeneration and to the regulation of oxidant stress [27]. After liver injury, HSCs transdifferentiate to an activated state

where they transition from a quiescent vitamin A-rich cell to highly proliferative and fibrogenic cells (Figure 4). This transdifferentiation event results in the acquisition of motility, contractile and pro-inflammatory properties promoting a wound-healing response and repair [24].

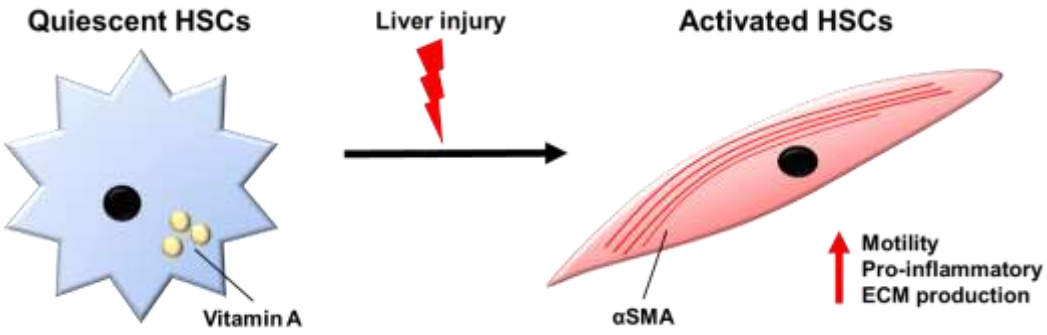


***Figure 4. HSC activation.***

*Schematic representation of hepatic stellate cells (HSCs), vitamin A storing cells, becoming activated during liver injury. Activated HSCs lose their vitamin A storing phenotype and acquire increased motility, αSMA expression, and ECM production. They also promote further inflammation including release of cytokines e.g. TGF-β1.*

Finally, KCs are another type of non-parenchymal cell, which are a critical component of the mononuclear phagocytic system and are essential in the innate immune response. Their localisation in the sinusoid allows them to act a first line of defence against immunoreactive material passing from the gastrointestinal tract via portal circulation. Their localisation also allows KCs to efficiently phagocytose pathogens entering portal or arterial circulation [28]. KCs are mediators of liver injury and repair and demonstrate plasticity as they express a range of polarised phenotypes dependent on the local metabolic immune environment [28]. They are capable of expressing a pro-inflammatory M1 phenotype and multiple M2 phenotypes that are involved in the resolution of inflammation and wound healing (Figure 5) [29].

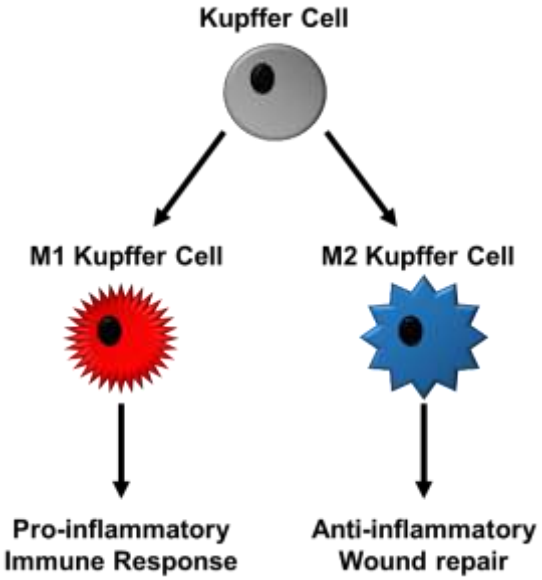


***Figure 5. KC activation to M1 and M2.***

*Schematic representation of Kupffer Cell (KC) activation. KCs can acquire two different phenotypes during liver injury and the wound healing process. M1 macrophages are pro-inflammatory and infiltrate during and after injury. M2 macrophages are anti-inflammatory and promotes wound healing e.g. by promoting fibroblasts proliferation and migration.*

## 3.2 Detoxification of xenobiotics

Depending on their physicochemical properties, chemicals can pass into hepatocytes passively or be taken up via different transport proteins. These transport proteins are located in the basolateral membrane and include members of the solute carrier (SLC) family, the organic anion transporting polypeptide (OATP) superfamily 39, the organic anion transporter (OAT) family and the organic cation transporter (OCT) family [30]. After uptake, the first metabolic step includes phase I oxidative reactions, often mediated by cytochrome p450 enzymes (CYPs) that utilise NADPH and oxygen in their catalytic cycle [31]. Following phase I metabolism, intermediate bioactive products are generated that can be hepatotoxic leading to hepatocyte dysfunction and cell death. These potentially toxic intermediate products are detoxified through inactivation by glucurono-, glutathione- or sulfa-conjugation via the most common phase II enzyme families including glutathione S-transferases (GSTs), UDP-glucuronosyltransferases (UGTs), sulfotransferases (SULTs), and N-acetyltransferases (NATs) [31]. These modifications typically result in a polar product, which does not usually have pharmacological activity. Drugs and metabolites efflux from hepatocytes into the bile or sinusoidal blood for excretion which is mainly mediated by ABC transporters such as multidrug resistance protein 1 (MDR1) and anion exchange mechanisms [32].

Although the liver has the ability to detoxify the hepatoxic intermediate products, the quantity of metabolite can exceed the capacity of the liver to carry out the following detoxification step due to depletion of phase II enzymes or conjugating molecules resulting in an accumulation of toxic metabolites. This formation of reactive metabolites is one possible mechanism through which drug-induced liver injury (DILI) occurs. A common example of this includes acetaminophen (APAP) toxicity. APAP is either glucuronylated or sulfa-conjugated to compounds that are excreted in urine. A fraction of the drug is metabolised by CYP2E1 and CYP1A2 to a toxic intermediate metabolite known as N-acetyl-p-benzo-quinone imine, (NAPQI) which interacts with intracellular proteins inducing hepatocyte death. Generated NAPQI is rapidly bound by glutathione (GSH), which prevents the toxic effects. When GSH is depleted or when NAPQI generation exceeds GST binding capacity the detoxification process cannot occur resulting in severe liver injury and failure [33].

Adverse drug reactions resulting in liver injury (DILI), are prevalent due to the role of the liver in the detoxification process. A large variety and quantity of medications including anesthetics, anticancer drugs, antibiotics, antituberculosis agents, antiretrovirals, and cardiac medications result in injury and many drugs are taken off the market as a result of their hepatotoxicity [33]. DILI is categorised as either chronic or acute based on the duration and histological location of the damage. Mechanisms of DILI can include direct toxicity from the administered

drug or their metabolite or may result from other immune related mechanisms [33]. An additional mechanism of DILI is inhibition of the bile salt export pump (BSEP) which leads to increased intracellular bile salt concentrations. These increased concentrations can damage mitochondria and result in hepatotoxicity and hepatic injury [32]. Examples of drugs that elicit this adverse outcome include, potent BSEP inhibitors such as cyclosporine A or bosentan which can lead to drug-induced cholestasis [34].

Extensive pre-clinical testing in the pharmaceutical industry aims to stop the development of compounds that may cause DILI. A population based study in the US demonstrated that the incidence of DILI was approximately 13.9 cases per 100,000 inhabitants over 3 years [35]. However, clinically relevant DILI incidence is dependent on the drug in question such as chlorpromazine, azathioprine and sulphasalazine, which show the highest incidence of DILI affecting approximately 1 per 1000 users [35,36]. In these cases, clinical management of DILI is based on correct diagnosis and identification of the hepatotoxic drug. The majority of cases of DILI can be resolved quickly through the removal of the injury-inducing drug. Therefore, early diagnosis and recognition of the cause is essential as prolonged exposure could progress to more severe damage or even result in liver failure [33,37]. Therefore, understanding hepatotoxicity and improving our ability to identify early signs of injury during drug development is required.

## 3.3 Liver fibrosis

Liver fibrosis is characterised by the accumulation of ECM, which distorts hepatic architecture through the formation of fibrous scars. If left untreated liver fibrosis ultimately progresses into cirrhosis resulting in hepatocellular dysfunction and reduced intrahepatic blood flow leading to hepatic insufficiency and portal hypertension [38,39]. It is thought to be the result of wound-healing due to persistent/repeated liver injury [38,40]. After acute liver injury, the parenchymal cells regenerate and replace the necrotic or apoptotic cells, eliciting an inflammatory response and a limited ECM deposition. However, if injury persists then the liver regeneration process fails and hepatocytes are substituted with abundant ECM, including fibrillary collagen (Figure 6) [38]. Major alterations in the tissue architecture occur and in advanced stages, the liver contains approximately 6 times more ECM due to increased synthesis and decreased degradation. Degradation of ECM is reduced due to decreased matrix metallopeptidase (MMPs) activity, which is mainly due to overexpression of their inhibitors, tissue inhibitor of metalloproteinases-1 (TIMPs). The ECM composition is rich in fibrillary collagens (mainly Collagen I, III and IV), fibronectin, undulin, elastin, laminin, hyraluronan and proteoglycans [38].

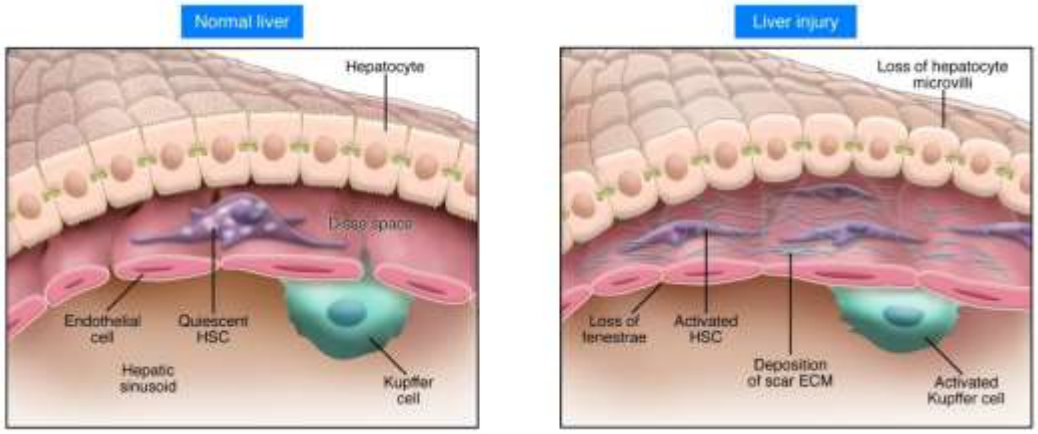


***Figure 6. Liver fibrosis progression.***

*Injury to hepatocytes resuls in recruitment and stimulation of inflammatory cells including Kupffer Cells (KCs). Activated KCs promote activation hepatic stellate cell (HSCs) resulting in increased producton of ECM and accumulation of scar tissue. Scar tissue build up results in loss of normal tissue architecture leading to impaired organ function. Image by Iredale et al.* [41]**.**

The events and cells involved in the progression of liver fibrosis have been investigated in great detail in the clinic, *in vitro* and *in vivo*, the results of which have resulted in the generation of the liver fibrosis adverse outcome pathway (AOP) [40]. The key events depicted in the AOP include hepatocellular death/injury, KC activation, transforming growth factor beta 1

(TGF-β1) expression, HSC activation and ultimately accumulation and changes in ECM composition (Figure 7) [40].

The first key event described is hepatocellular injury/death which is considered to be essential for triggering fibrogenesis [40]. Damaged/apoptotic hepatocytes release reactive oxygen species (ROS), cytokines and chemokines, which all contribute to oxidative stress, inflammatory signalling and ultimately KC activation. They also release apoptotic bodies that are engulfed by KCs leading to their activation [42]. Importantly, damaged hepatocytes release TGF-β1 and tumour necrosis factor alpha (TNF-α) [40]. Innate immune cells are also activated by damaged hepatocytes through the release of damage-associated molecular patterns (DAMPs), which activate KCs through toll-like receptors (TLRs) and recruit activated neutrophils and monocytes to the liver, resulting in the promotion of ROS formation [40,43,44]. Although, KC activation is associated with evident liver damage it also has a protective role, depending on the extent of activation. Excessive or prolonged KC activation shifts from a protective to a damaging inflammatory response, which is the second key event in the liver fibrosis AOP [40].

The next key event is the release of TGF-β1, which is a polypeptide member of the TGF-β superfamily of cytokines and is the most potent fibrogenic and plays a central role in fibrogenesis. TGF-β1 activates HSCs, which is the next key event in the fibrosis AOP and stimulates ECM synthesis which is the final key event [40]. Additionally, after activation HSCs express TGF-β1 and promote their own TGF-β1 expression to sustain high levels of TGF-β1 in sites of liver injury [45]. TGF-β1 also promotes the recruitment of inflammatory cells, portal fibroblasts and circulating myofibroblasts to the injured liver, which further triggers hepatocyte apoptosis [46]. TGF-β1 stimulates HSC transcription of collagen and the pro-fibrogenic peptide, connective growth factor (CTGF), which stimulates synthesis of Collagen 1 (Col I) and fibronectin. Transcription is also increased for TIMP-1, an inhibitor of the collagen cleaving enzymes MMP-8 and MMP-13 [25,40]. This leads to scarring and increased ECM stiffness which will ultimately result in hepatic insufficiency and portal hypertension [38].

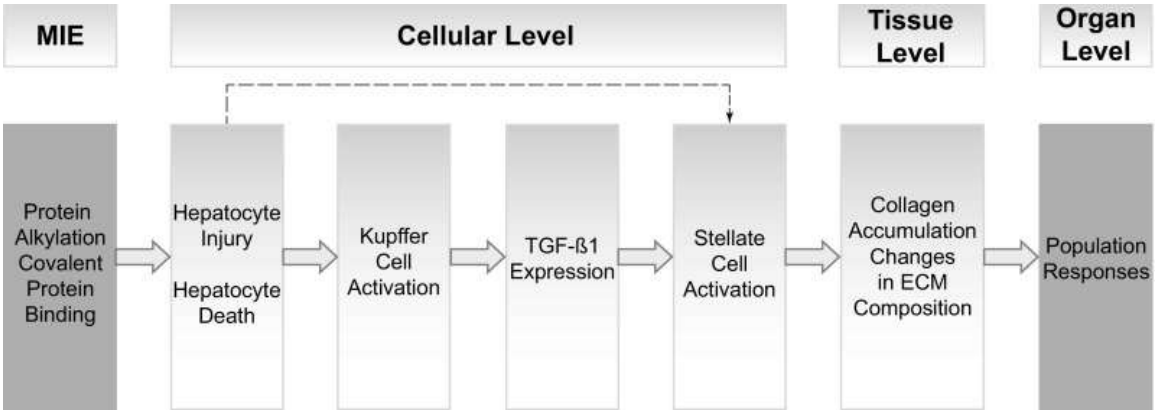


***Figure 7. Graphic representation of AOP.***

*Graphic representation of the adverse outcome pathway from protein alkylation to liver fibrosis. Molecular initiating pathway (MIE) is protein alkylation, which is then followed by the first key event (KE), hepatocyte injury/death. Hepatocellular injury and apoptosis promotes Kupffer cell (KC) activation, releasing TGF-β1 (the most potent pro-fibrogenic cytokine) and causing the next KE. HSC activation then leads to progressive collagen production and accumulation, thereby altering the extracellular matrix (ECM) composition resulting in scar development. These events ultimately result in impaired hepatic function. Image by Horvat et al.* [40]***.***

## 3.4 Liver fibrosis biomarkers and detection methods

Currently the most trusted method of diagnosing liver fibrosis is using liver biopsies, which are still considered the standard diagnostic method despite their invasive nature, sampling error and potential clinical complications [47,48]. Non-invasive methods (listed in table 1) are available including serum biomarkers such as alanine aminotransferase (ALT), aspartate aminotransferase (AST), alkaline phosphatase (ALP), albumin levels and total bilirubin (TBL) which are all associated with liver injury and fibrosis progression [49]. These are assessed using blood tests and are considered as 'liver function tests'. Albumin and TBL give information regarding the functional capacity of the liver, whereas ALT, AST and ALP levels detect liver injury [50]. Different combinations of serum markers and other parameters such as demographic and blood cell count known as serum aspartate aminotransferase/platelet ratio index (APRI), fibrosis-4 (FIB-4), FibroTest, Hepascore, FibroSpect II (FS) or Fibroindex produce scores which can be used for diagnosis of liver fibrosis [49].

APRI is calculated using normal AST levels and upper levels of normal, which is then divided by platelet counts and made into a percentage and expressed as absolute frequencies [51]. The APRI score has been shown to have the potential to correlate significantly to fibrosis stage [52]. However, other studies have demonstrated that this method is only useful to confirm or exclude significant fibrosis or cirrhosis. Thereby, indicating that staging fibrosis is not possible with this method [51]. FIB-4 is capable of predicting moderate or significant fibrosis and there are no additional costs as it utilises parameters measured in standard investigation of liver disease (age, AST, ALT, platelet count) [53]. Hepascore measures TBL, Gamma-glutamyl transpeptidase (GGT), hyaluronic acid and alpha-(2)-macroglobulin in combination with age and sex. It was found to be 67-80 % sensitive for significant fibrosis. Similar to Hepascore, FibroTest is calculated from the results of a six-parameter blood test which combines six serum markers, Alpha-2-macroglobulin, Haptoglobin, Apolipoprotein A1, GGT, TBL, and ALT with age and gender [54]. The results of comparing FibroTest to liver biopsy demonstrated that the results were best for advanced fibrosis and cirrhosis but only fair for lower stages [54]. The FS fibrosis panel includes serum hyaluronic acid, tissue inhibitor of metalloproteinase-1, alpha-2 macroglobulin, which are proteins involved in ECM remodelling. FS uses a logistic regression model established for this panel of fibrosis markers to detect significant fibrosis. [55]. Finally, Fibroindex is calculated from a combination of the platelet count, AST, and gamma globulin measurements [56]. APRI, FIB-4, Hepascore, FibroTest, FS and Fibroindex all include variations on a set of serum markers (Summarised in table 1) but were only able to detect significant fibrosis and were unable to discriminate between intermediate stages of fibrosis [53–57]. These serum biomarkers may be useful for excluding or confirming significant fibrosis but they lack sensitivity and are unable to identify early stages of liver fibrosis.

Other alternatives include ultrasonography (Examples: transient elastography, TE; Acoustic radiation force impulse, ARFI), computed tomography (CT) and magnetic resonance elastography (MRE) [58–60]. TE uses ultrasound to measure the propagation velocity of a wave, as it is proportional to elasticity and correlates to the amount of fibrosis in the liver as liver stiffness increases [61]. Although it is possible to measure liver stiffness there are limitations to this method as it is affected by necroinflammatory activity and/or a high body mass index [61]. ARFI uses ultrasound and combines conventional ultrasound and shear wave velocity to gauge liver stiffness [59]. ARFI has shown to have a sensitivity of 75% for diagnosing significant liver fibrosis, which increases to 90% for cirrhosis. TE has 70% sensitivity for diagnosing significant liver fibrosis/liver cirrhosis [59]. Advanced liver cirrhosis leads to shrinkage in liver volume and increased spleen volume, which can be measured using CT. It has also been suggested that liver and spleen volume may allow for liver fibrosis assessment in patients with chronic liver disease [62]. MRE uses propagating mechanical shear waves to assess mechanical properties of the liver. Waves propagate more rapidly in stiffer tissue and slower in softer tissue. If there is continuous application of waves, the speed of propagation is reflected in the wavelength [63]. As tissue stiffness increases, the wavelength becomes longer. The wave images are then processed with specialized software to generate quantitative cross-sectional images depicting the stiffness of tissue [63]. MRE is capable of differentiating between various stages (F2-4) of fibrosis as liver stiffness increases incrementally with fibrosis stages [63,64].

They detect a variety of liver diseases (i.e are non-specific), lack sensitivity for diagnosing early signs of liver injury/fibrosis, can be expensive and can carry radiological risks [49,58,65]. This highlights the need for sensitive and specific biomarkers that are capable of reliably detecting early signs of liver fibrosis.

***Table 1. Different methods of diagnosing liver fibrosis***

| *Method* | *Description* | *Stage of Fibrosis/Cirrhosis* |
|---|---|---|
| **Liver Biopsy** | Histopathological scoring of liver fibrosis | Identify multiple stages of injury/fibrosis |
| **APRI** | Serum aspartate aminotransferase/platelet ratio index | Significant fibrosis and cirrhosis |
| **FibroIndex** | platelet count, AST, and gamma globulin | Significant fibrosis and cirrhosis |
| **FIB-4** | Age, AST, ALT, platelet count | Significant fibrosis and Cirrhosis |
| **FibroTest/ Fibrosure** | Serum markers α2-macroglobulin, haptoglobin, apolipoprotein A1, bilirubin, gamma glutamyl transpeptidase & the patients age and gender. | Significant fibrosis and Cirrhosis |
| **Hepascore** | Serum markers bilirubin, GGT, α2 – macroglobulin and hyaluronic acid levels along with age and sex | Significant fibrosis and Cirrhosis |
| **Fibro-Spect II** | Serological test for hyaluronic acid, tissue inhibitor of metalloproteinases 1, and alpha-2-macroglobulin | Significant fibrosis and cirrhosis |
| **USE** | Ultrasound-based elastography such as transient elastrophgraphy and Acoustic radiation force impulse imaging (AFRI) | Cirrhosis & portal hypertension |
| **MRE** | Magnetic resonance elastography to measure liver stiffness | Stage 2 of fibrosis up to and including cirrhosis |
| **CT** | Computed tomography | Significant Fibrosis and cirrhosis |

## 3.5 Investigating liver toxicity *in vitro*

Liver function can be compromised by a variety of different causes such as DILI, non alcoholic fatty liver disease (NAFLD), cholestasis, infection with hepatitis B and C viruses (HBV and HCV, respectively) and hepatocellular carcinoma (HCC). All of these diseases represent a significant global health burden, for example 350 million people globally are infected with HBV and HCV. In addition, DILI is a leading cause of preclinical and clinical drug failures and withdrawals of marketed drugs [66]. Additionally, a common feature of liver disease is they increase patient risk of developing liver fibrosis, cirrhosis and ultimately HCC [38,40].

A large variety of animal models are used to investigate liver diseases and for evaluating compound toxicity. Examples of these *in vivo* models include: NAFLD which can be induced by controlling diets such as a methionine and choline deficient diet; fibrosis through carbon tetrachloride ($CCL_4$); cholestasis/fibrosis through bile duct ligation; HCC by knocking out specific tumor suppressor genes such as phosphatase and tensin homolog (*PTEN);* DILI through exposure to a variety of drugs [67]. Currently, pre-clinical drug testing requires the use of rodent and non-rodent models to perform risk assessment and minimise adverse outcome in humans. However, based on the number of drugs being withdrawn from the market it is clear that animal models do not completely suffice in identifying the potential risk. This could be due to the significant differences across species in drug metabolism [68]. In addition to the discrepancies in drug metabolism, rodents are also not always appropriate for studying diseases such as HBV and HCV, which are not infectious to rodents [68]. Finally, rodent models used for investigating certain diseases and drug toxicity are expensive and time-consuming. Finally, controversy surrounding *in vivo* experiments is also of concern due to the significant harm that might be caused to animals. Therefore, development of *in vitro* models contributes towards the 3Rs: Replacement, Reduction and Refinement [69].

These limitations have resulted in a considerable interest in developing *in vitro* models of the human liver, which could be employed to investigate metabolism and toxicity. *In vitro* models could also be used to understand disease development and testing potential therapies against liver disease. Primary cells are commonly used as an *in vitro* alternative, including primary hepatocytes (PHHs) and HSCs. PHHs are a useful alternative as they maintain key hepatic-specific functions including carbohydrate metabolism, ureogenesis, xenobiotic metabolism (through CYP enzymes) [70]. 2D culture of PHHs has drawbacks including rapid alteration of cellular morphology with loss of structural aspects and polarity. Thereby, bile canaliculi are no longer formed. More importantly, the drug metabolising capacity significantly decreases over time in 2D configurations [68,71]. Primary human HSCs have also provided a great deal of information as they have the capacity to recapitulate HSC activation seen during liver injury. However, primary HSCs have been known to spontaneously activate when cultured on plastic

surfaces meaning that primary HSCs have a limited useable life-span in 2D conditions [72]. Through culturing PHHs and primary human HSCs in 3D culture conditions, the cell-specific characteristics were maintained for longer periods.

Several protocols have been established to differentiated iPSCs into hepatocyte-like cell (HLCs). HLC production is carried out through the production of hepatic progenitors following an initial endoderm differentiation. The hepatic progenitors are then matured using specific growth factors and this method resulting in iHLC that express CK18 and CYPs. They also produce and release albumin, urea and glycogen [73–76]. Cholangiocytes have also been produced using iPSCs, by introducing SHH and the NOTCH ligand Jagged-1 during hepatic endoderm specification. The final stages of maturation include the addition of TGF-β which resulted in cholangiocyte-like cells [77]. iPSC-derived cholangiocytes were also generated using 3D conditions, Matrigel and the addition of specific growth factors such as fibroblast growth factor-10 [78–80]. HSCs have also been produced using iPSCs by two groups [81,82]. Coll *et al.* differentiated iPSCs on matrigel by introducing a variety of different growth factors such as BMP4, FGF1 and FGF3 [82]. These iPSC-derived HSCs were capable of being activated by TGF-β1 treatment and can be co-cultured with HepaRG in 3D microtissues [82]. On the other hand, Koui *et al.* followed an already established protocol for the induction of iPSCs into mesoderm and then selected HSC progenitors through ALCAM expression and then inhibited the Rho signalling pathway to produce mature HSCs that expressed ECMs and could be co-cultured with endothelial cells [81]. KCs have also been generated using iPSCs through supplementation with BMP4, ROCK inhibitor and stem cell factor (SCF) to obtain embryoid bodies. Following this, supplements such as macrophage colony stimulating factor (M-CSF) and Interleukin-3 were added to generate KCs over 3-4 weeks, which were functionally competent and similar to primary KCs [83]. Finally, LSECs have also been differentiated from iPSCs and is discussed in section 6.2.2.

Alternative cell lines exist including HepG2, a human hepatoma cell line that is characterised by unlimited life span, stable phenotype and high availability and are useful for understanding certain liver injuries such as gene toxicity [84,85]. However, HepG2 have much lower expression of metabolic activities compared with PHHs, which is an issue for drug toxicity studies [86]. Additionally, HepG2 lack many relevant hepatocyte specific transporters such as BSEP [86]. The hepatoma cell line HepaRG is a more suitable alternative for *in vitro* liver models. HepaRG cells have been shown to have enhanced metabolic activity in comparison to HepG2 making them a more suitable cell line. They also express more of the hepatocyte relevant transporters and are, therefore, more similar to PHHs [86].

There are also alternatives to primary HSCs including LX-1, LX-2 and hTERT-HSCs that are immortalised human HSCs [87,88]. LX-1 and LX-2 cells were shown to express key receptors

regulating hepatic fibrosis such as PDGF-βR and proteins involved in matrix remodelling including MMP-2, TIMP-2 and MT1-MMP. Additionally LX-2 cells respond to PDGF with increased proliferation and are responsive to TGF-β1 [87,89]. hTERT-HSCs were shown to have an extended life-span and be responsive to retinol and PDGF. They are also capable of becoming activated upon exposure to TGF-β1 [88,90]. However, it is important to carefully monitor HSC cell lines as they have been shown to be similar to activated HSCs [91]. Therefore, it is essential to maintain HSC cell lines at low passages and to take note of morphological changes and potentially use basement membrane-like matrices during expansion depending on the choice of cell line [1].

3D cultures involve both scaffold-free and scaffold-based systems. Scaffold-free systems can be made using ultra low adherence, inert surfaces or non-adhesive hydrogels such as alginate or collagen [92–94]. Scaffold-based 3D culture systems include 3D solid matrices derived from natural materials such as decellularised liver derived ECM or synthetic materials [95,96]. Culturing PHHs in 3D culture conditions demonstrated prolonged maintenance of hepatocyte-specific characteristics [71,97]. HSCs have also been shown to remain in a quiescent state for longer periods when cultured using 3D techniques [98]. Despite these advances in culturing primary cells to maintain characteristics there is still a need for extraction to collect these cells which involves invasive methods and there is a limited supply. Additionally, as primary cells lose characteristics in 2D culture they have limited expansion capacity. For these reasons, a large number of cell lines can be used as surrogates depending on the investigation.

As 3D models are more capable of recapitulating tissue microenvironments [99]. There are a number of 3D liver models published using one cell type or co-cultures of multiple cell types. Hepatotoxicity has been assessed in 3D-HepG2, 3D-HepaRG and 3D-PHHs [84,100–104]. These models have been useful in understanding hepatotoxicity. However, for elucidating fibrosis and other diseases that include the involvement of HSCs a multicellular model is required. Multicellular microtissue models using primary cells or cell lines have been characterised and are capable of recapitulating key events in the liver fibrosis AOP. These cell models include microtissues containing PHHs and NPCs [93,97,100,101,105,106], a combination of different cell lines [92,98] or iPSCs [107]. Additionally, a selection of 3D liver models has also been shown to recapitulate fibrosis including the models by Mukherjee *et al.* [108], Prestigiacomo *et al.* [92] and Leite *et al.* [98]. These models displayed hepatocellular death, HSC activation and accumulation of ECM in response to TGF-β1 and other pro-fibrotic compounds or conditions including methotrexate (MTX), thioacetamide (TAA) and lipid-loading [92,98,108].

Thus, advances *in vitro* models provide us with useful tools for understanding liver toxicity and disease, have the potential to be relevant to human physiology, and can be adapted for high-throughput screening.

## 3.6 miRNA biosynthesis and function

MicroRNAs (miRNAs) are small non-coding RNAs, typically 22 nucleotides (nt) in length, that play an important role in protein expression regulation. The majority of miRNAs are transcribed from DNA sequences into primary miRNAs (pri-miRNAs). These are then processed into precursor miRNAs (pre-miRNAs) and mature miRNAs [109]. Approximately half of miRNAs are intragenic and processed mostly from introns and to a lesser extent exons of protein coding genes. The remaining miRNAs are intergenic and are, therefore transcribed independently of a host gene and regulated by their own promoters [109,110]. miRNA biogenesis is classified into canonical and non-canonical (Figure 8). The canonical pathway is the dominant pathway for miRNA processing. Pri-miRNA is long and contains a stem-loop structure where mature miRNA sequences are embedded. Pri-miRNAs are transcribed and processed by RNA binding protein DiGeorge Syndrome Critical Region 8 (DGCR8) and a ribonuclease III enzyme Drosha, which form a microprocessor complex [111]. DGCR8 recognizes an N6-methyladenylated GGAC and other motifs within the pri-miRNA, while Drosha cleaves the pri-miRNA duplex at the base of the characteristic hairpin structure of pri-miRNA [111]. This results in the release of a small hairpin-shaped RNA of ~65 nucleotides in length which is the pre-miRNA that has a 2 nt 3' overhang [111].

Following the generation of pre-miRNA they are exported to the cytoplasm by an exportin 5 (XPO5)/RanGTP complex via nuclear pore complexes where maturation can be completed. Interestingly, knockdown of XPO5 resulted in reduction of total miRNA levels without a nuclear pre-miRNA accumulation. Pre-miRNA is then processed by the RNase III endonuclease Dicer. Dicer binds to pre-miRNA with a preference for a 2 nt long 3' overhang that was generated by Drosha. This processing step involves the removal of the terminal loop, and results in a mature miRNA duplex [112]. Two strands known as 5p and 3p arise from the 5' end and the 3' end of the pre-miRNA hairpin, respectively. Both strands derived from the mature miRNA duplex can be loaded into the Argonaute (AGO) family of proteins in an ATP dependent manner [113]. Interestingly, the proportion of AGO-loaded 5p or 3p strand varies greatly ranging from near equal proportions to predominantly one of the two strands. This loading proportion is dependent on the cell type or cellular environment [114]. There are multiple non-canonical miRNA biogenesis pathways and they can be grouped into Drosha/DGCR8-independent and Dicer-independent pathways and are summarised by O'Brien et al. and shown in figure 8.

The minimal miRNA-induced silencing complex (miRISC) consists of a guide strand and AGO [109]. The target specificity of miRISC is due to the interaction with complementary sequences on target mRNA, called miRNA response elements (MREs). MRE complementarity is responsible for whether there will be AGO-2 dependent splicing of target mRNA or whether there will be translational inhibition resulting in miRISC mediated mRNA decay [115]. When the

miRNA and MRE interaction is fully complementary AGO2 endonuclease activity is induced and targets mRNA cleavage [115]. miRNA is then degraded as this interaction destabilised the association between AGO and the 3' end of the miRNA [116]. The majority of miRNA-MRE interactions are not fully complementary in animals and most MREs contain central mismatches to their guide miRNA, which prevents AGO2 endonuclease activity [117]. In this case AGO2 acts as a mediator of RNA interference, similar to the non-endonucleolytic AGO family members (AGO1, 2 and 4) [118]. The miRNA-MRE interactions in many cases occurs via the 5' seed region and additional pairing at the 3' end provides stability and specificity of the miRNA-target interaction [119].

The molecular steps leading to microRNA-mediated gene silencing was reviewed in depth by Jonas *et al.* [117]. A silencing miRISC complex formation begins with the recruitment of GW182 family of proteins by mRISC. GW182 provides scaffolding that is required to recruit other effector proteins following miRNA-target mRNA interaction. Other effector proteins include poly(A)-deadenylase complexes PAN2-PAN3 and $CCR_4$-NOT [117]. PAN2/3 initiates target mRNA poly(A)-deadenylation and is completed by the $CCR_4$-NOT complex [117]. This leads to GW182 and poly(A)-binding protein C (PABPC) promoting efficient deadenylation. This results in a subsequent decapping which is facilitated by decapping protein 2 ($DCP_2$) and associated proteins. This causes rapid degradation by exoribonuclease 1 (XRN1) of the target mRNA [109,117].

miRNAs repress translation by mechanisms that have not been fully elucidated. However, it has been proposed that they interfere with the activity and/or assembly of the eukaryotic initiation factor 4f (eIF4F) complex which involve 43S pre-initiation complex recruitment and translation initiation [109,117]. Finally, Importin-8 and Exportin-1 shuttles Ago2 between the nucleus and cytoplasm and it has been shown that nuclear localised miRISC was found to regulate transcriptional and post-transcriptional levels of mRNA [120,121]. Some studies have shown that low molecular weight miRISC can interact with mRNAs in the nucleus and induce nuclear mRNA degradation. However, the exact mechanism is not fully understood [109].

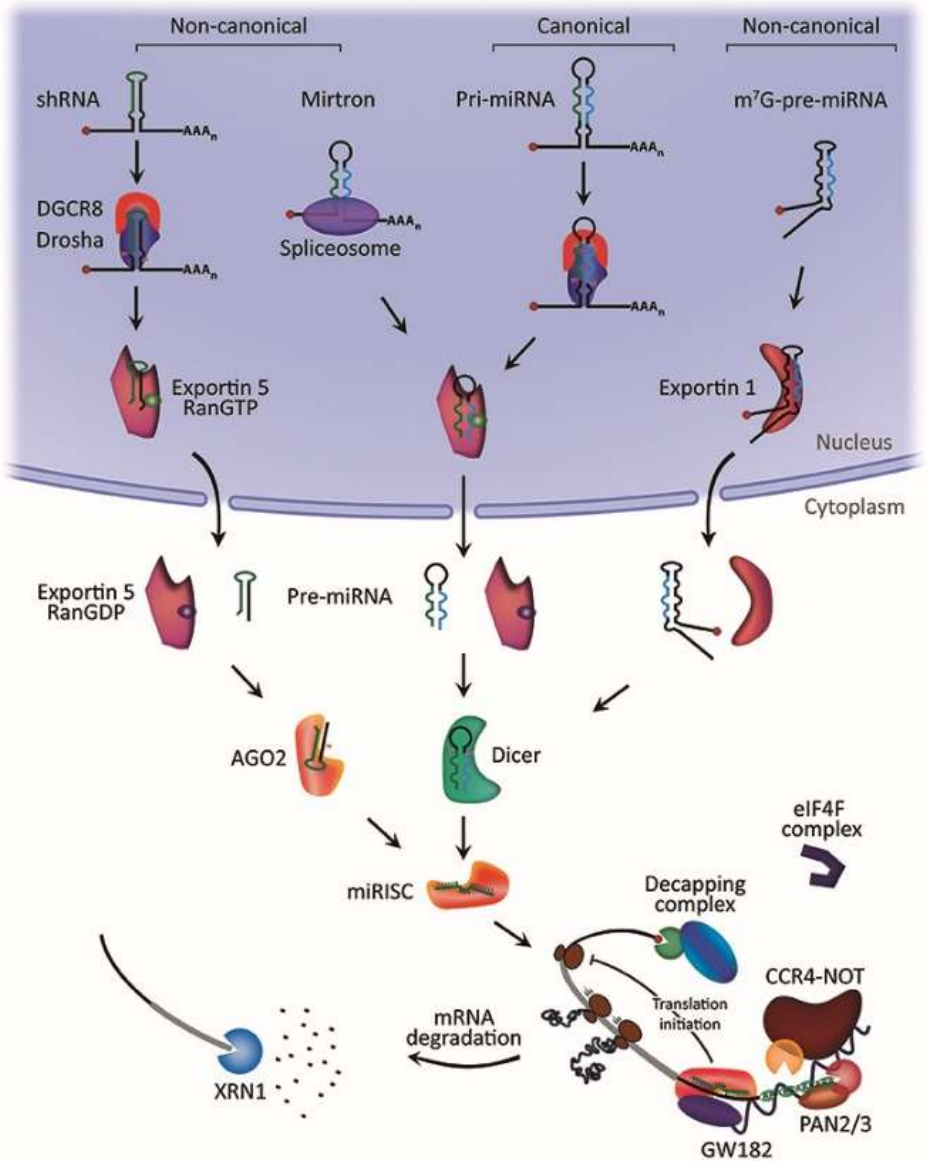


***Figure 8. miRNA biogenesis and gene silencing.***

*Canonical miRNA biogenesis starts with pri-miRNA transcript generation, which is then cleaved by Drosha and DiGeorge Syndrome Critical Region 8 (DGCR8), producing the precursor-miRNA (pre-miRNA). Exportin5/RanGTP export the pre-miRNA is exported to the cytoplasm to produce the mature miRNA duplex. The strands (5p or 3p) are loaded into the Argonaute (AGO) family of proteins forming miRNA induced silencing complex (miRISC). In the non-canonical pathways, DGCR8 cleaves small hairpin RNA (shRNA) and they are exported to the cytoplasm via Exportin5/RanGTP. AGO2-dependent, but Dicer-independent, cleavage is responsible for further maturation whereas, Mirtrons and 7-methylguanine capped (m7G)-pre-miRNA cytoplasmic maturation is Dicer dependent. Mirtrons are exported via Exportin5/RanGTP while m7G-pre-miRNA are exported via Exportin1. Both the canonical and non-canonical pathways lead to a functional miRISC complex. The majority of translational inhibition is by miRISC binding to target mRNAs, resulting in Argonaute-based recruitment of the poly(A)-deadenylases PAN2/3 and CCR4-NOT, which are responsible for initiating and completing the deadenylation process, respectively. This leads to the removal of the m7G cap on target mRNA by the decapping complex, which then undergoes 5′−3′ degradation via the exoribonuclease XRN1. Image by O'Brien et al.* [109]**.**

## 3.7 Extracellular/circulating miRNA: release mechanisms

In addition to the intracellular mechanisms, miRNAs can be released and elicit intercellular interactions. One release mechanism of miRNAs is through extracellular vesicles (EV) which are cell-derived membrane particles ranging from 30 to 5000 nm in size and include exosomes, microvesicles and apoptotic bodies. EVs are released under physiological conditions, but also during cellular activation, senescence and apoptosis. They play an important role in intercellular communication by carrying lipids, proteins, DNAs, mRNAs and functional mature miRNA from one cell to another [122]. Apoptotic bodies are the largest EV at approximately 1-5 µM in diameter, followed by microvesicles (MVs) at approximately 400-1500 nm and then exosomes, which are 30-100 nm in diameter, making them the smallest EVs [123,124].

Apoptotic bodies are released at the early stages of apoptosis and contain cytoplasmic contents originating from the parent cell. Due to enrichment with phosphatidylserine (PS) the apoptotic bodies signal to phagocytic cells (*e.g.* macrophages) to engulf and clear the cytoplasmic content [125,126]. Zernecke *et al.* demonstrated that miRNAs were also packaged in apoptotic bodies shown by the levels of miR-126 found to be released from endothelial cells (ECs) [127]. Hergenreider *et al.* went on to demonstrate that miR-126 was selectively loaded and released in apoptotic bodies by ECs, but not other MVs [128]

MVs are secreted under specific conditions by a number of different cells and are formed from the outward blebbing of the plasma membrane and are also enriched with PS and phosphatidylcholine (PC) [122]. MVs have been shown to carry functional proteins, mRNAs and miRNA to neighbouring cells (Figure 9A) [125,126]. An example of a miRNA released via MVs is miR-320b, released by platelets during myocardial infarction. Following release, MVs transfer the miR-320b to human microvascular endothelial cell line (HMEC-1) and results in downregulation of intercellular adhesion molecule-1 (ICAM-1) [129].

Exosomes are generated from a type of late endosomes known as multivesicular bodies which fuse with the plasma membrane releasing their contents into intraluminal vesicles (ILVs) [123]. Once extracellular, these ILVs are termed exosomes and are characterised by a variety of antigens including tetraspanins (CD9, CD63, CD37, CD81, CD82), heat shock proteins, tumor susceptibility gene 101 protein (Tsg101), and ALG2-interacting protein X (Alix) [123]. They are also enriched in ceramide, PC and phosphatidylethanolamine (PE) [126]. The content of exosomes is dependent on the cell type of origin, trigger or stimulus, but exosomes have been shown to carry miRNA into the extracellular space and to neighbouring cells (Figure 9A) [125,126]. miR-122, a putative marker of liver injury, has been shown to be released in exosomes from PHHs upon exposure to hepatotoxicants such as tolvaptan [130]. However, the intercellular target of miR-122 is still not fully understood.

miRNAs are not only selectively loaded into exosomes but extracellular/circulating miRNAs are also detected in the microvesicle-free fraction. This indicates an alternative release mechanism through association to protein complexes and it has been reported that Ago-2-miRNA complexes are released (Figure 9A) [122,131]. Results indicate that Ago2-protein complexes might also be involved in delivery of miRNAs from donor cell to recipient cells and facilitate cell-cell communication, similar to the miRNA released in exosomes [122]. Arroyo *et al.* demonstrated that miR-16, miR-92a and miR-122 were consistently enriched in the AGO2 immunoprecipitates extracted from human plasma/serum of healthy individuals [131]. Finally, miRNAs have also been identified to be released as high-density lipoprotein (HDL)-miRNA complexes, an example of this form of release is demonstrated in patients with familial hypercholesterolemia, who had increased release of miR-223 via HDL, which was transferred to recipient cells [132].

As miRNAs are expressed intracellularly and released into the extracellular space they have been identified in a wide range of bio-fluids including serum, plasma, urine, cerebrospinal fluid and saliva and more shown in Figure 9B [122]. miRNAs are also released by cells into culture supernatant *in vitro* [122,130,133,134]. Aberrant extracellular miRNAs are also released due to a variety of diseased states and have shown to be highly sensitive biomarkers [135]. Therefore, extracellular miRNAs are a promising method to detect early signs of liver injury, yet miRNAs specific to liver fibrosis are lacking and will be discussed further in section 4.2.1.

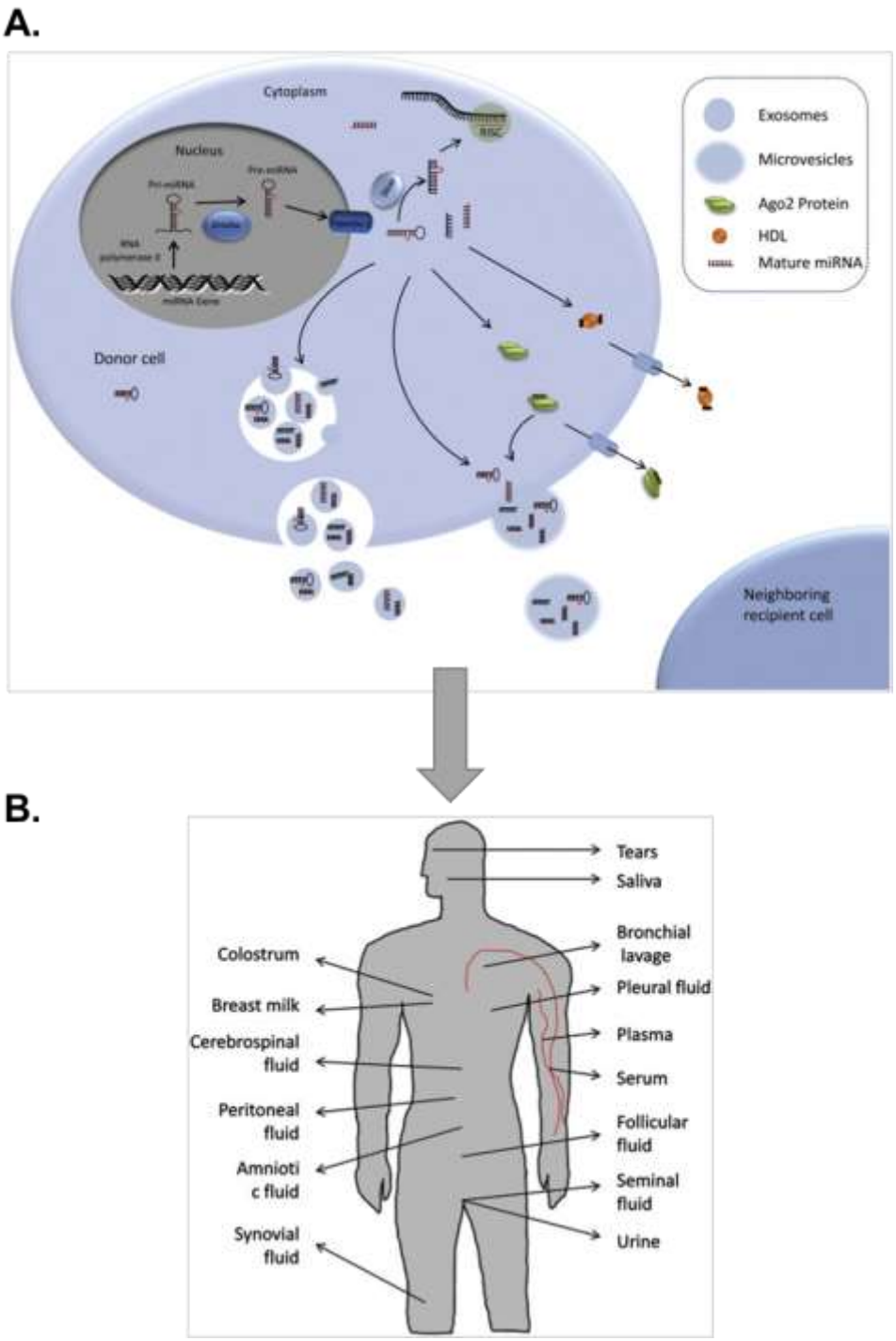


***Figure 9. Extracellular miRNA release.***

*miRNA biogenesis (described in section 3.6) and release of miRNAs into the extracellular environment. Mature miRNAs can be selectively released from the cell via incorporation into exosomes or coupled with Ago2 protein. Alternatively, miRNAs can be released enwrapped in microvesicles or attached high density lipoprotein (HDL). Extracellular/circulating miRNAs can then interact with neighbouring recipient cells (A). miRNAs have also been detected in a wide range of bio-fluids throughout the body (B). Images taken from Sohel et al. and modified for the purpose of this thesis* [122].

# 4 Project 1: Biomarkers of liver fibrosis

## 4.1 Aims

The aims of this section were to identify sensitive and fibrosis-specific biomarkers, which as discussed in section 3.4 are needed for detecting early signs of fibrosis. To this end, extracellular miRNAs were measured from MTs comprising HepaRG alone or co-cultured HepaRG, hTERT-HSC and THP-1, cellular models of DILI and liver fibrosis, respectively.

The first paper titled “Exosomal miRNAs release as a sensitive marker for drug-induced liver injury *in vitro*” investigates the sensitivity of extracellular miRNAs, focusing specifically on hepatocellular injury in a 3D-HepaRG cell culture model and on three putative miRNAs (miR-122-5p, miR-192-5p and miR-34a-5p) released in exosomes.

The second paper titled “Identification of miR-199a-5p, miR-214-3p and miR-99b-5p as extracellular biomarkers of fibrosis and promoters of HSC activation” focuses on identifying and characterising novel biomarkers for fibrosis by measuring extracellular miRNAs released by multicellular cultures into the cell culture supernatant. Here, the specific focus lies in differentiating hepatocellular damage (elicited by APAP-exposure) from liver fibrosis (elicited by exposure to MTX). Identification of miRNAs as biomarkers is accompanied by a functional genomics approach based on transfection of HSC with miRNA-mimics was pursued to establish the involvement of selected miRNAs in stellate cell activation, a key event in liver fibrosis.

## 4.2 Introduction

### 4.2.1 MiRNAs as biomarkers of liver injury, disease and fibrosis

As mentioned in section 3.4 serum biomarkers for liver fibrosis lack sensitivity and specificity and provide limited information. Achieving earlier detection of liver injury and fibrosis is required to improve disease management. Studies using different tissues and organs have demonstrated that injury or disease results in aberrant miRNA expression and miRNA release into a range of bio-fluids (described in section 3.7). Therefore, extracellular/circulating miRNAs are being investigated as non-invasive biomarkers of disease.

Genome-wide expression profiling has identified 277 miRNAs expressed in the liver, including miR-122 which is thought to make up 52% of all miRNA transcripts in the human liver and is liver-specific. miR-122 is involved in liver development, differentiation and homeostasis [136] and has been associated with liver injury, disease and HCC [137]. miR-122 expression decreases in liver tissue and release increases into serum/plasma upon exposure to hepatotoxicants such as APAP, paraquat and tolvaptan [130,138–141]. Other types of liver injury/disease also affect miR-122 expression/release such as HCV and HBV, alcoholic liver disease (ALD) and fibrosis [137,140,142]. Although, miR-122 is not specific to a single liver condition it has demonstrated the potential of miRNAs as biomarkers as it is released very early upon liver injury and outperforms other methods such as AST and ALT measurements [130,139]. Another miRNA linked to liver injury is miR-192 as release was elevated in the serum of alcoholic liver fibrosis (ALF) and APAP overdose patients [143–145]. Expression of miR-192 was also shown to decrease in liver tissue during fibrosis and HBV [146,147]. Both miR-122 and miR-192 are useful markers of liver injury but are not disease specific (*e.g.* fibrosis).

APAP is commonly used to investigate DILI as it elicits concentration dependent acute hepatotoxicity. The exact mechanism of APAP-induced hepatotoxicity is discussed further in section 4.2.3. Krauskopf *et al.* identified 36 circulating miRNAs associated with APAP-induced hepatotoxicity as a result of overdose in patient samples 5 of which were liver enriched: miR-122, miR-192, miR-194, miR-483, and miR-210 [145]. Krauskopf *et al.* carried out a follow up study using NGS where the differential release of 116 miRNAs was identified in patients who had suffered APAP overdose and once again included miR-122, miR-192, miR-194, miR-483, and miR-210 along with others such as hsa-miR-107, miR-150, miR-191, miR-21, miR-93, miR-223, miR-221 and more [143]. Of these miRNAs, miR-223 is associated with acute and chronic liver injury [148]. miR-223 was shown to be upregulated in the livers of mice with surgically induced ischemia and reperfusion (I/R) and in mice livers injured with $CCl_4$, APAP, and Conavalin A (Con A) [148]. This was also confirmed in patients with ALF which resulted in increased miR-223 hepatic expression and release [148,149].

ALD has also been studied with regards to miRNA expression and release. Mice fed with an ethanol-containing diet (Lieber–DeCarli diet) showed increased expression of miR-320, miR-486, miR-705, and miR-1224 and decreased expression of miR-27b, miR-214, miR-199a-3p, miR-182, miR-183, miR-200a, and miR-322 [150,151]. Dippold *et al.* demonstrated the deregulation of a panel of miRNAs, including miR-34a, miR-103, miR-107, and miR-122 in chronic EtOH fed rodents [152]. miR-155 was also shown to play a crucial role in ethanol-induced liver toxicity and it is thought to promote liver fibrosis and alcohol-induced steatophepatitis [150,153]. Hence, miRNAs have been suggested as putative biomarkers for a number of liver conditions.

There is a critical need for non-invasive yet sensitive and specific biomarkers of fibrosis that are better than those currently available (see section 3.4). As mentioned above, intracellular and extracellular deregulation of miR-122 and miR-192 are biomarkers of hepatocellular damage that are also detected during liver fibrosis progression. However they cannot be considered as specific to liver fibrosis but rather indicators of liver injury [140,141,144]. In pursuit of biomarkers specific for fibrosis, studies *in vitro* and *in vivo* have identified miRNAs that are specifically differentially expressed/released during fibrosis progression (listed in Table 2 with references). The role these miRNAs may play during HSC activation and liver fibrosis progression has been studied for some but not all of the listed miRNAs. Of the 31 miRNAs listed, twelve inhibited HSC activation: miR-30c, miR-193, miR-19b, miR-146a, miR-9, miR-24, miR-34, miR-150, miR-142, miR-29, miR-101 and miR-378 (Table 2). Whereas, ten of the listed miRNAs promoted HSC activation: miR-146b, miR-33a, miR-214, miR-199a, miR-221, miR-222, miR-181b, miR-125a, miR-17 and miR-31 (Table 2). Interestingly, of the miRNAs that promote HSC activation miR-33a, miR-181b, miR-125a and miR-17 were assessed in human serum samples, whereas miR-146b, miR-33a, miR-214, miR-199a, miR-221, miR-222 and miR-31 were studied intracellularly. Additionally, none of these miRNAs have been studied in the context of fibrosis as a result of chronic DILI as the serum samples were taken from patients with chronic hepatitis and NAFLD. Finally, the relationship between miRNA and tissue damage is complex: Krauskopf *et al.* demonstrated that some circulating miRNAs are less abundant (miR-30c, miR-150, miR-222 and miR-142) and some more abundant (miR-193, miR-34a, miR-221, miR-21 and miR-378) in patients with APAP-overdose [143]. Therefore, these miRNAs, although they may play a role in fibrosis progression, are not necessarily specific/suitable biomarkers for identifying liver fibrosis.

In summary, although circulating miRNAs have been investigated for patients with liver fibrosis, the majority has been identified in liver biopsy samples. In addition, specific miRNAs associated with DILI-induced fibrosis have not been extensively investigated and a panel of fibrosis-specific miRNAs would be desirable for early detection of fibrosis caused by medications in patients.

***Table 2. miRNAs associated with liver fibrosis.***

| *miRNA* | *Clinical Evidence* | *Study model* | *Effect* | *Ref.* |
|---|---|---|---|---|
| ***miR-30c*** | Decreased in serum (LC). | $CCL_4$ treated mice | Downregulation of miR-30C expression elevates HSC activation, proliferation & migration. Increased expression attenuates liver fibrosis. | 154,155 |
| ***mIR-125a*** | Increase in liver tissue (LC). Increased serum miR-125a (CHBV). | LX-2 | Potentially correlates to HSC activation. | 156,157 |
| ***miR-193*** | Elevated in serum (LC). | $CCL_4$ treated mice | Downregulated expression elevates HSC activation, proliferation & migration. Increased expression attenuates liver fibrosis. | 155 |
| ***miR-19b*** | Decrease in human liver tissue (LF). Increased in serum (LF). | Rat HSCs, LX-2 | Downregulated expression is linked to HSCs activation. Increased expression attenuates liver fibrosis. | 158 |
| ***miR-146a*** | Increased in serum (LF and LC). Decreased expression in liver tissue (LF and LC). | $CCL_4$ rats, Rat HSCs, LX-2 | Downregulated expression is associated with liver fibrosis. Increased expression attenuates liver fibrosis. | 159–161 |
| ***miR-146b*** | Increased in human liver (LF). | HSC-t6, LX-2, $CCL_4$ treated mice | Increased expressed is linked to HSC activation and increased proliferation. | 162,163 |
| ***miR-33a*** | Increased expression in liver tissue and serum quanity (CHBV). | LX-2 | HSC activation results in increased release. Increased expression/release linked to fibrosis progression. | 164,165 |
| ***miR-27a*** | Chronic hepatitis induced cirrhosis results in increased miR-27a release into serum. | rat DMN-induced liver cirrhosis | Serum quantity increased in rats with liver cirrhosis. | 166 |
| ***miR-9*** | Decreased expression in liver tissue (LF). | Primary human cells, LX-2, $CCL_4$ treated mice | Decreased expression is linked to fibrosis. Increased expression prevents HSC activation. | 167,168 |
| ***miR-24*** | N/A | Mdr2−/− mice | Downregulation significantly increases expression of fibrosis genes. | 169 |
| ***miR-214*** | Increased expression in liver tissue (LF). | LX-2, mouse liver | Increased miR-214 expression results in HSC activation and accumulation of ECM. | 170,171 |
| ***miR-34*** | Serum levels is increased (CHCV). Decreased in liver tissue (CHBV). | LX-2, $CCL_4$ treated mice | Increased expression ameliorates liver fibrosis progression. | 172–174 |
| ***miR-150*** | Serum quantity increased (LC). | Rats with BDL, primary rat HSCs | Decreased expression during liver fibrosis. Overexpression in HSCs results in decreased activation and proliferation. | 175–178 |
| ***miR-200*** | Increased expression in liver tissue (LF). | $CCL_4$ treated mice | Expression of fibrosis related genes increased by overexpression. | 163,172, 179 |

| | | | | |
|---|---|---|---|---|
| ***miR-182*** | Increased exoression in liver tissue (NAFLD-LF and CHCV). | DMN-induced LF in rats | Fibrosis resulted in increased plasma levels. | 180–182 |
| ***miR-183*** | Increased in liver tissue (NAFLD-LF). | DMN-induced LF in rats | Fibrosis resulted in increased plasma levels. | 180,182 |
| ***miR-199a*** | Expression increased in liver tissue (LF). | $CCL_4$ treated mice, rat primary HSCs, LX-2 | Increased expression elicits HSC activation and ECM production. | 163,183 |
| ***miR-221*** | Upregulated in human liver tissue (LF). | LX-2, mouse primary HSCs, $CCL_4$ treated mice | Upregulated expression in activated HSCs and during liver fibrosis. | 184,185 |
| ***miR-222*** | Upregulated in human liver tissue (LF). | LX-2, mouse primary HSCs, $CCL_4$ treated mice | Upregulated expression in activated HSCs and during liver fibrosis. | 185 |
| ***miR-142*** | Decreased serum levels (LC). | Rat primary HSCs | Increased expression results in HSC activation is reversed/decreased or prevents activation. | 186 |
| ***mIR-29*** | Decreased liver tissue expression and serum levels (LF, LC). | $CCL_4$ treated mice | Decreased expression is linked to fibrosis progression.<br>Increased expression prevents fibrosis progression. | 187 |
| ***miR-21*** | N/A | LX2 | Increased expression results in HSC activation.<br>Inhibited expression prevents HSC activation. | 188,189 |
| ***mIR-101*** | Serum levels and expression in liver tissue decreases (CHCV). | $CCL_4$ treated mice | Increased expression promoted reversal of HSC activation and was downregulated in the fibrotic liver. | 190,191 |
| ***miR-181b*** | Increased in serum (LC). | HSC-T6, LX-2, $CCL_4$ treated mice | Expression increases in activated HSCs and promotes HSC proliferation. | 192,193 |
| ***miR-17*** | Liver biopsies (NAFLD-LF) and serum samples (LC) resulted in increased expression/release | HSC-T6, $CCL_4$ treated mice | Increased expression during liver fibrosis.<br>Increased expression elicits ECM deposition and HSC activation. | 182,194 |
| ***miR-31*** | Increased expression in liver tissue (NAFLD-LF). | Primary rat, mouse and human HSCs | Increased expression in activated HSCs.<br>Decreased expression inhibits HSC activation. | 182,195 |
| ***miR-219a*** | Increased expression in liver tissue (NAFLD-LF). | N/A | N/A | 182 |
| ***miR-224*** | Increased expression in liver tissue (NAFLD-LF). | N/A | N/A | 165,182, 196 |
| ***miR-378*** | Increased expression in liver tissue (NAFLD-LF). | $CCL_4$ treated mice, LX2, primary mouse HSCs | Decreased expression during liver fibrosis progression.<br>Expression is reduced during HSC activation.<br>Increased expression suppresses HSC activation. | 182,197 |
| ***miR-590*** | Increased expression in liver tissue (NAFLD-LF). | N/A | N/A | 182 |

*Clinical data results shown with disease in brackets. Abbreviations include LF = Liver fibrosis, LC = Liver cirrhosis, CHBV = Chronic HBV resulting in fibrosis, CHCV = Chronic HCV resulting in fibrosis,* NAFLD-LF= NAFLD-induced liver fibrosis*. In vitro/In vivo study data are also briefly summarised. References (Ref.) are provided for each miRNA-type.*

### 4.2.2 Methotrexate, structure, metabolism and liver injury

Methotrexate (MTX) is an immunosuppressant drug and a chemotherapeutic agent. It is used to treat a variety of autoimmune diseases such as psoriasis and rheumatoid arthritis (RA). MTX is a folate antagonist but also affects other related metabolic pathways such as purine and pyrimidine metabolism [198]. MTX is composed of a pteridine ring, p-aminobenzoic acid and glutamic acid (Figure 10) and has a molecular weight of 454.5 g/mol ($C_{20}H_{22}N_8O_5$) and poor aqueous solubility [199]. MTX is structurally very similar to folic acid with the exception of a replacement of a carbonyl group for an amine in the pteridine ring and the addition of a methyl group on the p-aminobenzoic acid (Figure 10) [199].

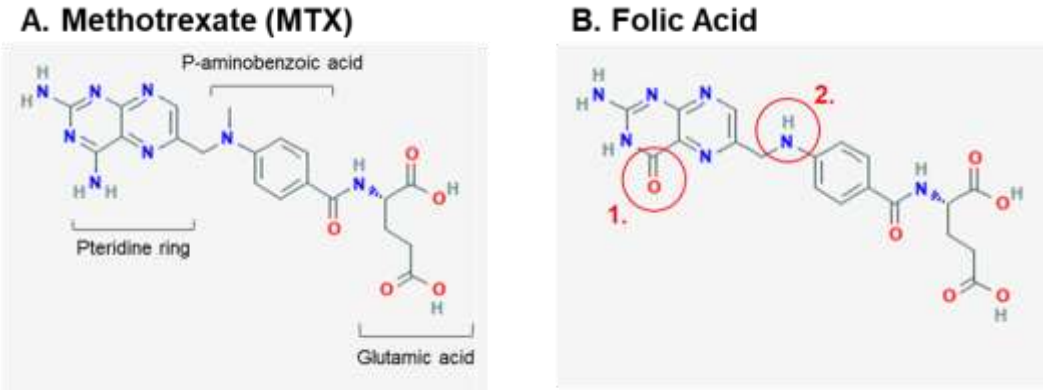


***Figure 10. Structure of methotrexate and folic acid.***

*Structure of MTX (A) and folic acid (B) are shown and the structural differences are highlighted, including replacement of a carbonyl group for an amine (position 1) and addition of a methyl group (position 2). Image modified from PubChem.*

MTX actively enters cells through folate transporter-1 (SLC19A1) while various ABC transporters mediate efflux of MTX. Once inside the cell MTX undergoes polyglutamation becoming methotrexate polyglutamate (MTXPG), which is catalysed by the enzyme folylpolyglutamate synthase (FPGS) and can be de-conjugated by gamma-glutamyl hydrolase (GGH) [198–200]. MTXPG inhibits several enzymes in folate metabolism including dihydrofolate reductase (DHFR), which results in the depletion of tetrahydrofolate (THF), a precursor of the folate cofactor 5-methyltetrahydrofolate (5-$CH_3$-THF) [200]. Reduced availability of 5-$CH_3$-THF reduces remethylation of homocysteine to methionine, leading to accumulation of homocysteine and decreased intracellular transmethylation capacity [198,200]. Inhibition of pyrimidine biosynthesis occurs via inhibition of thymidylate synthase (TYMS) by MTXPG and the indirect depletion of THF [198,200]. Purine biosynthesis is also inhibited by the failure to synthesize active folate compounds (Figure 11). MTXPG also inhibits bifunctional purine biosynthesis protein PURH

(ATIC), causing intracellular accumulation of 5-aminoimidazole-4-carboxamide ribonucleotide (AICAR), leading eventually to generation of adenosine [198–200].

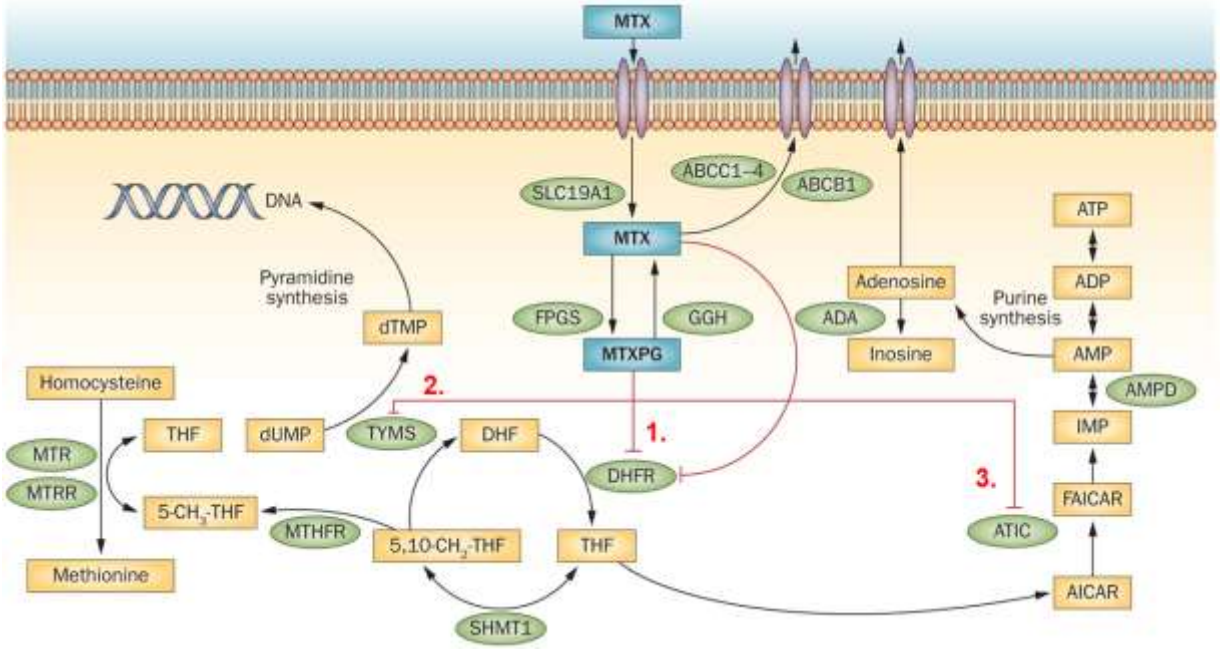


***Figure 11. Pathways of methotrexate metabolism.***

*MTX actively enters cells through SLC19A1, whereas transmembrane efflux is mediated by various ABC transporters. In the cell, MTX undergoes polyglutamation catalysed by the enzyme 10-formyl-5- aminoimidazole-4-carboxamide ribonucleotide (FPGS), which can be reversed by γ-glutamyl hydrolase (GGH).* ***1.*** *Several enzymes in folate metabolism are inhibited by MTX polyglutamate (MTXPG), including dihydrofolate reductase (DHFR), resulting in depletion of tetrahydrofolate (THF). THF is a precursor of the folate cofactor 5-CH3-THF is linked to both purine and pyrimidine biosynthesis. Remethylation of homocysteine to methionine is reduced due to decreased availability of 5-CH3-THF (due to depleted THF). This leads to accumulation of homocysteine and decreased intracellular transmethylation capacity.* ***2.*** *Inhibition of thymidylate synthase (TYMS) by MTXPG, and indirectly via depletion of THF, leads to inhibition of pyrimidine biosynthesis. Furthermore, when active folate compounds are not synthesised purine biosynthesis is also not possible.* ***3.*** *Finally, MTXPG inhibits bifunctional purine biosynthesis protein PURH (ATIC), resulting in intracellular accumulation of 5-aminoimidazole-4-carboxamide ribonucleotide (AICAR), leading to adenosine generation, which is an anti-inflammatory agent. Image taken from Schmeling et al. and edited for this thesis [198].*

Concerning the chemotherapeutic potential of MTX, it is thought that the inhibition of purine and pyrimidine biosynthesis results in the inhibition of DNA and RNA synthesis, a known therapeutic strategy used to treat a number of hyper-proliferative diseases including viral infections, autoimmune disorders and cancer [201,202]. The mechanism by which low-dose

MTX modulates inflammation is still not fully understood and might differ for each disease. However, when treating rheumatic diseases it has been shown that combining MTX treatment with folic acid prevents much of the toxic effects of MTX without interfering with its anti-inflammatory efficacy [203]. This suggests that the therapeutic effect of MTX in patients with rheumatic diseases relies on folate-independent mechanisms, including suppression of transmethylation reactions resulting in the promotion of adenosine release as an anti-inflammatory agent [198,200].

Although MTX is an effective treatment for RA and psoriasis, the adverse effects often result in therapy being discontinued [204]. Minor side effects include mouth ulcers and gastrointestinal intolerance. Major side effects include primarily bone marrow toxicity and liver function test abnormalities. Additionally, folate deficiency has been identified as a risk factor for MTX toxicity and supplementation with folic acid and folinic acid significantly reduced the rate of discontinuation of MTX in RA patients with no effect on MTX efficacy [203]. However, the exact reason how folate supplementation reduced MTX toxicity is not fully understood [203].

MTX has been shown to elicit DILI, resulting for some patients in elevated levels of AST and ALT [205]. A comparative study of 108 patients taking MTX as an RA treatment showed that 29 had increased AST, ALT and stiffness demonstrated by abnormal ultrasound and the larger cumulative doses were more likely to promote liver fibrosis. Additionally, this study demonstrated that patients with a higher BMI were more susceptible to developing fibrosis [206]. With regards to MTX as a treatment for RA it has been demonstrated that the risk of developing hepatic fibrosis and cirrhosis is low [205]. However, hepatic fibrosis is a potential consequence of MTX treatment for psoriasis yet the mechanism behind this is not fully understood [207,208]. Cobb *et al.* carried out genome-wide analyses for novel genes involved in the response to MTX where they demonstrated that there was an association with TGF-β/SMAD signalling and a member of the multi-drug resistance subfamily of the ATP-binding cassette transport protein, cystic fibrosis transmembrane conductase regulator (CFTR) [209]. TGF-β was also described by Moncrieffe *et al.* to be upregulated in patients with juvenile rheumatic arthritis treated with MTX [210]. This is interesting as TGF- β1 release is a key event in liver fibrosis progression due to its stellate cell activating capacity [40].

### 4.2.3 Acetaminophen structure, metabolism and toxicity

Acetaminophen (APAP) more commonly known as paracetamol is used worldwide as an analgesic and antipyretic that is a weak inhibitor of the synthesis of prostaglandins. Unlike non-steroidal anti-inflammatory drugs (NSAIDs), which selectively inhibit cyclooxygenase 2 (COX-2), APAP does not suppress inflammation of RA [211]. Chemically, APAP is a phenol substituted in the para-position by an amide group (Figure 12). Oxidation is essential to its mechanism of action as a substrate and an inhibitor of the peroxidase function of COX-1 and COX-2 [211] and also leads to the formation of toxic metabolite NAPQI [212].

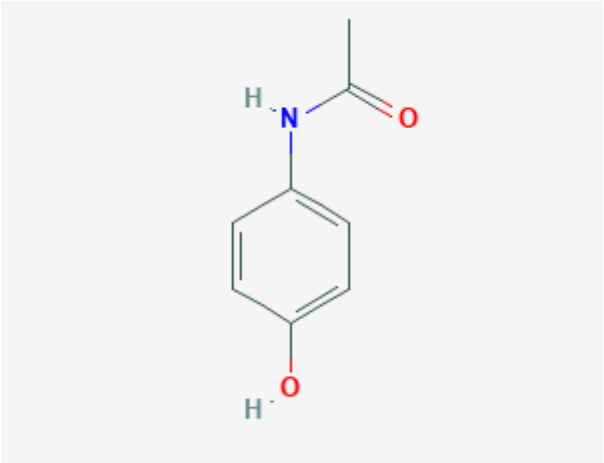


***Figure 12. Structure of acetaminophen.***

*Acetaminophen (APAP), a phenol substituted in the para-position by an amide group, is a substrate and an inhibitor of the peroxidase function of COX-1 and COX-2. APAP is commonly used as an analgesic and antipyretic. Image taken from PubChem.*

APAP is primarily metabolised in the liver and to a lesser extent in the kidneys and intestine. Therapeutic doses result in the majority of the APAP (52–57%) being converted to pharmacologically inactive glucuronide. Glucuronidation is catalysed by UDP-glucuronosyl transferases (UGT) resulting in a more water-soluble molecule. Studies in human liver microsomes and primary hepatocytes demonstrate that UGT1A1, UGT1A6, UGT1A9 and UGT2B15 are involved in APAP glucuronidation (Figure 13A). To a lesser extent APAP (30–44%) is converted to sulfate conjugates. A family of cytosolic enzymes called sulfotransferases (SULT) carries out sulfation of APAP. A sulfo group is transferred by SULTs to APAP increasing polarity, making it more prone to elimination. SULT1A1 and SULT1A3/4 were first shown to catalyze APAP sulfation using human platelet homogenates as a model for xenobiotic metabolism in the liver [213]. A minor fraction (5-10%) is oxidised to the reactive metabolite NAPQI and less than 5% of APAP is excreted unchanged [212,214]. Cytochrome P450 enzymes catalyse the oxidation of APAP to the toxic metabolite NAPQI and the exact contribution of particular CYP

isoforms to APAP bio-activation varies and is dependent on drug concentration. CYP2E1 has been shown to have a role in bio-activation and oxidation of APAP, but reports also suggest the involvement of CYP2A6 [215,216]. It has also been demonstrated that CYP2D6 is involved in oxidation of APAP but only at very high (toxic) doses *i.e.* when plasma levels reach 2 mM [217,218]. There have been suggestions that CYP3A4 is involved in APAP oxidation from experiments using hepatoma cell lines, yet experiments in human studies have demonstrated that the role of CYP3A4 is negligible [215].

NAPQI elicits hepatotoxicity and is detoxified through the binding of sulfhydryl group of GSH to form APAP-GSH, which is then excreted in the urine as APAP-cys. NAPQI conjugation to GSH occurs via a spontaneous process and an enzymatic reaction catalysed by glutathione- S-transferases (GSTs). The spontaneous and non-enzymatic reaction yields multiple products including GSH conjugate 3-(glutathione-S-yl)-acetaminophen (APAP-GSH), free APAP and glutathionine disulphide (GSSG). GST reaction yields APAP-GSH and free APAP [212]. There are seven distinct classes of enzymes that make the human cytosolic GST family with numerous genetic variants within each class [219]. The most effective catalysts of NAPQI conjugation with GSH is GSTP1, GSTT1 and GSTM1 [212]. Interestingly, GSTs have been proposed as a sensitive and early biomarker of acute liver damage as they are released as early as 4 hours after poisoning and remain elevated for 12 hours after ingestion [220,221].

As supratherapeutic doses (more than 4 g/day) the sulfation pathway becomes saturated, while glucuronidation and oxidation increased. However, after a highly toxic dose the glucuroinidation becomes saturated as well leading to higher quantities (~ 10%) of APAP being eliminated unchanged. There is also increased oxidation to NAPQI (> 15%), which eventually depletes GSH stores resulting in NAPQI forming protein adducts by binding to cysteine groups on cellular proteins. Due to the fact NAPQI primarily targets mitochondrial proteins and ion channels this leads to a loss of energy production, ion misbalance and cell death [212]. Lethal APAP doses can be effectively treated within 8-10 hrs after exposure with N-acetylcysteine (NAC). NAC replenishes GSH stores, scavenges reactive oxygen species in mitochondria and enhances the sulfation metabolic pathway (Figure 13B). This results in the risk of hepatotoxicity being reduced to less than 5% [222].

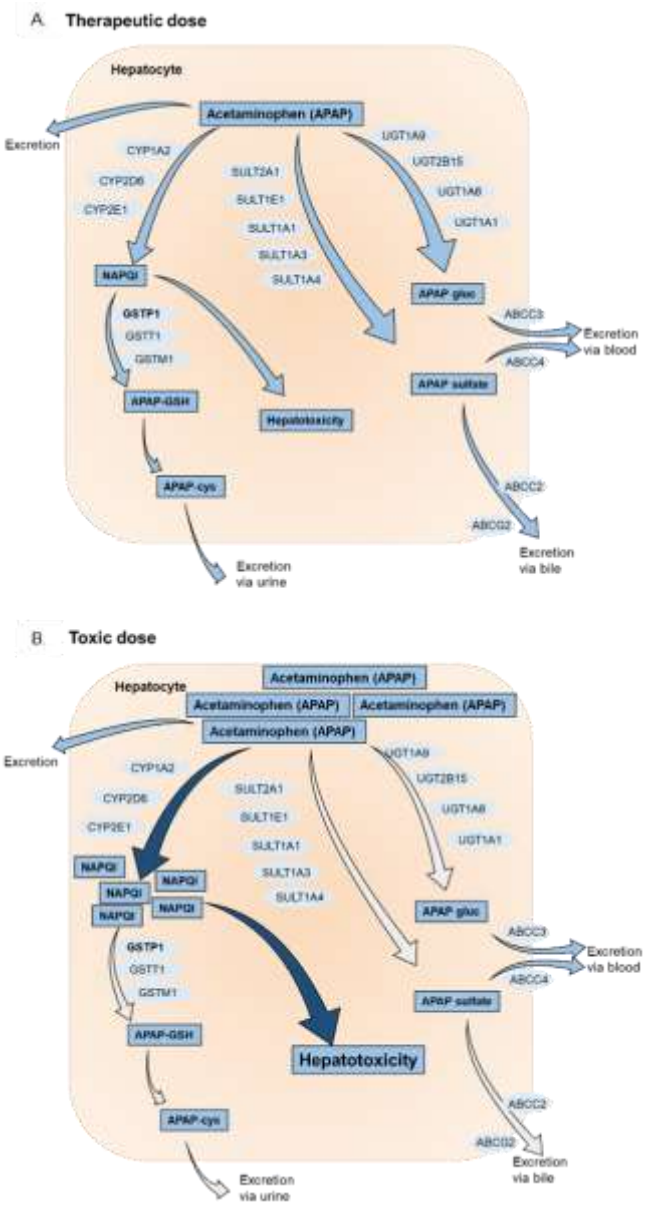


***Figure 13. APAP metabolism in the liver.***

*APAP metabolism is shown at a therapeutic dose (A) and toxic (B). APAP is metabolised via Glucuronidation (catalysed by UDP-glucuronosyl transferases, UGT) and sulfation (*catalysed by sulfotransferases, SULT) *into non-toxic metabolites APAP-gluc and APAP-sulfate are excreted via blood and bile, respectively. A small quantity of toxic NAPQI is produced*, which is catalysed by c*ytochrome P450 enzymes. NAPQI is subsequently detoxified by glutathione (GSH), catalysed by glutathione- S-transferases (GSTs), and excreted via urine (A). Large quantities of APAP result in increased production of NAPQI causing GSH depletion, thereby preventing the detoxification process resulting in increased hepatotoxicity and hepatocellular death (B).*

## 4.3 Paper 1: Exosomal miRNAs release as a sensitive marker for drug-induced liver injury *in vitro*

**Accepted: 12th of August 2020 in Applied *in vitro* Toxicology**

Catherine Jane Messner [1,2,4], Carine Premand [3], Carine Gaiser [1], Tanja Kluser[1], Eric Kübler [1], Laura Suter-Dick [1,4]

[1]University of Applied Sciences and Arts Northwestern Switzerland, 4132 Muttenz, Switzerland.
[2]University of Basel, Department of Pharmaceutical Sciences, 4056 Basel, Switzerland.
[3] University of Applied Sciences and Arts Western Switzerland, 1950 Sion, Switzerland.
[4] Swiss Centre for Applied Human Toxicology (SCAHT), 4055 Basel, Switzerland.

Corresponding author:
Laura Suter-Dick
University of Applied Sciences and Arts Northwestern Switzerland
Institute for Chemistry and Bioanalytics
Hofackerstrasse 30
CH-4132 Muttenz

Email: laura.suterdick@fhnw.ch

APPLIED IN VITRO TOXICOLOGY
Volume 6, Number 3, 2020
Mary Ann Liebert, Inc.
DOI: 10.1089/aivt.2020.0008

**ORIGINAL ARTICLES**

# Exosomal microRNAs Release as a Sensitive Marker for Drug-Induced Liver Injury *In Vitro*

Catherine Jane Messner,[1–3] Carine Premand,[4] Carine Gaiser,[1] Tanja Kluser,[1] Eric Kübler,[1] and Laura Suter-Dick[1,3]

## Abstract

***Introduction:*** *In vitro* models for liver disease suffer from the lack of well-established and sensitive biomarkers of cellular damage. MicroRNAs (miRNAs; small noncoding RNAs) represent potential biomarkers for the detection of drug-induced liver injury *in vivo* and *in vitro*. Altered physiological state caused by disease or tissue damage results in altered release of exosomal- or protein-bound miRNAs, detectable in body fluids and cell culture media.
***Materials and Methods:*** Here, we exposed 3D-HepaRG cultures to methotrexate (MTX) and acetaminophen (APAP) and used q-RT-PCR to investigate miRNAs as potentially sensitive markers of hepatotoxicity *in vitro*, with a specific focus on the exosomal release. We investigated three miRNAs, miR-122-5p and miR-192-5p, both associated with hepatic damage, and miR-34a-5p, involved with apoptosis. Metabolic activity, urea and albumin release were assessed to confirm key hepatocellular characteristics of 3D-HepaRG.
***Results:*** The 3D-HepaRG model was able to metabolise testosterone, produced urea and albumin. APAP treatment increased exosomal release of all three tested miRNAs, while MTX increased miR-122-5p release only. Absolute quantification of miR-122-5p corroborated the release of this miRNA by both treatments.
***Discussion:*** Exosomes could be efficiently isolated from 3D-HepaRG, characterized, and used for miRNA extraction and quantification. We identified that total extracellular and exosomal-miR-122-5p release occurred at concentrations lower than those leading to MTX-induced apoptosis/necrosis, which corroborate previous findings using other hepatotoxic compounds.
***Conclusion:*** Our results demonstrate the suitability of 3D-HepaRG combined with exosomal miRNA measurement for the detection of hepatotoxicity *in vitro*. Specifically, exosomal-miR-122-5p is a sensitive marker of APAP- and MTX-induced *in vitro* damage.

**Keywords:** 3D liver culture, biomarkers, DILI, drug-induced liver injury, exosomes, miRNA

## Introduction

DRUG-INDUCED LIVER INJURY (DILI) is a major challenge in clinical medicine and drug development. It is categorized as acute or chronic and can be the result of direct toxicity or immune-mediated mechanisms, as hepatocyte destruction may be further enhanced by a subsequent inflammatory reaction.[1] Acetaminophen (APAP) is a classic example of a drug causing acute dose-related DILI. High concentrations of APAP lead to acute hepatocellular necrosis/apoptosis and liver failure,[1,2] whereas methotrexate (MTX) elicits chronic DILI in patients, potentially leading to hepatic fibrosis and ultimately cirrhosis.[3–5]

Current diagnostic methods include serum biomarkers such as alanine aminotransferase (ALT), aspartate aminotransferase (AST), alkaline phosphatase, albumin levels, and total bilirubin that are incapable of detecting early signs of liver damage.[6] Liver biopsies are still the standard diagnostic method despite their invasive nature, sampling error, and potential clinical complications.[7] Similarly, there is a lack of appropriate *in vitro* biomarkers of hepatocellular damage. Therefore, novel methods for detecting early signs of hepatocellular damage in commonly used *in vitro* systems, such as HepaRG cultures, are required.

The small regulatory RNAs known as microRNAs (miRNAs) are single stranded noncoding RNAs consisting

[1]University of Applied Sciences and Arts Northwestern Switzerland, School of Life Sciences, Muttenz, Switzerland.
[2]Department of Pharmaceutical Sciences, University of Basel, Basel, Switzerland.
[3]Swiss Centre for Applied Human Toxicology (SCAHT), Basel, Switzerland.
[4]University of Applied Sciences Western Switzerland, Institute of Life Technologies, Sion, Switzerland.

of 21–25 nucleotides. They are not only present in cells but are also released into biofluids, including plasma, serum, urine, and cell culture media.[8] It has been shown that a variety of diseases such as cancer result in aberrant expression of miRNAs and selective miRNA release by injured cells.[9–13] Owing to the stability of extracellular miRNAs (ECmiRNAs) in biofluids they have already been described as circulating biomarkers for a variety of pathologies and evidence suggests that ECmiRNAs have increased sensitivity over other viability assays and traditional serum markers in kidney and liver models.[8,14–16] One described miRNA release mechanism is through extracellular vesicles (EV) known as exosomes that are 30–100 nm in diameter, making them the smallest EVs.[17,18] Exosomes are characterized by a variety of antigens, including tetraspanins (CD9, CD63, CD37, CD81, CD82), heat-shock proteins, tumor susceptibility gene 101 protein (Tsg101), and ALG2-interacting protein X (Alix).[17,19,20] miRNAs are not only selectively loaded into exosomes but ECmiRNAs are also detected in the microvesicle-free fraction indicating an alternative release mechanism through association to protein complexes that have been found in cell culture media.[21]

Several miRNAs have been identified as potential DILI biomarkers in clinical samples and using both 2D and 3D *in vitro* models. They include liver-specific miR-122-5p that is predominantly expressed in hepatocytes and released into the blood upon hepatocellular damage. Alongside miR-122-5p, miR-192-5p also appears elevated in serum during DILI and other forms of liver damage.[22–27] APAP-induced liver injury has been associated with increased release of miR-122-5p and miR-192-5p *in vivo* in animals and human.[23,28]

Less is known on the effect of MTX on miRNA release, but it has recently been described that bioprinted multicellular human liver tissue releases miR-122 into the cell culture supernatant after long-term MTX exposure.[29] Rodent *in vivo* studies showed that miR-122-5p can be released either in exosomes or attached to the AGO2 protein complex.[9,16,30] *In vivo* studies using APAP have quantitatively shown that miR-122 is predominantly released through the protein-rich fraction, but a significant increase in miR-122 has also been reported within the exosomal-fraction.[16,30] In primary human hepatocytes (PHHs) increased exosomal release of miR-122 has been reported after exposure to APAP and Tolvaptan, in both cases preceding treatment-induced necrosis.[14,16] Moreover, exosomal miR-122 release was detectable earlier in total ECmiR-122 than other traditional biomarkers such as ALT and albumin measurements.[14]

In this study, we extracted exosomes released by 3D-HepaRG to measure specific miRNAs associated with hepatocellular damage. The miRNAs selected include miR-122-5p and miR-192-5p due to their known association with DILI[26] and miR-34a-5p, which plays a role in regulating proliferator-activated receptor gamma and apoptosis[31] during disease and nephrotoxicity.[15,32–35] HepaRG is a cell line widely used for *in vitro* assays in toxicology and metabolism studies due to their suitable characteristics, including cytochrome p450 isoenzyme (CYP) expression, bile canaliculae formation as well as urea and albumin production.[36–39] HepaRG have also been shown to release exosomes,[40,41] yet the miRNA content of exosomes released by 3D-HepaRG has not been thoroughly investigated.

## Materials and Methods

### *Human cell lines*

HepaRG cells were obtained from Biopredic International (Rennes, France). The cells were seeded at $1 \times 10^5$ undifferentiated cells/cm$^2$ in medium with growth supplements ADD710 (Biopredic). The cells were cultured at 37°C in 5% $CO_2$ for 14 days before differentiation. After 14 days of culture, cell differentiation was induced with medium with differentiation supplements ADD720 (Biopredic) for 14 days. Then the cells were maintained in differentiation medium for up to 4 weeks. HepaRG were passaged using Trypsin-EDTA (Cat. No. 25300; Invitrogen).

### *Generation of 3D-HepaRG*

3D-HepaRG were generated using round bottomed ultralow adherence (ULA) plates (Nunclon™ Sphera™; 174929; ThermoFisher) or using the Sigma micro-mold system (Z764051-6EA; Sigma). Cells were counted and 2000 HepaRG/microtissue were resuspended in William's E Medium + GlutaMAX (Cat. No. 32551; Invitrogen), 2 mM L-glutamine (Cat. No. G7513; Sigma), 1X ITS (Cat. No. 11074547001; Sigma), 100 nM Dexamethasone (Cat. No. D1756; Sigma,), 20% fetal bovine serum (FBS), and 1% P/S named aggregation medium and 200 μL/well were added. After 72 hours of aggregation the 3D-HepaRG were maintained/treated in maintenance medium, which is aggregation medium without the 20% FBS to avoid exosomal contamination.

### *Induction of CYP3A4*

For functional characterization, CYP3A4 induction was carried out using 20 μM rifampicin (RIF; R3501; Sigma) directly after the aggregation phase of the 3D-HepaRG medium. RIF treatment was refreshed at 24 hours and ended at 48 hours. After this, the induced 3D-HepaRG were either tested for CYP3A4 activity, gene or protein expression as described hereunder.

### *mRNA analysis*

3D-HepaRG were collected and washed using phosphate-buffered saline then lysed using Qiazol Lysis Reagent (79306; Qiagen) and RNA was extracted using a standard TRIzol procedure with the addition of Glycogen (LT-02241; ThermoFisher). RNA was reverse transcribed using a M-MLV Reverse Transcriptase (M1705; Promega,), M-MLV RT buffer (M531A; Promega), dNTP Mix (02-31-00100; Solis BioDyne), and Oligo dT-Primer (79237; Qiagen). The quantitative real-time polymerase chain reaction (qRT-PCR) was carried out using TaqMan probes from ThermoFisher for Cytochrome P450 3A4 (Hs04260376_m1) and Beta-2 microglobulin as a housekeeping gene (Hs00187842_m1), using FastStart TaqMan Polymerase (04673433001; Roche), The program used: 10 minutes denaturation at 95°C, followed by 40 cycles of 15 seconds at 95°C and 1 minutes at 60°C. The Ct values were generated using the Corbett Rotorgene Analysis Software 6000 and processed on GraphPad Prism and data are expressed as fold change.

### *Cytochrome p450 assay*

P450-Glo™ CYP3A4 Assay with Luciferin-IPA (V9001; Promega) was used to determine the CYP3A4 activity in RIF treated and untreated 3D-HepaRG. The P450-Glo assay was carried out as described in the manufacturer's protocols

and adjusted to quantities necessary for the 3D-HepaRG. The luminescence was measured at 1000 m/s using a Flexstation 3 microplate reader (Molecular Devices).

### *High-performance liquid chromatography mass spectrometry*

Substrate conversion by 3D-HepaRG (35 microtissues/well) in a 24-well plate was determined in RIF treated and untreated 3D-HepaRG by measuring the conversion of 60 $\mu$g/mL testosterone (86500; Sigma) to hydroxytestosterone over time. Cell culture supernatant was collected at 0, 6, and 24 hours for the determination of testosterone and hydroxytestosterone. Medium samples were diluted in water supplemented with 2 mM ammonium fluoride solution and measurements were performed using high-performance liquid chromatography mass spectrometry (HPLC-MS/MS) (Agilent Technologies LC unit: Agilent Technologies, 1100; MS detector: Agilent Technologies, 6410; columns SB-C8, Zorbax, 4.6 × 50 mm, 1.8 mm, Agilent Technologies). Calibration standards were made of 1, 5, 10, 50, and 100 ng/mL testosterone in water supplemented with 2 mM ammonium fluoride. The absolute concentration of testosterone was calculated based on the calibration standards. Production of hydroxytestosterone was qualitatively assessed by determining the area under the curve.

### *Urea assay*

Urea production was measured in the supernatant from RIF treated and untreated 3D-HepaRG using the QuantiChrom™ Urea Assay Kit (DIUR-100; BioAssay Systems). The QuantiChrom assay was carried out as described in the manufacturer's protocols and adjusted to quantities necessary for the 3D-HepaRG. The absorbance was detected at 520 nm using a Flexstation 3 microplate reader (Molecular Devices).

### *Albumin enzyme-linked immunosorbent assay*

The albumin enzyme-linked immunosorbent assay (ELISA) analysis was performed using Human Albumin ELISA Quantitation Set kit (Cat. E80-129; Bethyl Laboratories). Supernatants from untreated, APAP-treated, and MTX-treated 3D-HepaRG were collected at 72 hours. Wells of a high binding 96-well plate were coated with goat anti-human albumin antibody for 1 hour, washed with buffer, blocked with blocking buffer for 1 hour, and washed with buffer again. Then 100 $\mu$L of the diluted medium samples were pipetted into the wells and incubated for 1 hour. After the incubation, the wells were washed again and the secondary antibody (horseradish peroxide-conjugated goat anti-human antibody) was added to the wells and incubated for 1 hour. After another wash step with buffer, 100 $\mu$L of enzyme substrate (tetramethylbenzidine) was added to the wells, incubated for 15 minutes in the dark, and the reaction was stopped by adding 100 $\mu$L stopping solution. All incubations were carried out at room temperature. The absorbance was detected at 450 nm using a Flexstation 3 microplate reader (Molecular Devices).

### *Immunostaining*

3D-HepaRG were fixed using 4% PFA (18814-20; Polysciences, Inc.) and stained whole using the protocol described by Ravenscroft et al.[42] using the primary anti-cytochrome p450 enzyme CYP3A4 antibody (A131254; Merck), the secondary goat anti-rabbit IgG H&L (Alexa Fluor® 488; A11070; Invitrogen) and DAPI (10236276001; Sigma). Images were taken using Colibri 7 LED system (Zeiss).

### *3D-HepaRG compound treatment*

For the determination of cytotoxicity, 3D-HepaRG were treated with MTX (M8307; Sigma) using the concentration range 3.75–120 $\mu$M and APAP (A5000; Sigma) using the concentration range of 1–8 mM. Medium with or without substances was exchanged every day. Subsequent experiments were performed with concentrations of 4 and 8 mM for APAP and 30 and 60 $\mu$M for MTX.

### *Cell viability assay*

Cell viability was assessed using the CellTiter-Glo® Luminescent Cell Viability Assay (Cat. No. G7570; Promega) to detect intracellular ATP content. The CellTiter-Glo assay was carried out as described in the manufacturer's protocols and adjusted to quantities necessary for the 3D-HepaRG. The luminescence was measured at 1000 mseconds using a Flexstation 3 microplate reader (Molecular Devices).

### *Exosome extraction*

The cell culture supernatant from the final 24 hours of the exposure period was collected from three wells each containing one 3D-HepaRG spheroid and used to extract exosome-rich fractions (ER-fractions) and collect the exosome poor fractions (EP-fractions). The cell culture supernatant was centrifuged at 800 *g* for 5 minutes followed by a second centrifugation at 3200 *g* for 10 minutes to remove dead cells or cellular debris.

Exosomes were collected using the exoRNeasy® Serum/Plasma Kit (Cat. No. 77044; Qiagen), which collects vesicles with an expected size range of 50–200 nm by using a membrane-based affinity binding step to isolate exosomes and other EVs. The supernatant was added to the column and after centrifugation, the flow-through was collected as an exosome-poor fraction (EP-fraction). Depending on the further processing, the exosomes were either eluted with elution buffer (76214; Qiagen) or collected in Qiazol, which was included in the kit.

### *miRNA analysis*

miRNA was extracted from cell culture supernatant samples using the miRNeasy Serum/Plasma Kit (Cat. No. 217184; Qiagen) and was carried out as described in the manufacturers protocol. Cell culture supernatant was centrifuged at 800 *g* for 5 minutes to remove dead cells and larger cell debris. ER-fractions and total ECmiRNA were processed using the columns from the miRNeasy Serum/Plasma Kit to extract miRNA. Reverse transcription and qRT-PCR was carried out using TaqMan MicroRNA Reverse Transcription Kit (Cat. No. 4366596; Thermofisher), qRT-PCR master mix (Cat. No. 4444557; Thermofisher) and all TaqMan qRT-PCR primers were purchased from Invitrogen (Table 1). miRNA extraction and processing were carried out using 80 $\mu$L supernatant. The reaction mix was prepared according to the manufacturer's instructions for a final reaction volume of 10 $\mu$L containing 3 $\mu$L miRNA extract.

The polymerase chain reaction (PCR) conditions were set for 30 minutes at 16°C followed for 30 minutes at 42°C and 5 minutes at 85°C. The qRT-PCR reaction mix contained TaqMan®

Table 1. TaqMan miRNA Primers

| *miRNA* | *Assay name* | *Assay number* |
|---|---|---|
| miR-122-5p | hsa-miR-122-5p | 002245 |
| miR-192-5p | hsa-miR-192-5p | 000491 |
| miR-34a-5p | hsa-miR-34a-5p | 000426 |
| Cel-miR-39/Spike-in | Cel-miR-39-3p | 000200 |
| RNU44 | RNU44 | 001094 |

Fast Advanced Master Mix 1x (4444557; Applied Biosystems™), TaqMan microRNA Assay primer 1x (Applied Biosystems; Table 1), and 1.3 $\mu$L cDNA in a final reaction volume of 20 $\mu$L. The PCRs were run at 95°C for 20 seconds followed by 40 cycles of 1 second at 95°C and 20 seconds at 60°C. Media samples were normalized using the cel-miR-39 spike in method, whereas total intracellular miRNA (ICmiRNA) were normalized using RNU44 to obtain the ($\Delta$CT). Data are expressed as $-\Delta\Delta$CT ($Log_2$FC) to give a relative abundance with respect to the untreated samples ($\Delta\Delta$CT).

### *Absolute quantification of miR-122-5p*

Pure synthetic miR-122-5p (5′ UGGAGUGUGACAAUGGUGUUUG 3′) was purchased from Microsynth. Reverse transcription and qRT-PCR was carried out using TaqMan MicroRNA Reverse Transcription Kit, qRT-PCR master mix (Cat. No. 4444557; Thermofisher), and miR-122-5p-5p TaqMan qRT-PCR primer was purchased from Invitrogen (Table 1). The reaction mix was prepared according to the manufacturer's instructions for a final reaction volume of 10 $\mu$L with 3 $\mu$L synthetic miR-122-5p-5p diluted to a range of concentrations (100 $\mu$M–0.0001 fM). The PCR conditions were set for 30 minutes at 16°C followed for 30 minutes at 42°C and 5 minutes at 85°C. The qRT-PCR reaction mix contained TaqMan Fast Advanced Master Mix 1x (4444557; Applied Biosystems), TaqMan microRNA Assay primer 1x (Applied Biosystems; Table 1), and 1.3 $\mu$L cDNA in a final reaction volume of 20 $\mu$L. The PCRs were run at 95°C for 20 seconds followed by 40 cycles of 1 second at 95°C and 20 seconds at 60°C. Standard was plotted as CT value versus miR-122-5p concentration. Unknowns were calculated using GraphPad Prism 8. The standard curve is depicted in Supplementary Figure S1.

### *Exosomal characterization*

The cell culture supernatant from three wells of 3D-HepaRG was used to extract ER-fractions and collect the EP-fraction. Samples for dot blot and for transmission electron microscopy (TEM) were collected using elution buffer (76214; Qiagen) and concentrated using 100,000 MWCO Vivaspin concentrator columns; 25 $\mu$L of exosome suspension was obtained for each sample (VS0141; Sartorius).

Lyophilized exosome standard (HBM-PES-30/2; HansaBioMed) was used as a positive control alongside the extracted samples. Samples were lysed using RIPA buffer (89900; ThermoFisher) and then 1 $\mu$L of exosome standard and sample was loaded onto a nitrocellulose membrane and blocked in 1 × Tris-buffered saline + 0.1% Tween 20 (TBS-T) containing 4% milk powder. The membrane was washed for 5 minutes three times and then incubated with the primary antibody (Table 2) overnight at 4°C. The wash step was repeated, and the membrane was incubated with the secondary antibody (Table 2) for 2 hours and washed once again. The membrane was visualized using the Odyssey CLx Infrared Imaging System by 700 nm.

The ER- and EP-fractions were concentrated and 4 $\mu$L was loaded onto a carbon film on a copper grid (1GC400; Ted Pella), then washed with water and stained with 2% uranyl acetate (73943; Fluka). The images were taken with a FEI T12 Spirit Electron microscope at 80 kV with a Morada CCD-camera by Olympus.

### *Statistical analysis*

Data were analyzed using GraphPad Prism 8 (Version 8.0.2; GraphPad Software) and expressed as mean values ± standard deviation. The unpaired Student's *t*-test was used for comparison between two groups. One-way analysis of variance (ANOVA), followed by a Dunnett's test for subsequent pairwise comparisons with the control group was used for dose–response analysis. $p < 0.05$ was considered to be significant: no significance (ns), $p > 0.05$; $*p \leq 0.05$; $**p \leq 0.01$; $***p \leq 0.001$.

## Results

### *Characterization of 3D-HepaRG*

3D-HepaRG were generated using 2000 predifferentiated HepaRG/microtissue and allowed to aggregate for 72 hours. The 3D-HepaRG showed basal and RIF-induced expression and activity of CYP3A4. qRT-PCR results demonstrate that 3D-HepaRG respond with a significant >10-fold increase of *CYP3A4* expression after induction with RIF (Fig. 1A). The increased expression led to significantly higher CYP3A4 activity as determined using the P450-Glo CYP3A4 assay and an increased conversion of testosterone to hydroxytestosterone as measured by HPLC-MS/MS. After 72 hours, the luminescence intensity measured using the P450-Glo CYP3A4 assay was significantly increased by RIF treatment (Fig. 1B). Time-course

Table 2. Antibodies Used in Dot Blot

| *Primary antibody* | *Dilution* | *Secondary antibody* |
|---|---|---|
| CD9 (10626D; ThermoFisher) | 1:250 | IRDye® (925-68070; LI-COR Biosciences) Diluted 1:20,000 |
| CD63 (10628D; ThermoFisher) | 1:250 | |
| Flotillin-1 (sc-133153; Santa-Cruz) | 1:100 | |
| TSG101 (MA123296; ThermoFisher) | 1:250 | |
| Alix (MA183977; ThermoFisher) | 1:250 | |
| Calnexin (MA3027; ThermoFisher) | 1:500 | |

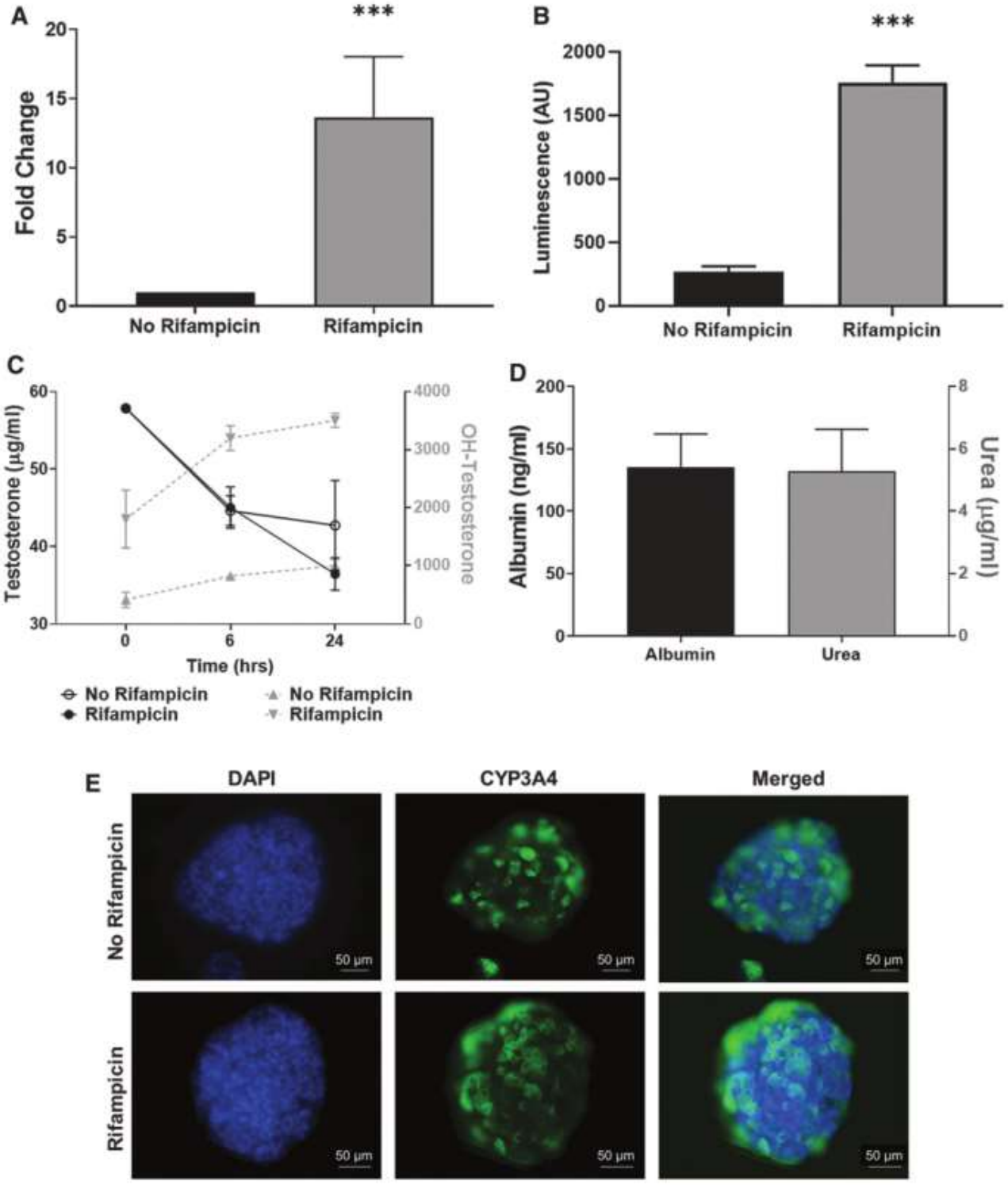


**FIG. 1.** Characterization of 3D-HepaRG. 3D-HepaRG were generated using 2000 HepaRG, allowed to aggregate for 72 hours and then exposed to 20 $\mu$M Rifampicin for 48 hours. Expression of *CYP3A4* determined by qRT-PCR, expressed as fold change in comparison with the control; $N=2$ biological and two technical replicates **(A)**. CYP3A4 activity determined by P450-Glo™ CYP3A4 assay and expressed in luminescence AU; $N=2$ biological and two technical replicates **(B)**. Conversion of testosterone (60 $\mu$g/mL) into hydroxytestosterone (OH-testosterone) at 6 and 24 hours determined by HPLC-MS/MS. Data are expressed as concentrations ($\mu$g/mL) calculated using a testosterone calibration curve or area under the curve in AU for OH-testosterone; $N=1$ biological and two technical replicates **(C)**. Urea concentration in the medium measured with the QuantiChrom™ Urea assay kit. Data are expressed as urea concentration ($\mu$g/mL) normalized per microtissue; $N=2$ biological and two technical replicates. Albumin was measured using Bethyl Laboratories ELISA kit. Data are expressed as albumin concentration (ng/mL) per microtissue; $N=3$ biological and three technical replicates **(D)**. Representative image of immunohistochemical detection of CYP3A4, scale bar = 50 $\mu$m **(E)**. Bar graphs represent means ± SD; statistical analysis based on Student's unpaired *t*-test, $*p \le 0.05$; $**p \le 0.01$; $***p \le 0.001$. AU, arbitrary units; qRT-PCR, quantitative real-time polymerase chain reaction; SD, standard deviation. Color images are available online.

experiments showed that the quantity of testosterone decreased in both the RIF-treated and untreated 3D-HepaRG at a similar rate in the first 6 hours. However, at 24 hours there were lower testosterone levels in the medium from the RIF-treated 3D-HepaRG, concomitant with an increase in the production of hydroxytestosterone (Fig. 1C). These results show that, under the current conditions, 3D-HepaRG display CYP3A4 activity that is inducible by RIF. In addition, the CYP3A4 activity is higher in 3D than in 2D cultures (Supplementary Fig. S1). Immunostaining for CYP3A4 demonstrated that both the untreated and RIF-treated 3D-HepaRG express CYP3A4 protein. However, the RIF-treated 3D-HepaRG appeared to have more CYP3A4 protein (Fig. 1E).

As an additional parameter, urea and albumin production were also measured to confirm 3D-HepaRG functionality. Untreated 3D-HepaRG released $\sim 1.5\,\mu g/mL$ urea and 130 ng/mL albumin into the cell culture supernatant for a 24-hour period.

### *HepaRG cells cultured in 3D microtissues release exosomes*

Exosomes were isolated from cell culture supernatants obtained from control (untreated) and treated (APAP, 8 mM) 3D-HepaRG and subsequently characterized. TEM images show EVs were present in both the ER- and EP-fractions (Fig. 2A). However, there were considerably fewer EVs in the EP-fraction (Fig. 2B, C) and the EVs were significantly smaller in size (Fig. 2B, C). Contrarily, the ER-fraction contained more than double the number of EVs (Fig. 2B, C) and

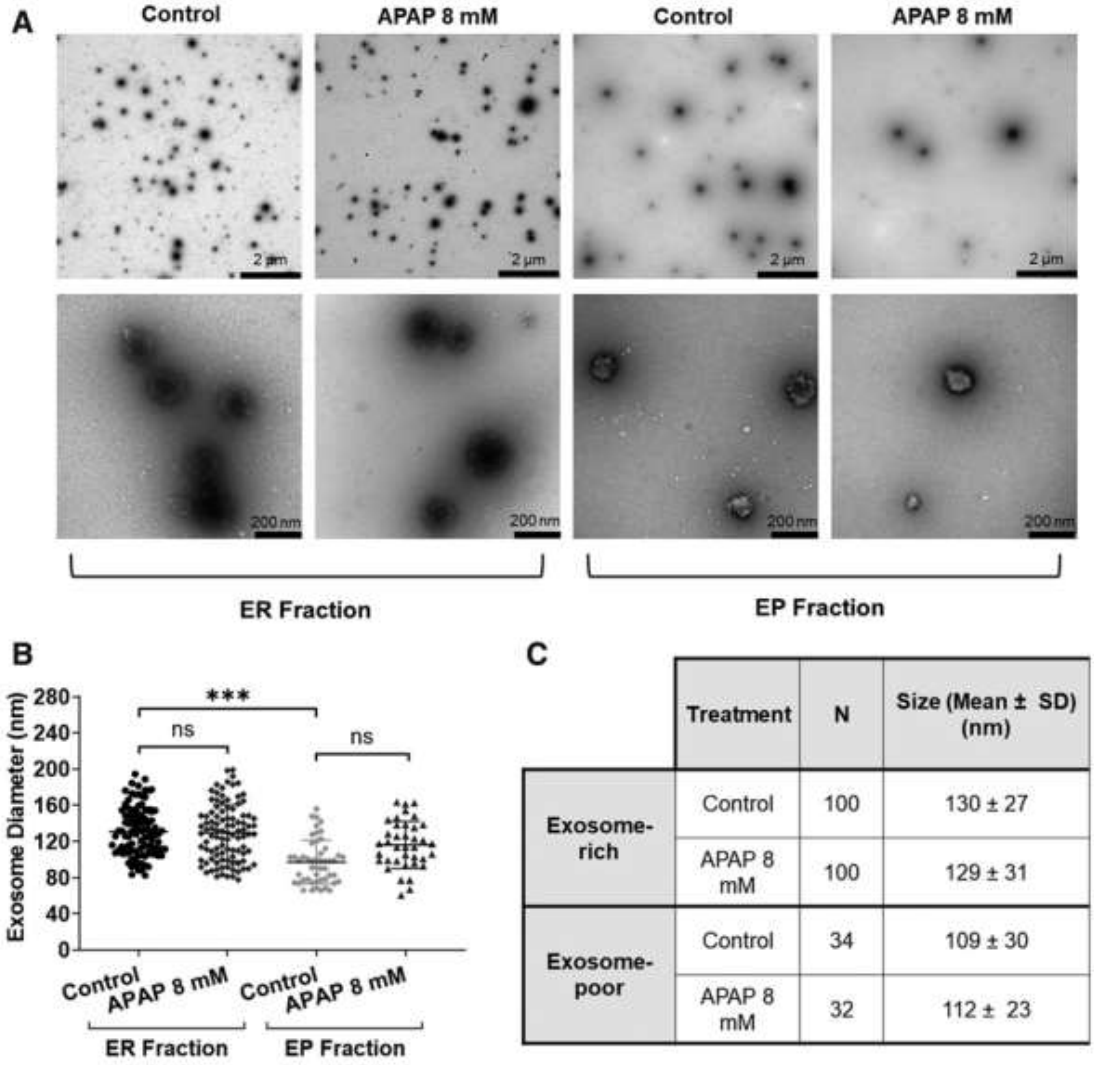


C

| | Treatment | N | Size (Mean ± SD) (nm) |
|---|---|---|---|
| Exosome-rich | Control | 100 | 130 ± 27 |
| | APAP 8 mM | 100 | 129 ± 31 |
| Exosome-poor | Control | 34 | 109 ± 30 |
| | APAP 8 mM | 32 | 112 ± 23 |

**FIG. 2.** Visualization and measurement of exosomal fractions. The cell culture supernatant from three wells of 3D-HepaRG was used to extract exosome-rich and collect the exosome-poor fraction. Samples for TEM were collected using elution buffer and concentrated using 100,000 MWCO Vivaspin concentrator columns until 25 $\mu$L of exosome suspension was obtained. Four microliters were loaded onto a carbon film on a copper grid and stained with 2% uranyl acetate. The images were taken with a FEI T12 Spirit Electron microscope at 80 kV. Two magnifications are shown, the scale bar for the top row is 2 $\mu$m and the second row is 200 nm **(A)**. Exosomes were measured using Image J to determine size distribution and counted manually **(B)**; Sizes are summarized **(C)**. Statistical analysis based on Student's unpaired *t*-test. ***$p \leq 0.001$; ns, not significant.

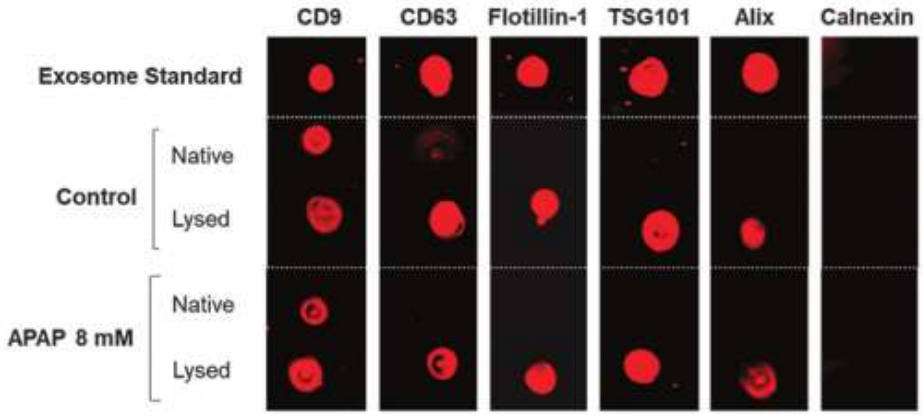


**FIG. 3.** Exosomal characterization by dot blot. The cell culture supernatant from three wells of 3D-HepaRG was used to extract exosome-rich samples collected using elution buffer and concentrated using 100,000 MWCO Vivaspin concentrator columns until 25 $\mu$L of exosome suspension was obtained. The exosome standard was purchased in a lysed form, whereas the samples were either lysed or left in the native form. One microliter of sample or exosome standard was loaded on a nitrocellulose membrane and processed according to the materials and methods section. The membrane was visualized using the Odyssey CLx Infrared Imaging System by 800 nm. Color images are available online.

the average size was significantly larger (Fig. 2B, C). The size of the EVs was not affected by the treatment, as no significant difference in diameter was observed between control and treated samples (Fig. 2). The EP-fraction did not contain any vesicles >150 nm in diameter, thereby demonstrating that the isolation method was efficient in retaining larger EVs and the small number that flowed through were smaller in size (Fig. 2B, C). In the ER-fraction EVs were found to be 80–200 nm, but the majority of EVs were ~100–150 nm in size (Fig. 2B).

Further characterization of the secreted vesicles with immunostaining of specific markers showed that the EVs express exosomal markers: CD9, CD63, Tsg101, Alix, and Flotillin-1 (Fig. 3). Calnexin was used as a negative control and was not detected in any of the samples, including the lyophilized exosome standard. The exosomal surface marker CD9 was detected in both native and lysed samples. Overall, the results confirmed that the HepaRGs in 3D culture release exosomes into the medium.

### *APAP toxicity leads to increased exosomal miRNA release*

3D-HepaRG were treated with a range of APAP concentrations (0–8 mM) leading to the expected concentration-dependent decrease in viability with an IC50 of 5.3 ± 0.65 mM, based on ATP content (Fig. 4A). APAP-induced hepatocellular injury was also confirmed by a decrease in albumin secretion measured by ELISA, which demonstrated a decrease in hepatocyte functionality caused by APAP at 4 and 8 mM (Fig. 4B). Microscopic observation further substantiated the findings as it showed a visible accumulation of debris and a reduction on the size of the microtissue after treatment with APAP (Fig. 4C and Supplementary Fig. S2A).

Total ECmiRNA from cell culture supernatant and total ICmiRNA from cell lysates were collected at 72 hours for miRNA analysis using qRT-PCR. The total ICmiRNA showed a small yet significant decrease in expression of miR-122-5p for 3D-HepaRG exposed to both concentrations of APAP (Fig. 4D). A significant decrease of miR-192-5p and miR-34a-5p was observed in 3D-HepaRG exposed to 4 mM APAP (Fig. 4E, F). Relative quantification of extracellular miRNA was carried out using qRT-PCR in the total ECmiRNA and the ER-fraction. Exposure to APAP elicited a significant concentration-dependent increase in release of miR-122-5p in the total ECmiRNA and the ER-fraction (Fig. 4D). Exposure to APAP also elicited a significant increase in miR-192-5p in the total ECmiRNA and ER-fraction (Fig. 4E). The total ECmiRNA showed a significant increase in miR-34a-5p release upon exposure to APAP similarly to the ER-fraction (Fig. 4F).

**FIG. 4.** Assessment of hepatocellular damage of 3D-HepaRG exposed to APAP. Differentiated HepaRG were cultured as 3D-HepaRG and were exposed to APAP for 72 hours. Upon exposure to APAP concentrations ranged from 1 to 8 mM viability was assessed using ATP assay and the IC50 was calculated to be 5.3 ± 0.65 mM. Viability data values are expressed as percentage ± SD of control (100%), $N = 3$ biological repeats with three technical replicates **(A)**. Albumin ELISA was used to assess the release at 72 hours of treatment to identify hepatocellular damage. ELISA data are expressed as albumin concentration (ng/mL) ± SD. $N = 3$ biological repeats with three technical replicates **(B)**. Microtissues were also observed for damage and imaged, scale bar is 100 $\mu$m **(C)**. Changes in expression and release of miRNA-122-5p **(D)**, miRNA-192-5p **(E)**, and miRNA-34a-5p **(F)** were assessed using qRT-PCR for ER-fraction, total extracellular miRNA, and intracellular miRNA. Relative expression was calculated using the untreated control of each fraction; intracellular expression was normalized to RNU44 and supernatant samples were normalized to cel-miR-39 spike in. Data are expressed as fold change ± SD. $N = 3$ biological repeats with three technical replicates. Quantitative assessment of exosomal miR-122-5p was done using a standard curve created using synthetic miR-122-5p. Data are expressed as miR-122-5p concentration (fM). $N = 3$ biological repeats with three technical replicates **(G)**. Statistical analysis: one-way ANOVA followed by Dunnett's pairwise comparison: $*p \le 0.05$; $**p \le 0.01$; $***p \le 0.001$. ANOVA, analysis of variance.

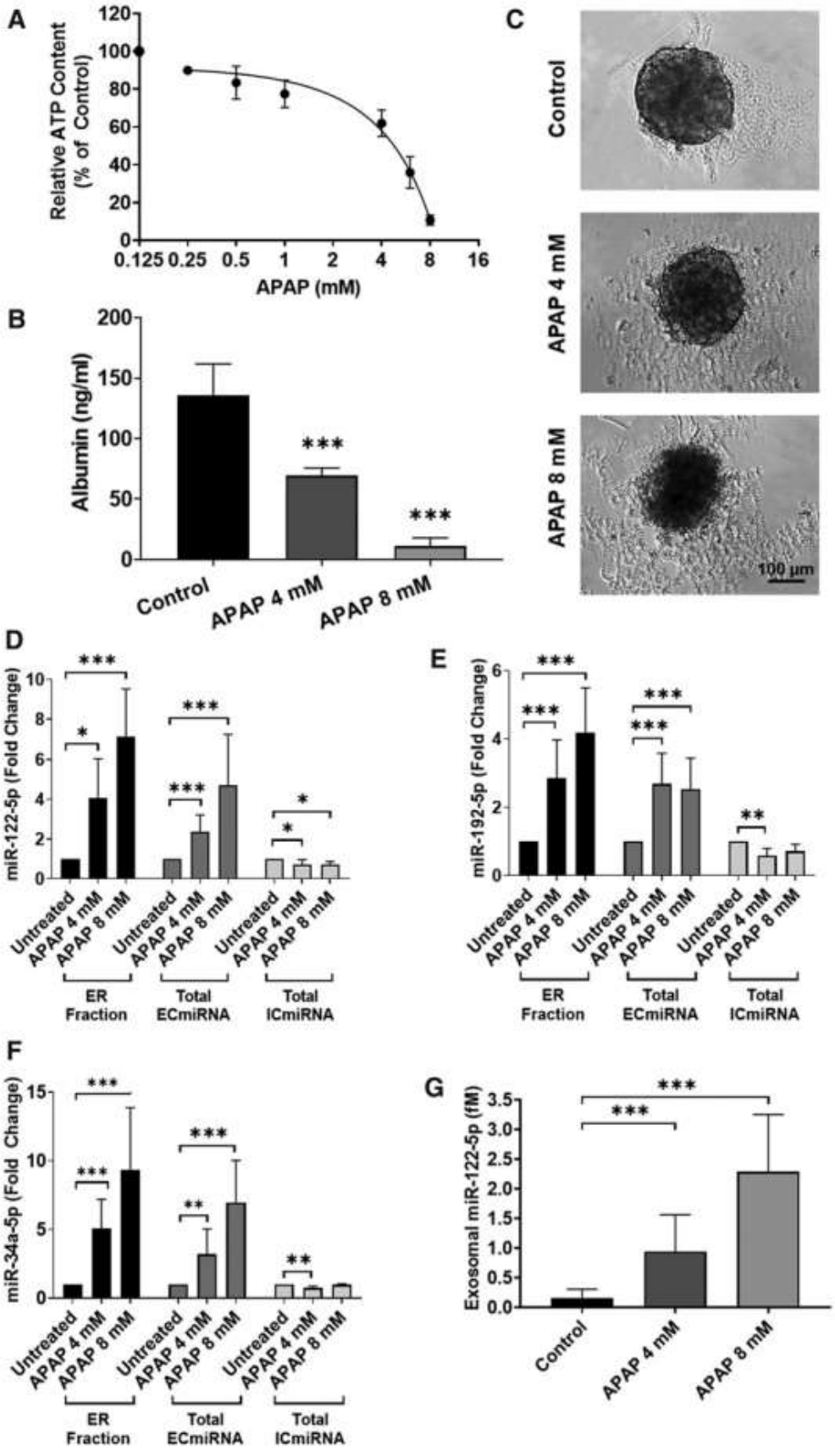
A
Relative ATP Content (% of Control)
120
100
80
60
40
20
0
0.125 0.25 0.5 1 2 4 8 16
APAP (mM)
B
Albumin (ng/ml)
200
150
100
50
0
***
***
Control
APAP 4 mM
APAP 8 mM
C
Control
APAP 4 mM
APAP 8 mM
100 µm
D
miR-122-5p (Fold Change)
10
8
6
4
2
0
Untreated
APAP 4 mM
APAP 8 mM
ER Fraction
Total ECmiRNA
Total ICmiRNA
E
miR-192-5p (Fold Change)
6
4
2
0
**
F
miR-34a-5p (Fold Change)
15
10
5
0
**
G
Exosomal miR-122-5p (fM)
3.5
3.0
2.5
2.0
1.5
1.0
0.5
0.0
Control
APAP 4 mM
APAP 8 mM

Using a standard curve produced with synthetic miR-122-5p, absolute quantification of the exosomal miRNA was carried out (Supplementary Fig. S3). Results show that there is a significant increase in miR-122-5p concentration upon exposure to both 4 and 8 mM APAP and we demonstrate small quantities (2.5 fM) can be detected by qRT-PCR (Fig. 4G), thus demonstrating the development of a successful protocol requiring small cell numbers and medium quantity ($\sim$6000 HepaRG and 300 $\mu$L) for analysis (Fig. 4G).

### *Exosomal miR-122-5p release increases upon subtoxic exposure to MTX*

To further extend our study, 3D-HepaRG were treated with a range of MTX concentrations (0–128 $\mu$M) and ATP content as a measure of viability was assessed. A small nonconcentration-dependent decrease in ATP content was detected in MTX-treated 3D-HepaRG (Fig. 5A). Albumin release was also measured by ELISA, which demonstrated that no significant decrease was observed after exposure of the microtissues to up to 60 $\mu$M MTX (Fig. 5B). Microscopic observation showed that there was no obvious morphological change in microtissues size and no accumulation of debris was visible (Fig. 5C and Supplementary Fig. S2B).

Isolated exosomes from MTX-treated 3D-HepaRG were also examined based on their content in miRNAs by qRT-PCR. Total ECmiRNA and total ICmiRNA were collected at 72 hours for miRNA relative quantification in the total ECmiRNA and ER-fraction. Exposure to MTX elicited a slight but significant decrease in intracellular miR-122-5p, miR-192-5p and miR-34a-5p expression and a significant increase in miR-122-5p release, in the ER-fraction (Fig. 5D–F). Neither concentration of MTX had a significant effect on the release of miR-192-5p or miR-34a-5p in the ER-fraction, but led to increased release of both miRNA species in the total ECmiRNA, suggesting a nonexosomal release mechanism for these two miRNAs (Fig. 5E, F). Quantitative measurement also confirmed a significant release of miR-122-5p in the exosomal fraction, although less marked than that observed after treatment with APAP (Fig. 5G).

## Discussion

In this study, we investigated the response of 3D-HepaRG to two compounds that show clinically relevant hepatotoxicity with the goal of assessing the suitability of exosomal miRNAs as markers of hepatocellular damage *in vitro*. To this end, we exposed 3D-HepaRG to the classic acute DILI compound APAP or to MTX is known to cause DILI in some patients undergoing chronic treatment.[1–3,5] We also successfully implemented methodologies to isolate exosomes and quantify miRNAs. We demonstrated that 3D-HepaRG released exosomes and that treatment did not affect this process: APAP had no significant effect on exosome size or composition but did affect their miRNA content. From a biomarker perspective, release of exosomal miR-122-5p, -192-5p, and -34a-5p was significantly increased upon APAP-induced toxicity. For miR-122-5p, absolute quantification in the ER-fraction corroborated the finding.

### *Characterization of the* in vitro *model and determination of compound concentrations*

Xenobiotic metabolism is a key function of hepatocytes and is mostly catalyzed by CYPs, some of which can be transcriptionally induced by RIF.[43] A large number of drugs (50%–60%) are metabolized by CYP3A4 and a variety of studies have demonstrated that RIF is able to induce this CYP in HepaRG grown in traditional monolayer and 3D cultures.[35,44–46] Therefore, we assessed expression and induction of CYP3A4 in our 3D-HepaRG.

We demonstrated basal and induced expression of CYP3A4 using immunostaining, qRT-PCR, and enzymatic activity measurements (using P450-Glo CYP3A4 assay and hydroxylation of testosterone with HPLC-MS/MS). Moreover, 3D-HepaRG showed increased basal and induced CYP3A4 activity when compared with HepaRG grown in monolayer cultures (Supplementary Fig. S1). These results are in accordance with findings by Berger et al. who demonstrate similar CYP3A4 activity in PHH and that 3D culture conditions results in enhanced basal CYP activity over monolayer cultures.[46] Furthermore, we also confirmed that 3D-HepaRG display other typical hepatocyte characteristics such as urea and albumin production as described elsewhere.[47–49] Taken together, these results show that this *in vitro* system represents a good surrogate model for the study of hepatocyte responses to chemicals.

Suitable concentrations of the test compounds APAP and MTX were determined based on known $C_{max}$, the maximal drug concentration in human plasma. The range surrounding the $C_{max}$ has been investigated by Xu et al. wherein they justified the use of doses up to $100\times C_{max}$ in PHH cultures to account for interindividual differences in drug concentrations within the liver.[50] The plasma concentration of MTX of psoriasis patients is $\sim$0.01–1.4 $\mu$M; therefore, the tested concentrations (3.5–120 $\mu$M) are within the $100\times C_{max}$.[51]

Determining the $C_{max}$ of APAP is problematic due to the nature of APAP-induced liver injury that occurs either by accidental or intentional overdose. Plasma levels vary between patients but have been reported to reach 400 mg/mL (2.6 mM).[52,53] In addition, previous reports *in vitro* and *ex vivo* demonstrated that APAP elicits toxicity at 5–20 mM dependent on the system.[54–56] Therefore, we investigated the concentration range of 0.5–8 mM and chose 4 and 8 mM for further analysis based on cell viability results in our system. Exposure of HepaRG to 4 and 8 mM APAP elicited the expected hepatocellular damage in 3D culture conditions. Contrarily, MTX did not exert significant toxicity in 3D-HepaRG. 3D-HepaRG shape, size, and albumin release were maintained when exposed to MTX suggesting hepatocellular function was not largely affected.

### *Exosomal miRNA release is significantly increased upon exposure to APAP*

To elucidate the potential of exosomal miRNAs as markers for hepatocellular responses, we extracted extracellular exosomes and confirmed their identity by immunostaining with specific markers (CD9, CD63, Tsg101, Alix, and Flotillin-1). These results strongly suggest that the ER-fraction contains exosomes.[17,19,20] In addition, TEM was used to visualize EVs and as expected, the ER-fraction contained more EVs than the EP-fraction. The EP-fraction consisted of mostly

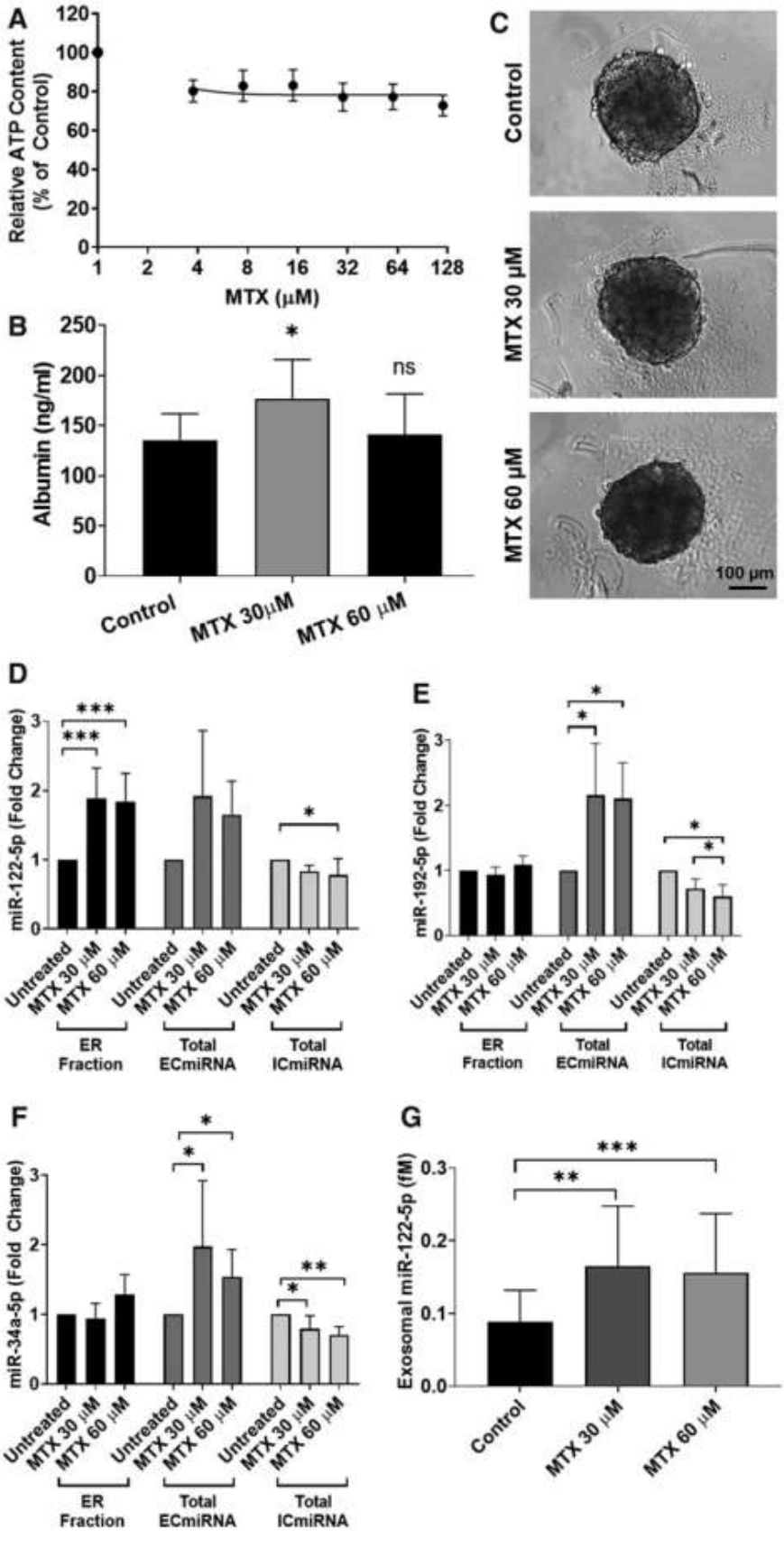


**FIG. 5.** Assessment of hepatocellular damage of 3D-HepaRG exposed to MTX. Differentiated HepaRG were cultured as 3D-HepaRG and were exposed to MTX for 72 hours. Upon exposure to MTX concentration ranged from 3.75 to 120 $\mu$M viability was measured but no IC50 could be calculated. Viability data values are expressed as percentage ± SD of control (100%). $N = 3$ biological repeats with three technical replicates **(A)**. Albumin ELISA was used to assess the release at 72 hours of treatment to identify hepatocellular damage. ELISA data are expressed as albumin concentration (ng/mL) ± SD. $N = 3$ biological repeats with three technical replicates **(B)**. Microtissues were also observed for damage and imaged, scale bar is 100 $\mu$m **(C)**. Changes in expression and release of miRNA-122-5p **(D)**, miRNA-192-5p **(E)**, and miRNA-34a-5p **(F)** were assessed using qRT-PCR for ER-fraction, total extracellular miRNA, and intracellular miRNA. Relative expression was calculated using the untreated control of each fraction; intracellular expression was normalized to RNU44 and supernatant samples were normalized to cel-miR-39 spike in. Data are expressed as fold change ± SD. $N = 3$ biological repeats with three technical replicates. Quantitative assessment of exosomal miR-122-5p was done using a standard curve created using synthetic miR-122-5p. Data are expressed as miR-122-5p concentration (fM) $N = 3$ biological repeats with three technical replicates **(G)**. Statistical analysis: one-way ANOVA followed by Dunnett's pairwise comparison: $^{*}p \leq 0.05$; $^{**}p \leq 0.01$; $^{***}p \leq 0.001$. MTX, methotrexate.

smaller EVs, whereas the majority of EVs in the ER-fraction were significantly larger (100–150 nm). The estimated diameter of the exosomes in the ER-fraction is slightly larger than expected based on previous publications.[17,18,57–59] However, the methodology of TEM by negative staining can result in desiccation and flattening of EVs, which may lead to a misinterpretation of their true morphology and size.[60] Interestingly, the number of exosomes for both treated and untreated 3D-HepaRG was not significantly affected, which is in agreement with previous findings where treatment of PHHs did not affect the number of exosomes being released.[16]

It has been previously shown that APAP elicits increased release of miR-122-5p and miR-192-5p *in vivo* and *in vitro*,[22–27] which we could also confirm using 3D-HepaRG. Interestingly, the increase of these miRNAs was more marked in the ER-fraction than in the total ECmiRNA. This may indicate that the exosomal fraction provides more precise measurements, as suggested by others.[14] The fact that the absolute quantification shows a clear dose-dependent increase of miR-122-5p further supports this assessment. Moreover, exosomal release of miR-192-5p and miR-34a-5p has also been observed in other biological systems[61–63]; and PHHs treated with 10 mM APAP release miR-122 in the ER-fraction.[16] In summary, 3D-HepaRG exposed to APAP results in increased release of exosomal miR-122-5p, miR-192-5p, and miR-34-5p.

### *Exosomal miR-122-5p is a sensitive marker of MTX-induced DILI*

Under the current experimental conditions, MTX did not cause overt toxicity to the 3D-HepaRG at concentrations up to 60 $\mu$M, as judged by albumin secretion, morphology of microtissues, and ATP content. The slight decrease in intracellular ATP depicted in Figure 5A lacked dose dependence and was, therefore, not considered a sign of MTX-induced toxicity.

At the same concentrations, a small but significant increase in release of miR-192-5p and miR-34a-5p was detected in the total ECmiRNA, whereas the levels in the ER-fraction remained unchanged. This may indicate that these two miRNA-species, related to liver damage or apoptosis,[26,31] are indicators of MTX-induced hepatocellular changes but are not released in exosomes. Contrarily, the levels of miR-122-5p were significantly increased in the ER-fraction, whereas minor changes were detected in the ECmiRNA. This suggests that exosomal miR-122-5p may be more sensitive than ECmiRNA and arguably than other markers of toxicity (such as ATP content and albumin production). The increase of exosomal miR-122-5p was consistent with the absolute quantification, although the levels reached with subtoxic concentrations of MTX were ~10-times lower than those measured with cytotoxic concentration of APAP.

The link between miR-122 release and liver damage after MTX-induced toxicity has been established in multicellular bioprinted tissues generated with human primary cells at cytotoxic concentrations.[29] However, exosomal miR-122 has not been investigated for MTX-induced DILI and our results show for the first time that exosomal miR-122-5p detects MTX-induced hepatocellular damage at concentrations that do not significantly affect albumin production or ATP content in 3D-HepaRG. This observation is in accordance with *in vitro* data from Mosedale et al. who demonstrated that exosomal miR-122 detected hepatocellular damage earlier than other measurements such as ALT and total ECmiRNA samples.[14] This is also in line with *in vivo* data from Bailey et al., as they state miRNAs outperform ALT and AST as toxicity biomarkers in terms of sensitivity and specificity.[64]

## Conclusion

Based on the characterization the model and its response to APAP, we deemed 3D-HepaRG a suitable model for investigating substances that lead to hepatocellular damage. The system can be easily adapted to 96- and 384-well plates and thus represents a scalable and automatable *in vitro* assay. In this study, we could successfully isolate exosomes released by 3D-HepaRG and determine exosomal miRNA content in a relative (to the control) and absolute (actual concentration) manner. Our results strongly support the use of miRNAs as markers of hepatocellular damage, in accordance with published clinical results and *in vitro* data.

We demonstrated that miR-122-5p is released in exosomes of 3D-HepaRG exposed to MTX and APAP, whereas exosomes released by untreated 3D-HepaRG contain significantly lower amounts of this miRNA. With this, we corroborate findings in similar systems indicating that miR-122-5p release is a suitable biomarker for hepatocyte injury and also show that absolute quantification of exosomal miR-122-5p may prove more precise. Thus, in our hands, quantitative measurement of exosomal miR-122-5p appears to be a sensitive marker of hepatocellular injury in a 3D-HepaRG-based cell culture system.

## Acknowledgments

We would like to acknowledge insight provided by Anna Weston and Michaela Caj that assisted the research. We are thankful to Frank Senner for his help with the analytical methods (HPLC/MS). We would also like to thank Dr. Mohamed Chami from the BioEM-Laboratory at the University of Basel for carrying out the TEM and for providing his expert advice on image interpretation. Finally, we would like to acknowledge the financial support of the Swiss Centre for Applied Human Toxicology (SCAHT) and the Institute for Chemistry and Bioanalytics at the University of Applied Sciences and Arts Northwestern Switzerland.

## Author Disclosure Statement

No competing financial interests exist.

## Funding Information

Funding was provided by the Swiss Centre for Applied Human Toxicology, Basel, Switzerland University of Applied Sciences of Northwestern Switzerland, School of LIfe Sciences, Muttenz, Switzerland.

## Supplementary Material

Supplementary Figure S1
Supplementary Figure S2
Supplementary Figure S3

## References

1. David S, Hamilton JP. Drug-induced Liver Injury. US Gastroenterol Hepatol Rev 2010:6;73–80.
2. Ramachandran A, Jaeschke H. Mechanisms of acetaminophen hepatotoxicity and their translation to the human pathophysiology. J Clin Transl Res 2017:3;157–169.

3. Barker J, Horn EJ, Lebwohl M, et al. Assessment and management of methotrexate hepatotoxicity in psoriasis patients: report from a consensus conference to evaluate current practice and identify key questions toward optimizing methotrexate use in the clinic. J Eur Acad Dermatol Venereol 2011:25; 758–764.
4. Aithal GP, Haugk B, Das S, et al. Monitoring methotrexate-induced hepatic fibrosis in patients with psoriasis: are serial liver biopsies justified? Aliment Pharmacol Ther 2004:19; 391–399.
5. Berends MAM, Oijen MGH, van Snoek J, et al. Reliability of the Roenigk Classification of liver damage after methotrexate treatment for psoriasis: a clinicopathologic study of 160 liver biopsy specimens. Arch Dermatol 2007:143; 1515–1519.
6. Lurie Y, Webb M, Cytter-Kuint R, et al. Non-invasive diagnosis of liver fibrosis and cirrhosis. World J Gastroenterol 2015:21;11567–11583.
7. Sebastiani G, Alberti A. Non invasive fibrosis biomarkers reduce but not substitute the need for liver biopsy. World J Gastroenterol 2006:12;3682–3694.
8. Sohel MH. Extracellular/circulating microRNAs: release mechanisms, functions and challenges. Achiev Life Sci 2016:10; 175–186.
9. Arroyo JD, Chevillet JR, Kroh EM, et al. Argonaute2 complexes carry a population of circulating microRNAs independent of vesicles in human plasma. Proc Natl Acad Sci 2011:108;5003–5008.
10. Usuba W, Urabe F, Yamamoto Y, et al. Circulating miRNA panels for specific and early detection in bladder cancer. Cancer Sci 2019:110;408–419.
11. Chen X, Ba Y, Ma L, et al. Characterization of microRNAs in serum: a novel class of biomarkers for diagnosis of cancer and other diseases. Cell Res 2008:18;997–1006.
12. Noferesti SS, Sohel MMH, Hoelker M, et al. Controlled ovarian hyperstimulation induced changes in the expression of circulatory miRNA in bovine follicular fluid and blood plasma. J Ovarian Res 2015:8;81.
13. Weber JA, Baxter DH, Zhang S, et al. The MicroRNA spectrum in 12 body fluids. Clin Chem 2010:56;1733–1741.
14. Mosedale M, Eaddy JS, Trask OJ, et al. miR-122 release in exosomes precedes overt tolvaptan-induced necrosis in a primary human hepatocyte micropatterned coculture model. Toxicol Sci Off J Soc Toxicol 2018:161;149–158.
15. Suter-Dick L, Mauch L, Ramp D, et al. Combining extracellular miRNA determination with microfluidic 3D cell cultures for the assessment of nephrotoxicity: a proof of concept study. AAPS J 2018:20;86.
16. Holman NS, Mosedale M, Wolf KK, et al. Subtoxic alterations in hepatocyte-derived exosomes: an early step in drug-induced liver injury? Toxicol Sci 2016:151;365–375.
17. Zhang Y, Liu Y, Liu H, et al. Exosomes: biogenesis, biologic function and clinical potential. Cell Biosci 2019:9.
18. Raposo G, Stoorvogel W. Extracellular vesicles: exosomes, microvesicles, and friends. J Cell Biol 2013:200;373–383.
19. Andreu Z, Yáñez-Mó M. Tetraspanins in extracellular vesicle formation and function. Front Immunol 2014:5;442.
20. Tetta C, Ghigo E, Silengo L, et al. Extracellular vesicles as an emerging mechanism of cell-to-cell communication. Endocrine 2013:44;11–19.
21. Turchinovich A, Weiz L, Langheinz A, et al. Characterization of extracellular circulating microRNA. Nucleic Acids Res 2011:39;7223–7233.
22. Schueller F, Roy S, Vucur M, et al. The role of miRNAs in the pathophysiology of liver diseases and toxicity. Int J Mol Sci 2018:19;261.
23. Starkey Lewis PJ, Dear J, Platt V, et al. Circulating microRNAs as potential markers of human drug-induced liver injury. Hepatol Baltim Md 2011:54;1767–1776.
24. Waidmann O, Bihrer V, Pleli T, et al. Serum microRNA-122 levels in different groups of patients with chronic hepatitis B virus infection. J Viral Hepat 2012:19;e58–e65.
25. Yamada H, Suzuki K, Ichino N, et al. Associations between circulating microRNAs (miR-21, miR-34a, miR-122 and miR-451) and non-alcoholic fatty liver. Clin Chim Acta 2013:424;99–103.
26. Howell LS, Ireland L, Park BK, et al. MiR-122 and other microRNAs as potential circulating biomarkers of drug-induced liver injury. Expert Rev Mol Diagn 2018:18; 47–54.
27. Kia R, Kelly L, Sison-Young RLC, et al. MicroRNA-122: a novel hepatocyte-enriched in vitro marker of drug-induced cellular toxicity. Toxicol Sci Off J Soc Toxicol 2015:144; 173–185.
28. Carroll EE, Ippolito DL, Permenter MG, et al. Utility of serum miR-122, liver enzymes, and hepatic histopathology in response to hepatotoxicants in Sprague-Dawley rats. Toxicol Pathol 2018:46;835–846.
29. Norona LM, Nguyen DG, Gerber DA, et al. Bioprinted liver provides early insight into the role of Kupffer cells in TGF-$\beta$1 and methotrexate-induced fibrogenesis. PLoS ONE 2019:14;e0208958.
30. Bala S, Petrasek J, Mundkur S, et al. Circulating microRNAs in exosomes indicate hepatocyte injury and inflammation in alcoholic, drug-induced and inflammatory liver diseases. Hepatol Baltim 2012:56;1946–1957.
31. Gerlach CV, Vaidya VS. MicroRNAs in injury and repair. Arch Toxicol 2017:91;2781–2797.
32. Hermeking H. The miR-34 family in cancer and apoptosis. Cell Death Differ 2010:17;193–199.
33. Bhatt K, Mi Q-S, Dong Z. microRNAs in kidneys: biogenesis, regulation, and pathophysiological roles. Am J Physiol Renal Physiol 2011:300;F602–F610.
34. Leite SB, Wilk-Zasadna I, Zaldivar JM, et al. Three-dimensional HepaRG Model as an attractive tool for toxicity testing. Toxicol Sci 2012:130;106–116.
35. Mandon M, Huet S, Dubreil E, et al. Three-dimensional HepaRG spheroids as a liver model to study human genotoxicity in vitro with the single cell gel electrophoresis assay. Sci Rep 2019:9;1–9.
36. Rubin K, Janefeldt A, Andersson L, et al. HepaRG cells as human-relevant in vitro model to study the effects of inflammatory stimuli on cytochrome P450 isoenzymes. Drug Metab Dispos 2014:43;119–125.
37. Hendriks DFG, Fredriksson Puigvert L, Messner S, et al. Hepatic 3D spheroid models for the detection and study of compounds with cholestatic liability. Sci Rep 2016:6; 35434.
38. Messner CJ, Mauch L, Suter-Dick L. Bile salts regulate CYP7A1 expression and elicit a fibrotic response and abnormal lipid production in 3D liver microtissues. Toxicol In Vitro 2019:60;261–271.
39. Prestigiacomo V, Weston A, Messner S, et al. Pro-fibrotic compounds induce stellate cell activation, ECM-remodelling and Nrf2 activation in a human 3D-multicellular model of liver fibrosis. PLoS One 2017:12;e0179995.

40. Thacker SE, Nautiyal M, Otieno MA, et al. Optimized methods to explore the mechanistic and biomarker potential of hepatocyte-derived exosomes in drug-induced liver injury. Toxicol Sci Off J Soc Toxicol 2018:163;92–100.
41. Duan L, Ramachandran A, Akakpo JY, et al. Role of extracellular vesicles in release of protein adducts after acetaminophen-induced liver injury in mice and humans. Toxicol Lett 2019:301;125–132.
42. Ravenscroft SM, Pointon A, Williams AW, et al. Cardiac non-myocyte cells show enhanced pharmacological function suggestive of contractile maturity in stem cell derived cardiomyocyte microtissues. Toxicol Sci 2016:152;99–112.
43. Ueyama T, Tsuji S, Sugiyama T, et al. Fluorometric evaluation of CYP3A4 expression using improved transgenic HepaRG cells carrying a dual-colour reporter for CYP3A4 and CYP3A7. Sci Rep 2017:7;2874.
44. Ferreira A, Rodrigues M, Silvestre S, et al. HepaRG cell line as an in vitro model for screening drug–drug interactions mediated by metabolic induction: amiodarone used as a model substance. Toxicol In Vitro 2014:28;1531–1535.
45. Gerets HHJ, Tilmant K, Gerin B, et al. Characterization of primary human hepatocytes, HepG2 cells, and HepaRG cells at the mRNA level and CYP activity in response to inducers and their predictivity for the detection of human hepatotoxins. Cell Biol Toxicol 2012:28;69–87.
46. Berger B, Donzelli M, Maseneni S, et al. Comparison of liver cell models using the basel phenotyping cocktail. Front Pharmacol 2016;7;443.
47. Levitt DG, Levitt MD. Human serum albumin homeostasis: a new look at the roles of synthesis, catabolism, renal and gastrointestinal excretion, and the clinical value of serum albumin measurements. Int J Gen Med 2016:9;229–255.
48. Lübberstedt M, Müller-Vieira U, Mayer M, et al. HepaRG human hepatic cell line utility as a surrogate for primary human hepatocytes in drug metabolism assessment in vitro. J Pharmacol Toxicol Methods 2011:63;59–68.
49. Nelson LJ, Morgan K, Treskes P, et al. Human hepatic HepaRG cells maintain an organotypic phenotype with high intrinsic CYP450 activity/metabolism and significantly outperform standard HepG2/C3A cells for pharmaceutical and therapeutic applications. Basic Clin Pharmacol Toxicol 2017:120;30–37.
50. Xu JJ, Henstock PV, Dunn MC, et al. Cellular imaging predictions of clinical drug-induced liver injury. Toxicol Sci Off J Soc Toxicol 2008:105;97–105.
51. Chládek J, Grim J, Martínková J, et al. Pharmacokinetics and pharmacodynamics of low-dose methotrexate in the treatment of psoriasis. Br. J Clin Pharmacol 2002:54;147–156.
52. Dargan PI, Ladhani S, Jones AL. Measuring plasma paracetamol concentrations in all patients with drug overdose or altered consciousness: does it change outcome? Emerg Med J 2001:18;178–182.
53. Shihana F, Dissanayake DM, Dargan PI, et al. A modified low cost colourimetric method for paracetamol (acetaminophen) measurement in plasma. Clin Toxicol Phila Pa 48;42–46.
54. Schreiter T, Sowa J-P, Schlattjan M, et al. Human *ex-vivo* liver model for acetaminophen-induced liver damage. Sci Rep 2016:6;31916.
55. Gamal W, Treskes P, Samuel K, et al. Low-dose acetaminophen induces early disruption of cell-cell tight junctions in human hepatic cells and mouse liver. Sci Rep 2017:7;37541.
56. Leite SB, Roosens T, El Taghdouini A, et al. Novel human hepatic organoid model enables testing of drug-induced liver fibrosis in vitro. Biomaterials 2016:78;1–10.
57. Garcia-Contreras M, Shah SH, Tamayo A, et al. Plasma-derived exosome characterization reveals a distinct microRNA signature in long duration type 1 diabetes. Sci Rep 2017:7;1–10.
58. Słomka A, Urban SK, Lukacs-Kornek V, et al. Large extracellular vesicles: have we found the holy grail of inflammation? Front Immunol 2018:9;2723.
59. Jung MK, Mun JY. Sample preparation and imaging of exosomes by transmission electron microscopy. J Vis Exp 2018:131;56482.
60. Scarff CA, Fuller MJG, Thompson RF, et al. Variations on negative stain electron microscopy methods: tools for tackling challenging systems. J Vis Exp 2018:132;57199.
61. Castaño C, Kalko S, Novials A, et al. Obesity-associated exosomal miRNAs modulate glucose and lipid metabolism in mice. Proc Natl Acad Sci 2018:115;12158–12163.
62. Falcone G, Felsani A, D'Agnano I. Signaling by exosomal microRNAs in cancer. J Exp Clin Cancer Res 2015:34;32.
63. Murakami Y, Toyoda H, Tanahashi T, et al. Comprehensive miRNA expression analysis in peripheral blood can diagnose liver disease. PLoS ONE 2012:;e48366.
64. Bailey WJ, Barnum JE, Erdos Z, et al. A performance evaluation of liver and skeletal muscle-specific miRNAs in rat plasma to detect drug-induced injury. Toxicol Sci 2019:168;110–125.

Address correspondence to:
*Prof. Laura Suter-Dick*
*University of Applied Sciences and Arts*
*Northwestern Switzerland*
*School of Life Sciences*
*Hofackerstrasse 30*
*Muttenz CH-4132*
*Switzerland*

*E-mail:* laura.suterdick@fhnw.ch

## 4.6 Paper 2: Identification of miR-199a-5p, miR-214-3p and miR-99b-5p as extracellular biomarkers of fibrosis and promoters of HSC activation.

Manuscript in preparation

Catherine Jane Messner[1,2,4], Dilek Özkul[1], Saskia Schmidt[1,2], Luigi Terracciano[3], Stephan Krähenbühl [2], Laura Suter-Dick[1,4].

[1]University of Applied Sciences Northwestern Switzerland, School of Life Sciences, Muttenz, Switzerland.
[2]University of Basel, Department of Pharmaceutical Sciences, Basel, Switzerland.
[3]University Hospital Basel, Institute of Pathology, Basel, Switzerland
[4] Swiss Centre for Applied Human Toxicology (SCAHT), Basel, Switzerland.

Corresponding author:
Catherine Jane Messner
Fachhochschule Nordwestschweiz
Hochschule für Life Sciences
Institut für Chemie und Bioanalytik
Hofackerstrasse 30
CH-4132 Muttenz

Email: catherine.messner@fhnw.ch

## Abstract:

Liver fibrosis is characterised by the accumulation of extracellular matrix (ECM) resulting in the formation of fibrous scars. In the clinic, liver biopsies are the standard diagnostic method despite potential sampling errors and clinical complications. Circulating miRNA-species are putative biomarkers of liver damage. miRNAs are single stranded, non-coding RNAs that can be detected in tissues, body fluids and cultured cells. The regulation of many miRNAs has been linked to tissue damage, including liver fibrosis in patients. Experimental evidence also suggests that miRNAs are regulated *in vitro*, and could thus serve as translational *in vitro-in vivo* biomarkers. Here, we focused on extracellular miRNAs released upon drug-induced injury from a multicellular 3D-liver model (MT) *in vitro*.

Following hepatocellular damage to the MT by methotrexate (MTX) and acetaminophen (APAP), we identified by NGS and qPCR four extracellular miRNAs (miR-199a-5p, miR-214-3p, miR-99b-5p and miR-125a-5p) that were differentially released from MTs displaying fibrotic phenotype (MTX-induced).

Using miRNA mimics in combination with immortalized human stellate cells (HSC), we could demonstrate that increased intracellular levels of miR-199a-5p, miR-214-3p and miR-99b-5p promoted HSC activation (αSMA expression) and fibronectin production. In addition, miR-199a-5p and miR-214-3p promoted HSC proliferation and migration. Thus, our data show that they play a role in HSC activation and fibrosis progression. The extracellular release and phenotypic anchoring of these three miRNAs suggest that they may represent liver fibrosis biomarkers. Investigations with primary human cell-based MT also corroborate the release of the selected miRNA-species into the medium, further supporting their broad applicability for the study of hepatic fibrosis.

In conclusion, we propose that extracellular miR-199a-5p, miR-214-3p, miR-99b-5p and miR-125a-5p could contribute towards a panel of miRNAs for identifying liver fibrosis and that miR-199a-5p, miR-214-3p, miR-99b-5p are promoters of HSC activation.

## Introduction:

Liver fibrosis is characterised by the accumulation of extracellular matrix (ECM), which distorts hepatic architecture through the formation of fibrous scars. If left untreated liver fibrosis ultimately progresses into cirrhosis resulting in hepatocellular dysfunction and reduced intrahepatic blood flow leading to hepatic insufficiency and portal hypertension [1,2]. Liver cirrhosis can also promote the development of hepatocellular carcinoma (HCC) [3]. Accurately diagnosing early stages of liver fibrosis is essential for disease management, due to the reversibility of fibrosis through the removal/treatment of the cause of injury [4,5]. A leading cause of liver damage is through the intake of drugs known as drug-induced liver injury (DILI) and is a major challenge in clinical medicine and drug development [6]. Certain drugs such as methotrexate (MTX) elicit chronic DILI in patients, potentially leading to hepatic fibrosis and ultimately cirrhosis [7,8]. Contrarily, acetaminophen (APAP) causes acute, dose-related DILI leading to hepatocellular necrosis/apoptosis and liver failure [6,9].

Currently the most trusted method of diagnosing liver fibrosis are liver biopsies, which are still considered the standard diagnostic method despite their invasive nature, sampling error and potential clinical complications [11]. Non-invasive methods are available including serum biomarkers such as alanine aminotransferase (ALT), aspartate aminotransferase (AST), alkaline phosphatase (ALP), albumin levels and total bilirubin (TBL) [12]. Different combinations of serum markers and other parameters (*e.g.* demographic and blood cell count) produce scores, which can be used for diagnosis of liver injury, examples of these tests include APRI, fibrosis-4 or Fibroindex [12]. Additional alternatives include ultrasonography, computed tomography, magnetic resonance and transient elastography [13–16]. These methods detect a variety of liver diseases, lack sensitivity, can be expensive and can carry radiological risks [12,13,17]. Thus, the quest for early and specific biomarkers of liver fibrosis is still ongoing.

Small regulatory RNAs known as microRNAs (miRNAs) are single stranded, non-coding RNAs consisting of 21-25 nucleotides. miRNAs are not only located intracellularly but can be released and circulate in a variety of bio-fluids (*e.g.* plasma, serum, urine) and cell culture media [18]. It has been shown that a variety of diseases such as cancer results in selective miRNA release making the identification of one or many of these miRNAs a promising potential biomarker for specific diseases [19–24]. Extracellular miRNAs are released via extracellular vesicles, protein-complexes or lipoproteins and mediate cell-cell signalling [18,25]. An example of intercellular communication from secreted miRNAs is the investigation by Zhang *et al*. who demonstrated miR-150 was selectively packed into microvesicles, which were actively secreted and able to enter and deliver miR-150 to immortalized human

microvascular endothelial cell line. The result being reduced c-Myb expression and increased cell migration [26].

Several miRNAs have been identified as potential DILI biomarkers in clinical samples, *in vivo* and i*n vitro* models [24,27–33], including liver specific miR-122-5p that is predominantly expressed by hepatocytes and released into the blood upon hepatocellular injury. An example of DILI eliciting liver injury and miR-122-5p release is APAP-induced liver injury [24,30–32,34]. MTX-induced miRNA release is less understood, but recently it has been described that long term exposure of bio-printed multicellular human liver tissue resulted in miR-122 release into the cell culture supernatant [35]. Additionally, miR-122-5p was released in exosomes prior to MTX-toxicity in 3D-HepaRG, demonstrating the sensitivity of miRNAs as early biomarkers [34]. Despite miR-122 being liver specific and promising for identifying liver injury, it is not specific to liver fibrosis.

Many miRNAs involved in liver fibrosis progression are typically measured intracellularly such as miR-199, miR-200, miR-2861, miR33a and many more [36]. However, measuring intracellular miRNAs is still an invasive procedure due to the need for liver biopsy. Therefore, circulating miRNAs are more suitable as they can be detected non-invasively. A small number of circulating miRNAs have shown aberrant release during fibrosis progression caused by NAFLD, HBV and HCV such as miR-34a, miR-19b, miR-33a, miR-27a, miR-17, miR-125a and miR-29 [37,38]. Yet fibrosis-specificity has not been confirmed and the role of extracellular miRNAs of DILI-induced fibrosis are less understood.

Scaffold-free multicellular 3D liver microtissues (MTs) comprising HepaRG, THP-1 and hTERT-HSC (surrogates for hepatocytes, Kupffer cells and hepatic stellate cells, respectively), have been shown to recapitulate key fibrotic events elicited by known pro-fibrotic stimuli such as TNF-α, TGF-β1 and pro-fibrotic compounds MTX and thioacetamide (TAA) [39]. In the present study, we used 3D human liver MTs and performed further characterisation by assessing CYP3A4 activity. We also investigated the effects of toxic concentrations of APAP in comparison to MTX. We then used next generation sequencing (NGS) to identify miRNAs released into the cell culture supernatant with the aims of identifying fibrosis-specific miRNAs. Furthermore, using miRNA mimics in combination with hTERT-HSCs we assessed the potential role that the selected miRNAs could play in HSC activation, thereby promoting liver fibrosis.

## Materials and Methods

### Human cell lines

HepaRG cells were obtained from Biopredic International (Rennes, France). The cells were seeded at 1 x $10^5$ undifferentiated cells/$cm^2$ in medium with growth supplements ADD710 (Biopredic). The cells were cultured at 37°C in 5% CO2 for 14 days before differentiation. After 14 days of culture, cell differentiation was induced with medium containing differentiation supplements ADD720 (Biopredic) for 14 days. Then the cells were maintained in differentiation medium for up to 4 weeks. HepaRG were passaged using Trypsin-EDTA (Invitrogen, Cat. 25300). HepaRG were used at passages below 20.

hTERT-HSC were kindly provided by Dr. Bernd Schnabl (UC San Diego, USA) and were cultured in DMEM High Glucose (Invitrogen, Cat. 41965) supplemented with 10% fetal bovine serum (FBS) (Invitrogen, Cat. 10270) and 1% P/S (Gibco, Cat.15070063) . The cells were maintained in the humidified incubator at 37°C in 5% CO2. hTERT-HSC were passaged using Trypsin-EDTA. hTERT-HSC were maintained at low passages (<12) to avoid spontaneous activation.

THP-1 monocytic cells (Cell Line Service) were cultured at 2–10 x $10^5$ cells/mL in RPMI 1640 containing (Bioconcept, Cat. 1-41F50-I) 10% FBS, 1% P/S and maintained at 37°C in 5% CO2. THP-1 cells were differentiated into macrophages over 48 hours in RPMI 1640 medium containing 10 ng/mL Phorbol 12-myristate 12-acetate (PMA) (Sigma, Cat. 79346) as described in previous literature [37] . The media containing PMA was removed and the differentiated THP-1 were washed with fresh medium and maintained in DMEM High Glucose supplemented with 10% FBS and 1% P/S. Differentiated THP-1 were detached using Accutase (Sigma, SCR005). THP-1 were used at passages below 30.

### Generation of microtissues

All co-culture (MTs) were generated using the MicroTissues 3D Petri Dish system from Sigma-Aldrich (Cat. Z764051-6EA) using UltraPure Agarose (ThermoFischer, Cat. 16500100). Differentiated HepaRG, differentiated THP-1 and hTERT-HSC were counted and resuspended in William's E Medium + GlutaMAX (Invitrogen, Cat. 32551), 5 µg/ml insulin, 5 µg/ml transferrin, 5 ng/ml sodium selenite (Sigma, Cat. 11074547001), 100nM dexamethasone (Sigma, Cat. D1756), 20% FBS and 1% P/S. After 72 hours of aggregation the MTs were maintained/treated in an FBS free version of the medium. Human liver MTs

were generated using 2000 cells per MT containing differentiated HepaRG, hTERT-HSC and differentiated THP-1.

Primary human microtissues (PHMTs) were generated using cryopreserved PHH (LOT: S1518T) and non-parenchymal cells NPCs (S1512T) (obtained from KalyCell, France) from the same donor. Cells were thawed and seeded at a ratio of 2:1 (PHH:NPC) at 2000 cells per MT in the 3D Petri Dish system. MTs were allowed to aggregate in Williams E medium + GlutaMax, 1% P/S, 10 µg/ml insulin, 5.5 µg/ml transferrin, 6.7 ng/ml sodium selenite (Sigma, I3146-5ML), 100 nM dexamethasone and 10% FBS. After spheroids were sufficiently compact (day 10) the medium was exchanged to an FBS free medium, which was used for cell treatments.

## Induction of CYP3A4

For functional characterisation, CYP3A4 induction was carried out using 20 µM rifampicin (RIF, Sigma, R3501) directly after the aggregation phase of the MTs medium. RIF treatment was refreshed at 24 h and ended at 48 h. Following this, the induced MTs were either tested for CYP3A4 activity, gene or protein expression as described below.

## Cytochrome p450 assay

P450-GloTM CYP3A4 Assay with Luciferin-IPA (Promega, V9001) was used to determine the CYP3A4 activity in RIF treated and untreated MTs. The P450-GloTM assay was carried out as described in the manufacturer's protocols and adjusted to quantities necessary for the MTs. The luminescence was measured at 1000 m/s using a Flexstation 3 microplate reader (Molecular Devices).

## HPLC-MS/MS

Substrate conversion by MTs was determined in RIF treated and untreated MTs by measuring the conversion of 25 µg/ml testosterone (Sigma, 86500) to hydroxytestosterone over time. Cell culture supernatant was collected at 6, 24 and 48 h and diluted in water supplemented with 2 mM ammoniumfluoride solution and measurements were performed using HPLC-MS/MS (Agilent Technologies LC unit: Agilent Technologies, 1100; MS detector: Agilent Technologies, 6410; columns SB-C8, Zorbax, 4.6 x 50 mm, 1.8 mm, Agilent Technologies). Calibration standards were made of 1, 5, 10, 50 and 100 µg/ml testosterone in water supplemented with 2 mM ammoniumfluoride. The absolute concentration of

testosterone was calculated based on the calibration standards. Production of hydroxytestosterone was qualitatively assessed by determining the area under the curve.

## Cell treatments

Co-cultures (MTs) were formed as described above and treatment was carried out using maintenance medium. For the determination of cytotoxicity, MTs were treated with methotrexate (MTX, Sigma, M8307) using the concentration range 3.75 - 120 µM and acetaminophen (APAP, Sigma, A5000) using the concentration range of 1 - 16 mM. Medium with or without substances was exchanged every 2-3 days. Subsequent experiments were performed with concentrations of 2 and 4 mM for APAP and 30 and 60 µM for MTX. In addition, 1 ng/ml TGF-β1 (Sigma, Cat. T5050), which is known to cause hepatocellular damage and to elicit a pro-fibrotic effect, was used as a positive control for fibrosis characterisation.

## Cell viability assay

Cell viability was assessed using the CellTiter-Glo® Luminescent Cell Viability Assay (Promega, Cat. G7570). The assay was carried out as described in the manufacturer's protocols and adjusted to quantities necessary for the MTs.

## Gene expression analysis

MTs were collected and washed using PBS then lysed using Qiazol Lysis Reagent (Qiagen, 79306) and mRNA was isolated following standard TRIzol extraction procedure with the addition of Glycogen (ThermoFisher, LT-02241). RNA was reverse transcribed using a M-MLV Reverse transcriptase (Promega, Cat. M1705) and oligo dT (Qiagen, 79237) and real time PCR was performed using FastStart TaqMan® Probe Master (Roche, Cat. 04673417001) and TaqMan probes from Invitrogen. Real time, TaqMan PCR was performed on selected genes (see Table 1). The qRT-PCR Program used: 10 minutes denaturation at 95°C, followed by 40 cycles of 15 seconds at 95°C and 1 minute at 60°C. The Ct values were generated using the Corbett Rotorgene Analysis Software 6000 and processed on GraphPad Prism. Beta-2-Microglobulin was used as an internal standard for the normalization. The Ct values were generated using the Corbett Rotorgene Analysis Software 6000 and processed on GraphPad Prism and data are expressed as fold change.

| Gene of Interest | Abbreviation | Invitrogen Ref. Nr |
|---|---|---|
| Beta-2-Microglobulin | B2M | Hs00187842_m1 |
| Actin, alpha 2, smooth muscle | ACTA2 (αSMA) | Hs00426835_g1 |
| Collagen 1 alpha 1 | COL1α1 | Hs00164004_m1 |
| Collagen 4 alpha 1 | COL4α1 | Hs00266237_m1 |
| Cytochrome P450 3A4 | CYP3A4 | Hs04260376_m1 |

Table 1. TaqMan primers used for gene expression analysis by q-RT-PCR

## Next Generation Sequencing

MTs were formed as described above and treatment was carried out using maintenance medium. Cell culture supernatant was collected from untreated MTs and treated MTs for MTX 30 uM and APAP 2 mM and sent to GenXPro. miRNA was extracted from 1 ml of cell culture supernatant of two biological replicates and processed using the TrueQuant method which contains „Unique Molecular Identifiers" (UMI) to avoid uneven amplification and artefact generation during the PCR stage. Data was initially processed by GenXPro to assign sequences to specific miRNAs and provide miRNA counts. Following this data was processed on R using packages: Bioconductor, DESeq2 and edgeR. Counts were initially normalised using TMM method and differential miRNAs were calculated using edgeR using GLM fit. PCA analysis was carried out using R. All data was plotted using ggplot2. miRNAs specific to MTX-induced fibrosis from our model were cross-checked with the publication by Krauskopf *et al.* [31] to confirm the specifity using clinical data from patients with APAP-induced toxicity. miRNAs were run through DIANA-miRpath v3.0 to identify potential links to fibrosis and targets to obtain the most promising miRNA panel to have fibrosis specificity.

## miRNA Analysis

miRNeasy Serum/Plasma Kit (Cat. 217184) was purchased from Qiagen and was carried out as described in the manufacturers protocol. Reverse transcription and q-RT-PCR was carried out using TaqMan MicroRNA Reverse Transcription Kit (ThermoFischer, Cat. 4366596), qRT-PCR master mix (ThermoFischer, Cat. 4444557) and all TaqMan q-RT-PCR primers were purchased from Invitrogen (Table 2). miRNA extraction and processing was carried out using 180µl supernatant. The reaction mix was prepared according to the manufacturer's instructions for a final reaction volume of 10 µL with 3 µL RNA extract. The PCR conditions were set for 30 min at 16 °C followed for 30 min at 42 °C and 5 min at 85 °C [38]. All values were expressed as -ΔCT values.

| miRNA of Interest | Assay name | Assay number |
|---|---|---|
| Cel-miR-39/Spike-in | Cel-miR-39-3p | 000200 |
| RNU44 | RNU44 | 001094 |
| miR-122-5p | hsa-miR-122-5p | 002245 |
| miR-199a-5p | hsa-miR-199a-5p | 000498 |
| miR-214-3p | hsa-miR-214-3p | 002306 |
| miR-125a-5p | hsa-miR-125a-5p | 002198 |
| miR-99b-5p | hsa-miR-99b-5p | 000436 |

Table 2. TaqMan primers used for miRNA analysis by q-RT-PCR

## Immunohistochemistry

MTs were fixed with 4% PFA 1h in PBS containing calcium and magnesium. Fixed MTs were either embedded in 2% agarose in PBS or stained whole using the protocol described by Ravenscroft et al [39] using primary and secondary antibodies listed below (Table 3). Images were taken using an Olympus FV3000 confocal microscope.

| Protein of Interest | Primary Antibody | Secondary Antibody |
|---|---|---|
| αSMA (ACTA2) | Mouse polyclonal antibody (Sigma A5228)/ 1:200 | Goat anti mouse Alexafluor 488 (A-11017)/ 1:1000 |
| Collagen I | Mouse monoclonal antibody (Abcam ab90395)/ 1:100 | Goat anti mouse Alexafluor 488 (A-11017)/ 1:1000 |
| Fibronectin | Rabbit polyclonal antibody (Abcam ab32457)/ 1:100 | Goat anti rabbit Alexafluor 546 (A-11071)/ 1:1000 |
| Albumin | Rabbit monoclonal antibody (Abcam ab207327)/ 1:800 | Goat anti rabbit Alexafluor 546 (A-11071)/ 1:1000 |
| Vimentin | Rabbit monoclonal antibody (Abcam ab92547)/ 1:100 | Goat anti rabbit Alexafluor 546 (A-11071)/ 1:1000 |
| CYP3A4 | Rabbit polyclonal antibody (Sigma, AB1254)/ 1:100 | Goat anti rabbit Alexafluor 488 (A-11070)/1:1000 |
| CD68 | Mouse monoclonal antibody (Abcam ab955) / 1:100 | Goat anti mouse Alexafluor 488 (A-11017)/ 1:1000 |

Table 3. Antibodies used for immunohistochemistry

## Enzyme-linked immunosorbent assay

Medium for protein determination was pooled over the whole treatment period. Human albumin ELISA (Cat. E80-129) was purchased from Bethyl Laboratories and all buffers, solutions were made according to the buffer preparation guidelines. High binding flat-bottomed plates (Cat. 655 061) were purchased from Greiner Bio-One. Human IL-6 ELISA kit (ThermoFischer, Cat. KHC0061C) was carried out as described in the manufacturer's protocol. ELISA results were calculated using a four-parameter fit using the SoftMax Pro software.

## Transfection of miRNA mimics

hTERT-HSC were plated in 96-well plates (5000 cells/well) or 24-well plates (20,000 cells/well) and allowed to adhere overnight. HiPerfect Reagent was combined with 40 nM of the specific miRCURY LNA miRNA Mimic from Qiagen (labelled with 5'FAM) and mixed with DMEM High Glucose (no supplements), vortexed briefly and incubated at RT for 20 minutes. Following this the transfection mixture was placed into each well containing 175 µl (96-well plate) and 525 µl (24-well plate) of DMEM with 10% FBS and 1% P/S and the cells were incubated at 37°C and 5% $CO_2$ for 72 h.

| Plate Size | HiPerfect Reagent | Mimic | DMEM without supplements | Final Quantity to add per well |
|---|---|---|---|---|
| 96-well | 0.75 µl | 0.12 µl | 24.25 | 25.12 µl |
| 24-well | 2.25 µl | 0.36 µl | 72.75 µl | 75.36 µl |

Table 4. Reagent quantities for miRNA mimic transfection

## Migration/Wound healing Assay

Migration assay was performed using ibidi culture inserts (Cat. No. 80209). hTERT-HSCs were transfected for 72 hrs then seeded at 20,000 cells per insert well and allowed to adhere overnight. Inserts were removed and fresh medium was added with or without treatments and imaged every h for 48 h in the cellVivo incubation system by Olympus. Data were analysed in ImageJ using the "Wound_healing_size_tool", which allows batch analysis of the stack of 48 images for each condition.

## Statistical Analysis

Data were analysed using GraphPad Prism 8 (GraphPad Software, Version 8.0.2) and expressed as mean values ± SD. The Student *t* test was used for comparison between two groups and One-way ANOVA was used for statistical analysis of multiple concentrations of the same treatment. $P < 0.05$ was considered to be significant: *, $P \leq 0.05$; ** , $P \leq 0.01$; ***, $P \leq 0.001$.

## Results

### Hepatic cell lines in 3D culture maintain CYP3A4 expression and activity

The ability to biotransform xenobiotics is key for the liver and should be displayed by HepaRG cells in 3D-cultures. To evaluate this in our system, 48 after aggregation we measured CYP3A4 expression and activity in MTs without (basal) and with (RIF) induction with rifampicin. Expression of CYP3A4 was detected under basal conditions and was strongly induced in MTs treated with RIF (Figure 1A). Enzymatic activity of CYP3A4 was also detectable under basal conditions and significantly induced by rifampicin. This is supported by results obtained with the P450-GloTM CYP3A4 assay (Figure 1B) and by measuring the metabolic transformation of testosterone to hydroxytestosterone using LC-MS (Figure 1C). Immunostaining of the MTs (Figure 1D) shows the marked induction elicited by rifampicin and the uniform distribution across the MT of CYP3A4 protein expression, further supporting basal and inducible expression of CYP3A4.

### 3D *in vitro* model can develop a fibrotic phenotype

In addition to HepaRG cells remaining metabolically active, immunostaining of untreated MTs confirmed that the three cell types are maintained in the MTs for 10 days following aggregation (20 days in total). All three cell types are required to develop a relevant fibrotic response. Immunostaining of MTs showed expression of specific protein markers: HepaRG express albumin; hTERT-HSC express the intermediate filament vimentin; and THP-1 express vimentin and CD68 (Figure 2A & B). Thus, co-staining of vimentin and CD68 is characteristic of THP-1 cells, while vimentin positive staining only identifies HSC. The cells in the MTs were also able to display a fibrotic response as shown by their response to treatment with the pro-fibrotic cytokine TGF-β1 (1 ng/ml) for 10 days. TGF-β1 treatment elicited a reduction of albumin stain, indicating hepatocellular damage probably to HepaRG cells. It also led to increased αSMA and Collagen I (Col I), showing that HSCs have become activated and ECM production has increased, thereby demonstrating TGF-β1 is capable of promoting a fibrotic phenotype in the MTs (Figure 2).

### Methotrexate but not acetaminophen induces fibrosis in the MTs

MTs were treated with MTX (3.75 – 60 µM) and APAP (0.5 - 16 mM) for 10 days. At the end of the treatment period, cellular ATP content was determined as a measure of cell viability. The EC50 was calculated for APAP and found to be 1.7 ± 0.38 mM, whereas MTX resulted in a 60-70% decrease in ATP content for all concentrations (Figure 3A & B). Cellular

glutathione (GSH) was also measured in APAP treated MTs as detoxification of APAP is expected to lead to GSH depletion. In our model, APAP exposure at 2 mM and above led to a large decrease in GSH (Figure 3D). Based on the EC50 of APAP and the GSH results we determined 2 and 4 mM to be appropriate for investigating APAP overdose. MTX concentrations 30 and 60 µM were selected for further investigation based on preliminary experiments. Specific damage of the compounds to the HepaRG cells was assessed by measuring a functional feature of HepaRG, albumin release. Both concentrations of APAP and MTX resulted in decreased albumin release. However, APAP elicited a larger decrease in albumin release at day 3 in comparison to MTX, which decreased more gradually (Figure 3D).

Evidence of liver fibrosis upon exposure to both toxicants was investigated using q-RT-PCR and immunostaining. q-RT-PCR results show that MTX induced a significant increase in Col I and Col IV expression at all concentrations. Significant αSMA expression was only seen in MTs treated with 30 µM MTX. APAP showed no significant increase in αSMA, Col I and Col IV expression for the toxic 2 and 4 mM concentrations (*i.e.* overdose) and sub-toxic 0.5 mM concentration of APAP. Finally, immunostaining results show albumin decrease for MTX and APAP treatment, which confirms both treatments cause damage to the albumin-producing HepaRG cells. However, both compounds differ in their effect on fibrosis markers: while MTX increased αSMA and Col I expression, APAP did not.

## Identification of fibrosis-specific miRNAs

Based on the results described above, we investigated further differences in the response of MT treated with a pro-fibrotic (MTX) and hepatotoxic yet not pro-fibrotic (APAP) compound. In order to identify fibrosis-specific markers, we collected cell culture supernatant from the final 72 h of the 10 day exposure period, when fibrosis was evident in the MTX treated MTs. All small RNAs also including miRNAs, piRNAs and tRNAs in the medium were analysed by NGS. Preliminary analysis of NGS data using PCA analysis demonstrated that the control, MTX and APAP samples grouped separately. More specifically the changes in small RNA release by treated (MTX and APAP) MTs shows the largest separation to the untreated samples based on the principal component 1 (PC1). This is likely due to the common toxic effects of both compounds. The more interesting differences between MTX and APAP-treated samples are represented in the second principal component (PC2), where effects of MTX and APAP differ (Figure 4A).

By calculating the differential small RNA release for each treatment we can see that the release of a large number of small RNAs is reduced through exposure to APAP and MTX, including 227 that were in common between the two treatments. We saw a decreased release

of 278 miRNAs specifically from the APAP treated MTs, whereas, MTX only had a decrease in release of 5 small RNAs (Figure 4B). Of the increased released small RNAs we see that there are 57 small RNAs in common between APAP and MTX. Only 9 small RNAs were released specifically due to APAP exposure. On the other hand, 43 small RNAs were released specifically due to MTX treatment and may be associated with liver fibrosis (Figure 4B).

Using these 43 small RNAs, we removed piRNA and tRNAs and focussed only on the miRNAs. Selection of putative miRNAs markers was based on known links to fibrosis or wound healing from *in vitro*, *in vivo* and/or clinical studies, on extensive literature search (summarized in Table 5), and on a screen in DIANA miRpath v3.0. This process led to the selection of four miRNAs for further investigations (miR-199a-5p, miR-214-3p, miR-125a-5p, and miR-99b-5p). The differential release of these miRNAs by MTX and APAP treated MTs is depicted in Figure 4 (C and D).

Further investigations on the four selected miRNA-species and on miRNA-122-5p, a known marker of hepatocellular damage, included confirmatory independent experiments to demonstrate their consistent release into the medium determined by q-RT-PCR. The results of these measurements are depicted in Figure 5 (A-E). As expected, miR-122a-5p was released upon exposure to both MTX and APAP due to the compounds toxicity to the MTs. APAP caused a more transient increase (at day 3) while MTX lead to an increase of miRNA-122-5p in the medium at days 3 and 5, consistent with their respective acute and chronic toxicity mechanisms (Figure 5A).

The predominant release of the selected four miRNAs by MTs treated with MTX was corroborated in these independent experiments and the evaluation of several time points uncovered additional kinetic differences. For each of the four miRNA tested, the release from MTX-treated samples was higher than that from APAP-treated samples. For example, miR-99b-5p release was increased upon exposure to MTX 30 and 60 µM at all time points, reaching an approximately 8-fold higher release, while APAP led to a maximum increase of approximately 3-fold. Similar effects were observed for the other miRNAs. This is also evident for miRNA 199 (at day 10) miRNA-214 (MTX 30 uM, at day 10), miRNA-99 (at days 5 and 7), and miRNA-125 (MTX 30 uM, at days 7 and 10). Taken together, these results confirm the findings obtained in the previous experiment using NGS on the differential release of the four selected miRNAs. It also shows that the effects of MTX appear generally later, with fewer effects at the earliest tested time point (Day 3). This is consistent with the chronic nature of fibrosis. Finally, the intracellular miRNA levels were investigated using q-RT-PCR, demonstrating that only the expression of miR-199a-5p and miR-214-3p was significantly increased upon exposure to 30 and 60 µM MTX, while miR-125a-5p and miR-99b-5p remained unchanged. APAP elicited a significant increase in miR-214-3p expression but did not affect the expression of miR-125a-5p, miR-199a-5p and miR-99b-5p (Figure 5F).

## Functional impact of selected miRNAs on hTERT-HSC

Following identification of the four miRNAs and confirmation that they are released upon exposure to MTX, we set to investigate their functional effect on HSC. To this end, we transfected miRNA mimics into hTERT-HSC and assessed their effect on down-stream signals and on functional responses related to HSC activation. Potential targets were identified (Table 5) and their expression was determined after transfection of the cells with the pertinent miRNA mimic. Suspected protein targets of the four miRNAs were investigated using immunostaining. For three of the four selected miRNAs, the target proteins were down-regulated by the miRNA mimics. Following 72 h of transfection with miR-199a-5p, we saw decreased staining for caveolin-1 (CAV1) (Figure 6A). Following 96 h of transfection, we saw that the miR-214-3p resulted in a decrease in negative regulator of hedgehog signalling (SUFU) and miR-99b-5p elicited a decrease in mammalian target of rapamycin (mTOR) as predicted based on previous literature (Figure 6B and C). However, miR-125a did not have a significant effect on signal transducer and activator of transcription 3 (STAT3) (Figure 6D).

Effects of the miRNA mimics on HSC activation status were assessed by immunostaining for αSMA and FN1 in the transfected cells (Figure 7). The pro-fibrotic cytokine TGF-β1 caused a large increase in αSMA and FN1 protein and was used as positive control throughout these experiments (Figure 7A). The growth factor PDGF is also involved in wound healing and plays a role in promoting migration/proliferation but does not promote increased αSMA and Collagen expression in HSCs (Figure 7A and B). The three miRNAs that elicited the down-regulation of the investigated target proteins (miR-199a-5p, miR-214-3p and miR-99b-5p) also led to an increase in αSMA protein. miR-125a-5p on the other hand did not increase in αSMA protein (Figure 7A). hTERT-HSC transfected with miR-199a-5p, miR-214-3p and to a lesser extent miR-99b-5p had increased FN1 protein levels. Once again, the miR-125a-5p had no effect on FN1 production (Figure 7A).

In addition to the expression of HSC activation markers, we evaluated the functional response of the hTERT-HSC in terms of cell migration and proliferation, key features of HSC during fibrosis. Consistent with previous data TGF-β1 treatment resulted in a decrease in proliferation shown by ki67 staining, whereas PDGF resulted in a significant increase in proliferation (Figure 7B & C). Staining results also show that miR-199a and miR-214 resulted in a significant increase in proliferation and to a lesser extent miR-99b-5p. miR-125a-5p and siRNA had no effect on hTERT-HSC proliferation (Figure 7B & C).

The migration capacity of the hTERT-HSC was assessed, following the 72 h transfection and each condition was imaged every hour for 48 h. Similar to the proliferation results, TGF-β1 treatment decreased and PDGF increased the migration capacity of hTERT-HSC (Fig 7D). Results also show that that migration was increased by miR-199a-5p and miR-

214-3p transfection (Figure 7D). miR-99b-5p, miR-125a-5p and negative control siRNA did not affect hTERT-HSC migration (Figure 7D & E).

## Relevance to the results in primary human cells

PHMTs were generated using a similar process to that for the cell line model (see materials and methods). Characterisation of cellular composition based on albumin, vimentin and CD68 immunostaining confirmed the successful incorporation of hepatocytes, HSCs and kupffer cells (KCs) into the PHMT. PHHs stained positive for albumin (Figure 8A) and both HSCs and KCs stained positive for vimentin (Figure 8B). KCs were distinguished from HSCs by CD68 staining within the PHMTs (Figure 8B). TGF-β1 (1 ng/ml) treatment of PHMTs elicited hepatocellular damage and HSC activation demonstrated by the reduction in albumin staining and increased αSMA-staining, respectively (Figure 8A).

Cell culture supernatant was collected at day 3 to identify whether the four miRNAs of interest and miRNA-122 were increased after TGF-β1-induced fibrosis in the PHMTs (Figure 8C). Q-RT-PCR results show that miR-122-5p was increased by TGF-β1 treatment, demonstrating the expected hepatocellular damage. We also identified increased release of the four putative fibrosis markers, in particular miRNA 199a-5p (approximately 5-fold) as well as miRNA 125, miR-214-3p, and miR-99b-5p, all approximately 2-fold higher in treated than in the untreated control (baseline). These results demonstrate the relevance and transferability of the findings in the cell-line based model to the primary model.

## Discussion

In this work, we set out to identify released fibrosis specific biomarkers that could be used *in vitro* and potentially clinically for research and diagnostic purposes. To this end, we focused on miRNAs released from hepatic 3D cultures (MT consisting of 3 cell line) exposed to two compounds: methothrexate, that causes toxicological insult leading to a fibrotic phenotype and acetaminophen, an acute hepatotoxicant that causes hepatocellular damage but does not lead to clinically relevant liver fibrosis. Using a 3D, MT-model, we demonstrated compound-specific responses: MTX induced a fibrotic response, and APAP did not. In order to identify potential biomarkers, we sequenced miRNAs released into the cell culture supernatant from the treated MTs and were able to identify four miRNAs for further investigations (miR-199a-5p, miR-214-3p, niRNA-125a-5p and miR-99b-5p). In addition to corroborating the findings in subsequent experiments with cell lines, we assessed the release of the miRNAs using primary human hepatic cells. Finally, we also established a mechanistic association between the miRNAs and the activation of the HSCs for three of the investigated miRNAs.

### Characterisation of human liver MTs

The capacity of hepatocytes to metabolise xenobiotics is a key hepatic function mostly catalysed by CYP450s. CYP3A4 is the most abundant isoform in the human liver, responsible for the metabolism of a large number of clinically used drugs (< 50%) [40]. RIF is capable of transcriptionally inducing CYP3A4 and is a common method used to assess CYP induction and metabolic capacity of hepatocytes *in vitro* [32,41–43]. In accordance with our previous studies using 3D-HepaRG model, this cell line displays basal and inducible CYP3A4-activity in the MT [32]. Furthermore, we confirmed that the MTs display other typical hepatic characteristics such albumin production as described elsewhere [44,45]. THP-1 and hTERT-HSC were assessed using CD68 and vimentin staining, confirming successful incorporation of all three cells lines, as previously reported by Prestigiacomo *et al.* [37]. TGF-β1 is a key cytokine in liver fibrosis progression as it is involved in HSC activation, which elicits ECM deposition as described in the AOP for liver fibrosis [46]. The ability of the 3D human liver MTs to result in a fibrotic phenotype in response to TGF-β1 was confirmed by the increased αSMA and Col I expression.

Taken together, these results show that this MT model represents a suitable *in vitro* alternative for the study of metabolism and liver fibrosis progression.

## Compound-specific response of MTs exposed to MTX and APAP

High concentrations of APAP lead to acute hepatocellular necrosis/apoptosis and liver failure [6,9], whereas, MTX elicits chronic DILI in some patients, potentially leading to hepatic fibrosis and ultimately cirrhosis [7,8]. Therefore, we investigated the adverse outcome in the MTs exposed to both these compounds.

As described in our previous study, suitable concentrations of the test compounds MTX and APAP were determined based on the known $C_{max}$ (maximal drug concentration in human plasma) and is described in more detail in Messner *et al.* 2020 [32]. APAP elicited significant toxicity, specifically hepatocellular death shown by reduced albumin release and increased release of miR-122-5p. APAP exposure also significantly decreased GSH quantities and depletion was observed at >1 mM APAP exposure, which correlated to the EC50 (1.7 ± 0.38 mM). GSH depletion by N-acetyl-p-benzoquinoneimine (NAPQI) accumulation occurs clinically during APAP overdose, resulting in acute hepatotoxicity and liver failure [9,48]. APAP-induced hepatocellular toxicity has been shown *in vitro* using PHH carried out by Bell *et al.*, who present an EC50 of 1.5- 2.5 mM, dependent on donor, after 7 days of exposure [49]. Finally, although APAP does not elicit a fibrotic response in the clinic, some *in vitro* studies have shown APAP is capable of activating HSCs [50]. Interestingly, in our hands APAP exposure did not elicit fibrosis, underlying the relevance of the obtained results.

MTX, on the other hand, caused hepatotoxicity in the MTs (decreased albumin release and increased miR-122-5p release) that led to a fibrotic phenotype (increased αSMA and Col I). This is in agreement with *in vitro* data hepatotoxicity and/or fibrosis [33,37,50,51] and with clinical findings from psoriasis patients[7,10]. In summary, the data demonstrate that our *in vitro* model is sensitive to MTX- and APAP-induced hepatotoxicity and that, as in the clinic, only MTX-induced hepatocellular damage leads to a fibrotic response.

## Extracellular miRNAs as potential markers of fibrosis

Based on the response of the MTs to APAP and MTX we hypothesized that the two compounds could be used to identify biomarkers able to differentiate responses due to acute hepatocellular necrosis/apoptosis from DILI-induced fibrosis. We focused on differentially released miRNAs identified using NGS and subsequent database (DIANA miRPath v3.0) and literature analysis, excluding in particular miRNAs known to be released in patients who have suffered an APAP overdose [31]. The chosen panel consisted of miR-199a-5p, miR-214-3p, miR-99b-5p and miR-125a-5p. miR-199a has been shown to be increased in liver fibrosis biopsy samples and the severity of liver fibrosis correlated with increased expression of miR-199a [34,52,53]. Additionally, TGF-β1 has been shown to upregulate miR-199a-3p in HSCs [54]. Our data suggest that miR-199a-5p is a suitable candidate as a fibrosis-specific miRNA as we

show that intracellular expression and extracellular release of miR-199a-5p was induced by MTX, but not by APAP. Intracellular miR-214 has also been reported to be increased during liver fibrosis and HSC activation [34,55,56]. We not only identified increased miR-214-3p expression; we also show an increase in extracellular levels upon exposure to MTX.

A correlation has been identified between miR-125a and HBV induced liver fibrosis, HCV-associated hepatotoxicity and HSC activation [58–60]. We identified a large and significant increase in miR-125a-5p release upon exposure to MTX 30 μM and only a small increase by APAP 2 mM. Finally, miR-99b has been linked to pericellular fibrosis from NAFLD and wound healing/regeneration during from dermal and spinal cord injury [61–63]. Extracellular levels of miR-99b-5p increased upon exposure to both MTX and APAP. Interestingly, MTX demonstrated a sustained miR-99b-5p release (*i.e.* chronic release) as both concentrations elicited a significant increase in release at all the times measured. In comparison, the increase caused by APAP was much smaller and less consistent overtime.

In summary, the four relevant miRNAs showed potential regulation by MTX: both intracellular and extracellular miRNA levels of miR-199a-5p and extracellular miR-214-3p levels were increased by MTX-induced fibrosis. Furthermore, miR-125a-5p and miR-99b-5p release increased upon exposure to MTX and to a lesser extent APAP.

## miR-199a-5p, miR-214-3p and miR-99b-5p promote hTERT-HSC activation

Acceptance of novel biomarkers highly increases when there is evidence of a causal association to the disease. Thus, we evaluated the effect of the four miRNAs in promoting HSC activation, proliferation and migration. TGF-β1 has been shown to upregulate miR-199a-3p and decrease CAV1 in HSCs. CAV1 internalizes TGF receptors into caveolae and this internalisation represses the TGF-β signalling pathway [64], thereby establishing an important link between miR-199a-5p and CAV1/2 in liver fibrosis progression [54]. Moreover, a recent publication using primary rat HSCs and the immortalised human HSC cell line LX2 demonstrated that miR-199a-3p transfection resulted in inhibition of CAV2 and TGFβRI level subsequently enhancing TGF-β signalling pathway, promoting HSC activation [65]. A similar mechanism involving miR-199a-5p has been proposed to exacerbate lung fibrosis [66]. Our results are in agreement with these findings as CAV1 expression was decreased by both miR-199a-5p transfection and TGF-β1 treatment (Figure S1). We also detected increased αSMA and FN1 in agreement with the findings of Yang *et al.* [65]. The effect of miR-199a-5p on migration and proliferation has only been assessed in tumours, where miR-199a-5p was shown to reduce cell proliferation and promote apoptosis [67]. Contrarily, we observed that miR-199a-5p promoted migration and cell proliferation in the hTERT-HSCs without impacting cell

viability (Figure S2). In summary, these results confirm that miR-199a-5p plays an important role in HSC activation, migration, proliferation and subsequently in fibrosis progression.

It has been shown that miR-214 is increased intracellularly during liver fibrosis [34] and that miR-214 plays a role in HSC activation promoting αSMA and FN1 production and suppressing the expression of SUFU protein [55]. We could corroborate those findings with these results as a decrease in SUFU staining and increase in αSMA and FN1 was observed in hTERT-HSC. Ma *et al.* also demonstrated using MTT assay that miR-214 promoted proliferation in HSCs and LX2 cells [55]. We could also demonstrate that miR-214 promotes proliferation and migration of HSC, supporting the hypothesis that miR-214-3p plays a role in liver injury through HSC activation, proliferation and migration.

miR-99b-5p has been shown to target mTOR and plays a role in wound healing and regulating cell proliferation and cell migration [62,63,68]. In accordance to previous findings, we demonstrate that miR-99b-5p elicited a decrease in mTOR protein. Interestingly, Turcatel *et al.* demonstrated using murine mammary gland cells that inhibition of miR-99b-5p decreased TGF-β activity by inhibiting SMAD3 phosphorylation [69], suggesting that miR-99b-5p is involved in the regulation of TGF-β signalling. Here we identified that miR-99b-5p can elicit an increase in αSMA and FN1 expression by HSC and also foster they cellular migration and proliferation [69]. Interestingly, it has been seen that rapamycin-induced repression of mTOR in hepatic progenitor cells elicited ROS generation and subsequently activated TGF-β-Smad2 signalling [70]. However, the link between miR-99a-5p, mTOR and HSC activation requires further investigation.

miR-125a-5p is released during chronic hepatitis B and serum concentrations of miR-125a-5p show a strong correlation to liver fibrosis staging [60,71]. miR-125a-5p has been shown to negatively regulate cell migration and proliferation and suppress tumor activity, through STAT3 inhibition [72,73]. It has also been shown that TGF-β was capable of inducing an upregulation of miR-125a-5p in HBV infected hepatocytes. Interestingly, downregulation of miR-125a-5p prevented activation of HSCs *in vitro* as suggested by Li *et al.* [59]. Following transfection of hTERT-HSC with miR-125a-5p, we observed no changes in αSMA expression, FN1 expression, proliferation and migration. Further investigation would be required to assess the effects miR-125a-5p may have on HSCs. It would be beneficial to identify other potential targets as we saw no decrease in STAT3. However, the transfection may not have been optimal for this miRNA and requires additional testing (*e.g.* longer transfection period, higher mimic concentrations, different mimic supplier). However, it has been shown that exceeding certain concentrations of miRNA mimics can elicit non-specific responses [74], so would need to be carried out with caution.

PHMTs were exposed to TGF-β1 in order to elicit HSC activation. We confirmed hepatocellular injury and HSC activation by decrease in albumin and increase in αSMA

staining, respectively. miRNA release was assessed in the cell culture supernatant from the first 72 h of treatment. Hepatocellular damage was confirmed by increased miR-122-5p release. We also identified that TGF-β1 exposure to the PHMTs elicited an increase in miR-214-3p and miR-199a-5p by a similar amount elicited by the cell-line based MTs. miR-99b-5p and miR-125a-5p release was also increased by the treated PHMTs.

In summary, we demonstrate using hTERT-HSC that miR-199a-5p, miR-214-3p and miR-99b-5p play a role in HSC activation and proliferation, whereas miR-125a-5p did not show any evidence of promoting HSC activation. We also confirm that these miRNAs are released by primary liver cells upon exposure to pro-fibrotic cytokine TGF-β1 are detectable from first 72 h, demonstrating that the miRNAs allow the early detection of HSC activation.

## Conclusion

In conclusion, we demonstrate the ability of the MTs to respond to both chronic and acute DILI compounds, resulting in a phenotype that corresponds to clinical data. The MTs show basal and RIF-induced CYP3A4 activity and TGF-β1 treatment induced fibrosis. We identified four miRNA biomarkers, which could be used to detect liver fibrosis, which we confirmed in both the cell line model and primary model, highlighting their suitability as *in vitro* models for assessing miRNA release during fibrosis.

Using miRNA mimics and hTERT-HSCs we were able to identify a link between three of the miRNAs (miR-199a-5p, miR-214-3p and miR-99b-5p) to HSC activation and two of the miRNAs (miR-199a-5p, miR-214-3p) to increased proliferation and migration. Finally, due to the specificity of the miRNAs and the link to HSC activation, we suggest these miRNAs could be useful contributing biomarkers to a non-invasive panel for detecting fibrosis

# Abbreviations

| | |
|---|---|
| ALP | alkaline phosphatase |
| ALT | alanine aminotransferase |
| AOP | Adverse outcome pathway |
| APAP | Acetaminophen |
| AST | aspartate aminotransferase |
| CAV1 | Caveolin-1 |
| CAV2 | Caveolin-2 |
| Col 4 | Collagen IV alpha 1 |
| Col I | Collagen I alpha 1 |
| CYP | Cytochrome P450 |
| ECM | Extracellular matrix |
| ECM | Extracellular matrix |
| FBS | Fetal bovine serum |
| FBS | fetal bovine serum |
| FN1 | Fibronectin |
| GSH | Glutathione |
| HSC | Hepatic stellate cell |
| hTERT-HSC | Immortal activated human hepatic stellate cells |
| miRNA | Micro RNA |
| mRNA | Messenger RNA |
| mTOR | Mammalian target of rapamycin |
| MTs | Microtissues |
| MTX | Methotrexate |
| NPC | Non-parenchymal cells |
| PFA | Paraformaldehyde |
| PHH | Primary human hepatocytes |
| PHMTs | Primary human microtissues |
| PMA | Phorbol 12-myristate 12-acetate |
| RIF | Rifampicin |
| STAT3 | Signal transducer and activator of transcription 3 |
| SUFU | Negative Regulator Of Hedgehog Signaling |
| TAA | Thioacetamide |
| TBL | total bilirubin |
| TGF-β1 | Transforming growth factor-β |
| TNF-α | Tumour necrosis factor alpha |
| UMI | Unique Molecular Identifiers |
| αSMA | α-smooth muscle actin |

## References


1. Bataller, R. & Brenner, D. A. Liver fibrosis. *J. Clin. Invest.* **115**, 209–218 (2005).
2. BENYON, R. & IREDALE, J. Is liver fibrosis reversible? *Gut* **46**, 443–446 (2000).
3. O'Rourke, J. M., Sagar, V. M., Shah, T. & Shetty, S. Carcinogenesis on the background of liver fibrosis: Implications for the management of hepatocellular cancer. *World J. Gastroenterol.* **24**, 4436–4447 (2018).
4. Zoubek, M. E., Trautwein, C. & Strnad, P. Reversal of liver fibrosis: From fiction to reality. *Best Pract. Res. Clin. Gastroenterol.* **31**, 129–141 (2017).
5. Trautwein, C., Friedman, S. L., Schuppan, D. & Pinzani, M. Hepatic fibrosis: Concept to treatment. *J. Hepatol.* **62**, S15–S24 (2015).
6. David, S. & Hamilton, J. P. Drug-induced Liver Injury. *US Gastroenterol. Hepatol. Rev.* **6**, 73–80 (2010).
7. Aithal, G. P. *et al.* Monitoring methotrexate-induced hepatic fibrosis in patients with psoriasis: are serial liver biopsies justified? *Aliment. Pharmacol. Ther.* **19**, 391–399 (2004).
8. Berends, M. A. M. *et al.* Reliability of the Roenigk Classification of Liver Damage After Methotrexate Treatment for Psoriasis: A Clinicopathologic Study of 160 Liver Biopsy Specimens. *Arch. Dermatol.* **143**, 1515–1519 (2007).
9. Ramachandran, A. & Jaeschke, H. Mechanisms of acetaminophen hepatotoxicity and their translation to the human pathophysiology. *J. Clin. Transl. Res.* **3**, 157–169 (2017).
10. Barker, J. *et al.* Assessment and management of methotrexate hepatotoxicity in psoriasis patients: report from a consensus conference to evaluate current practice and identify key questions toward optimizing methotrexate use in the clinic. *J. Eur. Acad. Dermatol. Venereol. JEADV* **25**, 758–764 (2011).
11. Sebastiani, G. & Alberti, A. Non invasive fibrosis biomarkers reduce but not substitute the need for liver biopsy. *World J. Gastroenterol. WJG* **12**, 3682–3694 (2006).
12. Nallagangula, K. S., Nagaraj, S. K., Venkataswamy, L. & Chandrappa, M. Liver fibrosis: a compilation on the biomarkers status and their significance during disease progression. *Future Sci. OA* **4**, (2017).
13. Lurie, Y., Webb, M., Cytter-Kuint, R., Shteingart, S. & Lederkremer, G. Z. Non-invasive diagnosis of liver fibrosis and cirrhosis. *World J. Gastroenterol.* **21**, 11567–11583 (2015).
14. Koda, M. *et al.* FibroIndex, a practical index for predicting significant fibrosis in patients with chronic hepatitis C. *Hepatol. Baltim. Md* **45**, 297–306 (2007).
15. Allan, R., Thoirs, K. & Phillips, M. Accuracy of ultrasound to identify chronic liver disease. *World J. Gastroenterol.* **16**, 3510–3520 (2010).
16. Arena, U. *et al.* Acute viral hepatitis increases liver stiffness values measured by transient elastography. *Hepatol. Baltim. Md* **47**, 380–384 (2008).
17. Bellan, M., Castello, L. M. & Pirisi, M. Candidate Biomarkers of Liver Fibrosis: A Concise, Pathophysiology-oriented Review. *J. Clin. Transl. Hepatol.* **6**, 317–325 (2018).
18. Sohel, M. H. Extracellular/Circulating MicroRNAs: Release Mechanisms, Functions and Challenges. *Achiev. Life Sci.* **10**, 175–186 (2016).
19. Arroyo, J. D. *et al.* Argonaute2 complexes carry a population of circulating microRNAs independent of vesicles in human plαSMA. *Proc. Natl. Acad. Sci.* **108**, 5003–5008 (2011).
20. Usuba, W. *et al.* Circulating miRNA panels for specific and early detection in bladder cancer. *Cancer Sci.* **110**, 408–419 (2019).

21. Chen, X. *et al.* Characterization of microRNAs in serum: a novel class of biomarkers for diagnosis of cancer and other diseases. *Cell Res.* **18**, 997–1006 (2008).
22. Noferesti, S. S. *et al.* Controlled ovarian hyperstimulation induced changes in the expression of circulatory miRNA in bovine follicular fluid and blood plαSMA. *J. Ovarian Res.* **8**, 81 (2015).
23. Weber, J. A. *et al.* The MicroRNA Spectrum in 12 Body Fluids. *Clin. Chem.* **56**, 1733–1741 (2010).
24. Starkey Lewis, P. J. *et al.* Circulating microRNAs as potential markers of human drug-induced liver injury. *Hepatol. Baltim. Md* **54**, 1767–1776 (2011).
25. Schueller, F. *et al.* The Role of miRNAs in the Pathophysiology of Liver Diseases and Toxicity. *Int. J. Mol. Sci.* **19**, (2018).
26. Waidmann, O. *et al.* Serum microRNA-122 levels in different groups of patients with chronic hepatitis B virus infection. *J. Viral Hepat.* **19**, e58–e65 (2012).
27. Yamada, H. *et al.* Associations between circulating microRNAs (miR-21, miR-34a, miR-122 and miR-451) and non-alcoholic fatty liver. *Clin. Chim. Acta* **424**, 99–103 (2013).
28. Howell, L. S., Ireland, L., Park, B. K. & Goldring, C. E. MiR-122 and other microRNAs as potential circulating biomarkers of drug-induced liver injury. *Expert Rev. Mol. Diagn.* **18**, 47–54 (2018).
29. Kia, R. *et al.* MicroRNA-122: a novel hepatocyte-enriched in vitro marker of drug-induced cellular toxicity. *Toxicol. Sci. Off. J. Soc. Toxicol.* **144**, 173–185 (2015).
30. Carroll, E. E. *et al.* Utility of Serum miR-122, Liver Enzymes, and Hepatic Histopathology in Response to Hepatotoxicants in Sprague-Dawley Rats. *Toxicol. Pathol.* **46**, 835–846 (2018).
31. Krauskopf, J. *et al.* Serum microRNA signatures as 'liquid biopsies' for interrogating hepatotoxic mechanisms and liver pathogenesis in human. *PLoS ONE* **12**, (2017).
32. Messner, C. J. *et al.* Exosomal microRNAs Release as a Sensitive Marker for Drug-Induced Liver Injury In Vitro. *Appl. Vitro Toxicol.* **6**, 77–89 (2020).
33. Norona, L. M. *et al.* Bioprinted liver provides early insight into the role of Kupffer cells in TGF-β1 and methotrexate-induced fibrogenesis. *PLOS ONE* **14**, e0208958 (2019).
34. Devaraj Ezhilarasan. Role of MicroRNAs in Hepatic Fibrosis Progression. *J. Appl. Pharm. Sci.* (2018) doi:10.7324/JAPS.2018.8524.
35. Loosen, S. H., Schueller, F., Trautwein, C., Roy, S. & Roderburg, C. Role of circulating microRNAs in liver diseases. *World J. Hepatol.* **9**, 586–594 (2017).
36. Iacob, D. G., Rosca, A. & Ruta, S. M. Circulating microRNAs as non-invasive biomarkers for hepatitis B virus liver fibrosis. *World J. Gastroenterol.* **26**, 1113 (2020).
37. Prestigiacomo, V., Weston, A., Messner, S., Lampart, F. & Suter-Dick, L. Pro-fibrotic compounds induce stellate cell activation, ECM-remodelling and Nrf2 activation in a human 3D-multicellular model of liver fibrosis. *PLOS ONE* **12**, e0179995 (2017).
38. Suter-Dick, L. *et al.* Combining Extracellular miRNA Determination with Microfluidic 3D Cell Cultures for the Assessment of Nephrotoxicity: a Proof of Concept Study. *AAPS J.* **20**, 86 (2018).
39. Ravenscroft, S. M., Pointon, A., Williams, A. W., Cross, M. J. & Sidaway, J. E. Cardiac Non-myocyte Cells Show Enhanced Pharmacological Function Suggestive of Contractile Maturity in Stem Cell Derived Cardiomyocyte Microtissues. *Toxicol. Sci.* **152**, 99–112 (2016).
40. Zhou, S., Chan, E., Li, X. & Huang, M. Clinical outcomes and management of mechanism-based inhibition of cytochrome P450 3A4. *Ther. Clin. Risk Manag.* **1**, 3–13 (2005).

41. Ueyama, T., Tsuji, S., Sugiyama, T. & Tada, M. Fluorometric evaluation of CYP3A4 expression using improved transgenic HepaRG cells carrying a dual-colour reporter for CYP3A4 and CYP3A7. *Sci. Rep.* **7**, 2874 (2017).
42. Berger, B. *et al*. Comparison Of Liver Cell Models Using The Basel Phenotyping Cocktail. *Front. Pharmacol*. **7**, (2016).
43. Mandon, M., Huet, S., Dubreil, E., Fessard, V. & Hégarat, L. L. Three-dimensional HepaRG spheroids as a liver model to study human genotoxicity in vitro with the single cell gel electrophoresis assay. *Sci. Rep*. **9**, 1–9 (2019).
44. Levitt, D. G. & Levitt, M. D. Human serum albumin homeostasis: a new look at the roles of synthesis, catabolism, renal and gastrointestinal excretion, and the clinical value of serum albumin measurements. *Int. J. Gen. Med.* **9**, 229–255 (2016).
45. Lübberstedt, M. *et al.* HepaRG human hepatic cell line utility as a surrogate for primary human hepatocytes in drug metabolism assessment in vitro. *J. Pharmacol. Toxicol. Methods* **63**, 59–68 (2011).
46. Horvat, T. *et al.* Adverse outcome pathway development from protein alkylation to liver fibrosis. *Arch. Toxicol.* **91**, 1523–1543 (2017).
47. Nelson, L. J. *et al.* Human Hepatic HepaRG Cells Maintain an Organotypic Phenotype with High Intrinsic CYP450 Activity/Metabolism and Significantly Outperform Standard HepG2/C3A Cells for Pharmaceutical and Therapeutic Applications. *Basic Clin. Pharmacol. Toxicol*. **120**, 30–37 (2017).
48. Hinson, J. A., Roberts, D. W. & James, L. P. Mechanisms of Acetaminophen-Induced Liver Necrosis. *Handb. Exp. Pharmacol.* 369–405 (2010) doi:10.1007/978-3-642-00663-0_12.
49. Bell, C. C. *et al*. Comparison of Hepatic 2D Sandwich Cultures and 3D Spheroids for Long-term Toxicity Applications: A Multicenter Study. *Toxicol. Sci*. **162**, 655–666 (2018).
50. Leite, S. B. *et al*. Novel human hepatic organoid model enables testing of drug-induced liver fibrosis in vitro. *Biomaterials* **78**, 1–10 (2016).
51. Kim, J. *et al*. Recapitulation of methotrexate hepatotoxicity with induced pluripotent stem cell-derived hepatocytes from patients with rheumatoid arthritis. *Stem Cell Res. Ther.* **9**, (2018).
52. Roy, S., Benz, F., Luedde, T. & Roderburg, C. The role of miRNAs in the regulation of inflammatory processes during hepatofibrogenesis. *Hepatobiliary Surg. Nutr.* **4**, 24–33 (2015).
53. Murakami, Y. *et al.* The Progression of Liver Fibrosis Is Related with Overexpression of the miR-199 and 200 Families. *PLoS ONE* **6**, e16081 (2011).
54. Mungunsukh, O. & Day, R. M. Transforming growth factor-β1 selectively inhibits hepatocyte growth factor expression via a micro-RNA-199-dependent posttranscriptional mechanism. *Mol. Biol. Cell* **24**, 2088–2097 (2013).
55. Ma, L. *et al.* MicroRNA-214 promotes hepatic stellate cell activation and liver fibrosis by suppressing Sufu expression. *Cell Death Dis.* **9**, 718 (2018).
56. Iizuka, M. *et al.* Induction of microRNA-214-5p in human and rodent liver fibrosis. *Fibrogenesis Tissue Repair* **5**, 12 (2012).
57. Okada, H. *et al*. Inhibition of microRNA-214 ameliorates hepatic fibrosis and tumor incidence in platelet-derived growth factor C transgenic mice. *Cancer Sci*. **106**, 1143–1152 (2015).
58. Coppola, N. *et al*. Correlation Between the Hepatic Expression of Human MicroRNA hsa-miR-125a-5p and the Progression of Fibrosis in Patients With Overt and Occult HBV Infection. *Front. Immunol.* **9**, 1334 (2018).

59. Li, G. *et al.* MicroRNA-125a-5p Contributes to Hepatic Stellate Cell Activation through Targeting FIH1. *Cell. Physiol. Biochem. Int. J. Exp. Cell. Physiol. Biochem. Pharmacol.* **38**, 1544–1552 (2016).
60. Oura, K. *et al.* Serum microRNA-125a-5p as a potential biomarker of HCV-associated hepatocellular carcinoma. *Oncol. Lett.* **18**, 882–890 (2019).
61. Estep, M. *et al.* Differential expression of miRNAs in the visceral adipose tissue of patients with non-alcoholic fatty liver disease. *Aliment. Pharmacol. Ther.* **32**, 487–497 (2010).
62. Jin, Y. *et al.* MicroRNA-99 Family Targets AKT/mTOR Signaling Pathway in Dermal Wound Healing. *PLOS ONE* **8**, e64434 (2013).
63. Cao, F., Liu, T., Sun, S. & Feng, S. The role of the miR-99b-5p/mTOR signaling pathway in neuroregeneration in mice following spinal cord injury. *Mol. Med. Rep.* **16**, 9355–9360 (2017).
64. O'Reilly, S. MicroRNAs in fibrosis: opportunities and challenges. *Arthritis Res. Ther.* **18**, (2016).
65. Yang, X. *et al*. Twist1-induced miR-199a-3p promotes liver fibrosis by suppressing caveolin-2 and activating TGF-β pathway. *Signal Transduct. Target. Ther.* **5**, 1–12 (2020).
66. Lino Cardenas, C. L. *et al.* miR-199a-5p Is Upregulated during Fibrogenic Response to Tissue Injury and Mediates TGFbeta-Induced Lung Fibroblast Activation by Targeting Caveolin-1. *PLoS Genet*. **9**, (2013).
67. Wang, Q. *et al.* Overview of microRNA-199a Regulation in Cancer. *Cancer Manag. Res.* **11**, 10327–10335 (2019).
68. Zhang, Y., Huang, B., Wang, H.-Y., Chang, A. & Zheng, X. F. S. Emerging Role of MicroRNAs in mTOR Signaling. *Cell. Mol. Life Sci.* **74**, 2613–2625 (2017).
69. Turcatel, G., Rubin, N., El-Hashash, A. & Warburton, D. MIR-99a and MIR-99b Modulate TGF-β Induced Epithelial to Mesenchymal Plasticity in Normal Murine Mammary Gland Cells. *PLoS ONE* **7**, (2012).
70. Wu, Y. *et al*. Rapamycin Upregulates Connective Tissue Growth Factor Expression in Hepatic Progenitor Cells Through TGF-β-Smad2 Dependent Signaling. *Front. Pharmacol.* **9**, (2018).
71. Zheng, J. *et al*. Serum microRNA-125a-5p, a useful biomarker in liver diseases, correlates with disease progression. *Mol. Med. Rep.* **12**, 1584–1590 (2015).
72. Wang, G., Mao, W., Zheng, S. & Ye, J. Epidermal growth factor receptor-regulated miR-125a-5p – a metastatic inhibitor of lung cancer. *FEBS J.* **276**, 5571–5578 (2009).
73. Zhong, L. *et al*. MicroRNA-125a-5p plays a role as a tumor suppressor in lung carcinoma cells by directly targeting STAT3. *Tumour Biol. J. Int. Soc. Oncodevelopmental Biol. Med.* **39**, 1010428317697579 (2017).
74. Jin, H. Y. *et al.* Transfection of microRNA Mimics Should Be Used with Caution. *Front. Genet.* **6**, (2015).

# Figures

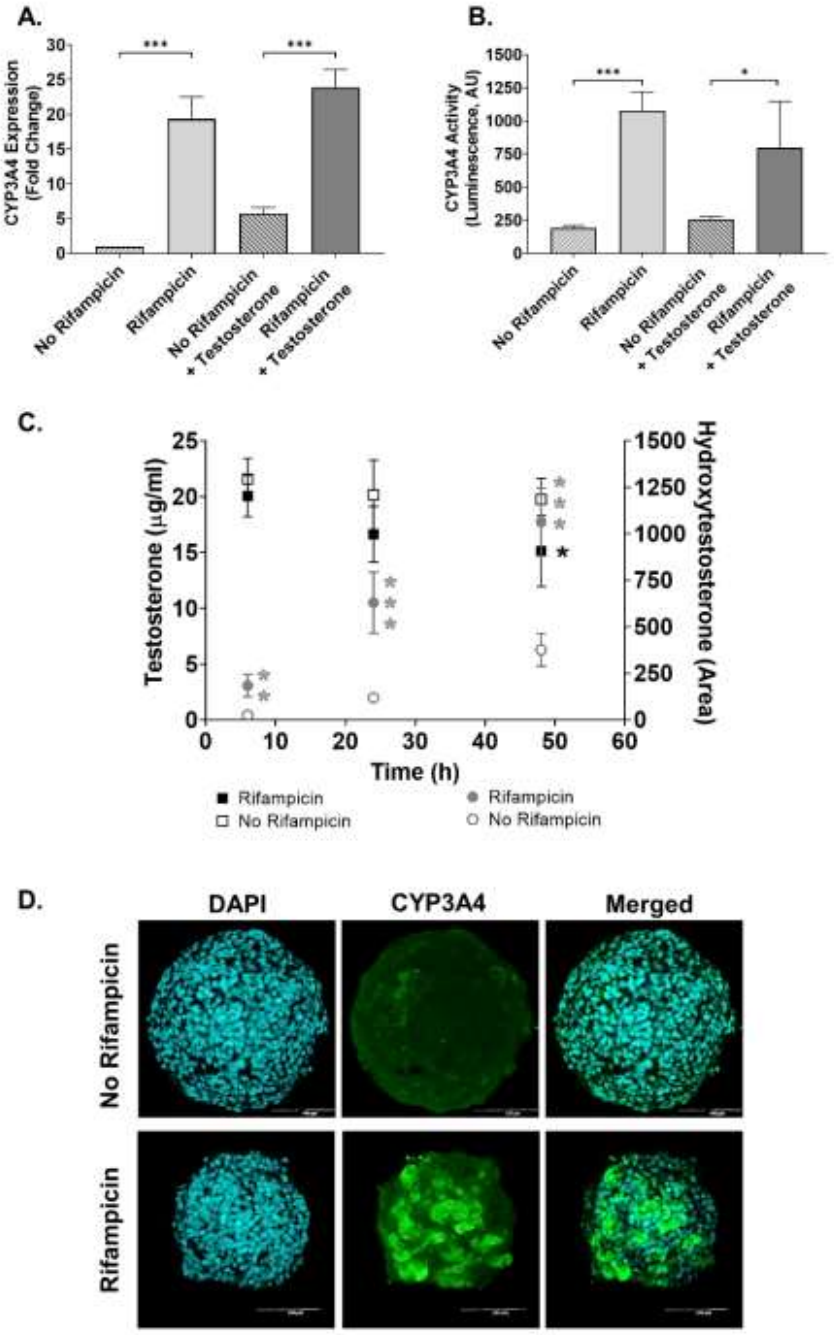


**Figure 1: Characterisation of CYP3A4 Activity in 3D human liver MTs**
MTs were exposed to 20 µM Rifampicin (RIF) and RIF treated and untreated MTs were exposed to 25 µg/ml testosterone for a further 48 hrs. CYP3A4 activity was measured by P450-GloTM CYP3A4 assay and expressed in luminescence arbitrary units (AU); N = 3 biological and 3 technical replicates (A). Expression of CYP3A4 determined by q-RT-PCR, expressed as fold change in comparison with the control; N = 1 biological and 3 technical replicates (B). Conversion of testosterone (25 µg/ml) into hydroxytestosterone (OH-testosterone) at 6, 24 and 48 h was determined by HPLC-MS/MS. Data are expressed as concentrations (µg/ml) calculated using a testosterone calibration curve. Area under the curve in arbitrary units (AU) was used for calculating OH-Testosterone; N = 2 biological and 3 technical replicates (C). Representative image of immunohistochemical detection of CYP3A4, scale bar = 100 µm (D). Bargraphs represent means ± SD; statistical analysis based on Students unpaired T Test; Boxplot represents means ± SD; statistical analysis based on Students unpaired T Test for Rifampicin v.s No Rifampicin for each timepoint *, $P \leq 0.05$; **, $P \leq 0.01$; ***, $P \leq 0.001$.

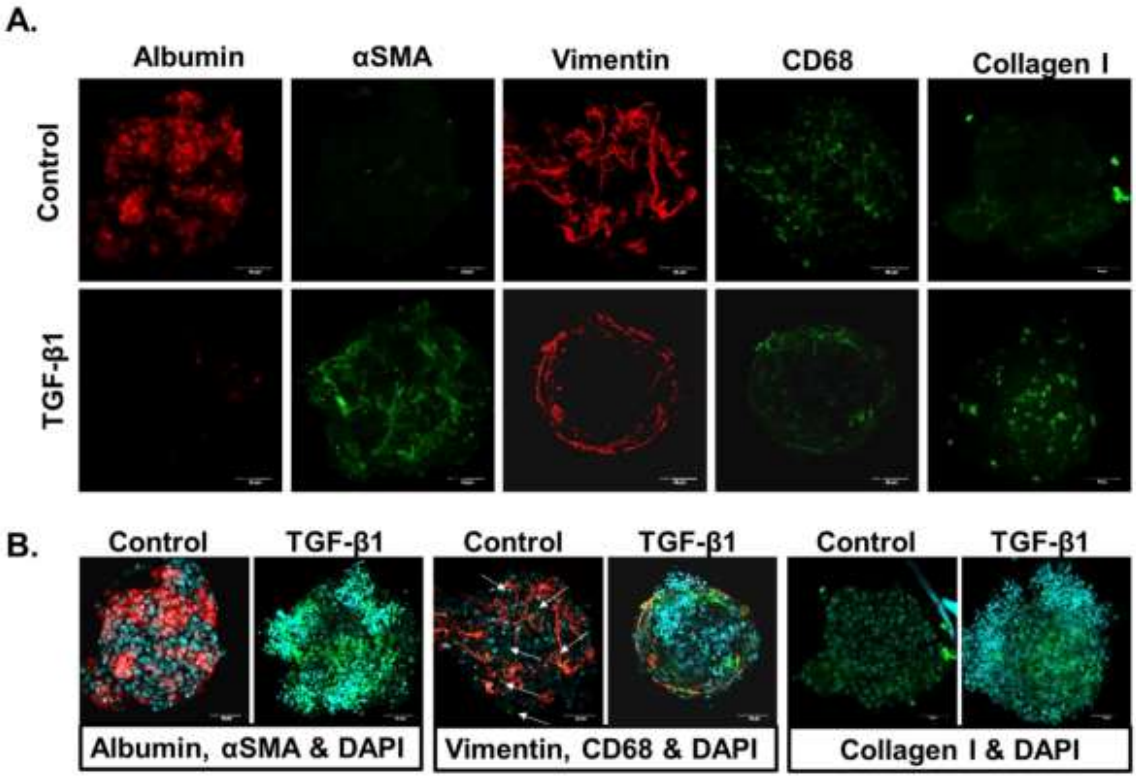


**Figure 2: TGF-β1 induces fibrosis in human liver MTs.**
MTs were exposed to 1 ng/ml TGF-β1 for 10 days which was refreshed every 2-3 days. The MTs were fixed and stained to demonstrate localisation of the three cell types: HepaRG cells stain positive for albumin; hTERT-HSC stain positive for aSMA and vimentin; THP-1 stain positive for CD68 and vimentin. HSC activation and ECm deposition were shown through increased aSMA and collagen I staining, respectively. Images are shown as a maximum intensity projection for each staining (A) and the merged images with DAPI with and without TGF- β1 exposure (B) Arrows identify THP-1 as these cells are positive for both CD68 and vimentin (B).

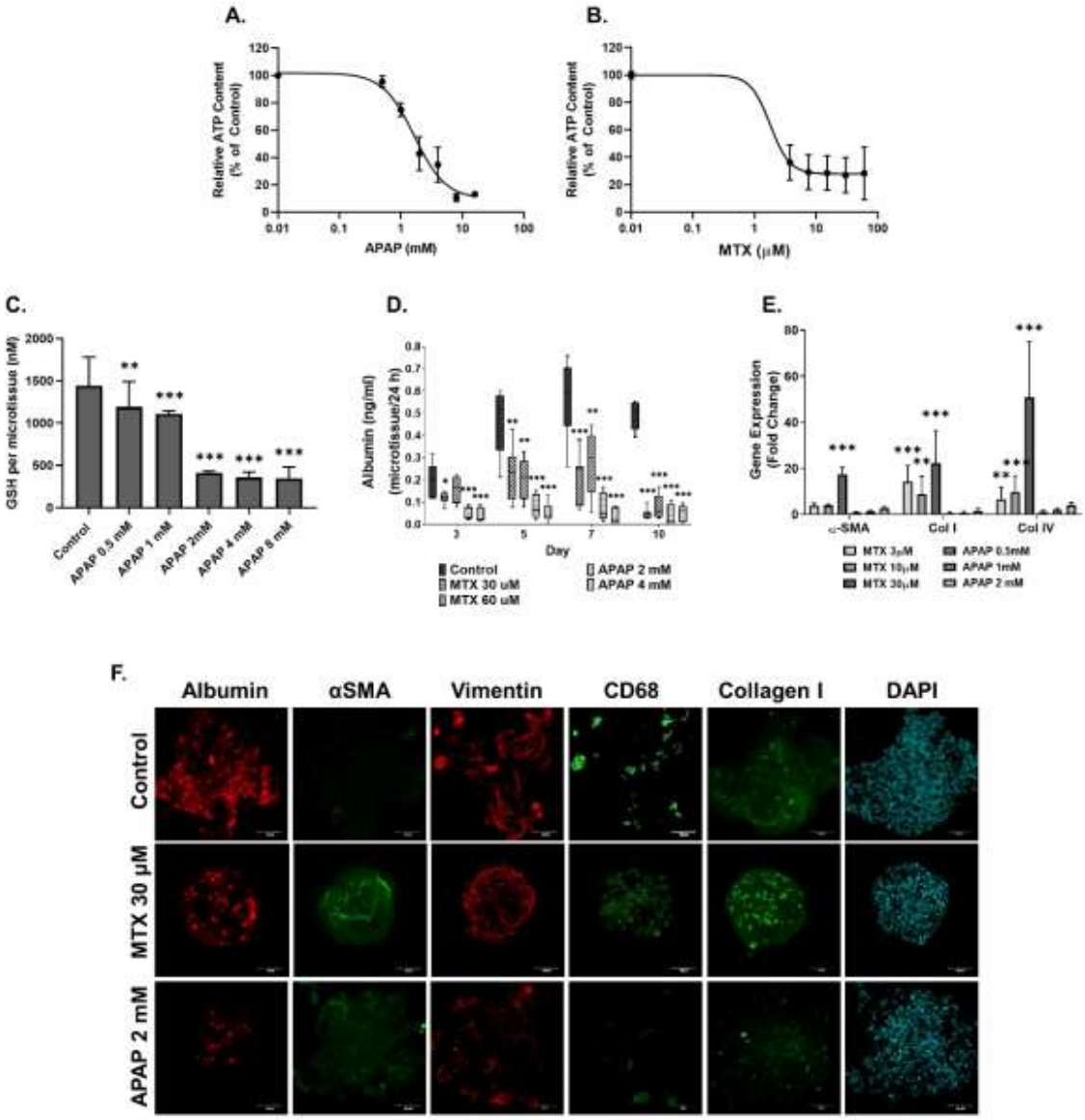


**Figure 3: MTX & APAP elicit compound-specific responses in human liver MTs**
MTs were exposed to MTX and APAP for 10 days, which was refreshed every 2-3 days. Viability was assessed for APAP (A) and MTX (B) treated MTs using the CellTiterGlo luminescence kit and expressed as relative ATP content (% of control), N= 3 biological and 3 technical replicates. IC50 for APAP was calculated to be 1.7 ± 0.38 mM but IC50 for MTX was not able to be calculated accurately. GSH was measured using GSH-Glo™ Assay for APAP treated MTs, N= 3 biological and 3 technical replicates. (C). Albumin release was measured for treated MTs using albumin ELISA, N= 3 biological and 3 technical replicates (D). Gene expression of aSMA, Col I and Col IV was measured using q-RT-PCR in treated MT samples. N= 2 biological and 3 technical replicates (E). MTs were fixed and stained for albumin, aSMA, vimentin and CD68. HSC activation and ECM deposition was shown through increased aSMA and collagen I staining, respectively. Images are shown as a maximum intensity projection for each staining (F). Bargraphs and boxplots represent means ± SD; statistical analysis based on One-way ANOVA (C) and Students unpaired T Test (D & E); *, P ≤ 0.05; **, P ≤ 0.01; ***, P ≤ 0.001.

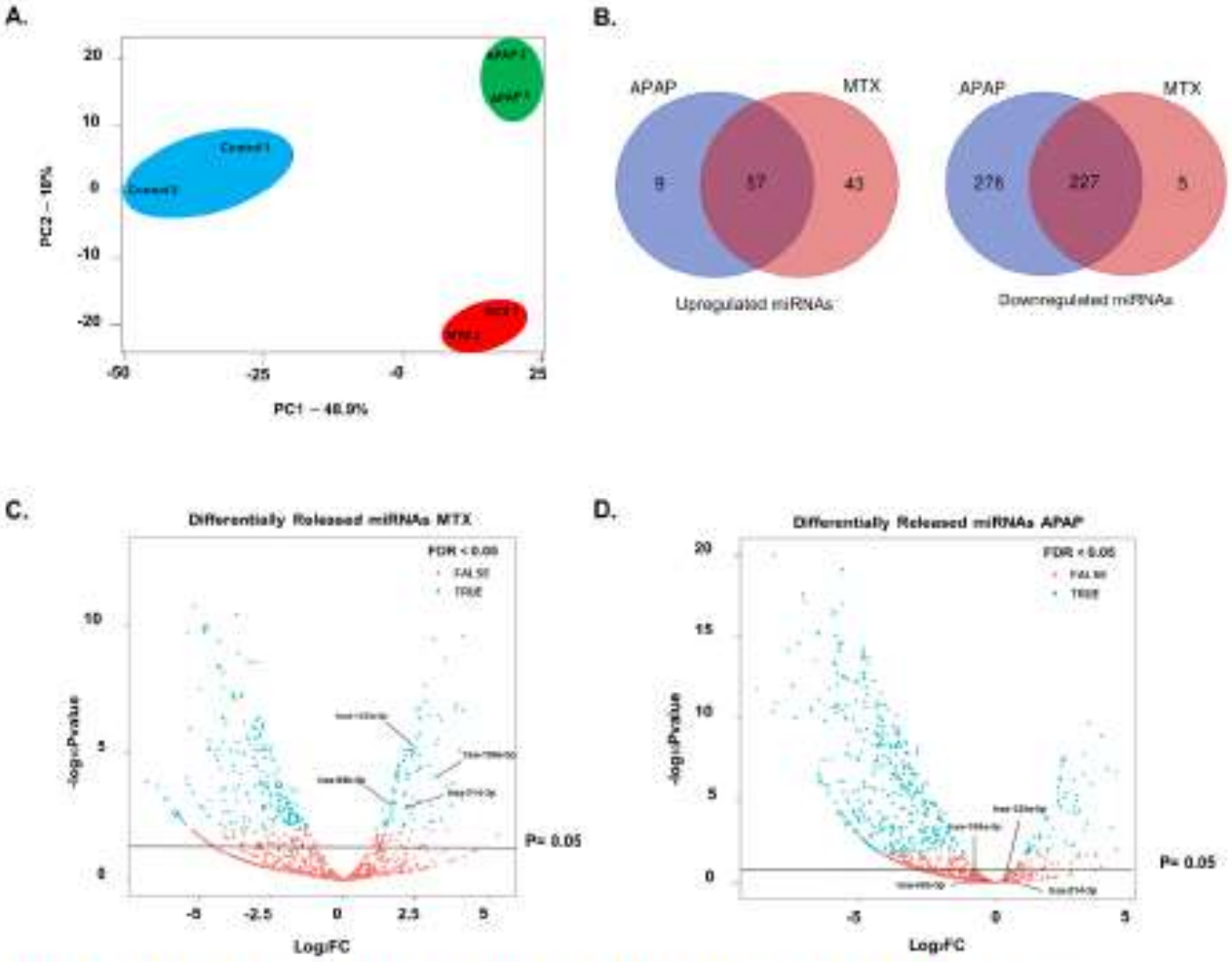


**Figure 4: Using NGS to investigate miRNAs released by MTs treated with MTX & APAP**
Cell culture supernatant from MTs exposed to MTX and APAP for 10 days were collected to perform miRNA analysis using NGS. PCA analysis of differentially released miRNAs was carried out using R as described in methods section (A). NGS demonstrated that MTX and APAP differentially released miRNAs. Venn diagram result show that release was increased for 57 miRNAs decreased for 225 common between the treatments (B) Four of the MTX-specific miRNAs were chosen based on literature search and volcano plots for MTX (D) and APAP (E) demonstrate the release of the four miRNAs (miR-199a-5p, mIR-214-3p, miR-125a-5p, miR-99b-5p) is significantly increased by MTX treatment but not APAP.

**Table 5.Literature used for miRNA selection**

| miRNA | *in vitro* | *in vivo* | Clinical | Target | Publications |
|---|---|---|---|---|---|
| **miR-199a-5p** | 1. Increased in activated stellate cells.<br>2. Mimic resulted in increased HSC activation.<br>3. AntagomiR decreased HSC activation. | 1. Links to lung fibrosis.<br>2. Intracellular miR-199a levels correlate with liver fibrosis development.<br>3. miR-199a is linked to ECM synthesis in CCl4 treated mice. | 1. Increased in human fibrotic liver samples.<br>2. Intracellular levels correlate with liver fibrosis development. | CAV-1/-2 | Cardenas et al., 2013<br>Yang et al., 2020<br>Ezhilarasan, 2018.<br>Roy et al., 2015 |
| **miR-214-3p** | 1. Intracellular miR-214 promotes HSC activation.<br>2. Reduction in intracellular miR-214 ameloriates liver fibrosis. | 1. Knockdown of intracellular miR-214 results in enhanced Sufu and decreased liver fibrosis.<br>2. Upregulated intracellular miR-214 is overexpressed in mouse models resulting in liver fibrosis. | 1. Intracellular miR-214 is linked to HCV induced liver fibrosis.<br>2. Circulating miR-214 decreases in APAP overdose patients. | SUFU | Ma et al., 2018<br>Ezhilarasan, 2018.<br>Krauskopf et al., 2017 |
| **miR-125a-5p** | 1. Intracellular miR-125a is shown to be upregulated in activated HSCs. | 1. miR-125a expression was increased in mouse livers with CCL4 induced fibrosis. | 1. Intracellular miR-125a linked to liver fibrosis from HBV infection.<br>2. Circulating miR-125a is linked to HCC. | STAT3<br>FIH1 | Coppola et al., 2018<br>Oura et al., 2019<br>Li et al., 2016 |
| **miR-99b-5p** | 1. miR-99b expression is linked to dermal wound healing response *using in vitro* models.<br>2. Involved in regulating cell proliferation and cell migration. | 1. miR-99b expression in mice is linked to dermal wound healing response.<br>2. miR-99b expression linked to spinal cord regeneration. | 1. Expression of miR-99b is significantly associated with pericellular fibrosis from NAFLD. | mTOR | Estep et al., 2010<br>Jin et al., 2013<br>Cao et al., 2017 |

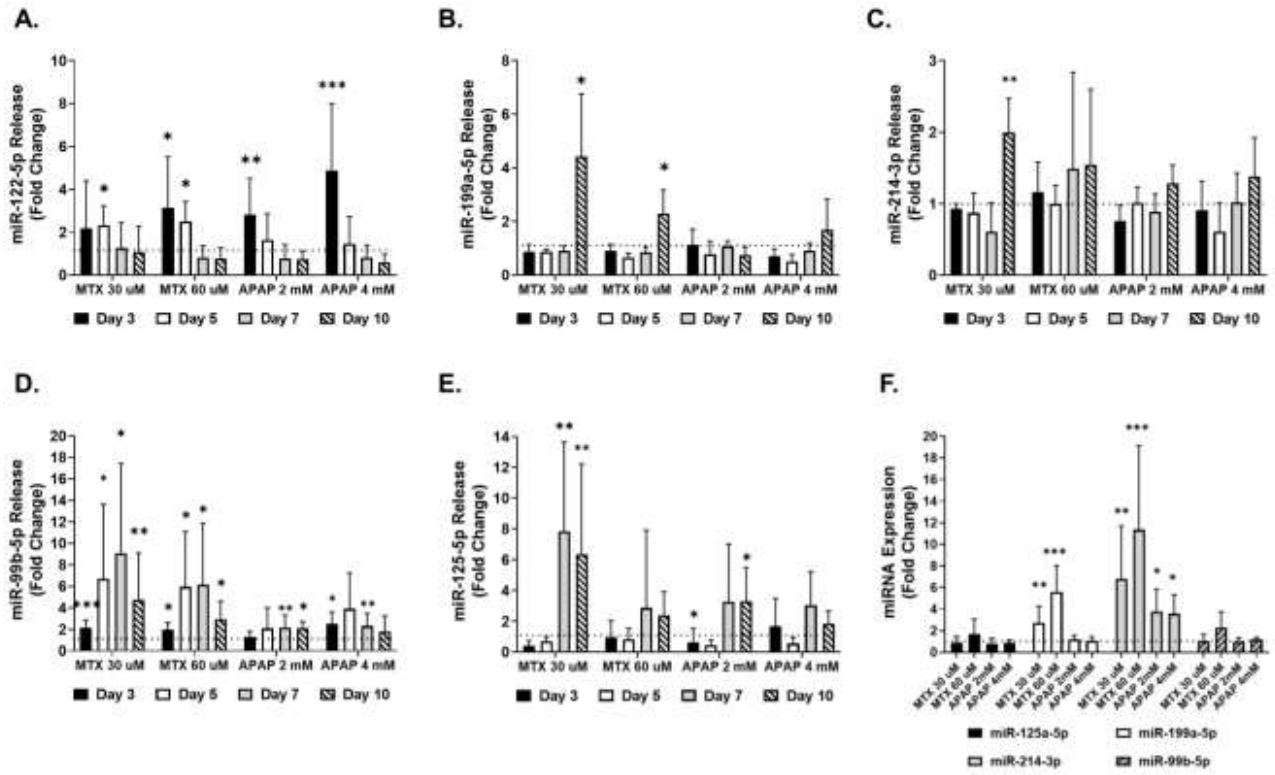


**Figure 5: miRNA corroboration using q-RT-PCR**

MTs were exposed MTX or APAP for 10 days and cell culture supernatant was collected to investigate miRNA release using q-RT-PCR. Release of miR-122-5p (A), miR-199a-5p (B), miR-214-3p (C), miR-99b-5p (D) and miR-125a-5p (E) were measured at day 3, day 5 day 7 and day 10 and analysed using q-RT-PCR. miRNA was also measured intracellularly to assess changes in miR-125a-5p, miR-199a-5p, miR-214-3p and miR-99b-5p expression (F). Data are expressed as fold change, N= 2 biological and 3 replicates for B and F, whereas, N= 3 biological and 3 replicates for A, C, D and E. Bargraphs represent means ± SD; statistical analysis based on Students unpaired T Test; *, $P \leq 0.05$; **, $P \leq 0.01$; ***, $P \leq 0.001$.

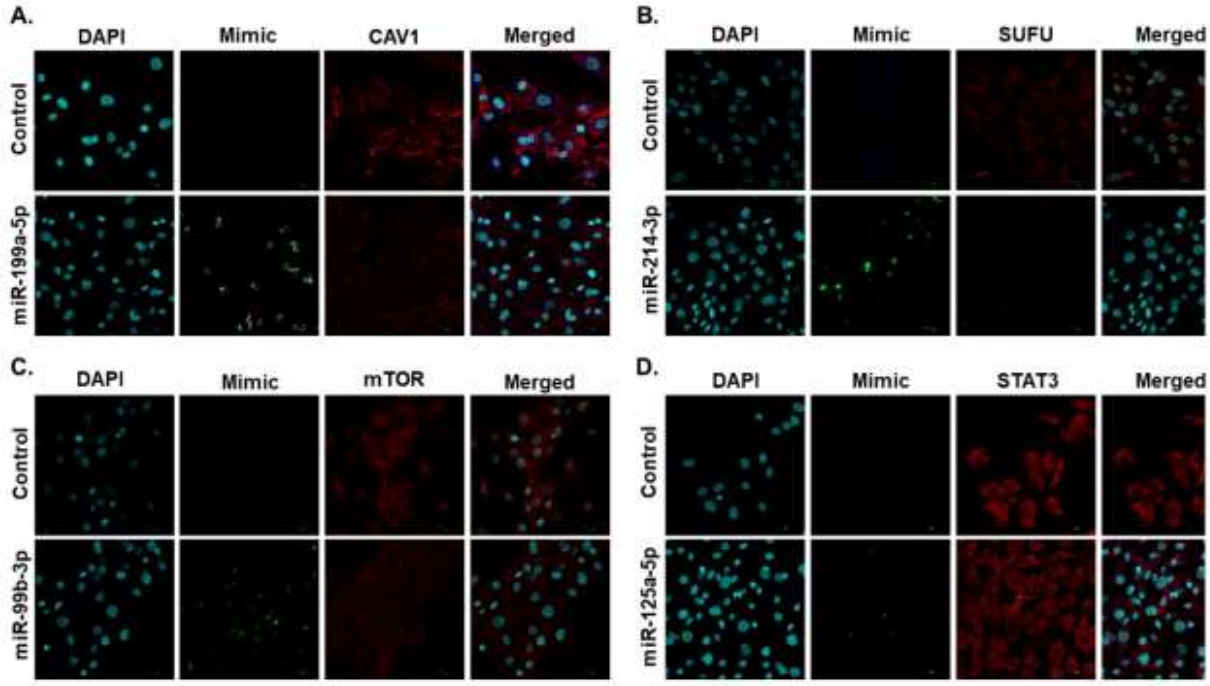


**Figure 6: Identification of potential targets of the four selected miRNAs**
Transfected hTERT-HSC with miRNA mimics were fixed at 72 h and 96 h. Potential targets CAV1 (miR-199a-5p), SUFU (miR-214-3p), mTOR (miR-99b-5p) and STAT3 (miR-125a-5p) were assessed. At 72 h we demonstrate that CAV1 was decreased by miR-199a-5p (A). At 96 h SUFU and mTOR were decreased by miR-214-3p and miR-99b-5p, respectively (B, C). At 96 h no effect was seen on STAT3 demonstrating miR-125a-5p had no inhibitory effect (D).

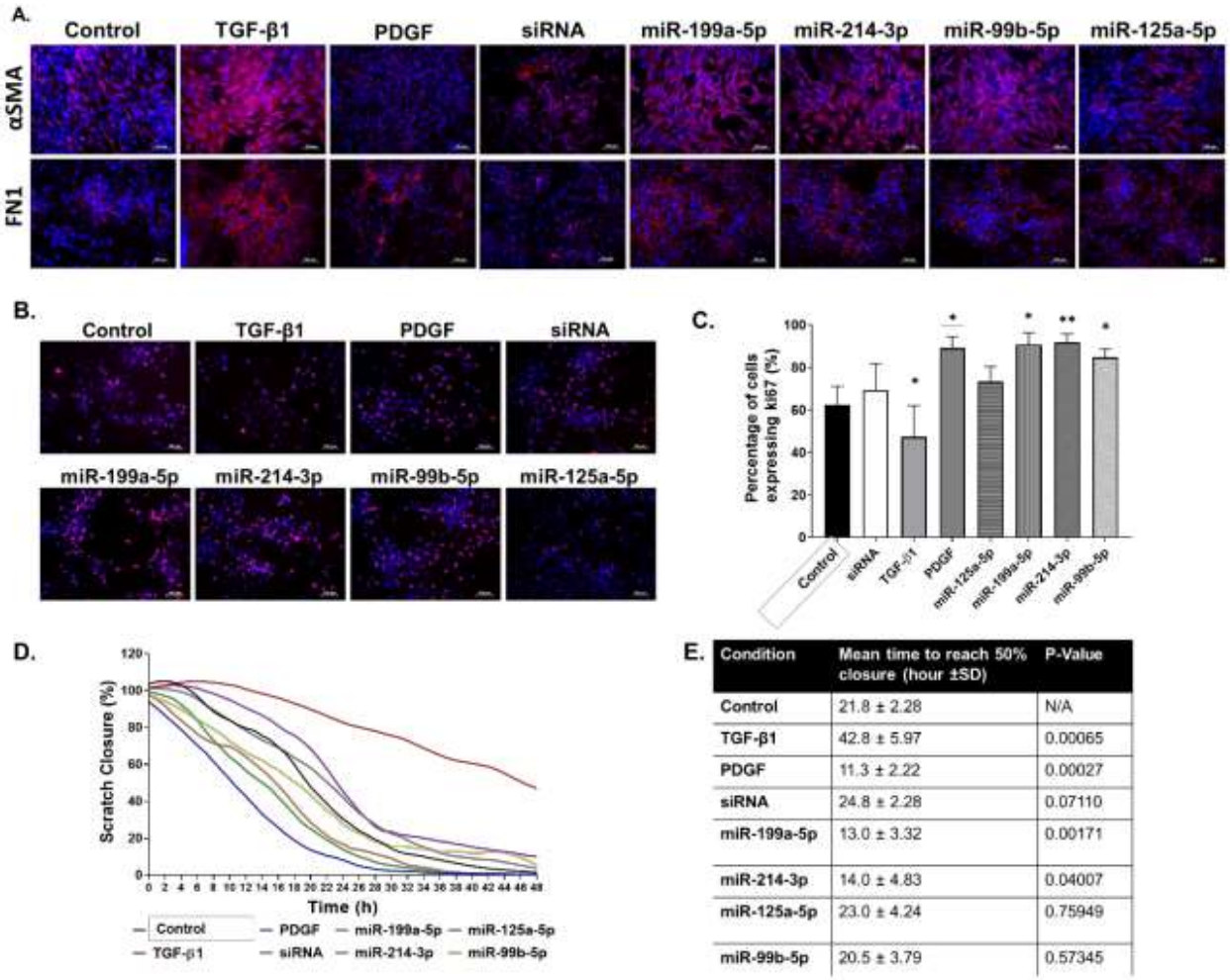


E.

| Condition | Mean time to reach 50% closure (hour ±SD) | P-Value |
|---|---|---|
| Control | 21.8 ± 2.28 | N/A |
| TGF-β1 | 42.8 ± 5.97 | 0.00065 |
| PDGF | 11.3 ± 2.22 | 0.00027 |
| siRNA | 24.8 ± 2.28 | 0.07110 |
| miR-199a-5p | 13.0 ± 3.32 | 0.00171 |
| miR-214-3p | 14.0 ± 4.83 | 0.04007 |
| miR-125a-5p | 23.0 ± 4.24 | 0.75949 |
| miR-99b-5p | 20.5 ± 3.79 | 0.57345 |

**Figure 7: miR-199a-5p, miR-214-3p and miR-99b-5p elicit hTERT-HSC activation**
aSMA and FN1 staining was carried to investigate the potential of the 4 miRNA mimics to elicit HSC activation which were compared to positive control TGF-β1 (A). Proliferation was assessed using ki67 staining, which was quantified on ImageJ (B & C). Migration was assessed using a mgration assay that was imaged every h over 48 h and quantified using ImageJ to assess the speed of wound closure (D). The time for each condition to reach 50% wound closure was assessed to calculate significance between migration capacities for each condition. N= 2 biological repeats of 2-3 replicates (E). Students unpaired T Test; *, P ≤ 0.05; **, P ≤ 0.01; ***, P ≤ 0.001

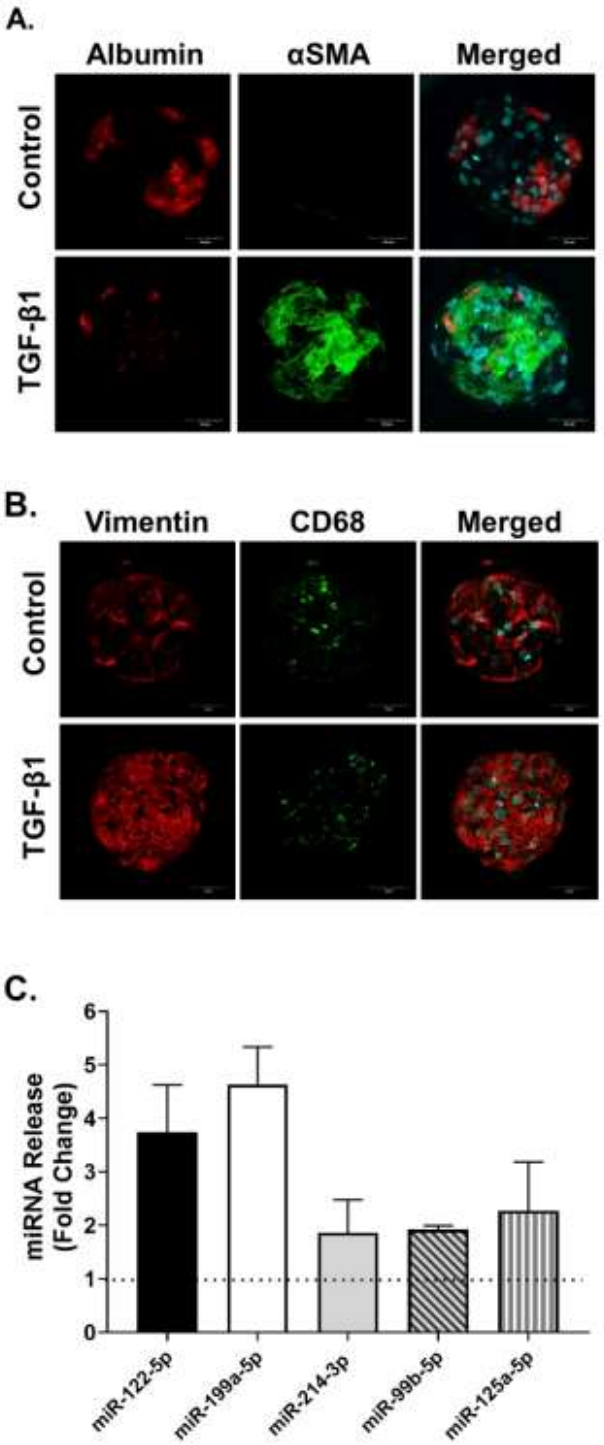


**Figure 8: Measurement of miRNAs in Primary MTs exposed to TGF-β1**
Primary MTs were exposed to TGF-β1 for 3-10 days. Primary MTs were fixed at day 10 and stained for co-stained for αSMA and albumin (A) or vimentin and CD68 (B). Cell culture supernatant was collected at 72 h to investigate miRNA release of primary MTs exposed to TGF-β1 using q-RT-PCR. miRNAs measured included: miR-122-5p, miR-199a-5p, miR-214-3p, miR-99b-5p and miR-125a-5p were measured at day 3, day 5 day 7 and day 10 and analysed using q-RT-PCR (C). Data are expressed as fold change, N= 1 biological and 3 replicates.
**Figure S1.**

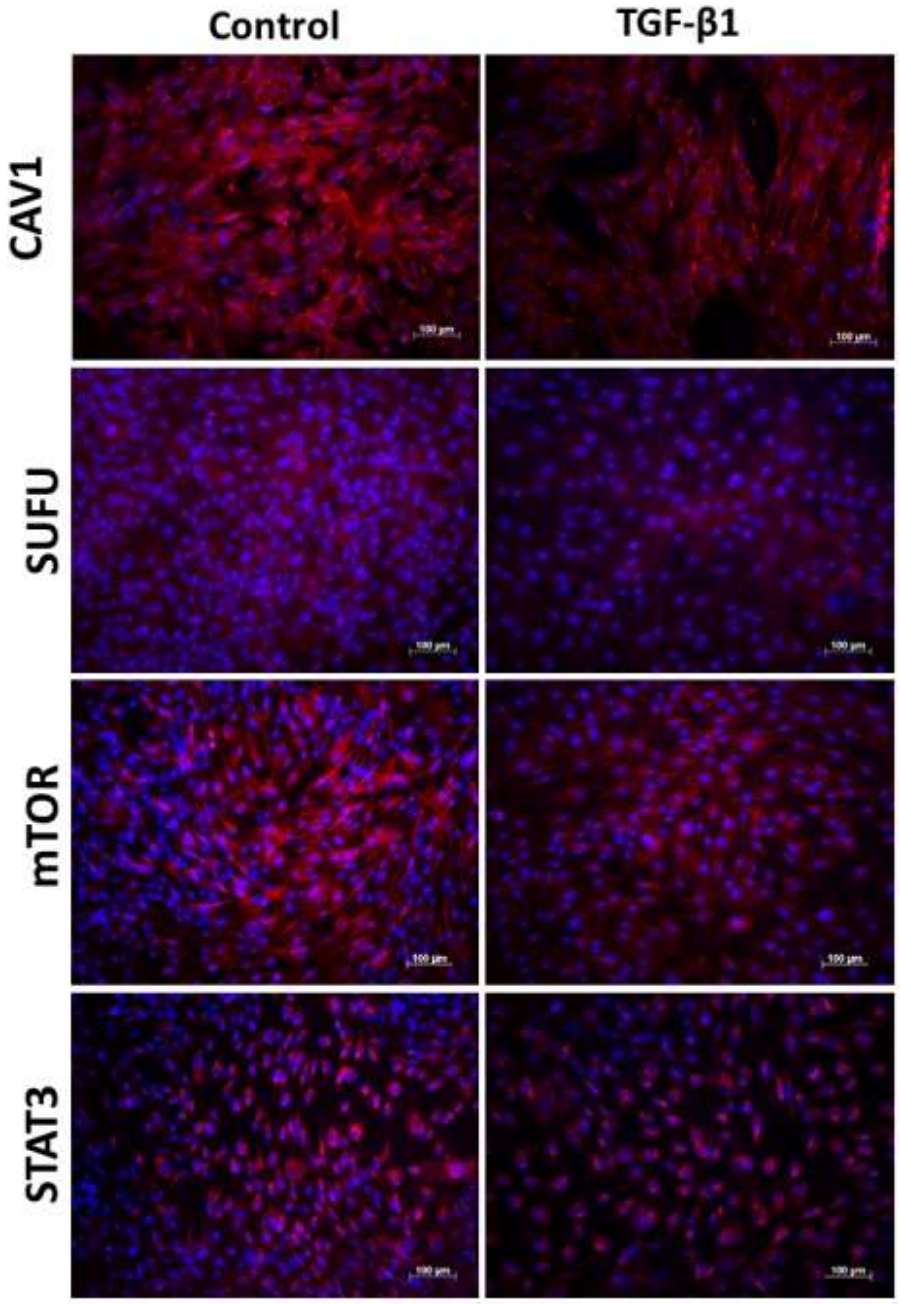


**Figure S1: Effects of TGF-β1 on miRNA targets CAV1, SUFU, mTOR & STAT3**
hTERT-HSC were exposed to TGF-β1 for 72 hrs, fixed and stained for CAV1, SUFU, mTOR, STAT3. TGF-β1 appears to elicit a decrease in CAV1, SUFU and mTOR protein. No effect was seen in STAT3 protein. However, further confirmation and quantification is required.

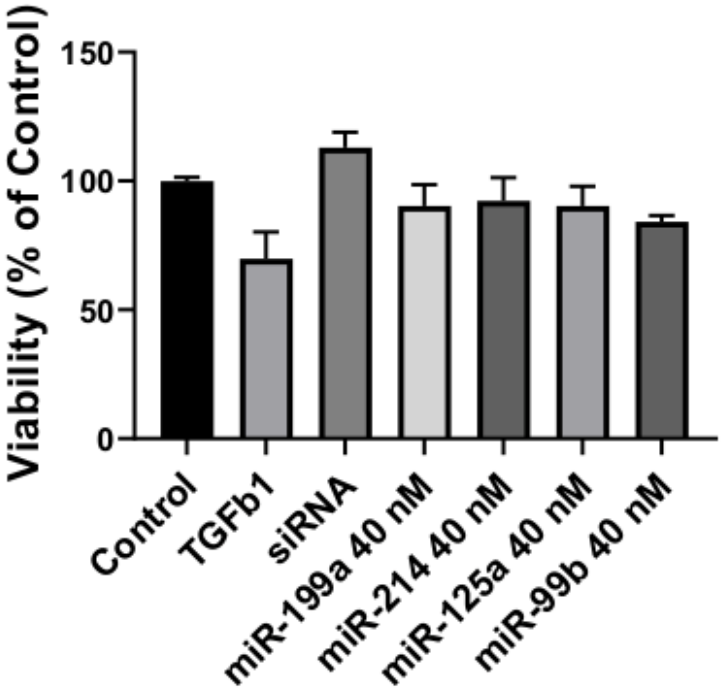


**Figure S2: Viability of transfected cells**
hTERT-HSC were transfected or exposed to TGF-β1 for 72 hrs. Viability was measured using CCK-8 assay and expressed at % relative to the control.

## 4.7 Conclusion

The research goal addressed in project 1 was to assess the potential of miRNAs as biomarkers of liver toxicity *in vitro*, with a specific focus on early detection of hepatic fibrosis. Moreover, the functional involvement of selected miRNAs in the activation of the HSC was also investigated.

In the first paper (Messner *et al.* Applied *In vitro* Toxicology, 2020) miRNAs were extracted from cell culture supernatant from HepaRG cells grown in 3D culture conditions upon exposure to chronic DILI compound MTX and acute DILI compound APAP. We confirm that HepaRG are a suitable model for assessing DILI due to their response to the compounds and to the maintenance of some key hepatocyte functions in the 3D-culture, namely stable viability, albumin release and CYP3A4 activity. Our data show that HepaRG in 3D have basal and rifampicin induced CYP3A4 activity. We also demonstrate that the ability of HepaRG to metabolise testosterone in 3D-cultures exceeds that of 2D cultures. In HepaRG MTs, APAP-induced toxicity resulted in increased release (exosome isolation and total extracellular miRNA sample) miRNAs associated with hepatocellular damage. Using MTX to recapitulate chronic DILI, we demonstrated that HepaRG MTs significantly released miRNAs into the medium at concentrations and exposure times at which only minimal toxicity was observed. Interestingly, exosomal miR-122 outperformed all other parameters (including total extracellular miRNA) in terms of detecting very early signs of MTX-induced liver injury. These results support the use of exosomal miRNAs as sensitive biomarkers of liver injury and provides a strong methodological basis that could translate from an *in vitro* to an *in vivo* situation.

In the second paper (Messner *et al.* in progress), we identified four extracellular fibrosis-specific miRNAs that were differentially released into cell culture supernatant by human liver MTs upon exposure to MTX but not APAP. Mimics of these four miRNAs (miR-199a-5p, miR-214-3p, miR-99b-5p and miR-125a-5p) were transfected into hTERT-HSCs to assess their role in the activation of the stellate cell. Increased intracellular levels of miR-199a-5p, miR-214-3p and miR-99b-5p promoted a-SMA expression and fibronectin production. In addition, miR-199a-5p and miR-214-3p promoted HSC proliferation and migration. Taken together, our results show that these miRNAs can play a role in fostering fibrosis by activating the hepatic stellate cell.

This leads us to propose that extracellular miR-199a-5p, miR-214-3p, miR-99b-5p and miR-125a-5p could contribute towards a panel of miRNAs to identify liver fibrosis. We were also able to demonstrate a functional link between the proposed biomarkers and a fibrotic

phenotype: miR-199a-5p, miR-214-3p and miR-99b-5p are involved in HSC activation and thereby fibrosis progression.

In conclusion, we demonstrate that the 3D-HepaRG and 3D multicellular MTs are useful tools for investigating miRNA markers of hepatotoxicity and fibrosis, respectively. Finally, we were also able to identify four extracellular miRNAs that could contribute towards a non-invasive method to detect liver fibrosis, including three that show direct links to HSC activation.

# 5 Project 2: Investigating hepatotoxicity and pro-fibrotic potential of additional compounds

## 5.1 Aims

Following, the investigation carried out using MTX and APAP, which demonstrated compound-specific responses of the MTs, the aim of this section was to assess the response of the MTs to additional hepatotoxic compounds, to assess fibrotic potential and identify the broad uses of this multicellular *in vitro* model.

The first paper titled “Bile salts regulate CYP7A1 expression and elicit a fibrotic response and abnormal lipid production in 3D liver microtissues” investigated whether the MTs were capable of recapitulating cholestatic injury upon exposure to large quantities of bile salts and to assess whether the resultant hepatocellular injury would elicit fibrosis.

The second paper titled “A 3D-human liver microtissue model for the assessment of fibrotic potential of environmental chemicals” Investigated the pro-fibrotic potential of environmental pollutants TCDD (dioxin), PCB126 (dioxin-like) and B[a]P (PAH). Previous evidence has suggested that some dioxins may have an effect on HSC activation but these chemicals have not been introduced to a model capable of liver fibrosis *in vitro.*

## 5.2 Introduction

### 5.2.1 Bile biogenesis and cholestatic injury

Bile formation is a unique function of the liver and serves a number of important functions including excretion of harmful exogenous lipophilic substances as well as other endogenous substrates. It is also involved in elimination of cholesterol. Bile salts are involved in emulsification of dietary fats, and facilitate intestinal absorption [6,13]. Bile is a complex aqueous secretion that originates from hepatocytes and consists of a number of endogenous solid constituents including bile salts, bilirubin phospholipid, cholesterol, amino acids, steroids, enzymes, porphyrins, vitamins, heavy metals, as well as exogenous drugs, xenobiotics and environmental toxins [6]. Hepatocytes secrete bile through the apical membrane through relevant transporters (*e.g.* BSEP) into bile canaliculae. Bile is secreted out of the liver via the biliary tree, which consists of a series of bile ducts, common hepatic duct and the gallbladder. Once bile flows through these ducts it flows to the gallbladder where it is concentrated and stored [6]. The bile ducts contain cholangiocytes which regulate the flow, composition and pH of the primary bile [17]. In the small intestine, bile salts facilitate lipid digestion and absorption. Only approximately 5% of bile salts are excreted as the other 95% are recycled as needed through enterohepatic circulation to maintain the bile pool [6]. Enterohepatic circulation and bile salt concentrations at each stage are shown in Figure 14.

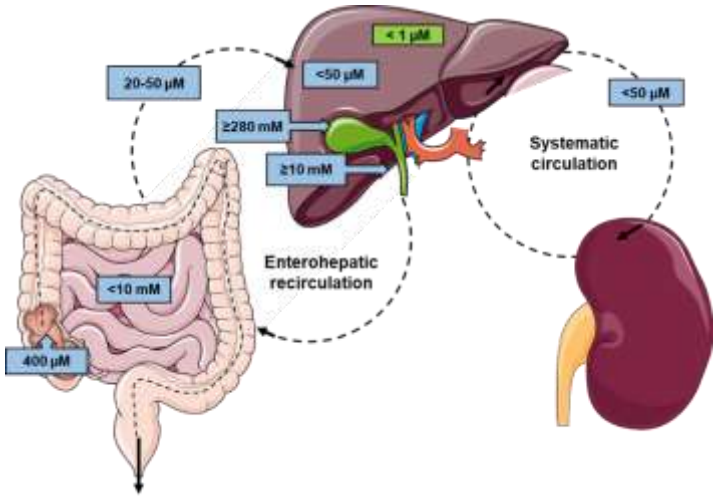


***Figure 14. Enterohepatic circulation with bile salt concentrations.***

*Illustration shows enterohepatic circulation of bile including basal concentrations of bile flowing through each stage of the enterohepatic cycle (blue). Concentration in green represents the concentration of bile salts in the hepatic tissue. Image was based on a figure by Fickert et al. [223] then created using the 'Servier Medical Art' website. Concentrations were collected from 4 publications [223–226].*

Bile consist of organic and inorganic solutes, the inorganic solutes are typically passively secreted ions at a similar concentration to those in plasma [6]. In contrast, organic anions and cations are highly concentrated through active transport mechanisms at the canalicular membrane, the most prevalent organic anion being bile salts. It is important to note that the chemistry of bile salts varies significantly among different species [6]. In humans, two primary bile salts are synthesised from cholesterol: cholic acid (CA), a trihydroxylated bile salt, and chenodeoxycholic acid (CDCA), a dihydroxy bile salt. Both CA and CDCA can conjugate taurine or glycine via a side chain [227]. These conjugated bile salts are stronger acids, which limits their passive reabsorption. However, intestinal bacteria produce "secondary bile salts" by converting CA to deoxycholic acid (DCA) and by metabolising CDCA into lithocholic acid (LCA) (Figure 15). The bile salt ratio is approximately 40% CA, 40% CDCA and 20% DCA and <1% LCA. DCA and LCA are the most hydrophobic and cytotoxic, the order of decreasing toxicity is LCA > DCA > CDCA > CA [228]. Additionally, increased levels of DCA and LCA in the liver have been linked to cholestasis [229].

Two mechanistic pathways known as the classical pathway and the alternative pathway produce bile (Figure 15). The classical pathway is initiated by the rate-limiting enzyme cholesterol 7α-hydrolase (CYP7A1), which is transcriptionally regulated by a variety of nuclear receptors and is involved in the tight regulation of bile production by a negative feedback loop [230]. This is necessary as dysregulation leads to hepatocytes being exposed to cytotoxic concentrations of bile salts resulting in inflammatory infiltration and injury, *i.e*. cholestasis [231]. The majority of bile salts are produced via the classical pathway (82%). CA synthesis requires sterol 12a-hydroxylase (CYP8B1) which hydroxylates 7a-hydroxy-4-cholesten-3-one, an intermediate product and marker for the rate of bile salt synthesis [230]. Mitochondrial steroid 27-hydroxylase (CYP27A1) catalyses steroid side-chain oxidation, which is followed by oxidative cleavage of a 3-carbon-side-chain to form CA and CDCA [230].

In the alternative pathway, CYP27A1 initiates bile salt synthesis by hydroxylation and oxidation of cholesterol to 3b-hydroxy-5-cholestenoic acid, which is then 7a-hydroxylated by oxysterol 7a-hydroxylase (CYP7B1) to form CDCA [230]. In the intestine, gut microbial bile salt hydrolases deconjugate conjugated-bile salts and bacterial 7a-dehydroxylases convert the primary bile salts CA and CDCA to deoxycholic acid and LCA, respectively [230]. Following this, most bile salts are re-conjugated to glycine or taurine and then reabsorbed into the ileum. Conjugated bile salts can then be transported back to the liver via the portal vein to go into enterohepatic circulation [230].

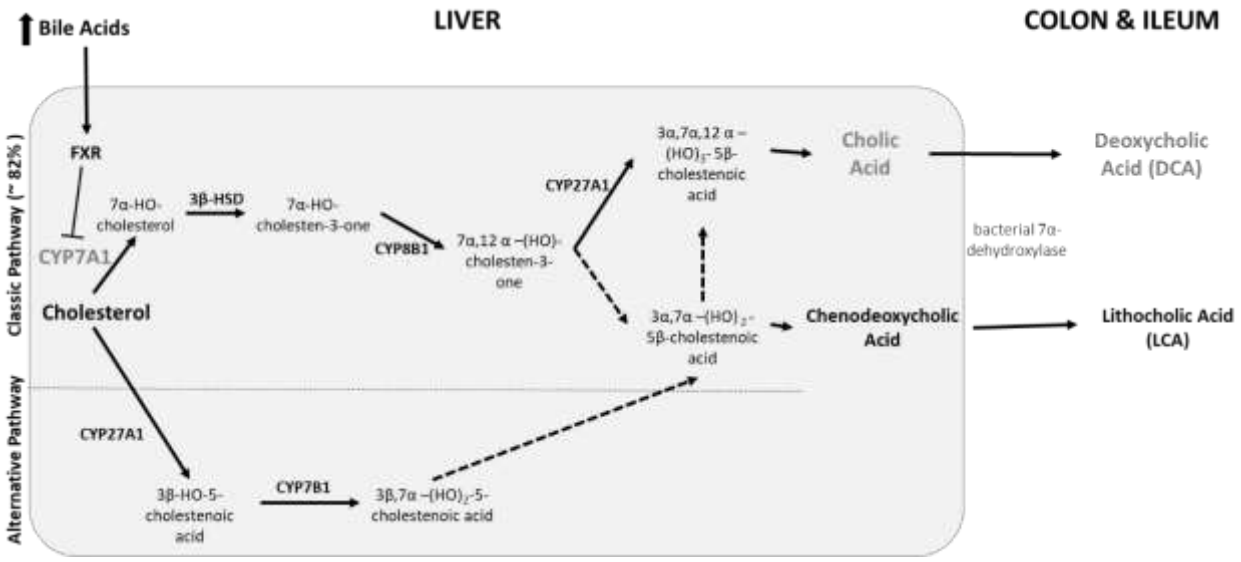


***Figure 15. Bile salt production.***

*Bile production pathway showing the two mechanistic pathways known as the classical pathway (produces 82% of bile salts) and the alternative pathway produce bile. The classical pathway is initiated by the rate-limiting enzyme cholesterol 7α-hydrolase (CYP7A1), which is tightly regulated by a negative feedback loop. Cholic acid (CA) synthesis requires sterol 12a-hydroxylase (CYP8B1) which hydroxylates intermediate product 7a-hydroxy-4-cholesten-3-one. Mitochondrial steroid 27-hydroxylase (CYP27A1) catalyses steroid side-chain oxidation, which is followed by oxidative cleavage of a 3-carbon-side-chain to form CA and chenodeoxycholic acid (CDCA). In the alternative pathway, CYP27A1 initiates synthesis by hydroxylation and oxidation of cholesterol to 3b-hydroxy-5-cholestenoic acid this is Following this, oxysterol 7a-hydroxylase (CYP7B1) then carries out a 7a-dehydroxylation to form CDCA. In the intestine, gut microbial bile salt hydrolases deconjugate conjugated-bile salts and bacterial 7a-dehydroxylases convert the CA and CDCA (primary bile salts) to deoxycholic acid (DCA) and LCA (secondary bile salts), respectively.*

There are specific uptake and export systems for biliary components in hepatocytes relevant for enterohepatic recirculation and excretion (Figure 16). Bile salt uptake transporters include sodium taurocholate co-transporting polypeptide (NTCP) and a family of multi-specific organic anion transporters (OATPs) [232,233]. These are mainly responsible for clearance of conjugated bile salts returning to the liver via the portal vein [233]. ATP-binding cassette (ABC) transporters mediate excretion of bile salts into the bile canaliculi. The canalicular membrane contains bile-salt export pump (BSEP) for excretion of monovalent bile salts and conjugate export pump MRP2 for excretion of bilirubin and divalent bile salts [233–235]. The multidrug export pump MDR1 assists in the excretion of cationic drugs. The phospholipid export pump MDR3 transports phosphatidyl-choline from the inner to the outer leaflet of the bile canaliculi membrane, the phosphatidyl-choline in combination with bile salts and cholesterol form micelles [233,236]. Other bile salt export pumps, MRP3, MRP4 and organic solute transporter (OSTa/b)

[233]. MRP3 and (OSTa/b) are present at the basolateral membrane and function as back-up pumps for alternative sinusoidal bile salt export [233].

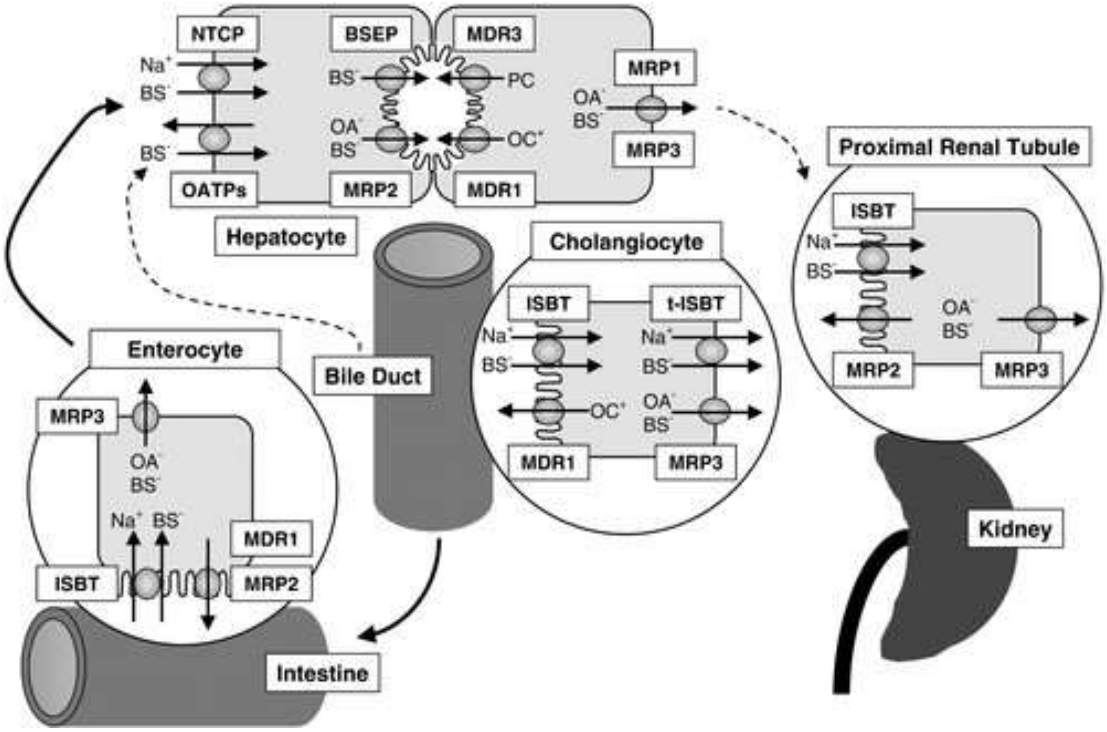


***Figure 16. Bile salt transporters.***

*Hepatobiliary transport systems in liver and extrahepatic tissues in humans. Hepatocytes, via the basolateral $Na^{2+}$/taurocholate cotransporter (NTCP) and organic anion transporting proteins (OATPs), take up bile salts (BS). Canalicular bile salt export pump (BSEP) is responsible for excreted monovalent BS, while canalicular conjugate export pump (MRP2) excretes divalent BS together with anionic conjugates (OA). The phospholipid export pump (MDR3) facilitates excretion of phosphatidylcholine (PC), which forms mixed micelles in bile together with BS and cholesterol. The multidrug export pump (MDR1) excretes cationic drugs (OC). Other basolateral isoforms of the multidrug resistance-associated protein (MRP1 and MRP3) provide an alternative route for the elimination of BS and non-bile salt OA into the systemic circulation. Finally, reabsorption of BS in the terminal ileum occurs via ileal $Na^{2+}$-dependent BS transporter (ISBT) and then effluxed by MRP3. Proximal renal tubules (PRTs) and cholangiocytes have similar mechanisms, where an additional, truncated isoform (t-ISBT) may be involve in BS efflux from cholangiocytes. MRP2 is also located in the apical membrane of enterocytes and PRTs. MDR1 has also been located in the intestines and bile ducts. Image by Trauner and Boyer [233] .*

### 5.2.2 Cholestatic liver injury

Cholestasis is a clinical syndrome that is a result of impaired bile secretion and flow and can be either extra- or intrahepatic. Extrahepatic cholestasis is defined as a mechanical obstruction to the flow of bile from the liver [237]. Causes include choledocholithiasis and tumours. Intrahepatic cholestasis is caused by immune-mediated conditions like cholangitis, exposure to several medications (steroids, nonsteroidal anti-inflammatory drugs, antibiotics, antidiabetic agents) and inborn errors of cholesterol/bile salt biosynthesis and/or metabolism [238]. Cholestasis causes progressive bile duct injury and drives further retention of toxic hydrophobic bile salts, which cause persistent and extensive damage to the bile ducts and liver [6].

A large range of drugs elicit cholestatic injury, either due to toxicity of the drug causing direct injury to bile ducts or through eliciting an adverse immune response directed against the liver. Chlorpromazine (CPZ) has been demonstrated to cause toxicity, oxidative stress and inflammation resulting in cholestatic injury [239–241]. Drugs can also interfere with the bile excretory mechanisms such as ATP-binding cassette transporters [242]. An example being bosentan, which is an endothelin receptor antagonist that inhibits BSEP and MRP2 leading to intracellular accumulation of bile salts, while increasing bile salt-independent bile flow [34].

The ability of drugs to cause cholestatic injury is a challenge for drug-development, which means that a greater understanding of cholestatic injury and development of relevant models of cholestasis would be a useful research tool and could result in preventative or therapeutic methods.

There are both *in vitro* and *in vivo* cholestasis models, which have been proposed as suitable for assessing initiators of the injury process and elucidating relevant mechanisms. Different models have drawbacks and considering these is necessary prior to experimentation and is dependent on the research question. Common models typically use rodents such as the bile duct ligation model (BDL) [243], administration of lithocholic acid [244] or alphanaphthylisothiocyanate [245], multi-drug transporter knockout mice [246] or involving the inhibition of BSEP [247]. Although these models have aided in elucidating a variety of different potential causes and mechanisms it is important to address *in vivo* differences in species with regard to bile salt toxicity [228]. Rodent models are flawed, as their bile composition is different to that of humans. For example murine bile contains much larger quantities of hydrophilic bile salts, making their bile less toxic at high concentrations. In mouse liver, CDCA is converted to a-muricholic acid (a-MCA), which is then epimerized to b-MCA and u-MCA and are highly soluble [230]. Additionally, the mouse liver is capable of converting LCA formed in the intestine to CDCA and can be epimerized to ursodeoxycholic acid (UDCA), a highly soluble bile salt that is less toxic than other bile salts [230]. *In vivo* models using rodents with BDL, multi-drug transporter knockout mice and inhibition of BSEP tend to produce more hydrophilic bile salts that are non-toxic up

to mM concentrations and do not reflect the toxicity of bile salts seen in humans [228,248,249]. Therefore, these animal models may not suitable for assessing the effects of accumulation of bile salts in the liver. LCA-feeding in rodents is also a popular cholestasis model as LCA is the most toxic of the bile salts produced, thereby eliciting hepatotoxicity [244]. However, LCA only contributes to <1% of the total BS composition and does not reflect a physiologically relevant composition of bile [229].

As hepatocellular damage by high bile salt concentrations (toxic hepatic concentration > 0.1 µg/ml or 1 µM [223]) is thought to be the initiator of the injury process, a variety of *in vitro* models using hepatocytes have been established [250] including hepatocytes cultured in mono-layers [251], sandwich cultures [252] and MTs [104]. Using these methods, it has been demonstrated that exceeding physiological concentrations of bile salts results in reactive oxygen species (ROS) generation and hepatocellular death. It is important to note that PHHs [253] tend to quickly lose hepatocellular characteristics when cultured in monolayers. Therefore, 3D cell culture techniques are becoming increasingly accepted as these methods have been shown to help maintain the phenotypic characteristics of cells for longer periods [93,104]. MTs created using PHHs by Hendricks *et al.* and confirmed the protein expression of BSEP and MRP2, which are export pumps found in hepatocytes in the liver. They also demonstrate exacerbation of cholestatis in PHH through co-exposure to bile salts and compounds with cholestatic potential. This study demonstrated that PHHs can be used to investigate cholestatic injury elicited by compounds such as CCPZ *in vitro* [104]. This is corroborated through transcriptomic evidence of PHHs exposed to a range of drugs with cholestatic potential (CPZ, cyclosporin A, ibuprofen, amiodarone) against those that do not elicit cholestatic injury (APAP).

Although PHHs are considered the gold standard for *in vitro* models alternatives are commonly used due to difficulty in acquiring primary liver cells as described above in section 3.5. Alternatives typically include the use of hepatoma cell lines of which the most commonly used are Huh7 and HepG2. However, both these cell lines lack or have very low expression of important transporters such as NTCP and BSEP, leading to transfection being required in order to achieve active uptake of bile salts [254–257]. HepaRG cells express a variety of essential cytochromes that other hepatoma cell lines do not [86] and they also express both canalicular and basolateral transporters [253,258]. This makes these cells an alternative more relevant to human pathophysiology. HepaRG cells have already been used to carry out a variety of drug toxicity studies including the investigation of drug-induced cholestasis in both 2D and 3D cell culture systems [104,239,240,259,260]. Hendricks *et al.* demonstrated that HepaRG cells are a suitable cell line especially in 3D models to assess the effects of cholestatic compounds such as chlor-promazine [104].

### 5.2.3 Link between cholestasis and fibrosis

If cholestasis is left untreated it can progress to liver fibrosis, cirrhosis and eventually liver failure [261]. This has been evidenced both clinically [262] and in a variety of *in vivo* models including BDL [243], BSEP inhibition [252] and administration of alphanaphthylisothiocyanate and lithocholic acid [244,245].

Accumulation of bile results in the exposure of the hepatocytes to toxic concentrations of bile salts causing hepatocellular death and inflammation, which are key events in the liver fibrosis AOP [263]. PHHs exposed to bile salts and mice fed with LCA showing that hepatocytes undergo necrosis upon exposure to high concentrations of bile [249,260] and could be a contributing factor to liver fibrosis development. However, Allen *et al.* suggested that although hepatocytes promote an inflammatory response, it was not through the release of damage-associated molecular pattern molecules (DAMPs) from the dying hepatocytes [251]. Instead they hypothesised that hepatocytes exposed to bile salts may contribute to the chemokine milieu that is responsible for lymphocyte and neutrophil recruitment into the liver [251]. Additionally, neutrophil inflammation through ROS production has been shown in BDL rodents [264,265]. It is still unclear what role the exact hepatocytes play in the development of fibrosis elicited by cholestatic injury. KCs are thought to be involved in cholestatic injury as patients with cholestasis due to extrahepatic obstruction show increased ICAM-1 expression, which was thought to occur due to KC activation and release of cytokines [266]. Cholestatic injury also results in upregulated IL-17 [267], which has been shown to play a role in inducing IL-1β, TGF-β1, IL-6, and TNF-α in KCs [268]. However, further investigation is required to confirm this link between cholestatic injury and fibrosis and the potential role KCs may play.

Cholangiocytes also play a role in bile salt toxicity as they have been shown to proliferate in order to handle increased bile load to prevent infarction [269]. They also play a role in bile flow through the release of anions ($Cl^-$) and ($HCO3^-$), which regulate water flux and drive biliary flow [270,271]. Despite these protective methods, cholangiocyte proliferation could also actively play a role in fibrosis progression, as increased secretin and secretin receptor in cholangiocytes, which is seen in cholestatic injury, results in increased proliferation and fibrogenesis promoting in bile duct hyperplasia and fibrosis, respectively [272].

*In vitro* studies using LX2 cells and primary rat HSCs have demonstrated that bile salts are capable of eliciting HSC activation and proliferation, respectively. Saga *et al.* demonstrated that secondary unconjugated bile salts (DCA) are capable of inducing HSC activation, shown by increased α-SMA production [273]. Yarde *et al.* found that CA, CDCA and LCA promote HSC activation and proliferation [274]. In summary, these two publications demonstrate that CA, DCA, CDCA and LCA are all capable of eliciting HSC activation. Using primary rat HSCs, Svegliati-Baroni *et al.* demonstrated that bile salts activated epidermal growth factor receptor (EGFR)

and induce proliferation at concentrations of 25 μM to 200 μM [275]. These concentrations are closer to concentrations seen during cholestatic injury and these data suggest that bile salts could play a role in exacerbating HSC activation in the areas of injury [266].

It is clear that cholestatic liver fibrosis is multicellular process as different relevant liver cells play different roles in potentially eliciting/exacerbating liver fibrosis. Therefore, having a suitable *in vitro* model will allow us to better understand cholestatic liver fibrosis but also could be useful in the development of disease management and therapies.

## 5.3 Paper 3: Bile salts regulate CYP7A1 expression and elicit a fibrotic response and abnormal lipid production in 3D liver microtissues

**Accepted: 3rd of June 2019 in Toxicology *in vitro***

Catherine Jane Messner[1,2], Linda Mauch[1], Laura Suter-Dick[1].

[1]University of Applied Sciences Northwestern Switzerland, School of Life Sciences, Muttenz, Switzerland.
[2]University of Basel, Department of Pharmaceutical Sciences, 4056-Basel, Switzerland.

Corresponding author:
Catherine Jane Messner
Fachhochschule Nordwestschweiz
Hochschule für Life Sciences
Institut für Chemie und Bioanalytik
Hofackerstrasse 30
CH-4132 Muttenz
Email: catherine.messner@fhnw.ch

Toxicology in Vitro 60 (2019) 261–271

Contents lists available at ScienceDirect

Toxicology in Vitro

journal homepage: www.elsevier.com/locate/toxinvit

# Bile salts regulate CYP7A1 expression and elicit a fibrotic response and abnormal lipid production in 3D liver microtissues

Catherine Jane Messner[a,b,*], Linda Mauch[a], Laura Suter-Dick[a]

[a] School of Life Sciences, University of Applied Sciences Northwestern Switzerland, Muttenz, Switzerland
[b] Department of Pharmaceutical Sciences, University of Basel, 4056 Basel, Switzerland

ABSTRACT

Disrupted regulation and accumulation of bile salts (BS) in the liver can contribute towards progressive liver damage and fibrosis. Here, we investigated the role of BS in the progression of cholestatic injury and liver fibrosis using 3D scaffold-free multicellular human liver microtissues (MTs) comprising the cell lines HepaRG, THP-1 and hTERT-HSCs. This *in vitro* model has been shown to recapitulate cellular events leading to fibrosis including hepatocellular injury, inflammation and activation of HSCs, ultimately leading to increased deposition of extracellular matrix (ECM). In order to better differentiate the contribution of individual cells during cholestasis, the effects of BS were evaluated either on each of the three cell types individually or on the multicellular MTs. Our data corroborate the toxic effects of BS on HepaRG cells and indicate that BS exposure elicited a slight increase in cytokines without causing stellate cell activation. Contrarily, using the MTs, we could demonstrate that low concentrations of BS led to cellular damage and triggered a fibrotic response. This indicates that cellular interplay is required to achieve BS-triggered activation of HSC. Moreover, BS were capable of down-regulating CYP7A1 expression in MTs and elicited abnormal lipid production (accumulation) concordant with clinical cases where chronic cholestasis results in hypercholesterolemia.

## 1. Introduction

Cholestasis is the result of a disrupted regulation of bile salt (BS), also known as bile acids and leads to intrahepatic accumulation of bile salts, which contributes towards progressive liver damage and fibrosis. This condition can result from a variety of factors including drug induced liver toxicity, genetic defects in canalicular transporters (e.g. bile salt export peptide), pregnancy, autoimmune destruction of bile ducts and finally mechanical obstructions such as gallstones or tumours. Bile formation and secretion in the healthy liver is fundamental for the successful intestinal absorption of lipids and fat-soluble vitamins but also have other critical roles in signalling of key cellular pathways (Houten et al., 2006; Keitel et al., 2008; Nguyen and Bouscarel, 2008). Moreover, bile formation is also involved in the excretion of xenobiotics. Bile salts are synthesised from cholesterol through two pathways: the classic pathway, which accounts for 90% of bile salt production and the alternative pathway, which accounts for 10% of production to obtain cholic acid (CA) and chenodeoxycholic acid (CDCA). CA and CDCA are further processed in the intestine where bacterial 7α-dehydroxylase activity converts CA to deoxycholic acid (DCA) and CDCA to either ursodeoxycholic acid (UDCA) or lithocholic acid (LCA). The physiological ratio of bile salts is approximately 40% CA, 40% CDCA and 20% DCA and < 1% LCA of which DCA and LCA are the most hydrophobic and cytotoxic ones; elevated levels of DCA and LCA in the liver have been linked to cholestasis (Li and Apte, 2015). All bile salts show toxicity, the order of decreasing toxicity is LCA > DCA > CDCA > CA (Woolbright et al., 2016). However, the exact composition of bile present in the liver during cholestasis has not been confirmed. Bile salts are not excreted as free carboxylic acids but are conjugated in the liver prior to secretion (Chiang, 2009). Bile salt production is tightly regulated by a negative feedback loop (Goodwin et al., 2000; Li and Chiang, 2014; Mishra et al., 2014) involving cholesterol 7α-hydrolase (CYP7A1)

*Abbreviations:* αSMA, α-smooth muscle actin; AOP, Adverse outcome pathway; BDL, Bile duct ligation model; BS, Bile salts; CA, Cholic acid; CDCA, Chenodeoxycholic acid; CDF, 5 (and 6)-carboxy-2′,7′-dichlorofluorescein; CDFDA, 5 (and 6)-carboxy-2′,7′-dichlorofluorescein diacetate; COL1α1, Collagen I alpha 1; COL4α1, Collagen IV alpha 1; CYP7A1, cholesterol 7 alpha-hydroxylase; DCA, Deoxycholic acid; ECM, Extracellular matrix; HSC, hepatic stellate cells; hTERT-HSC, Immortal activated human hepatic stellate cells; FBS, Fetal bovine serum; FN1, Fibronectin; H&E, Haematoxylin and eosin stain; IL-6, Interleukin-6; KC, Kupffer cells; LCA, Lithocholic acid; LpX, Lipoprotein X; MMP2, matrix metalloproteinase-2; mRNA, messenger RNA; MTs, Microtissues; PFA, Paraformaldehyde; PMA, Phorbol 12-myristate 12-acetate; ROS, Reactive oxygen species; TNF-α, Tumour necrosis factor-α; TGF-β1, Transforming growth factor-β; QSIV, Quantitative IHC staining value; UDCA, Ursodeoxycholic acid; WST-8, Water-soluble tetrazolium salt −8

* Corresponding author at: Institut für Chemie und Bioanalytik, Hochschule für Life Sciences, Fachhochschule Nordwestschweiz, Hofackerstrasse 30, CH-4132 Muttenz, Switzerland.
*E-mail address:* catherine.messner@fhnw.ch (C.J. Messner).

https://doi.org/10.1016/j.tiv.2019.06.002
Received 3 April 2019; Received in revised form 26 May 2019; Accepted 3 June 2019
Available online 10 June 2019
0887-2333/ 

which is transcriptionally regulated by a variety of nuclear receptors (Goodwin et al., 2000; Crosignani et al., 2007). This is necessary as dysregulation leads to the exposure of hepatocytes to cytotoxic concentrations of bile salts resulting in inflammatory infiltration and injury (Li et al., 2017), *i.e.* cholestasis. When left untreated, chronic cholestasis has been shown to result in liver fibrosis and ultimately liver cirrhosis. Liver fibrosis is characterised by an accumulation of fibrillary extracellular matrix and involves several intermediate steps. These steps include hepatocyte injury and cell death, oxidative stress, activation of Kupffer cells (KC), activation of hepatic stellate cells (HSC), and chronic inflammation. Importantly HSCs have been identified as the primary effector cells of fibrosis as they orchestrate extracellular matrix deposition in normal and fibrotic liver (Horvat et al., 2017).

In addition to the development of liver fibrosis cholestasis has been linked to hypercholesterolemia (Papakonstantinou et al., 2017; Longo et al., 2001; Phatlhane and Zemlin, 2015) due to the production of lipoprotein-X (Phatlhane and Zemlin, 2015; Fellin and Manzato, 2019). Abnormal lipoprotein build up, specifically lipoprotein X (LpX) is used as a serum marker for cholestasis and has been suggested as a cause for hypercholesterolemia in the liver (Fellin and Manzato, 2019). This is especially the case with biliary obstruction as LpX is formed as a result of a physicochemical, non-metabolic process involving bile salts and albumin (Fellin and Manzato, 2019; Manzato et al., 1976). The obstructed flow of bile initiates this process resulting in a build-up of LpX causing the feedback loop to become disrupted (Fellin and Manzato, 2019) which is thought to lead to increased hepatic fatty acid production.

There are both *in vitro* and *in vivo* cholestasis models, which have been proposed as suitable for assessing initiators of the injury process and elucidating relevant mechanisms. Examples of common models include rodent models such as the bile duct ligation model (BDL) (Woolbright et al., 2013), administration of lithocholic acid (Fickert et al., 2006) or alphanaphthylisothiocyanate (Krell et al., 1987), multidrug transporter knockout mice (Fickert et al., 2002) or involving the inhibition of bile salt export pump (BSEP) (Rodrigues et al., 2014). These models have aided in elucidating a variety of different potential causes and mechanisms involved in cholestatic injury. However, it is important to address differences between species with regard to bile salt toxicity (Woolbright and Jaeschke, 2015). For example rodents with BDL tend to produce more hydrophilic bile salts that are non-toxic up to millimolar concentrations (Woolbright and Jaeschke, 2015; Zhang et al., 2012; Woolbright et al., 2014). Therefore, animal models may not always be the most suitable model for assessing the effects of toxic concentrations of bile salts in the liver meaning a relevant model is necessary for elucidating mechanisms in humans. As hepatocellular damage by high bile salt concentrations is thought to be the initiator of the injury process, *in vitro* models using hepatocytes have been established (Malhi et al., 2010). Current *in vitro* models available include cultured hepatocytes in monolayers (Allen et al., 2011), sandwich cultures (Jackson et al., 2018) and MTs (Hendriks et al., 2016) Using 2D and 3D cell-culture methods of primary hepatocytes and cell lines it has been demonstrated that exceeding physiological concentrations of bile salts results in hepatocellular death and reactive oxygen species (ROS) generation. It is important to note that primary hepatocytes from humans and rodents (Szabo et al., 2013) tend to quickly lose hepatocellular characteristics when cultured in 2D. Therefore, 3D cell culture techniques are becoming increasingly used as cells have been shown to maintain their phenotypic characteristics for longer (Hendriks et al., 2016; Messner et al., 2013). In addition, due to the difficulty in acquiring primary cells, alternatives typically used are hepatoma cell lines of which the most commonly used are Huh7 and HepG2. However, neither of these cell lines natively express the sodium taurocholate co-transporting polypeptide (NTCP) which is the primary bile salt uptake transporter (Mühlfeld et al., 2012; Denk et al., 2012; Denk et al., 2010; Decaens et al., 2008). HepaRG cells are becoming increasingly popular as they express a variety of essential cytochromes that other cell lines do not (Gerets et al., 2012) and they also express both canalicular and basolateral transporters (Szabo et al., 2013; Le Vee et al., 2006). This makes these cells an alternative more relevant to human pathophysiology. HepaRG cells have already been used to carry out a variety of drug toxicity studies including the investigation of drug-induced cholestasis in both 2D and 3D cell culture systems (Woolbright et al., 2016; Hendriks et al., 2016; Sharanek et al., 2014; Azzi et al., 2014; Anthérieu et al., 2013). They have also been compared to primary hepatocytes and it was concluded that HepaRG is a suitable cell line to use in 3D models to assess the effects of cholestatic compounds (Hendriks et al., 2016)

Although a limited number of HepaRG microtissue models are currently being used to investigate the mechanisms of hepatocellular damage, multicellular models are not currently used to elucidate mechanisms associated with bile salt toxicity or to identify the potential role that bile salts play in fibrosis progression. Multicellular 3D liver MTs comprising HepaRG, THP-1 and hTERT-HSC which are surrogates for hepatocytes, Kupffer Cells (KCs) and hepatic stellate cells (HSC), respectively have been shown to recapitulate key fibrotic events elicited by known pro-fibrotic stimuli such as lipopolysaccharide, TNF-α, TGF-β1 and pro-fibrotic compounds methotrexate and thioacetamide (Prestigiacomo et al., 2017). Therefore, we used this 3D human *in vitro* model to investigate the role of bile salts in the progression of cholestatic injury and fibrosis. Furthermore, we investigated the direct effects that bile salts have on the three separate cell types using standard 2D monolayer cultures. In addition, micro RNAs (miRNAs) have already been described as circulating biomarkers for liver damage (Loosen et al., 2017; Starkey Lewis et al., 2011; Starkey Lewis et al., 2012), and due to their cell-type specificity could be optimal biomarkers *in vivo* (clinics) and *in vitro* (liver co-culture systems) for activation and damage of specific cell types. To this end, we used three putative miRNAs that are associated with hepatic injury and liver fibrosis miR-122, miR-192 and miR-34a. These three miRNA species have been previously related to tissue damage and hepatic damage. In addition, miR-122 expression is liver specific and the release thereof has been linked with hepatocellular damage (Starkey Lewis et al., 2011; Jiang et al., 2017; Szabo and Bala, 2013; Kia et al., 2015; Jopling, 2012).

The exact composition of BS differs between different cholestatic disorders and has not been fully elucidated (Luo et al., 2018; Chiang, 2017) making it difficult to define the ideal composition for *in vitro* investigations. We exposed the cells either individually in 2D or as 3D-MTs to a 50/50 mixture of extracted mammalian CA and DCA (this mix was termed BS throughout this manuscript). DCA has been shown to activate cellular cytokine release such as TNF-α and IL-6 (Li and Apte, 2015) making it an appropriate choice for eliciting cholestatic injury and inflammation in the 3D MTs. CA has been shown to be the predominant primary bile salt in certain forms of cholestasis (Zhang et al., 2016); and CA concentrations significantly increase during cholestasis (Matsuzaki et al., 2002; Menzyk et al., 2018). LCA was excluded due to it contributing < 1% of the total BS composition and being highly cytotoxic (Li and Apte, 2015). With this BS composition we were able to elicit the expected toxicity in the multicellular microtissues.

The results show that bile salt treatment at both sub-toxic and toxic concentrations result in specific cellular responses and in a fibrotic phenotype in 3D-co-cultures but not in 2D-monolayer cultures of individual cells.

## 2. Results

### 2.1. Hepatocellular damage and CYP7A1 regulation by bile salt treatment in HepaRG monolayers

Bile salts concentrations of 100 μg/ml and above were cytotoxic to HepaRG cells with a calculated $IC_{50}$ of 120 ± 2.3 μg/ml (Fig. 1a). Despite there being no decrease in viability at BS concentrations below 100 μg/ml we observed functional impairment of the cells, evidenced by a decrease in albumin expression and release (Fig. 1). In addition,

both TGF-β1 and BS caused a significant increase in miR-122, -192 and -34a release by 2D HepaRG (Fig. 1b). Hepatocytes also tightly regulate bile production in the liver *via* a negative feedback loop, therefore it was important to identify whether the HepaRG cells could respond in a similar manner when treated with bile salts. The results show that bile salts at sub-toxic concentrations elicited a significant decrease in mRNA expression of CYP7A1 (Fig. 1d). Finally, bile canaliculi were visualised using an MRP2 fluorescent substrate, CDF, formed from non-fluorescent CDFDA *via* intracellular esterases. CDF results show that the HepaRG form bile canaliculi and that BS treatment at sub-toxic concentrations did not have any effect on them, whereas as expected toxic concentrations reduced on excretory capacity and bile canaliculi formation (Fig. 1e). HepaRG cells were also exposed to 1 ng/ml TGF-β1 as a comparator. The results show that 1 ng/ml TGF-β1 caused a significant decrease in viability (Fig. S1) and in albumin expression and release, as well as morphological changes and loss of bile canaliculi (Fig. 1).

### 2.2. Bile salts induce a pro-inflammatory response in THP-1 monolayers

After differentiation of THP-1 monocytes to macrophages as described in the methods section the cells were treated with a range of bile salts concentrations. Viability determined using a WST-8 assay shows a large increase in viability during TGF-β1 treatment, meaning that there is an increase in cellular dehydrogenase activity due to the significant increase in the WST-8 measurement (Fig. S1). Concentrations of bile salts above 150 μg/ml caused a decrease in viability after 7 days and IC50 was calculated to be 193 ± 5.6 μg/ml (Fig. 2a). In addition, THP-1 treated with 1 ng/ml TGF-β1 or 30 μg/ml bile salts for 48 h resulted in a slight inflammatory response demonstrated by an increase in mRNA expression of TGF-β1. BS treated THP-1 also resulted in a small but significant increase in TNF-α mRNA expression (Fig. 2b). In addition, THP-1 did not form bile canaliculi, confirming the specificity of using CDFDA to visualise bile canaliculi (Fig. S2).

### 2.3. Activation of stellate cell monolayers is not initiated by bile salts

The hTERT-HSC cells were cultured and regularly inspected to ensure typical stellate cell morphology with dendritic structure was maintained prior to experimentation. TGF-β1 treated hTERT-HSCs demonstrated a slight decrease in viability (Fig. S1), whereas bile salts reduced viability with a calculated $IC_{50}$ of 155 ± 2.9 μg/ml (Fig. 2c). Untreated, not activated hTERT-HSCs showed low levels of expression of stellate cell activation markers. Exposure to TGF- β1 elicited the activation of hTERT-HSCs as demonstrated by increased αSMA immunostaining and increased transcription of αSMA, COL1α1 and COL4α1. Contrarily, hTERT-HSCs were not activated by bile salts and all tested activation markers remained unchanged (Fig. 2d). In addition, hTERT-HSC did not exhibit bile canaliculi formation, which, along with the THP-1 data, confirms the specificity of using CDFDA to visualise bile canaliculi in 2D HepaRG and multicellular microtissues (Fig. S2).

### 2.4. Bile salt treatment elicits hepatocellular damage and regulates CYP7A1 expression in human liver microtissues

Liver MTs are more sensitive to bile salts treatment than each of the three cell types cultured separately as concentrations as low as 60 μg/

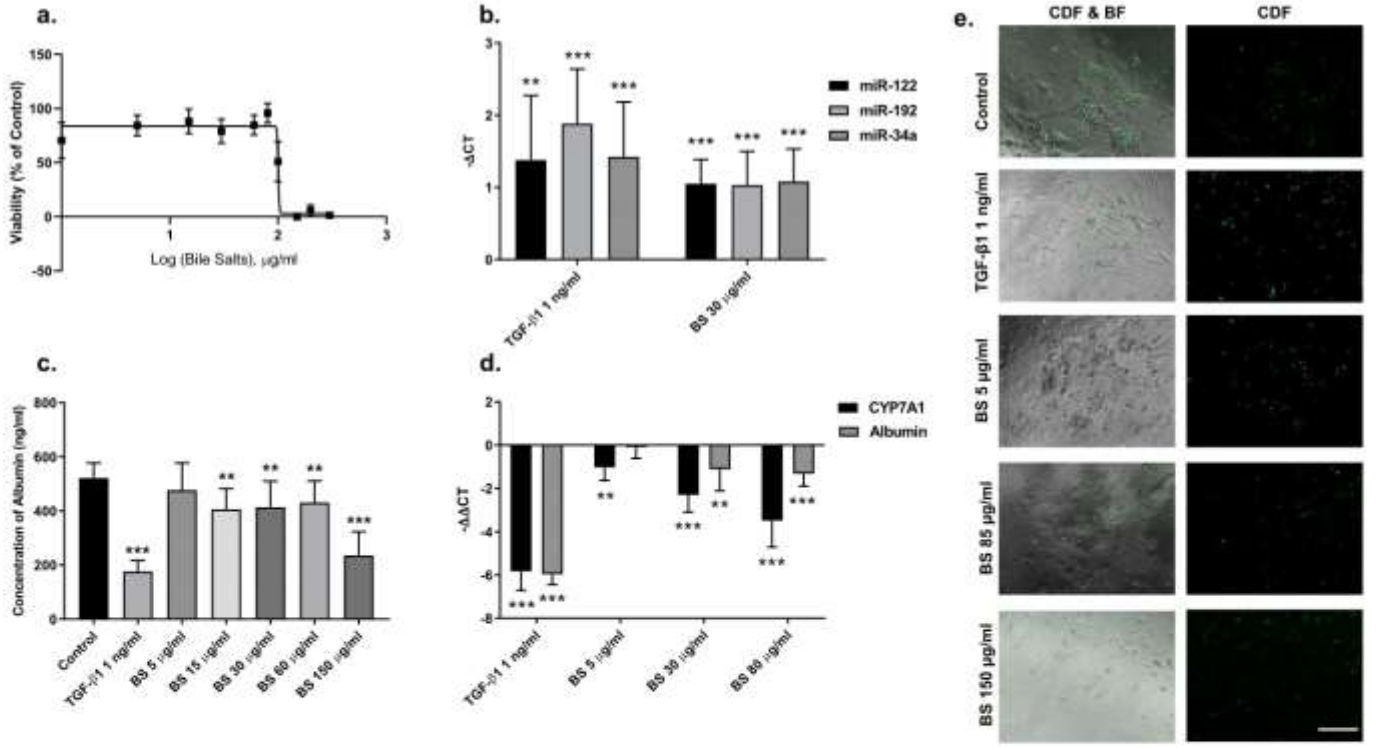


**Fig. 1.** Albumin and CYP7A1 expression decreases in HepaRG upon exposure to BS.
Differentiated HepaRG monolayers were exposed to 1 ng/ml TGF-β1 and BS of which the concentrations ranged from 5 μg/ml to 300 μg/ml for 1–7 days. Viability was assessed using WST-8 Assay at day 7 and IC50 was calculated to be 120 ± 2.3 μg/ml (a). Changes in release of miRNA-122, miRNA-192 and miRNA-34 a by HepaRG exposed to 1 ng/ml TGF-β1 and 30 μg/ml BS for 24 h were also assessed using q-RT-PCR and expressed as −ΔCT, control = 0 (b). Albumin ELISA was used to assess protein amount in pooled supernatant medium collected over 7 days of exposure to TGF-β1 and BS and expressed as concentration (ng/ml) (c). q-RT-PCR was used to identify changes in expression of albumin and CYP7A1 when exposed to 1 ng/ml TGF-β1, 5 μg/ml BS, 30 μg/ml BS and 80 μg/ml for 7 days and expressed as −ΔΔCT, control = 0, (d). CDF was used on day 7 to detect the formation of bile canaliculi and assess excretory capacity in treated and untreated HepaRG, scale bar is 100 μm (e). Viability data values are expressed as percentage ± SD of control of three repeats with 3–6 replicates (a). qRT-PCR data values are expressed as −ΔCT or −ΔΔCT ± SD of three repeats with three replicates each, control is "0", "1" and "-1" indicates 2-fold upregulation and 2-fold downregulation, respectively (b, d). ELISA is expressed as concentration ± SD of albumin release of three repeats with three replicates.

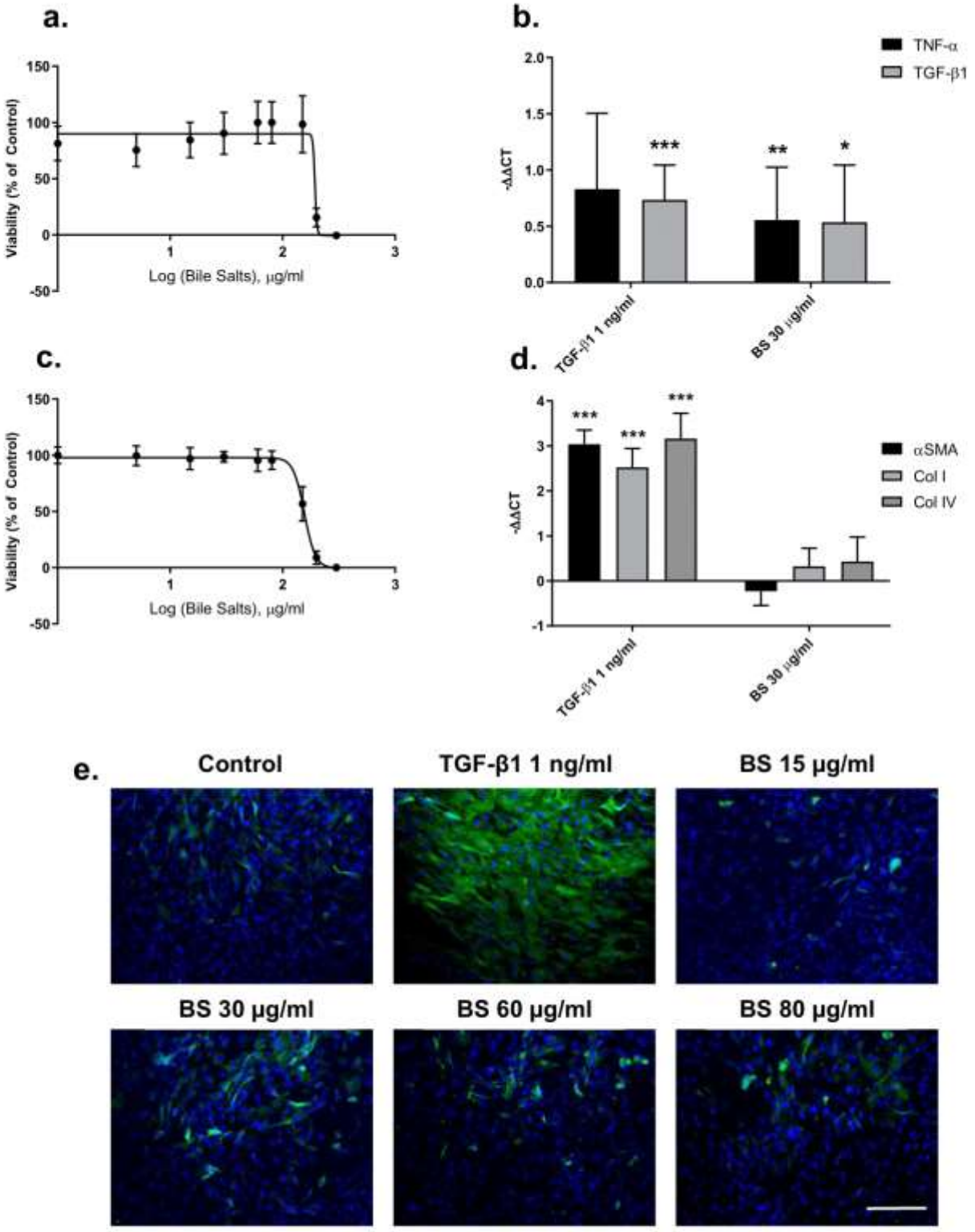


**Fig. 2.** The effect of BS on differentiated THP-1 and hTERT-HSC monolayer cultures.
Differentiated THP-1 and hTERT-HSC monolayers were exposed separately to 1 ng/ml TGF-β1 and BS of which the concentrations ranged from 5 µg/ml to 300 µg/ml for 2–7 days. Viability for THP-1 was assessed using WST-8 assay at day 7 and IC50 was calculated to be 193 ± 5.6 µg/ml (a). q-RT-PCR was used to identify changes in expression of TNF-α and TGF-β1 when THP-1 were exposed to 1 ng/ml TGF-β1 and 30 µg/ml BS for 48 h and expressed as –ΔΔCT, control = 0 (b). Viability for hTERT-HSC was assessed using WST-8 assay at day 7 and IC50 was calculated to be 155 ± 2.9 µg/ml (c). q-RT-PCR was used to identify changes in expression of αSMA, Col I and Col IV when hTERT-HSCs were exposed to 1 ng/ml TGF-β1 and 30 µg/ml BS for 7 days and expressed as –ΔΔCT, control = 0 (d). hTERT-HSCs were exposed to 1 ng/ml TGF-β1 and varying concentrations of BS and stained for αSMA after 5 days of treatment, scale bar is 100 µm (e). Viability data values are expressed as percentage ± SD of control of three repeats with 3–6 replicates, control is "0", "1" and "-1" indicates 2-fold upregulation and 2-fold downregulation, respectively (a,c). qRT-PCR data values are expressed as –ΔΔCT ± SD of three repeats with three replicates each (b,d).

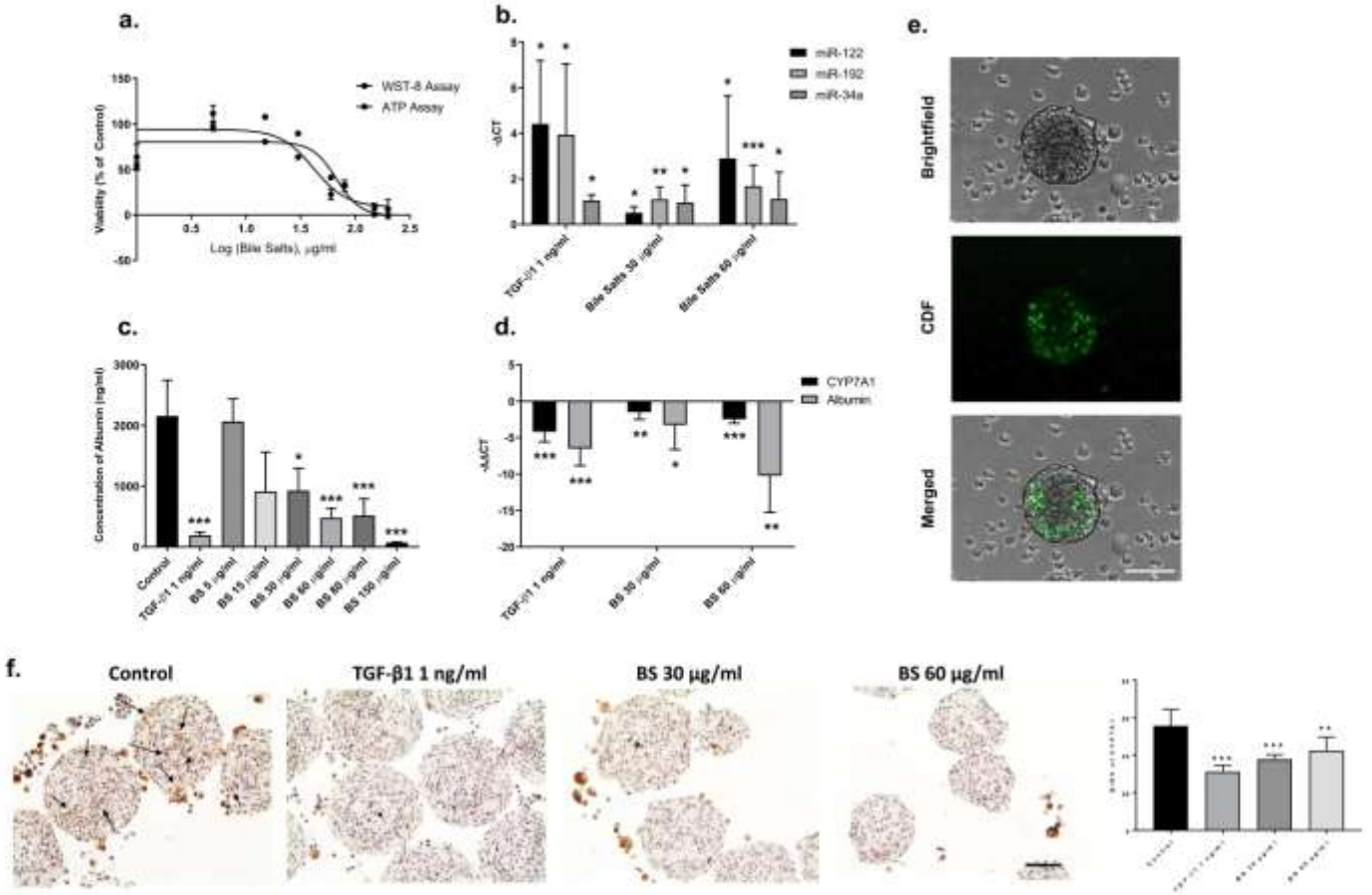


**Fig. 3.** BS cause hepatocellular damage and reduce CYP7A1 expression in human liver multicellular microtissues.
MTs were exposed to 1 ng/ml TGF-β1 and BS of which the concentrations ranged from 5 µg/ml to 200 µg/ml for 10 days. Viability for MTs was assessed using WST-8 and ATP assays at day 10 and IC50 was calculated at 41 ± 12.8 µg/ml and 67.5 ± 6.7 µg/ml, respectively (a). Changes in release of miRNA-122, miRNA-192 and miRNA-34 a by HepaRG exposed to 1 ng/ml TGF-β1 and 30 µg/ml BS for 10 days were assessed using q-RT-PCR and expressed as –ΔCT, control = 0 (b). Albumin ELISA was used to assess protein amount in pooled supernatant medium collected over days 7–10 of exposure to TGF-β1 and BS and expressed as concentration (ng/ml) (c). q-RT-PCR was used to identify changes in expression of albumin and CYP7A1 when MTs were exposed to 1 ng/ml TGF-β1, 30 µg/ml BS and 60 µg/ml BS for 10 days and expressed as –ΔΔCT (d). CDF was used on day 7 MTs to detect the formation of bile canaliculi, scale bar is 100 µm (e). Immunostaining of formalin fixed paraffin embedded human microtissues was carried out to identify whether microtissues expressed CYP7A1 protein, QSIV was calculated as described in methods section, scale bar is 100 µm (f). Viability data values are expressed as percentage ± SD of control of three repeats with 3 replicates. qRT-PCR data values are expressed as –ΔCT or –ΔΔCT ± SD of three repeats with three replicates each, control is "0", "1" and "-1" indicates 2-fold upregulation and 2-fold downregulation, respectively (b, d). ELISA is expressed as concentration ± SD of albumin release of three repeats with three replicates. QSIV was calculated as described in methods section using two exposures of 4–6 replicates for immunostaining.

ml cause a decrease in viability. The $IC_{50}$ was calculated by using two methods to assess viability. The two methods resulted in an average $IC_{50}$ of 55 µg/ml (Fig. 3a) as opposed to 120–193 µg/ml that was seen previously using traditional monolayer culture. Hepatocellular damage was also observed in 3D-MT with a significant decrease in albumin expression (Fig. 3d) and albumin release starting at concentrations as low as 30 µg/ml (Fig. 3c). TGF-β1 also reduced albumin expression, which could be due to hepatocellular damage supported by results that demonstrated increased miR-122 release (Fig. 3b). Hepatic damage was further confirmed by measuring miR-122, -192 and -34a release, which increased during treatment with 30 µg/ml bile salts (Fig. 3b) similar to the HepaRG monolayer culture. The exact cell type from which the miRNAs are released was not investigated. The liver MTs also responded to the bile salts as expected with a decrease in CYP7A1 expression after exposure to 30 µg/ml and 60 µg/ml bile salts (Fig. 3d). This was further confirmed using CYP7A1 immunostaining (Fig. 3f). The liver MTs also showed excretory capacity and bile canaliculi formation, which was visualised using CDF (Fig. 3e). Human liver MTs were also stained using Nile red in order to identify whether TGF-β1 or BS treatment would affect lipid production. Untreated MTs showed a small amount of positive staining, whereas following exposure to TGF-β1 the quantity of intracellular lipid appeared to decrease (Fig. 6). When the MTs were treated with either concentration of BS we observed an increase in Nile red staining (Fig. 6), which suggests there is an increase in lipid production concordant with the increased fatty acid production of hypercholesterolemia typically seen during cholestasis.

### 2.5. Bile salts promote fibrosis in human liver microtissues

Unlike the results obtained in the monocultures of individual cell types, BS treatment of 3D-multicellular MTs led to a fibrotic phenotype. As already described in the previous section there is evidence of hepatocellular damage occurring during bile salts treatment. The MTs were exposed to 1 ng/ml TGF-β1 and bile salts at 30 µg/ml and 60 µg/ml for 10 days resulting in a significant increase in mRNA expression of the inflammatory marker TNF-α and the pro-fibrotic cytokine TGF-β1 (Fig. 4a). Further evidence of inflammation was provided by an increase in IL-6 release when the MT were exposed to TGF-β1 or bile salts (Fig. 4c). Both treatments also elicited a significant increase in expression of the stellate cell activation marker αSMA as well as in mRNA

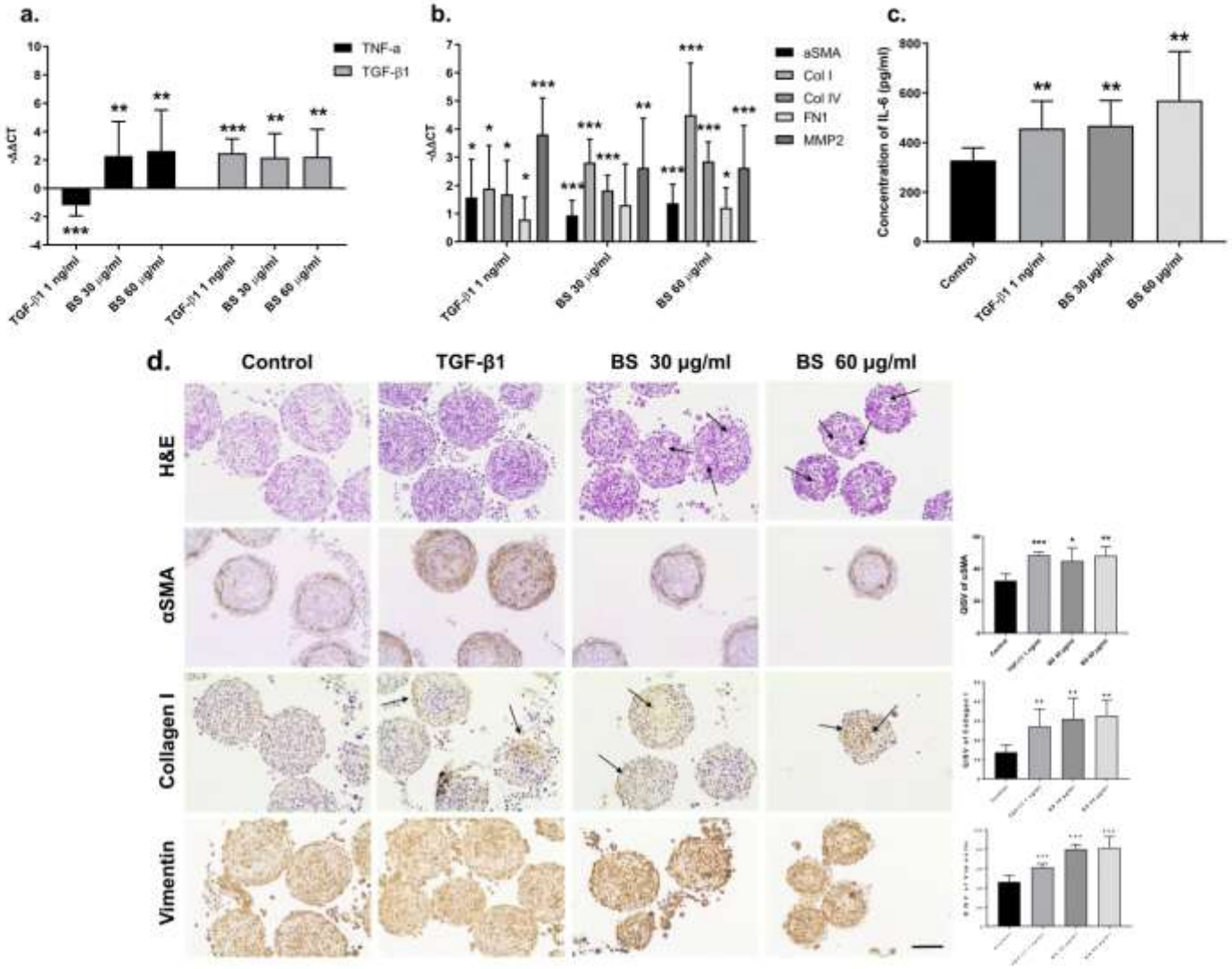


**Fig. 4.** BS exposure elicits a fibrotic response in human liver multicellular microtissues.
MTs were exposed to 1 ng/ml TGF-β1 and 30 μg/ml BS and 60 μg/ml BS 10 days. q-RT-PCR was used to identify an inflammatory response through changes in expression of TNF-α and TGF-β1 and expressed as –ΔΔCT, control = 0 (a). q-RT-PCR was used to identify stellate cell activation or ECM deposition through changes in expression of α SMA, Col I, Col IV, FN1 and MMP2 and expressed as –ΔΔCT, control = 0 (b) IL-6 ELISA was used to assess protein amount in supernatant medium after 10 days of exposure and expressed as concentration (pg/ml) (c). Immunostaining of formalin fixed paraffin embedded human microtissues was carried out to identify fibrosis progression by α SMA, Col I and Vimentin protein QSIV was calculated as described in methods section, scale bar is 100 μm (d) qRT-PCR data values are expressed as –ΔΔCT ± SD of three repeats with three replicates each, control is "0", "1" and "-1" indicates 2-fold upregulation and 2-fold downregulation, respectively (a,b). ELISA is expressed as concentration ± SD of IL-6 release of three repeats with three replicates (c). QSIV was calculated as described in methods section using two exposures of 4–6 replicates for immunostaining (d).

expression of COL1α1, COL4α1, FN1 and MMP2, which are all associated with extracellular matrix deposition (ECM) deposition (Fig. 4b). Using immunohistochemistry, we also demonstrated that microtissues showed a small but significant increase in αSMA protein and a significant increase in COL1α1 protein when treated with TGF-β1 and BS 30 μg/ml and BS 60 μg/ml (Fig. 4d). Whole MT staining confirmed these results (Fig. 5a and b). Vimentin staining, which stains NPCs within the microtissues, was used to identify whether treatment would have an effect on the overall microtissue composition. Staining results demonstrated that TGF-β1 and BS exposure resulted in a significant increase in vimentin expression (Fig. 4d). However, additional experimentation would need to be carried out to identify which specific cell type is proliferating and causing the composition to be altered. Finally, using immunostaining for fibronectin (FN1) it appears that more FN1 was produced when the MTs were treated with TGF-β1 and bile salts (Fig. 5b). In addition, H&E staining shows that BS 60 μg/ml and to a lesser extent BS 30 μg/ml affected the microtissue morphology as there are multiple areas where macrovesicles have formed. These changes appear similar to prolonged cholestasis which results in feathery degeneration of hepatocytes (shown by arrows). This finding was specific of BS-exposure while untreated and TGF-β1 treated MT did not show this feature (Fig. 4d).

## 3. Discussion

Based on our findings, we provide evidence that prolonged BS exposure results in cholestatic injury and abnormal accumulation of lipids concordant with clinical cases. We also provide evidence that BS exposure elicits key events involved in fibrosis progression including hepatocellular injury, inflammation and activation of HSC and increased deposition of ECM.

In the healthy liver tissue bile salt concentrations were measured to be approximately 56–90 nmol/g (≈ 0.022–0.037 μg/ml) (Setchell et al., 1997; Fickert and Wagner, 2017), whereas biliary concentrations

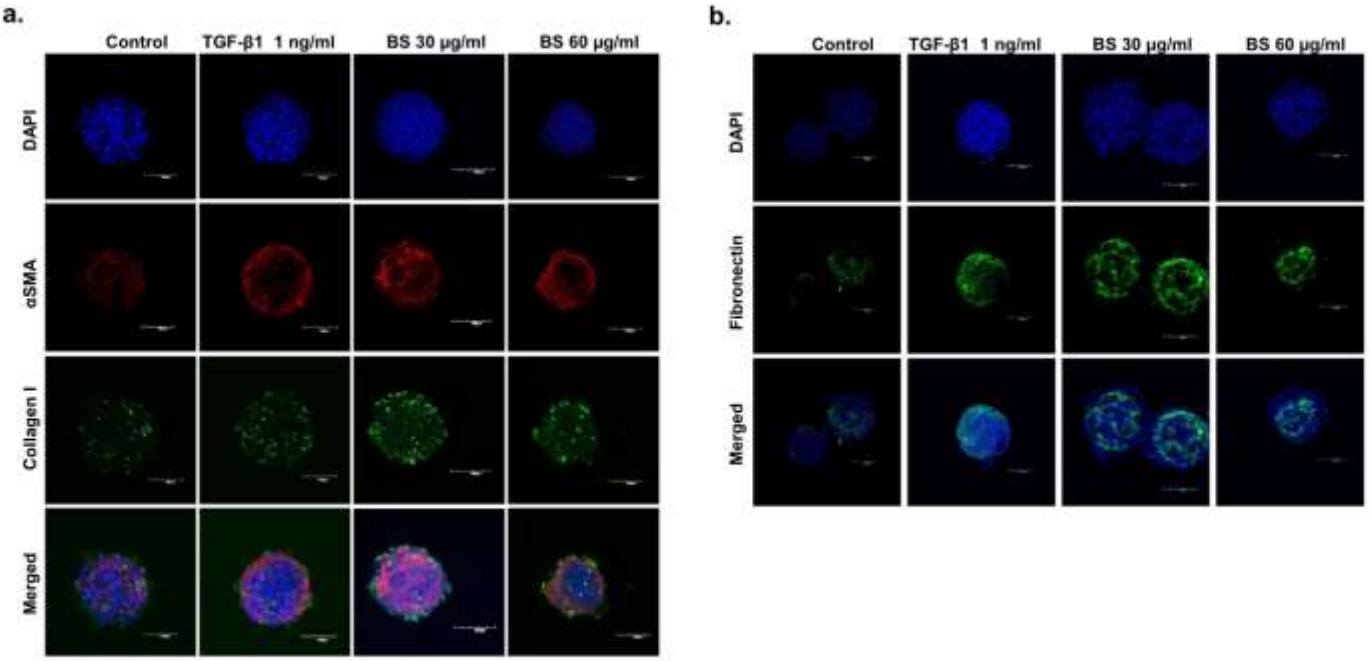


**Fig. 5.** Immunostaining of ECM deposition upon exposure to BS.
MTs were exposed to 1 ng/ml TGF-β1, 30 µg/ml BS and 60 µg/ml BS 10 days. Whole MT staining was performed using different antibodies to confirm the increase in intensity seen in Fig. 4d to corroborate staining results for αSMA and Collagen I quantity (a) and to identify changes in FN1 quantity (b) and imaged on an Olympus Fluoview FV1000 Confocal Microscope, scale bar is 100 µm.

are much higher at approximately 11–21 mmol/L (≈ 4500–8500 µg/ml) (Fickert and Wagner, 2017). Cholestasis and liver cirrhosis have been shown to increase hepatic bile salt concentrations to approximately 176–254 nmol/g (≈ 0.07–0.1 µg/ml) (Fickert and Wagner, 2017). The concentrations, which we use, are higher than the concentrations typically seen in the liver. However, as demonstrated by the $IC_{50}$ results the increased sensitivity of the 3D model ($IC_{50}$ ≈ 55 µg/ml) allows us to reduce the concentration necessary to elicit a toxic response as opposed to the very high concentrations monolayer cultures require ($IC_{50}$ ≈ 120–193 µg/ml). In addition, the HepaRG in the 3D model release a much larger quantity of albumin into the medium than the monolayer culture with quantities of 0.6 ng and 0.02 ng per HepaRG, respectively (Fig. S1). These results provide us with evidence that the enhanced sensitivity is not due to the 3D environment causing cellular damage rather the recreation of a more physiological environment is enhancing the cellular characteristics.

HepaRG have previously been shown to have the relevant bile salt synthesis and transport capacities which makes them a more suitable option over other hepatoma cell lines which are lacking these capacities (Ni et al., 2016). We confirmed this by using CDF, which labels fluorescently labels MRP2, to demonstrate that monolayer and HepaRG express efflux transporters and bile canaliculi are formed. Most importantly, however, we show that they retain this capability in the MTs in the presence of the additional cell types. We have also provided evidence that the HepaRG also express CYP7A1, which plays a relevant role in cholestasis models as this expression, is the rate-limiting step in bile production. We also provide evidence that not only do HepaRG in monolayers express CYP7A1 upon exposure to bile salts but also that the expression levels reduce in a concentration dependent manner which would suggest the HepaRG regulates bile production similarly to hepatocytes in the liver. In addition, it has been shown that CYP7A1 expression decreases in patients with cholestasis (Crosignani et al., 2007), to prevent further increases in bile salt concentration. This means that CYP7A1 expression in our model responds in accordance with clinical data. As is seen in cholestasis, high concentrations of bile salts can result in hepatic damage, specifically hepatocellular damage/death (Allen et al., 2011). This is also observed when exposing the HepaRG to bile salts in both 2D and 3D culture. Viability data and the release of miR-122, −192 and -34a provides us with evidence of hepatic damage. More specifically, albumin expression and release reduces significantly in the 2D HepaRG and the multicellular MTs, which is evidence that there is hepatocellular damage and this is further confirmed by the increase in miR-122 release that has been linked specifically to hepatocellular damage (Loosen et al., 2017). These results are consistent with our positive control as TGF-β1 also resulted in increase miRNA release and albumin expression and a reduction in albumin release (Figs. 1 and 3).

Chronic cholestasis has been linked with dysregulated lipid production (Papakonstantinou et al., 2017; Phatlhane and Zemlin, 2015). Therefore, we assessed the lipid content in MTs treated with BS. In untreated microtissues low level lipid staining is visible, probably due to the presence of vitamin A storing lipid droplets, a characteristic of stellate cells which is retained in the hTERT-HSCs (Jophlin et al., 2018; Schnabl et al., 2002). When treated with we see a decrease in intracellular lipids (Fig. 6). This could be explained by the fact the stellate cells become activated and their vitamin A-storing phenotype may be reduced (Shang et al., 2018). However, additional experiments would need to be carried out to unequivocally identify the lipid-containing cell type. Contrarily to the decrease in nile red positive cells caused by TGF-β1, both BS 30 µg/ml and 60 µg/ml show increased intracellular lipid content. The cause of this increase may be due to the observed decrease in CYP7A1 expression that may lead to disrupted production of fatty acids. This hypothesis would be in line with *in vivo* results showing increased fatty acid deposition in CYP7A1 deficient mice (Erickson et al., 2003). An alternative explanation could also be the production of LpX caused by the BS treatment mimicking bile accumulation in the liver. As described before, LpX is formed from bile and albumin and can dysregulate CYP7A1 expression resulting in hypocholesteraemia, which includes abnormal production of hepatic lipids (Horvat et al., 2017; Longo et al., 2001). This could explain why we measure a decrease in CYP7A1 after treatment with BS. However, additional experiments need to be carried out to fully understand the mechanisms that lead to

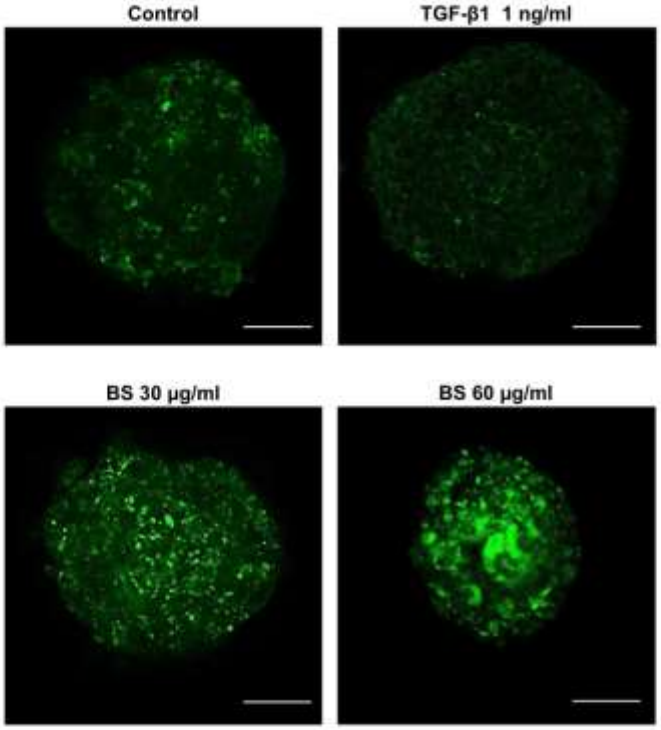


**Fig. 6.** Nile red staining of intracellular lipid droplets of human liver microtissues treated with BS.
MTs were exposed to 1 ng/ml TGF-β1, 30 μg/ml BS and 60 μg/ml BS 10 days. Whole MT staining using Nile red was performed to identify changes in intracellular lipid droplets an Olympus Fluoview FV1000 Confocal Microscope was used to image a single section of the microtissues, scale bar is 100 μm.

this response including isolating LpX in cell culture media. In addition, it would be interesting to elucidate the lipid composition in the MTs more specifically as this is not possible using Nile Red.

As mentioned previously, hepatocellular damage is relevant in the initiation of inflammatory infiltration during cholestasis but it also contributes towards fibrosis progression. The MTs treated with BS results in hepatocellular damage which is one of the key initial events in published fibrosis AOP as hepatocellular damage/death results in the release of ROS, cytokines and chemokines into the liver, which promotes KC activation and inflammation (Seki and Schwabe, 2015). We have also provided evidence that bile salt exposure promotes an inflammatory response in the MTs, evidenced by the increase in expression of TNF-α, TGF-β1 and increased IL-6 release. As mentioned previously TNF-α and TGF-β1 play a key role in fibrosis progression and specifically the significant increase in expression of TGF-β1, produced either by the THP-1 cells or by the hTERT-HSC is indicative of a described autocrine loop in which HSCs are stimulated (Dooley and ten Dijke, 2012). In addition, TGF-β1 expression is a key event in AOP. We also show increased IL-6 release in our model and IL-6 is thought to have some involvement in the progression of fibrosis (Prestigiacomo et al., 2017). Studies *in vitro* using HepaRG would suggest that IL-6 could be promoting cholestatic features (Osawa et al., 2010) and primary mouse hepatocytes treated with bile salts have also shown increased IL-6 production (Allen and Copple, 2010). However, the role of IL-6 is not fully understood and evidence suggests that IL-6 plays a protective role in the liver and promotes liver regeneration as BDL models demonstrated that IL-6 was only expressed at early stages of injury (Crosignani et al., 2007).

We provide evidence of HSC activation and ECM deposition that are the final key events in fibrosis progression. By exposing the multicellular MTs to BS 30 μg/ml for 10 days, we see activation of hTERT-HSC shown by a small but significant increase in αSMA expression and the number of αSMA-positive cells and we also show significant transcriptional induction of ECM components including COL1α1, COL4α1, FN1 and MMP2. These changes in ECM composition were also confirmed by immunostaining that showed increased quantities of COL1α1 and FN1. NPC proliferation was also seen by the increase in vimentin positive cells and that the overall microtissue composition is being altered. These results are interesting as they demonstrate that sub-lethal concentrations of BS are capable of eliciting a fibrotic response. Finally, by exposing the multicellular MTs to BS 60 μg/ml for 10 days we also see stellate cell activation and ECM deposition. In addition to this, we see a change in the microtissue composition, which is similar to the feathery degeneration seen during cholestasis.

The potential role of the individual cell types was investigated by culturing the three cell types separately in monolayers. Upon exposure to BS only some of the responses observed in the clinic and in the 3D-system were recreated. As mentioned previously BS exposure to 2D HepaRG does provide us with some information on the role that the HepaRG are potentially playing in cholestasis and fibrosis. We show that the HepaRG respond to BS with the negative feedback loop seen in the liver and are capable of forming the bile canaliculi in monolayers. We also confirm that BS do elicit hepatocellular damage by the viability data as the hepatocytes had the lowest $IC_{50}$ of the three cell types but also by the decrease in albumin release and increased miRNA release. We demonstrated that there is an inflammatory response in the co-culture MTs. However, the specific role that the KCs play is not fully elucidated. KCs have been thought to have an initial protective role during cholestasis by promoting liver regeneration by increased production of relevant cytokines including TNF-α and TGF-β1. However, prolonged production of these cytokines then has a promoting effect on fibrosis through the activation of HSCs (Li et al., 2017; Prestigiacomo et al., 2017; Dooley and ten Dijke, 2012; Osawa et al., 2010). Based on clinical findings and monolayer cultures of differentiated THP-1, it is possible to propose that the bile salts could promote a slight inflammatory response in macrophages and increase TGF-β1 expression. However, in our experiments TGF-β1 expression levels remained low in the differentiated THP-1. This could be due to the lack of apoptotic or necrotic bodies from other cells (*e.g.* hepatocytes) which have been shown to activate KCs or the THP-1 in monolayers could be less sensitive to the treatment.

Finally, HSC activation is a key event as described in the published AOP for liver fibrosis and interestingly, bile salts have been shown to have no effect on apoptosis induction but do increase proliferation *in vitro* in activated HSCs (Svegliati-Baroni et al., 2005). In our experiments, the hTERT-HSCs in monoculture show very low expression of activation markers upon exposure to BS in comparison to TGF-β1 treated hTERT-HSCs. Using this 2D model system we do not see any evidence of stellate cell activation in absence of other cell types. Further experiments would be required to discern the exact contribution of the architecture (2D *vs.* 3D culture conditions) and that of the cellular interplay (multicellular microtissues *vs.* monoculture). But our findings are in line with reports indicating that HSCs alone grown in 3D do not become activated by MTX, further supporting the necessity of cellular interplay between hepatocytes and HSCs (Leite et al., 2016). Taken together, our data supplies evidence supporting that hepatocellular damage and cellular interplay are required to elicit BS-induced liver fibrosis. In addition, the MTs have the capacity to recapitulate cell-cell interactions and key events leading to fibrosis *in vitro*. These results confirm that co-cultures can more faithfully recreate a physiological environment and model clinical research, which allows us to obtain information that is not possible using monolayer culture alone. Therefore, the multicellular model that incorporates all three cell types is a suitable *in vitro* model to explore synergistic effects between the three cell types, mimicking hepatocellular damage, inflammation and activation of stellate cells resulting in ECM deposition.

## 4. Conclusion

In conclusion, we have demonstrated that BS-induced hepatocellular damage occurs in both 2D and 3D culture systems by reduced albumin released and increased miRNA release. We also confirmed HepaRG express CYP7A1 and upon exposure to BS, expression decreased in accordance with the negative feedback loop. We also demonstrated that the bile salt treatment only causes a low transduction of inflammatory markers in THP-1 and did not result in activation of stellate cells in 2D monolayer culture. In contrast, we provide evidence that 3D multicellular MT model can recapitulate BS induced liver damage and chronic cholestasis demonstrated by CYP7A1 regulation and dysregulated lipid production. Finally using the MTs, we provide further evidence of the importance of cellular interplay and that BS are capable of eliciting hepatocellular damage, inflammation and activating stellate cells resulting in ECM deposition all of which are key events involved in fibrosis progression thus demonstrating a link between cholestasis and fibrosis.

## 5. Materials and methods

### 5.1. Human cell lines

HepaRG cells were obtained from Biopredic International (Rennes, France). The cells were seeded at $1 \times 10^5$ undifferentiated cells/cm$^2$ in medium with growth supplements ADD710 (Biopredic). The cells were cultured at 37 °C in 5% CO2 for 14 days before differentiation. After 14 days of culture, cell differentiation was induced with medium with differentiation supplements ADD720 (Biopredic) for 14 days. Then the cells were maintained in differentiation medium for up to 4 weeks. HepaRG were passaged using Trypsin-EDTA (Invitrogen, Cat. 25300).

hTERT-HSC were kindly provided by Dr. Bernd Schnabl (UC San Diego, USA) [21] and were cultured in DMEM High Glucose (Invitrogen, Cat. 41965) supplemented with 10% fetal bovine serum (FBS) (Invitrogen, Cat. 10270) and 1% P/S (Gibco, Cat.15070063). The cells were maintained in the humidified incubator at 37 °C in 5% CO2. hTERT-HSC were passaged using Trypsin-EDTA.

THP-1 monocytic cells (Cell Line Service) were cultured at 2–10 × $10^5$ cells/mL in RPMI 1640 containing (Bioconcept, Cat. 1-41F50-I) 10% FBS, 1% P/S and maintained at 37 °C in 5% CO2. THP-1 cells were differentiated into macrophages over 48 h in RPMI 1640 medium containing 10 ng/mL Phorbol 12-myristate 12-acetate (PMA) (Sigma, Cat. 79346) as described in previous literature (Starkey Lewis et al., 2012). The media containing PMA was removed and the differentiated THP-1 were washed with fresh medium and maintained in DMEM High Glucose supplemented with 10% FBS and 1% P/S. Differentiated THP-1 were detached using Accutase (Sigma, SCR005).

### 5.2. Generation of microtissues

All MTs were generated using the MicroTissues 3D Petri Dish system from Sigma-Aldrich (Cat. Z764051-6EA) using UltraPure Agarose (ThermoFischer, Cat. 16500100). Cells were counted and resuspended in William's E Medium + GlutaMAX (Invitrogen, Cat. 32551), 2 mM L-Glutamine (Sigma, Cat.G7513), 1× ITS (Sigma, Cat. 11074547001), 100 nM Dexamethasone (Sigma, Cat. D1756), 20% FBS and 1% P/S named aggregation medium. After 72 h of aggregation the MTs were maintained/treated in Williams Medium E + GlutaMax, 2 mM L-Glutamine, 1× ITS, 100 nM Dexamethasone and 1% P/S named maintenance medium. Human liver MTs were generated using 2000 cells per MT containing differentiated HepaRG, hTERT-HSC and differentiated THP-1 at a cell-ratio of 2:1:1 (HepaRG:hTERT-HSC:THP-1).

### 5.3. Cell treatments

All three cell types were seeded individually at appropriate cell densities in 96-well plates. THP-1 were allowed to differentiate for 48 h prior to treatment as described above, whereas HepaRG and hTERT-HSC were treated 24 h after seeding. Co-cultures (3D MTs) were formed as described above and treatment was carried out using maintenance medium. All three cell types and the MTs were exposed to a variety of concentrations of BS consisting of 50% CA & 50% DCA purified from bile extracts (Sigma, Cat. 48305), with medium exchange every 2–3 days. In addition, 1 ng/ml TGF-β1 (Sigma, Cat. T5050), which is known to cause hepatocellular damage and to elicit a pro-fibrotic effect was used as a positive control throughout all experiments.

### 5.4. Cell viability assay

Cell viability was assessed using the Cell Counting Kit-8/WST-8 Assay (Sigma, Cat. 96992) and the CellTiter-Glo® Luminescent Cell Viability Assay (Promega, Cat. G7570). Both were carried out as described in the manufacturer's protocols and adjusted to quantities necessary for the MTs.

### 5.5. Gene expression analysis

mRNA was isolated following standard TRIzol extraction procedure. RNA was reverse transcribed using a M-MLV Reverse transcriptase (Promega, Cat. M1705) and oligo dT (Qiagen,) and real time PCR was performed using FastStart TaqMan® Probe Master (Roche, Cat. 04673417001) and TaqMan probes from Invitrogen. Real time, TaqMan PCR was performed on selected genes (see Table 1). The qRT-PCR Program used: 10 min denaturation at 95 °C, followed by 40 cycles of 15 s at 95 °C and 1 min at 60 °C. The Ct values were generated using the Corbett Rotorgene Analysis Software 6000 and processed on GraphPad Prism. Data are expressed as ΔCT to give a relative abundance with respect to the house keeping gene (ΔCT) and to the untreated samples (ΔΔCT). An average of Beta-2-Microglobulin and GAPDH was used as an internal standard for the normalization of the ΔΔCT values.

### 5.6. miRNA analysis

miRNeasy Serum/Plasma Kit (Cat. 217184) was purchased from Qiagen and was carried out as described in the manufacturers protocol. Reverse transcription and q-RT-PCR was carried out using TaqMan MicroRNA Reverse Transcription Kit (ThermoFischer, Cat. 4366596), qRT-PCR master mix (ThermoFischer, Cat. 4444557) and all TaqMan q-RT-PCR primers were purchased from Invitrogen (Table 2). miRNA extraction and processing was carried out using 80 µl supernatant. The reaction mix was prepared according to the manufacturer's instructions for a final reaction volume of 10 µl with 3 µl RNA extract. The PCR conditions were set for 30 min at 16 °C followed for 30 min at 42 °C and 5 min at 85 °C The qRT-PCR reaction mix contained TaqMan® Fast Advanced Master Mix 1x (Applied Biosystems™, 4444557), TaqMan microRNA Assay primer 1x (Applied Biosystems™, see Table 2), and

**Table 1**
Gene transcripts analysed with qRT-PCR.

| Gene of interest | Abbreviation | Invitrogen Ref. Nr |
|---|---|---|
| Beta-2-Microglobulin | B2M | Hs00187842_m1 |
| Glyceraldehyde 3-phosphate dehydrogenase | GAPDH | Hs02758991_g1 |
| Actin, alpha 2, smooth muscle | ACTA2 (αSMA) | Hs00426835_g1 |
| Collagen 1 alpha 1 | COL1α1 | Hs00164004_m1 |
| Collagen 4 alpha 1 | COL4α1 | Hs00266237_m1 |
| Transcription growth factor Beta 1 | TGF-β1 | Hs00998133_m1 |
| Tumour necrosis factor alpha | TNF- α | Hs01113624_g1 |
| Albumin | ALB | Hs00609403_m1 |
| Cholesterol 7α-hydrolase | CYP7A1 | Hs00167982_m1 |
| Matrix metalloproteinase-2 | MMP2 | Hs01548727_m1 |
| Fibronectin | FN1 | Hs00415006_m1 |

**Table 2**
miRNAs analysed with qRT-PCR.

| miRNA | Assay name | Assay number |
|---|---|---|
| miR-122 | hsa-mir-122-5p | 002245 |
| miR-192 | hsa-mir-192 | 000491 |
| miR-34a | hsa-mir-34a | 000426 |

**Table 3**
Antibodies used for immunohistochemical (IHC) analysis.

| Protein of interest | Primary antibody | Secondary antibody |
|---|---|---|
| αSMA (ACTA2) | Mouse polyclonal antibody (Sigma A5228)/1:200 | Rabbit anti mouse Alexafluor 546 LOT:1549811/1:1000 |
| Collagen Iα2 | Goat polyclonal antibody (Santa Cruz Biotechnology Inc.)/1:50 | Rabbit anti goat Alexafluor 488 LOT: 1613914/1:1000 |
| Fibronectin | Rabbit polyclonal antibody (Abcam ab32457)/1:100 | Goat anti rabbit Alexafluor 546 LOT: 1896381/1:1000 |

1.3 µl cDNA in a final reaction volume of 20 µl. The PCRs were run at 95 °C for 20 s followed by 40 cycles of 1 s at 95 °C and 20 s at 60 °C. (Suter-Dick et al., 2018). Data are expressed as ΔCT to give a relative abundance with respect to the untreated samples (ΔCT). No normalization was performed due to a lack of a correct and universally accepted method for extracellular miRNA quantification.

### 5.7. Immunohistochemistry

Monolayer cultures of hTERT-HSC were fixed in 4% paraformaldehyde (PFA) for 15 min, followed by permeabilisation with 0.1% Triton-X-100 for 20 min. Blocking was performed with 1% BSA in PBS for 60 min and washing with PBS; all steps were performed at RT αSMA antibody was used for the staining (Table 3). MTs were fixed with 4% PFA 1 h in PBS containing calcium and magnesium. Fixed MTs were either embedded in 2% agarose in PBS or stained whole using the protocol described by Ravenscroft et al. (2016) using primary and secondary antibodies listed below (Table 3). Images were taken using an Olympus Fluoview FV1000 Confocal Microscope.

Nile red (Sigma,19123) staining was carried out using a 1 mg/ml stock solution dissolved in acetone. MTs were washed using PBS + $Mg^{2+}$ and $Ca^{2+}$ and fixed in 4% PFA for 1 h. Nile red was diluted to 1.5 µg/ml PBS + $Mg^{2+}$ and $Ca^{2+}$ and added to the fixed microtissues and incubated at RT for 1 h. MTs were washed and transferred onto slides for imaging. Images were taken using an Olympus Fluoview FV1000 Confocal Microscope.

The samples were subjected to paraffin embedding, cut, stained for αSMA, Collagen I, vimentin and H&E then imaged on an Olympus CKX41. Quantification was carried out using the IHC Toolbox on the image analysis software NIH ImageJ (version 2.0.0-rc-56/1.51 h). Brown-positive area (staining) and blue positive area (nuclei) were segmented and integrated optical density was calculated as total number of brown pixels multiplied by brown pixel intensity. Quantitative IHC staining value (QSIV) was calculated as integrated optical density divided by total area occupied by the positive staining (brown area) and total number of cells (blue area).

### 5.8. ELISA

Medium for protein determination was pooled over the whole treatment period. Human albumin ELISA (Cat. E80-129) was purchased from Bethyl Laboratories and all buffers, solutions were made according to the buffer preparation guidelines. High binding flat-bottomed plates (Cat. 655061) were purchased from Greiner Bio-One. Human IL-6 ELISA kit (ThermoFischer, Cat. KHC0061C) was carried out as described in the manufacturer's protocol. ELISA results were calculated using a four-parameter fit using the SoftMax Pro software.

### 5.9. CDFDA

As described above, MTs were aggregated over 72 h and maintained for 7 days. On day 7 MTs were collected and washed with PBS to remove any remaining medium. MTs were incubated with 1 ml of 5 (and 6)-carboxy-2′,7′-dichlorofluorescein (CDFDA) diluted in William's E Medium no phenol red (Invitrogen, Cat. A1217601) to obtain a 2 µM solution. The MTs were then washed 3 times with PBS, resuspended in William's E Medium, and imaged immediately using a Zeiss Axiovert 40 CFL using a blue excitation filter.

### 5.10. Statistical analysis

Data were analysed using GraphPad Prism 8 (GraphPad Software, Version 8.0.2) and expressed as mean values ± SD. The Student *t*-test was used for comparison between two groups and $P < .05$ was considered to be significant: *, $P \leq .05$; **, $P \leq .01$; ***, $P \leq .001$.

Supplementary data to this article can be found online at https://doi.org/10.1016/j.tiv.2019.06.002.

## Acknowledgements

We would like to acknowledge the financial support of the Swiss Centre for Applied Human Toxicology (SCAHT) and insight provided by Dr. Vincenzo Prestigiacomo that assisted the research. We are also very thankful to Dr. B. Schnabl for making the hTERT-HSC available for our research.

## References

Allen, K.M., Copple, B., 2010. Bile acids increase proinflammatory gene expression in hepatocytes. FASEB J. 24, 349.1.
Allen, K., Jaeschke, H., Copple, B.L., 2011. Bile acids induce inflammatory genes in hepatocytes. Am. J. Pathol. 178, 175–186.
Anthérieu, S., et al., 2013. Oxidative stress plays a major role in chlorpromazine-induced cholestasis in human HepaRG cells. Hepatology 57, 1518–1529.
Azzi, P.B.-E., et al., 2014. Impact of inflammation on chlorpromazine-induced cytotoxicity and cholestatic features in HepaRG cells. Drug Metab. Dispos. 42, 1556–1566.
Chiang, J.Y.L., 2009. Bile acids: regulation of synthesis. J. Lipid Res. 50, 1955–1966.
Chiang, J.Y.L., 2017. Bile acid metabolism and signaling in liver disease and therapy. Liver Res. 1, 3–9.
Crosignani, A., et al., 2007. Changes in classic and alternative pathways of bile acid synthesis in chronic liver disease. Clin. Chim. Acta 382, 82–88.
Decaens, C., Durand, M., Grosse, B., Cassio, D., 2008. Which in vitro models could be best used to study hepatocyte polarity? Biol. Cell. 100, 387–398.
Denk, G.U., et al., 2010. Conjugation is essential for the anticholestatic effect of NorUrsodeoxycholic acid in taurolithocholic acid-induced cholestasis in rat liver. Hepatology 52, 1758–1768.
Denk, G.U., et al., 2012. Tauro-β-muricholic acid restricts bile acid-induced hepatocellular apoptosis by preserving the mitochondrial membrane potential. Biochem. Biophys. Res. Commun. 424, 758–764.
Dooley, S., ten Dijke, P., 2012. TGF-β in progression of liver disease. Cell Tissue Res. 347, 245–256.
Erickson, S.K., et al., 2003. Hypercholesterolemia and changes in lipid and bile acid metabolism in male and female cyp7A1-deficient mice. J. Lipid Res. 44, 1001–1009.
Fellin, R., Manzato, E., 2019. Lipoprotein-X fifty years after its original discovery. Nutr. Metab. Cardiovasc. Dis. 29, 4–8.
Fickert, P., Wagner, M., 2017. Biliary bile acids in hepatobiliary injury – what is the link? J. Hepatol. 67, 619–631.
Fickert, P., et al., 2002. Ursodeoxycholic acid aggravates bile infarcts in bile duct-ligated and Mdr2 knockout mice via disruption of cholangioles. Gastroenterology 123, 1238–1251.
Fickert, P., et al., 2006. Lithocholic acid feeding induces segmental bile duct obstruction and destructive cholangitis in mice. Am. J. Pathol. 168, 410–422.
Gerets, H.H.J., et al., 2012. Characterization of primary human hepatocytes, HepG2 cells, and HepaRG cells at the mRNA level and CYP activity in response to inducers and their predictivity for the detection of human hepatotoxins. Cell Biol. Toxicol. 28, 69–87.
Goodwin, B., et al., 2000. A regulatory cascade of the nuclear receptors FXR, SHP-1, and LRH-1 represses bile acid biosynthesis. Mol. Cell 6, 517–526.
Hendriks, D.F.G., Fredriksson Puigvert, L., Messner, S., Mortiz, W., Ingelman-Sundberg,

M., 2016. Hepatic 3D spheroid models for the detection and study of compounds with cholestatic liability. Sci. Rep. 6, 35434.
Horvat, T., et al., 2017. Adverse outcome pathway development from protein alkylation to liver fibrosis. Arch. Toxicol. 91, 1523–1543.
Houten, S.M., Watanabe, M., Auwerx, J., 2006. Endocrine functions of bile acids. EMBO J. 25, 1419–1425.
Jackson, J.P., Freeman, K.M., St. Claire, R.L., Black, C.B., Brouwer, K.R., 2018. Cholestatic drug induced liver injury: a function of bile salt export pump inhibition and farnesoid X receptor antagonism. Appl. Vitro Toxicol. 4, 265–279.
Jiang, X.-P., Ai, W.-B., Wan, L.-Y., Zhang, Y.-Q., Wu, J.-F., 2017. The roles of microRNA families in hepatic fibrosis. Cell Biosci. 7.
Jophlin, L.L., Koutalos, Y., Chen, C., Shah, V., Rockey, D.C., 2018. Hepatic stellate cells retain retinoid-laden lipid droplets after cellular transdifferentiation into activated myofibroblasts. Am. J. Physiol. Gastrointest. Liver Physiol. 315, G713–G721.
Jopling, C., 2012. Liver-specific microRNA-122. RNA Biol. 9, 137–142.
Keitel, V., Kubitz, R., Häussinger, D., 2008. Endocrine and paracrine role of bile acids. World J. Gastroenterol. 14, 5620–5629.
Kia, R., et al., 2015. MicroRNA-122: a novel hepatocyte-enriched in vitro marker of drug-induced cellular toxicity. Toxicol. Sci. Off. J. Soc. Toxicol. 144, 173–185.
Krell, H., Metz, J., Jaeschke, H., Höke, H., Pfaff, E., 1987. Drug-induced intrahepatic cholestasis: characterization of different pathomechanisms. Arch. Toxicol. 60, 124–130.
Le Vee, M., et al., 2006. Functional expression of sinusoidal and canalicular hepatic drug transporters in the differentiated human hepatoma HepaRG cell line. Eur. J. Pharm. Sci. 28, 109–117.
Leite, S.B., et al., 2016. Novel human hepatic organoid model enables testing of drug-induced liver fibrosis in vitro. Biomaterials 78, 1–10.
Li, T., Apte, U., 2015. Bile acid metabolism and signaling in cholestasis, inflammation and cancer. Adv. Pharmacol. San Diego Calif 74, 263–302.
Li, T., Chiang, J.Y.L., 2014. Bile acid signaling in metabolic disease and drug therapy. Pharmacol. Rev. 66, 948–983.
Li, M., Cai, S.-Y., Boyer, J.L., 2017. Mechanisms of bile acid mediated inflammation in the liver. Mol. Asp. Med. 56, 45–53.
Longo, M., Crosignani, A., Podda, M., 2001. Hyperlipidemia in chronic cholestatic liver disease. Curr. Treat. Options Gastroenterol. 4, 111–114.
Loosen, S.H., Schueller, F., Trautwein, C., Roy, S., Roderburg, C., 2017. Role of circulating microRNAs in liver diseases. World J. Hepatol. 9, 586–594.
Luo, L., et al., 2018. Assessment of serum bile acid profiles as biomarkers of liver injury and liver disease in humans. PLoS One 13.
Malhi, H., Guicciardi, M.E., Gores, G.J., 2010. Hepatocyte death: a clear and present danger. Physiol. Rev. 90, 1165–1194.
Manzato, E., et al., 1976. Formation of lipoprotein-X. its relationship to bile compounds. J. Clin. Invest. 57, 1248.
Matsuzaki, Y., et al., 2002. Selective inhibition of CYP27A1 and of chenodeoxycholic acid synthesis in cholestatic hamster liver. Biochim. Biophys. Acta (BBA) - Mol. Basis Dis. 1588, 139–148.
Menżyk, T., Bator, M., Derra, A., Kierach, R., Kukla, M., 2018. The role of metabolic disorders in the pathogenesis of intrahepatic cholestasis of pregnancy. Clin. Exp. Hepatol. 4, 217–223.
Messner, S., Agarkova, I., Moritz, W., Kelm, J.M., 2013. Multi-cell type human liver microtissues for hepatotoxicity testing. Arch. Toxicol. 87, 209–213.
Mishra, S., Somvanshi, P.R., Venkatesh, K.V., 2014. Control of cholesterol homeostasis by entero-hepatic bile transport – the role of feedback mechanisms. RSC Adv. 4, 58964–58975.
Mühlfeld, S., et al., 2012. Short-term feedback regulation of bile salt uptake by bile salts in rodent liver. Hepatol. Baltim. Md 56, 2387–2397.
Nguyen, A., Bouscarel, B., 2008. Bile acids and signal transduction: role in glucose homeostasis. Cell. Signal. 20, 2180–2197.
Ni, X., et al., 2016. Functional human induced hepatocytes (hiHeps) with bile acid synthesis and transport capacities: a novel *in vitro* cholestatic model. Sci. Rep. 6, 38694.
Osawa, Y., et al., 2010. Role of acid sphingomyelinase of Kupffer cells in cholestatic liver injury in mice. Hepatology 51, 237–245.
Papakonstantinou, P., Theodoraki, E., Koulentaki, M., Papadakis, J., 2017. New-onset severe hypercholesterolemia in a patient with cholestatic liver disease. Should we treat the lipids? Atherosclerosis 263, e253–e254.
Phatlhane, D.V., Zemlin, A.E., 2015. Severe hypercholesterolemia mediated by lipoprotein X in a patient with cholestasis. Ann. Hepatol. 14, 924–928.
Prestigiacomo, V., Weston, A., Messner, S., Lampart, F., Suter-Dick, L., 2017. Pro-fibrotic compounds induce stellate cell activation, ECM-remodelling and Nrf2 activation in a human 3D-multicellular model of liver fibrosis. PLoS One 12, e0179995.
Ravenscroft, S.M., Pointon, A., Williams, A.W., Cross, M.J., Sidaway, J.E., 2016. Cardiac non-myocyte cells show enhanced pharmacological function suggestive of contractile maturity in stem cell derived cardiomyocyte microtissues. Toxicol. Sci. 152, 99–112.
Rodrigues, A.D., et al., 2014. Drug-induced perturbations of the bile acid pool, cholestasis, and hepatotoxicity: mechanistic considerations beyond the direct inhibition of the bile salt export pump. Drug Metab. Dispos. 42, 566–574.
Schnabl, B., Choi, Y.H., Olsen, J.C., Hagedorn, C.H., Brenner, D.A., 2002. Immortal activated human hepatic stellate cells generated by ectopic telomerase expression. Lab. Investig. 82, 323–333.
Seki, E., Schwabe, R.F., 2015. Hepatic inflammation and fibrosis: functional links and key pathways. Hepatology 61, 1066–1079.
Setchell, K., et al., 1997. Bile acid concentrations in human and rat liver tissue and in hepatocyte nuclei. Gastroenterology 112, 226–235.
Shang, L., Hosseini, M., Liu, X., Kisseleva, T., Brenner, D.A., 2018. Human hepatic stellate cell isolation and characterization. J. Gastroenterol. 53, 6–17.
Sharanek, A., et al., 2014. Different dose-dependent mechanisms are involved in early cyclosporine A-induced Cholestatic effects in HepaRG cells. Toxicol. Sci. 141, 244–253.
Starkey Lewis, P.J., et al., 2011. Circulating microRNAs as potential markers of human drug-induced liver injury. Hepatology 54, 1767–1776.
Starkey Lewis, P.J., et al., 2012. Serum microRNA biomarkers for drug-induced liver injury. Clin. Pharmacol. Ther. 92, 291–293.
Suter-Dick, L., et al., 2018. Combining extracellular miRNA determination with microfluidic 3D cell cultures for the assessment of nephrotoxicity: a proof of concept study. AAPS J. 20 (86).
Svegliati-Baroni, G., et al., 2005. Bile acids induce hepatic stellate cell proliferation via activation of the epidermal growth factor receptor. Gastroenterology 128, 1042–1055.
Szabo, G., Bala, S., 2013. MicroRNAs in liver disease. Nat. Rev. Gastroenterol. Hepatol. 10, 542–552.
Szabo, M., Veres, Z., Baranyai, Z., Jakab, F., Jemnitz, K., 2013. Comparison of human hepatoma HepaRG cells with human and rat hepatocytes in uptake transport assays in order to predict a risk of drug induced hepatotoxicity. PLoS One 8, e59432.
Woolbright, B.L., Jaeschke, H., 2015. Critical factors in the assessment of cholestatic liver injury in vitro. Methods Mol. Biol. 1250, 363–376.
Woolbright, B.L., et al., 2013. Plasma biomarkers of liver injury and inflammation demonstrate a lack of apoptosis during obstructive cholestasis in mice. Toxicol. Appl. Pharmacol. 273, 524–531.
Woolbright, B.L., et al., 2014. Lithocholic acid feeding results in direct hepato-toxicity independent of neutrophil function in mice. Toxicol. Lett. 228, 56–66.
Woolbright, B.L., McGill, M.R., Yan, H., Jaeschke, H., 2016. Bile acid-induced toxicity in HepaRG cells recapitulates the response in primary human hepatocytes. Basic Clin. Pharmacol. Toxicol. 118, 160–167.
Zhang, Y., et al., 2012. Effect of bile duct ligation on bile acid composition in mouse serum and liver. Liver Int. 32, 58–69.
Zhang, Y., et al., 2016. Bile acids evoke placental inflammation by activating Gpbar1/NF-κB pathway in intrahepatic cholestasis of pregnancy. J. Mol. Cell Biol. 8, 530–541.

## 5.4 Introduction

### 5.4.1 Environmental Pollutants: dioxins and dioxin-like compounds.

Environmental pollution is the deterioration in the physical, chemical, and biological quality of the environment. Pollution can directly or indirectly affect human health. Pollutants can be classified as biodegradable and non-biodegradable [276]. Biodegradable pollutants include sewage effluents and organic matter that are readily decomposed. Whereas non-biodegradable substances are not degraded by microorganisms, *e.g.* heavy metals, plastics, and detergents [276]. Dioxins are included in the non-biodegradable category of pollutants and are persistent in the environment [277].

Dioxins usually refer to polychlorinated dibenzo-dioxins (PCDDs) and polychlorinated dibenzofurans (PCDFs) and are colourless solids or crystals and enter the environment as mixtures containing individual components and impurities [278]. PCDDs and PCDFs are formed of two benzene rings bonded via oxygen atoms. The two rings of PCDDs are joined by two oxygen bridges whereas PCDFs are joined by a carbon bond and one oxygen bridge (Figure 17) [278]. Chlorine atoms can be attached to eight different places on the molecule (numbered 1-8 on figure 17) [278]. Dioxins have no known natural use and the only natural source is from forest fires and volcano activity. Therefore, most are formed and released as by-products of human activities such as industrial processes and waste incineration [278,279]. Other sources include coal-fired power plants and burning of chlorinated compounds such as polychlorinated biphenyls (PCBs) [277,278,280]. Dioxins are hydrophobic and strongly lipophilic and the increased chlorine content increases solubility [278]. Due to the lack of solubility, they attach strongly to any material with high organic content such as aquatic microscopic plants and animals which then get eaten by larger animals and thus dioxins circulate through the food chain [278]. It has been shown that about 90-98% of the average human exposure to dioxin and dioxin-like compounds results from dietary intake, with animal-based products (*e.g* milk) as the predominant source due to contaminations in their feed [281,282]. However, there have also been contaminations found in citrus pulps [282]. In Belgium, in 1999, 500 tonnes of animal feed became contaminated with dioxin/dioxin-like compounds, leading to testing of over 40,000 samples of food showing 6.5% of poultry samples and 8.1% of the egg samples tested positive for toxic concentrations of dioxin/dioxin-like compounds [283]. Accidental exposure has also occurred for example in 1976 a chemical plant in Seveso Italy. An uncontrolled reaction occurred resulting in an explosion that released TCDD into the surrounding environment reaching up to 100 ppm (100 times higher than the accepted range), which ultimately affected the surrounding community members demonstrated by the development of skin lesions [284]. This demonstrates the requirement to understand the contamination patterns but also to understand the effects and concentrations of dioxins and dioxin-like compounds could have on human health.

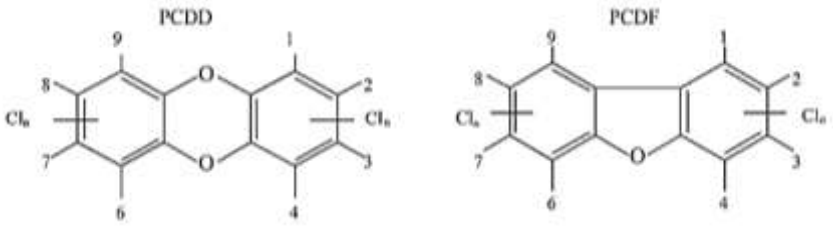


***Figure 17. PCDD and PCDF structure.***

*Two benzene rings bonded via oxygen atoms form PCDDs and PCDFs. Two oxygen bridges in PCDDs join the two rings, whereas a carbon bond and one oxygen bridge join PCDFs. Chlorine atoms can be attached in eight different places on the molecule, which are marked by numbers 1-8. Image by Marinković et al.* [278]*.*

### 5.4.2 Toxicity mechanism of dioxins and dioxin-like compounds.

Dioxins induce phase I and phase II metabolising enzymes through activation of aryl hydrocarbon receptor (AhR). AhR is a member of the basic Helix–Loop–Helix (bHLH)— Per-ARNT-Sim (PAS) family of transcription factors that regulate various physiological and developmental processes [285]. AhR is localised in the cytoplasm and is activated by xenobiotic compounds (including dioxins and dioxin-like compounds) that diffuse through the plasma membrane due to their lipophilic properties. Following the activation of AhR the resultant signalling pathway leads to metabolism of the lipophilic compounds [285]. In the canonical pathway, AhR is localised in the cytoplasm and maintained in an inactive form in the absence of agonists. They are maintained in this form by chaperone proteins prostaglandin E synthase 3 (PTGES3), heat shock protein 90 (HSP90) and AhR-interacting protein (AIP) [285]. When an agonist such as a dioxin or dioxin-like compound diffuses through the plasma membrane and binds to AhR the chaperone proteins are released and dioxin-AhR complex binds to the transcription factor AhR nuclear translocator protein (Arnt) [285]. The dioxin-AhR complex migrates to the nucleus and it binds to xenobiotic-response elements (XRE), which are found on promotor regions of various genes. The process of dioxin-AhR complex binding to XRE modulates the expression of downstream genes including: phase I enzymes CYP1A1, CYP1B1 and CYP1A2; phase II enzymes GST-A1, UGT1A1 and UGT1A6; AhR repressor (AHRR) [285]. The non-canonical pathway involves AhR interacting with other receptor-mediated signalling pathways.

There are a wide variety of phenotypical changes AhR signalling can elicit, including cell cycle regulation, mitogen-activated protein kinase cascades, immediate-early gene induction and cross-talk with other nuclear receptors [286] There is also evidence of a cross-talk between AhR and estrogen receptor signalling pathways [287]. Links between AhR and immune system modulation through the transcription factor NF-κB have been identified and occur by inducing regulatory T cells expansion, repressing IL-17 or enhancing IL-22 [288–290].

Organ toxicities have also been observed and acute exposure to dioxins damages the gastrointestinal tract, liver, pancreas and causes nausea, vomiting and loss of appetite. Acute exposure has also been linked to chloracne, which is a chronic inflammatory skin condition [278]. Additionally, dioxins have been shown to be risk factors for cancer [291], immune deficiency [292], reproductive and developmental abnormalities [284], endocrine disruption (*e.g.* diabetes and thyroid disorders) [293] and many more conditions which are listed by Schecter *et al.* [285]. For this reason, understanding the effects and toxicity of dioxins and dioxin-like compounds on humans and animals is essential for developing stringent regulations regarding dioxin contaminations and general intake.

For the purpose of this thesis, three pollutant compounds capable of inducing AhR signalling were chosen (Figure 18). The first compound is the well characterised dioxin 2,3,7,8-tetrachlorodibenzo-p-dioxin (TCDD), a PCDD with the addition of four chlorine atoms [294]. The second compound is the dioxin-like compound PCB126, which is a bicyclic chlorinated hydrocarbon, known to elicit developmental toxicity. The third compound is B[a]P, a polycyclic aromatic hydrocarbon (PAH), known carcinogen and environmental pollutant.

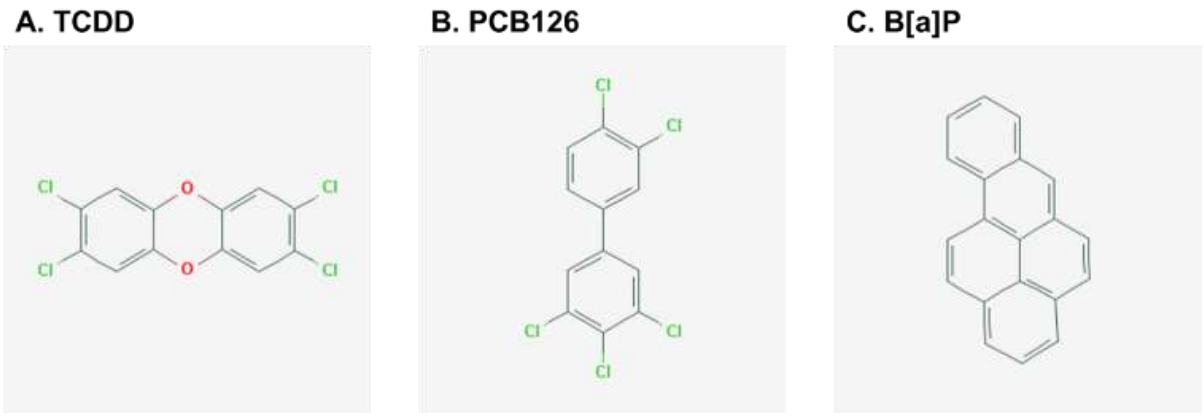


***Figure 18. Structure of TCDD, PCB126, B[a]P.***

*The structure of TCDD (A), PCB126 (B), B[a]P (C) are shown.TCDD corresponds to PCDD structure with the addition of four chlorine atoms (A). PCB126 is a bicyclic chlorinated hydrocarbon with structural similarity and toxic mode of action to dioxins (B). B[a]P is a polycylic aromatic hydrocarbon (PAH) formed by a benzene ring fused to a pyrene (C). Similar to dioxins it also induces AhR signalling. Images taken from PubChem.*

Rodent models are often used to assess dioxin toxicity. However, there are large differences in lethality and phenotypic responses to TCDD exposure. This could be explained by small differences in the gene/structure of AhR. Despite these varied responses a variety of studies have been carried out and have provided important information regarding TCDD toxicity and transcriptomic responses [295,296]. Specifically, rodent models unveiled the association between TCDD

and tumorigenesis [297,298]. PCB126 is linked in rodents to metabolic disruption and induces gluconeogenesis disruption and fatty acid oxidation [299–301]. Finally, using rodent models it has been shown that B[a]P elicits tumorigenesis and also affects reproduction [302,303].

There are concerns involved with using *in vivo* models to extrapolate human safety and predict adverse effects in humans [304] . Typically, *in vivo* models require high doses and there is a risk of species specific effects [285,305]. Human models to assess dioxin and dioxin-like compound toxicity include the use of skin, lung cells, HepaRG, neuronal cells, MCF-7, PHHs, Caco-2, LX-2 and primary humans HSCs [306–312]. These studies cover a wide range of topics including intestinal absorption [311], potency to the lungs [309], cholinergic enzymes in neuronal studies [308], tumour growth [307] and metabolism/toxicity in the liver [306,310].

### 5.4.3 Hepatotoxicity of dioxins and dioxin-like compounds.

Dioxins and dioxin-like compounds have been shown to have gastrointestinal effects in humans. TCDD has been shown to increase the overall liver size after exposure to TCDD due to industrial accidents. Additionally, acute exposures to TCDD have also shown increase ALT and AST levels [313,314]. Using *in vivo* models it has been shown that dioxins and dioxin-like compounds are capable of eliciting hepatotoxicity, HSC activation and ECM deposition [315–322]. Additionally, TCDD also elicited a pro-inflammatory response in mice [316,317,323,324].

Chang *et al.* assessed hepatotoxicity in mice exposed to TCDD. Their results show that TCDD elicited dose-related pathological changes including centrilobular fatty change, cellular swelling and degeneration and hepatocellular necrosis [321]. Multiple studies have demonstrated that TCDD exposure in mice elicits HSC activation shown by increased αSMA protein [316,317,323]. ECM deposition has also been confirmed by increased Col I [316,317] and general collagen staining by PicroSirius Red [320]. Interestingly, a study by Lamb *et al.* demonstrated that TCDD was capable of increasing necroinflammation and HSC activation, but liver fibrosis was not exacerbated as no deposition of Col I was observed [323]. Additionally, exposure of TCDD amplified liver impairment and not only promoted liver fibrosis in obesity-related NAFLD using C57BL/6Jmice, but also worsened hepatic steatosis [315]. Dioxin and dioxin-like compounds can promote fatty liver, including TCDD [325]. PCB126 exposure promoted lipid accumulation in rats *in vivo* [300]. Additionally, Shan *et al.* co-exposed ApoE$^{-/-}$mice (Atherosclerosis-prone apolipoprotein E-deficient mice) to TCDD and PCBs, which worsened NAFLD [326]. PCB126 has been linked to disrupted liver function, lipid accumulation and inflammation and Wahlang *et al.* exposed fibrotic-mice to PCB126 which demonstrated that PCB exacerbated fibrosis [327]. B[a]P has also been shown to have hepatotoxic effects, elicit oxidative stress and DNA damage [328–331] and induce lipid metabolic diseases [332]. No direct link has been made that demonstrates that PCB126 or B[a]P are capable of directly causing liver fibrosis

The small number of *in vitro* systems used to investigate dioxin induced liver toxicity are typically human primary cells or cell lines cultured in monolayers. These include hepatocyte-based models using primary hepatocytes, HepaRG or HepG2. Additionally, two publications report that assessed the effect of dioxins *in vitro* using primary HSCs or the LX-2 cell line [312,333].

Studies with HepG2 have demonstrated they are useful for assessing toxicity, AhR signalling, metabolomics and transcriptional signatures upon exposure to dioxins [334–338]. However, as mentioned in previous sections it has already been shown that HepG2 do not express essential drug-metabolising genes and do not respond in a similar manner to primary hepatocytes [339,340]. Comparative studies of HepG2 and HepaRG for the purpose of chemical hazard identification has been carried out by Jennen *et al*. In order to understand the biological effects (including adverse outcomes) that environmental pollutants may cause, they demonstrate that HepaRG most closely resemble PHHs[341]. HepaRG have only been used for a very small number of dioxin toxicity studies [341–343]. Mesnage *et al.* demonstrated that PCB 126 (concentrations >100 pM) activated the AhR receptor in HepaRG. PCB 126 also provoked a decrease in polyunsaturated fatty acids and an increase in sphingolipid levels. They also show an increase in oxidative stress [342]. AhR activation and signalling have also been studied in PHH [306,344,345].

As mentioned previously, dioxins and dioxin-like compounds have the potential to elicit fibrosis in *in vivo* models. However, there is currently conflicting data on whether TCDD elicits fibrosis, despite the fact that it is the most potent dioxin [346]. The majority of studies demonstrate that TCDD appears to elicit stellate cell activation at high concentrations [316,317,333]. Additionally, the *in vitro* study by Harvey *et al.* identified that TCDD directly activated immortalised HSCs (LX-2 cells) and promoted proliferation, but have no effect on Col I mRNA levels [333]. HSC activation was also demonstrated by Lamb *et al.* using LX-2 cells exposed to TCDD, which also resulted in HSC activation [333].

To the best of our knowledge, no human co-culture system has been used to assess adverse effects of dioxin and dioxin-like compounds to investigate whether environmental pollutants have any fibrotic potential.

## 5.5 Paper 4 Assessment of fibrotic pathways induced by environmental chemicals using 3D-human liver microtissue model

**Manuscript currently under review**

Lu Yan*[1], Catherine Jane Messner*[2,3,4], Xiaowei Zhang[1], Laura Suter-Dick[2,4]

[1] State Key Laborator of Pollution Control & Resource Reuse, School of the Environment, Nanjing, P. R. China, 210023
[2] University of Applied Sciences and Arts Northwestern Switzerland, 4132 Muttenz, Switzerland.
[3] University of Basel, Department of Pharmaceutical Sciences, 4056 Basel, Switzerland.
[4] Swiss Centre for Applied Human Toxicology (SCAHT), 4055 Basel, Switzerland.

*Both authors contributed equally

**Corresponding Author:**
Prof. Xiaowei Zhang
Nanjing University
School of the Environment
Email: zhangxwnju.cn

Environmental Research 194 (2021) 110679

Contents lists available at ScienceDirect

Environmental Research

journal homepage: www.elsevier.com/locate/envres

# Assessment of fibrotic pathways induced by environmental chemicals using 3D-human liver microtissue model

Lu Yan [a], Catherine Jane Messner [b,c,d], Xiaowei Zhang [a,*], Laura Suter-Dick [b,d]

[a] State Key Laboratory of Pollution Control & Resource Reuse, School of the Environment, Nanjing University, Nanjing, 210023, PR China
[b] School of Life Sciences, University of Applied Sciences Northwestern Switzerland, Muttenz, 4132, Switzerland
[c] Department of Pharmaceutical Sciences, University of Basel, Basel, 4003, Switzerland
[d] Swiss Centre for Applied Human Toxicology (SCAHT), 4056, Switzerland

ARTICLE INFO

*Keywords:*
Liver microtissues
Fibrotic potential assessment
Environmental chemicals

ABSTRACT

Exposure to environmental chemicals, particularly those with persistent and bioaccumulative properties have been linked to liver diseases. Induction of fibrotic pathways is considered as a pre-requirement of chemical induced liver fibrosis. Here, we applied 3D *in vitro* human liver microtissues (MTs) composed of HepaRG, THP-1 and hTERT-HSC that express relevant hepatic pathways (bile acid, sterol, and xenobiotic metabolism) and can recapitulate key events of liver fibrosis (e.g. extracellular matrix-deposition). The liver MTs were exposed to a known profibrotic chemical, thioacetamide (TAA) and three representative environmental chemicals (TCDD, benzo [a] pyrene (BaP) and PCB126). Both TAA and BaP triggered fibrotic pathway related events such as hepatocellular damage (cytotoxicity and decreased albumin release), hepatic stellate cell activation (transcriptional upregulation of α-SMA and Col1α1) and extracellular matrix remodelling. TCDD or PCB126 at measured concentrations did not elicit these responses in the 3D liver MTs system, though they caused cytotoxicity in HepaRG monoculture at high concentrations. Reduced human transcriptome (RHT) analysis captured molecular responses involved in liver fibrosis when MTs were treated with TAA and BaP. The results suggest that 3D, multicellular, human liver microtissues represent an alternative, human-relevant, *in vitro* liver model for assessing fibrotic pathways induced by environmental chemicals.

## Credit author statement

L.Y., X.Z., and L.S. designed the study. X.Z., and L.S. provided the funding. L.Y. and C.M. collected the data and conducted the statistical analyses. L.Y. and C.M. wrote the first draft of the manuscript. L.Y., X.Z., C.M. and L.S. contributed to the discussion and revisions.

## 1. Introduction

Environmental organic pollutants, particularly those with persistent and bioaccumulative properties, have become a common health hazard. These pollutants can enter human body through diet, drinking water, air, dust and direct contact with products resulting in risk of chronic disease (Harrad et al., 2019; Sutherst, 2004). Increasing epidemiological evidence shows that chronic exposure to environmental organic pollutants may promote the development of liver injuries and metabolic diseases in humans (Deierlein et al., 2017; Magliano et al., 2014). Although animal experiments have demonstrated that 2,3,7,8-tetrachlorodibenzo-pdioxin (TCDD), Benzo[a]pyrene (BaP), polychlorinated biphenyl (PCB) 126 and other organic pollutants can cause liver damage, direct evidence demonstrating that these chemicals induce human liver dysfunction is scarce (Dere et al., 2011; Nault et al., 2016; Zhu et al., 2020). One of the main reasons is the lack of suitable human-relevant hepatotoxicity models for assessing the effects of environmental pollutants.

Hepatic fibrosis, defined as the excessive extracellular matrix (ECM) accumulation in the liver, is a major concern as the fibrotic response underlies virtually all the complications of end-stage liver disease (Friedman, 2008). The pathway leading to fibrosis has been summarized in the liver fibrosis adverse outcome pathway (https://aopwiki.org/aops/38). The key events include hepatocyte injury and cell death, increased production of TGF-β, activation of kupffer cells (KC), activation of hepatic stellate cells (HSC), chronic inflammation and increased deposition of ECM. Among these, HSC activation and the subsequent

* Corresponding author. Nanjing University School of the Environment, China.
*E-mail address:* zhangxw@nju.edu.cn (X. Zhang).

https://doi.org/10.1016/j.envres.2020.110679
Received 10 October 2020; Received in revised form 22 December 2020; Accepted 23 December 2020
Available online 30 December 2020
0013-9351/

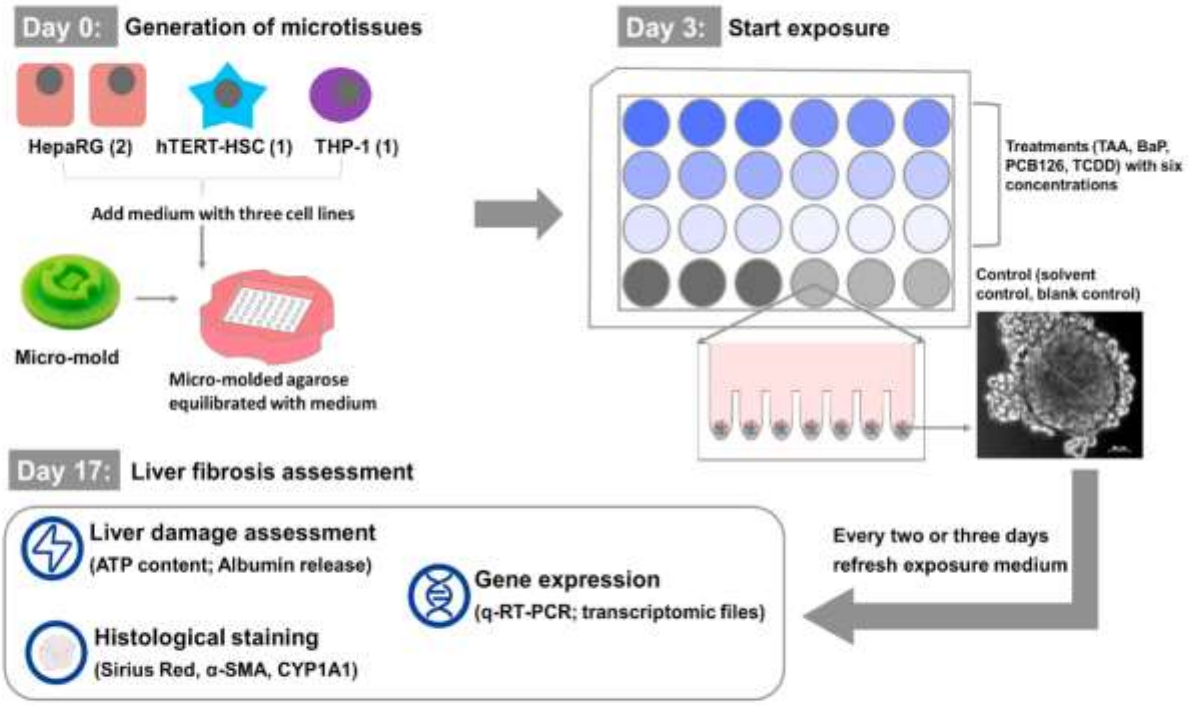


**Fig. 1. Schematic representation of the experimental setup.** Differentiated HepaRG, hTERT-HSC and differentiated THP-1 were used to make Microtissues (MTs) at d0 and allowed to aggregate over 3 days. On the third day, the exposure started through the addition of chemicals to the maintenance medium and treatments were refreshed with every medium exchange every 2–3 days. MTs were collected at d17 and used for liver fibrosis assessment.

deposition of collagens and other ECM proteins are the central events in the process of liver fibrosis (Horvat et al., 2017; Takaaki et al., 2017). Widely used 2D-cultures using a single cell type (such as HSC, human LX-1 or LX-2 cell line) are readily available *in vitro* models of liver fibrosis, while these models are not optimal because of lacking multicellular interaction and activation of HSC in 2D-attachment culture (Jennen et al., 2010; Jetten et al., 2013; Ramaiahgari et al., 2017; van Grunsven, 2017).

In recent years, increasing evidence supports that co-culture systems in 3D have improved capability to mimic liver-like microenvironments (Lauschke et al., 2016; van Grunsven, 2017). Most co-culture experiments using hepatocytes and HSCs show improved longevity, preserved cytochrome P450 inducibility and quiescent HSCs (Kostadinova et al., 2013; Ramaiahgari et al., 2017). These models appear to outperform 2D monolayer experiments in assessing liver toxicity of environmental chemicals, especially liver fibrosis. As mentioned earlier, activation of KCs is also a key event leading to liver fibrosis (van Grunsven, 2017), the tri-culture spheroids involving three relevant cell types (hepatocytes, HSCs and KCs) could have an improved ability to reflect the process of liver fibrosis. Here we used a cell-line based, novel human hepatic microtissue (MT) model representing the three cell types that recapitulates key fibrotic events when exposed to pro-fibrotic stimuli such as lipopolysaccharide, TNF-α, TGF-β1 and the pro-fibrotic xenobiotics (methotrexate and thioacetamide (TAA)) (Prestigiacomo et al., 2017).

Transcriptomic profiling provides a powerful tool to capture the occurrence of key events at transcriptional level during the course of adverse health outcome. It does not only identify specific genes modulated by certain compounds but also provides information that is essential for a holistic understanding of molecular mechanisms of compound-induced hepatotoxicity (Jiang et al., 2019). To efficiently examine the key biological processes relevant to adverse health outcome, an alternative approach to whole genome transcriptome analysis is to select a panel of genes representative of specific toxicological relevant pathways. We have recently developed the reduced human transcriptome (RHT) of 1200 genes, including all genes involved in molecular initiating events and key events currently available in AOP wiki. This RHT approach has been successfully applied in pathway-based assessment of single chemicals and mixtures by a high throughput transcriptomics approach in human cell-based system (Xia et al, 2017, 2020bib_Xia_et_al_2020bib_Xia_et_al_2017).

Here the combination of human 3D multicellular liver microtissue (MT) and reduced human transcriptome was applied to characterize the capability of MTs models to assess the biological pathways related to liver fibrosis induced by environmental chemicals. The 3D liver MT comprise HepaRG, THP-1 and hTERT-HSC which are surrogates for hepatocytes, KCs and HSCs, respectively (Messner et al., 2019; Prestigiacomo et al., 2017). Firstly, transcriptomic pathways relevant to toxicological outcomes were characterized in this human-relevant *in vitro* system. Secondly, the biological pathways relevant to liver fibrosis were analyzed by a combination of biochemical, molecular and transcriptomic assays in human 3D MTs exposed to chemicals. The chemicals used to challenge the system were a known profibrotic chemical, TAA, and the three typical environmental chemicals (TCDD, BaP, and PCB126). Finally, RHT analysis was used to evaluate changes in biological pathways caused by exposure to the chemicals.

## 2. Methods and materials

**Cell culture.** HepaRG cells were obtained from Biopredic International (Rennes, France). The cells were seeded at $1 \times 10^5$ undifferentiated cells/cm$^2$ in medium with growth supplements ADD710 (Biopredic). The cells were expanded at 37°C in 5% $CO_2$ for 14 days prior to differentiation. After 14 days of culture, cells were differentiated using medium with differentiation supplements ADD720 (Biopredic) for 14 days. Following differentiation, the cells were maintained in differentiation medium for up to 4 weeks. hTERT-HSC were kindly provided by Dr. Bernd Schnabl (UC San Diego, USA) and were cultured in DMEM High Glucose (Invitrogen, Cat. 41965, USA) supplemented with 10% fetal bovine serum (FBS) (Invitrogen, Cat. 10270, USA) and 1% Penicillin-Streptomycin (P/S) (Gibco, Cat.15070063, USA). THP-1 monocytic cells (Cell Line Service) were cultured at 2–10 × $10^5$ cells/ml in RPMI 1640 (Bioconcept, Cat. 1–41F50–I, Switzerland)

supplemented with 10% FBS and 1% P/S and maintained at 37°C in 5% $CO_2$. THP-1 cells were differentiated into macrophages over 48 h in RPMI 1640 medium containing 10 ng/ml Phorbol 12-myristate 12-acetate (PMA) (Sigma, Cat. 79346, Switzerland) (Prestigiacomo et al., 2017). After 48 h the media containing PMA were removed and the differentiated THP-1 were maintained in DMEM High Glucose supplemented with 10% FBS and 1% P/S.

**3D microtissues experiments.** The workflow of the whole experiment is depicted in Fig. 1.

**Generation of microtissues (MT).** Human liver MTs were generated using 2000 cells/MT containing differentiated HepaRG, hTERT-HSC and differentiated THP-1 at a cell-ratio of 2:1:1 (HepaRG: hTERT-HSC: THP-1). Cell-ratios were chosen based on a previous study, where the usual liver cell ratio (80% hepatocytes and 20% non-parenchymal cells) was adjusted to be able to capture specific cellular responses and the key events of liver fibrosis (Messner et al., 2019; Prestigiacomo et al., 2017). MTs generation was carried out using the MicroTissues 3D Petri Dish system from Sigma-Aldrich (Cat. Z764051-6EA, Switzerland) using UltraPure Agarose (ThermoFischer, Cat. 16500100, USA). Cells were counted and resuspended in William's E Medium + GlutaMAX (Invitrogen, Cat. 32551, USA), 2mM L-Glutamine (Sigma, Cat.G7513, Switzerland), 1 × ITS (Sigma, Cat. 11074547001, Switzerland), 100nM Dexamethasone (Sigma, Cat. D1756, Switzerland), 20% FBS and 1% P/S named aggregation medium. After three days' aggregation, the human liver MTs formed in a regular spherical shape in the center where hTERT-HSC and macrophages were located and surrounded by HepaRG cells. The diameter of one MT was approximately 200–300 μm, and cells in this microtissue model did not proliferate any more in the following 14 days culture. The generated MTs were maintained/treated in maintenance medium (Williams Medium E + GlutaMax, 2mM L-Glutamine, 1 × ITS, 100nM Dexamethasone and 1% P/S).

**Chemical exposure.** TAA was directly dissolved in the maintenance media. BaP and PCB 126 were dissolved in DMSO with maximal concentrations of 5 g/L (19.8mM) and 2 g/L (6.1mM), respectively. 10 μg/ml TCDD (3.1nM) were prepared in toluene. Cell treatment was carried out using maintenance medium and MTs were exposed to a variety of concentrations of TAA, BaP, PCB126 and TCDD (Table S1) with medium exchange on d6, d8, d10, d13, d15.

**Assays used for detecting hepatocellular damage and fibrosis.** Cell viability was assessed using the CellTiter-Glo® Luminescent Cell Viability Assay (Promega, Cat. G7570, USA) which is based on intracellular ATP quantity to determine the number of viable cells. Human albumin ELISA (Cat. E80-129, Switzerland) was used to test liver function. Regarding fibrosis assessment, gene expression of αSMA and Col1α1 (liver fibrosis gene makers) were evaluated by Real time TaqMan PCR. In addition, AhR and CYP1A1 were also evaluated by Real time TaqMan PCR. Relative expression was calculated using $2^{-}(-\Delta\Delta Ct)$ method. Protein expression in the MTs after 14-day treatment was determined histologically. Briefly, MTs were fixed with 4% paraformaldehyde (PFA) 1h in phosphate buffer saline (PBS) containing calcium and magnesium. Fixed MTs were embedded in 2% agarose and were subjected to paraffin embedding, cut, and stained with antibodies against αSMA (Sigma, Cat. F3777, Switzerland) and CYP1A1 (Proteintech, Cat. 13241-1-AP, USA), or with Sirius Red and H&E. Imaging was performed on an Olympus CKX41, details about processes are given in the supplementary information.

**Reduced Transcriptomics.** RNA sequencing was performed based on reduced transcriptomes including a panel of crucial genes which were described in published paper of our lab (Xia et al., 2017). In order to further analyze transcriptomic response of the liver MT to the samples from the vehicle, the BaP (19.8, 198, 1980 nM), TAA (0.16, 0.8, 4 mM), and TCDD (310, 3100 pM) treatment groups, reduced transcriptome sequencing were applied. The transcriptional expression of 1200 genes were measured by an amplicon-seq technology. A total of twenty-six libraries were prepared from 10 ng of RNA of each sample using Ion AmpliSeq Transcriptome Human Gene Expression Kit (Life Technologies, USA), followed by sequencing on Ion Torrent Proton (Life Technologies, USA). Raw data, namely read counts were submitted to R package for gene expression analysis. Normalization of gene expression was performed with the method of the weighted trimmed mean of M-values (TMM), then the normalized expressions of each gene across control to treatment groups (measured concentrations) were submitted to analysis of differentially expressed genes (DEGs) using correlation analysis between fold change and concentrations. Upregulated DEGs were identified with positive correlation ($p < 0.05$), while down-regulated DEGs with negative correlation. Next, DEGs of each treatment were submitted to principle component analysis (PCA) using FactoMineR package. Gene Ontology (GO) enrichment and Kyoto Encyclopedia of Genes and Genomes (KEGG) pathway of the DEGs were analyzed by using DAVID (the Database for Annotation, Visualization and Integrated Discovery, https://david.ncifcrf.gov). GO terms and KEGG pathway with P-value <0.05 and Fold enrichment >1.5 were considered significantly enriched. For Venn diagrams, we used an on-line tool (http://bioinformatics.psb.ugent.be/webtools/Venn/).

Comparison of gene expression among four gene sets (Human Liver, Microtissues, HepG2 cell line and HepaRG cell line) was conducted. Firstly, the human liver and HepaRG transcriptomic data were compared to the 1200 genes analyzed using the reduced transcriptomic method of which 844 and 721 genes were expressed in the liver and HepaRG cell line, respectively. This could then be compared to the genes expressed in the human liver microtissues. Human liver transcript was carried out by using published data: GEO Accession GSE30611.

**Table 1**
Critical biological pathways and genes associated with liver toxicity and liver fibrosis that are expressed in the human 3D liver microtissues.

| Biological Pathways | Expressed Genes Of Interest | Remarks |
|---|---|---|
| Xenobiotic metabolism | CYP1A1, CYP1B1, CYP1A2, AHR | AhR & AhR-mediated cytochromes (Phase I) |
| | CYP4F12, CYP2C9, CYP2C19, CYP3A4, CYP4A11, CYP3A7, CYP2J2, CYP2E1, CYP2B6, CYP2D6, ALDH2, NR1H4, FDX1, FDXR, ARNT | Phase I of drug-metabolism |
| | SULT2A1, MGST1, UGT1A1, GSTP1, GGT1, MTR, COMT | Phase II of drug-metabolism |
| Transporters | ABCB1, ABCA1, ABCB11, ABCG2, ABCC3, ABCC1, ABCC2, | Relevant transporters |
| Bile & Cholestasis biosynthesis | CYP27A1, CYP7B1, CYP7A1, NR1H3 | Involved in bile and cholesterol biosynthesis |
| ECM remodelling genes | COL11A2, COL17A1, COL18A1, COL1A1, COL1A2, COL3A1, COL7A1, ELN | ECM remodelling genes necessary for wound healing and fibrosis progression |
| | MMP11, MMP13, MMP14, MMP15, MMP16, MMP17, MMP19, MMP2, MMP24, MMP7 | |
| | ITGA1, ITGA2, ITGA3, ITGA4, ITGA5, ITGA6, ITGAM, ITGAV, ITGB1, ITGB2, ITGB3, ITGB4 | |
| General inflammatory genes | CXCL1, CXCL10, CXCL13, CXCL2 | Necessary for eliciting an inflammatory response upon exposure to xenobiotics |
| | IL15, IL18, IL1B, IL1R1, IL1RN, IL23A, IL6 | |
| | CCL2, CCL20, CCL22, CCL3, CCL5 | |
| | CD14, CD40, CD44 | |
| TGF-β Signalling | TGFB1, TGFB2, TGFB3, TGFBR1, TGFBR2 | Pro-inflammatory and key event in liver fibrosis AOP. |
| TNF Signalling | TNF, TNFRSF1A, TNFRSF1B | Involved in Kupffer cell activation |
| PDGF Signalling | PDGFA, PDGFB, PDGFRA, PDGFRB | Involved in hepatic stellate cell activation |

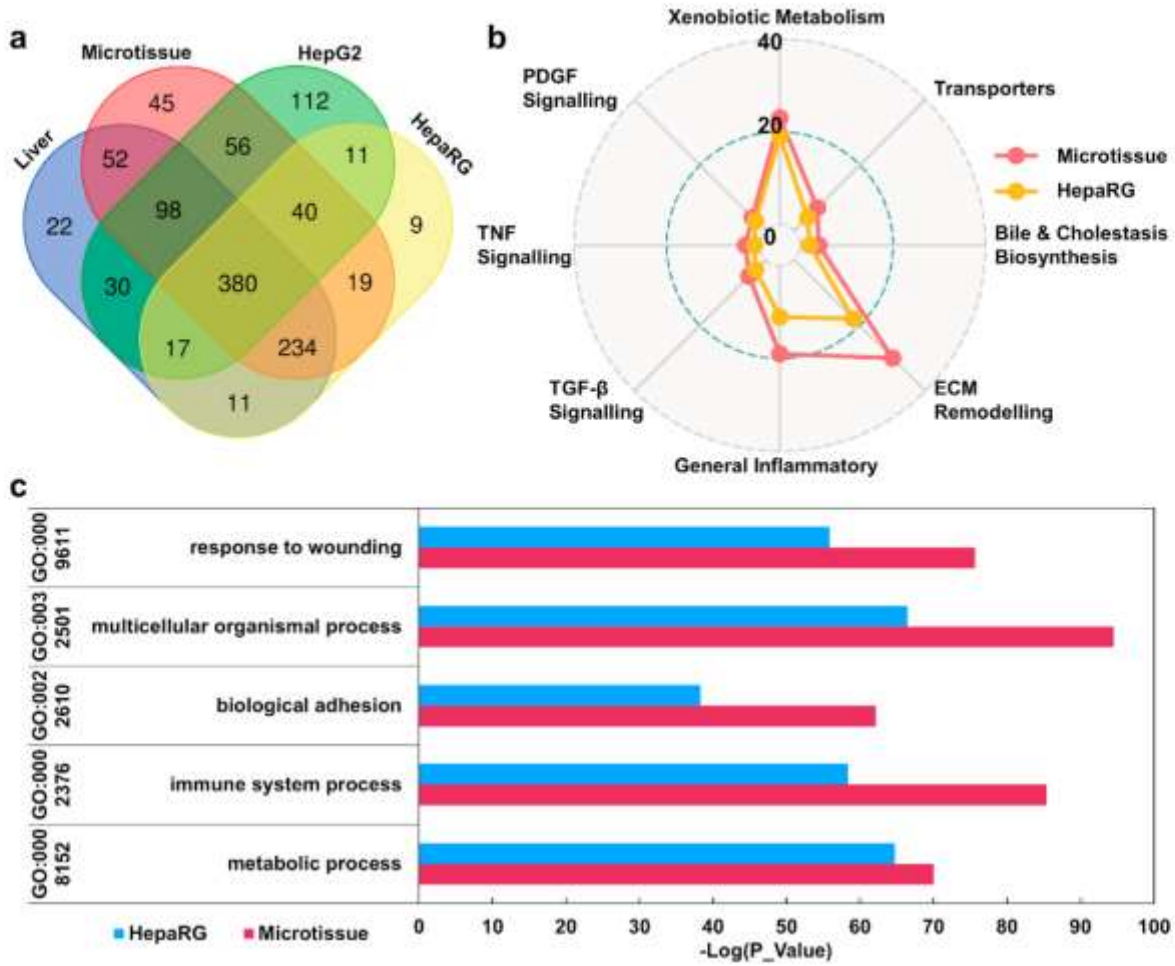


**Fig. 2. Gene expression and targeted biological processes comparison of microtissues with other models.** A Venn diagram was generated by overlapping four sets of genes: the first data set (Human liver) contains the human liver genes (n = 844) involved in the core and toxicity-related 1200 genes set; the second data set (Liver microtissues) contains the genes (n = 924) expressing in Liver microtissues; the third data set (HepG2) contains 744 genes which were identified using the same method with this study; the forth data set (HepaRG) contains 721 genes which are involved in the core and toxicity-related 1200 genes set (a); Radar plots of microtissues and HepaRG for eight biological pathways listed in Table 1. Values indicate the number of interested gene involved in eight biological pathways (b); Targeted biological process of microtissues and HepaRG (c).

Microtissue transcript was obtained from six blank controls in this study. HepG2 transcript identified using the same sequencing method with this study, was generated by Xia et al., (2017) (Xia et al., 2017). HepaRG transcript was from the literature which provided a whole genome sequencing analysis for differentiated HepaRG (Ivanova et al., 2018).

**Statistical Analysis.** Unless stated differently, all data are represented as mean ± SD. p values $< 0.05$ were considered significant-*$p < 0.05$, **$p < 0.01$, and ***$p < 0.001$. All experiments were performed at least three times. All statistical analyses were performed on GraphPad Prism using unpaired two-tailed student's t-test.

## 3. Results and discussion

### 3.1. MTs express essential genes involved in liver fibrotic pathways

The transcriptomic profile of multicellular MTs included essential genes relevant to metabolism, extracellular matrix formation, platelet-derived growth factor signaling, and inflammatory response, especially TNF and TGF-β signaling (Table 1), among which many genes are vital in the development of liver fibrosis (Crespo Yanguas et al., 2016; Zhan et al., 2019). Compared with the gene expression of the liver (Data: GEO Accession GSE30611), MTs showed 76.1% similarity. While HepG2 and HepaRG, the two cell line frequently used in 2D monolayer experiments, had 53.7% and 69.6% similarity, respectively with the liver (Fig. 2a, S1a) (Leite et al., 2016; Zhang et al., 2016). Among the 98 genes that are associated with fibrotic pathways and were expressed in the human 3D liver microtissues (Table 1), 34 genes were missing in HepaRG. In accord with GO enrichment analysis, the 34 genes missing in HepaRG but present in the 3D liver MTs belong to ECM modeling and inflammatory response (Fig. 2b and c), which indicated that hTERT-HSC and THP-1 contribute to gene expression of MTs in these targeted biological processes.

Liver-specific pathways were expressed in the MT, including bile acid metabolism, bile secretion, and sterol metabolism, besides common basal cell processes such as cell cycle and MAPK signaling pathway (Table 1). More essential biochemical pathways represented in the MTs are demonstrated by KEGG analysis of the genes expressed (Figure S1b). MTs express 21 of the 26 CYP-P450 selected in RHT sequencing, including CYP3A4 and CYP2E1, which are very important in drug metabolism and detoxification (Anzenbacher and Anzenbacherova, 2001). Many liver-specific transporters are expressed in the model, such as cholesterol efflux regulatory protein gene (ABCA1), multidrug resistance-related protein gene (ABCC1) and bile salt export pump gene (ABCB11), all of which are involved in the hepatobiliary excretion of

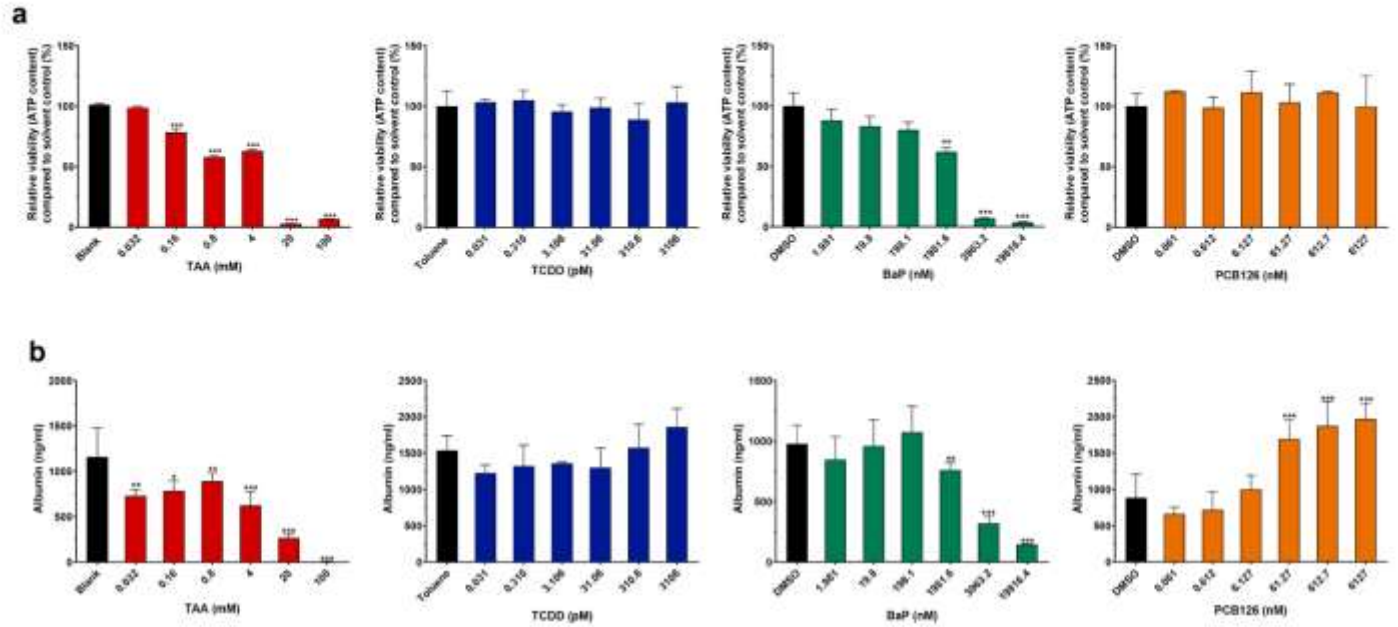


**Fig. 3. Viability and albumin production of liver microtissues exposed to TAA, TCDD, BaP and PCB126.** After 14 days of treatment the liver microtissues were collected and the relative ATP content was measured to assess the microtissues viability. The results were expressed as relative percentage of either the blank or solvent control ± SD (a). After 12 days of exposure the medium/treatment was refreshed and then at day 14 the medium was collected for assessing the quantity of albumin released over the final 48 h of TAA, TCDD, BaP and PCB126 exposure. Albumin was measured using ELISA and data is expressed as albumin concentration ± SD (b). *, $P \leq 0.05$; **, $P \leq 0.01$; ***, $P \leq 0.001$ determined using unpaired *t*-test.

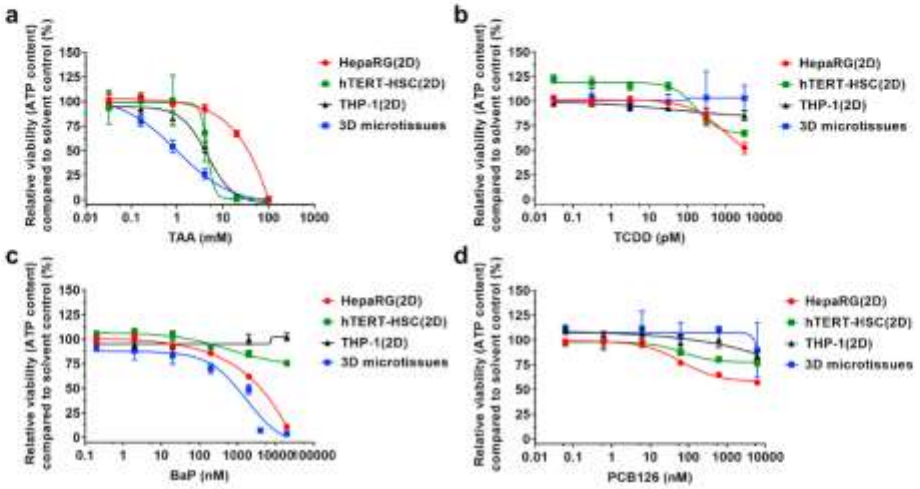


**Fig. 4. Effect of TAA, BaP, TCDD and PCB126 on ATP content in liver microtissues and monolayer culture.** Relative ATP content was measured in human liver microtissues and monolayer culture of differentiated HepaRG, hTERT-HSC and differentiated THP-1 upon exposure to TAA (a), TCDD(b), BaP(c) and PCB126 (d).

hormones and bile (Table 1) (Zhan et al., 2019). More importantly, MTs express genes related to hepatic stellate cell activation (such as PDGFB and PDGFRB) (Table 1) (Borkham-Kamphorst et al., 2015).

### 3.2. TAA and BaP, but not PCB126 and TCDD caused hepatocellular damage and fibrosis in the MT model

The positive control TAA and BaP caused concentration-dependent liver cell damage in the MT model. Relative ATP content showed that TAA and BaP caused marked cytotoxicity to MT at concentration range of 0.16–100 mM and 1981–19816 nM, respectively (Fig. 3a). TCDD and PCB126 did not significantly affect the ATP content in the range of measured concentrations (Fig. 3a), even though PCB126 had reached the highest feasible concentration (2 g/L) based on its solubility in DMSO. Consistent with reduced ATP content, albumin release was significantly decreased by TAA and BaP at concentration range of 0.032–100 mM and 1981–19816 nM, respectively (Fig. 3b), indicating reduced hepatocyte function (Carvalho and Machado, 2018). TCDD did not have any significant effects on albumin release and PCB126 caused a significant increase in albumin release at concentrations of 61 nM and above (Fig. 3b).

The responses in 2D monoculture exposed to the four tested chemicals were different from that in 3D MTs (Fig. 4). In monoculture of HepaRG, THP-1 and HSC cells, TAA (≥4mM) adversely affect the viability of the three cell lines in concentration-dependent manner, and the most sensitive cell line to TAA was THP-1. For TCDD, only the highest experimental concentration (3106pM) reduced viability of HepaRG cells and hTERT-HSC cells in monolayer experiments. HepaRG cell was the most sensitive cell line reacting to the toxicity of BaP and PCB126 in ATP levels. We observed cytotoxicity induced by PCB126 in

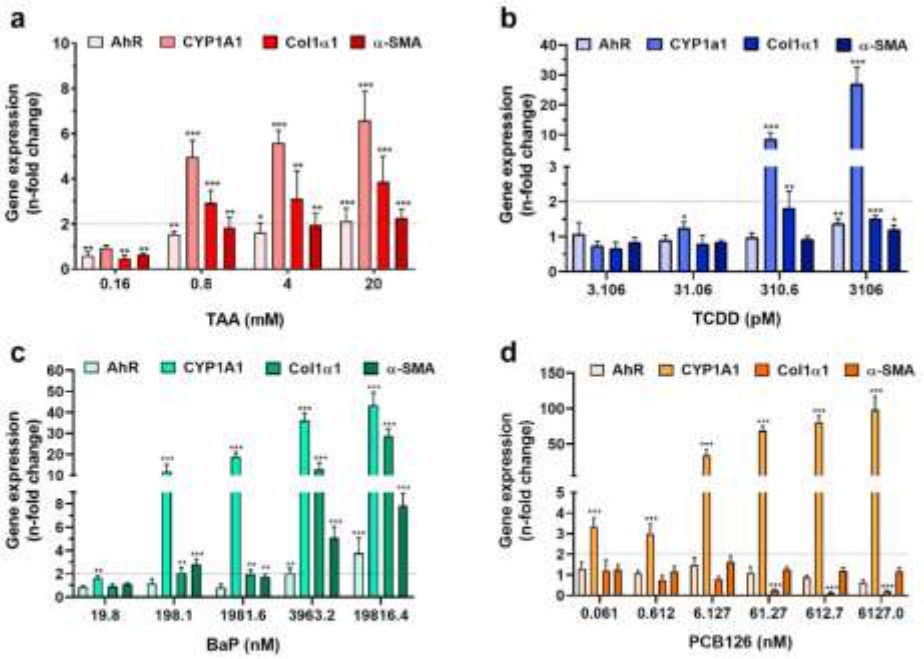


**Fig. 5. Effects of TAA, TCDD, BaP and PCB126 on AhR, CYP1A1, α-SMA and COL1α1 expression in liver microtissues.** Human liver microtissues were created using differentiated HepaRG, hTERT-HSC and differentiated THP-1 and allowed to aggregate for 72 h. Following this the medium was exchanged and treatments TAA (a), TCDD (b), BaP (c) and PCB126 (d) were added and refreshed 2 times per week for 14 days. After 14 days of treatment the liver microtissues were collected and RNA was extracted for further analysis using q-RT-PCR to assess the expression of AhR, CYP1A1, α-SMA and COL1α1 and data are expressed as $2^{-}(-\Delta\Delta Ct) \pm SD$. $^{*}p \leq 0.05$, $^{**}p \leq 0.01$, $^{***}p \leq 0.001$ determined using unpaired *t*-test.

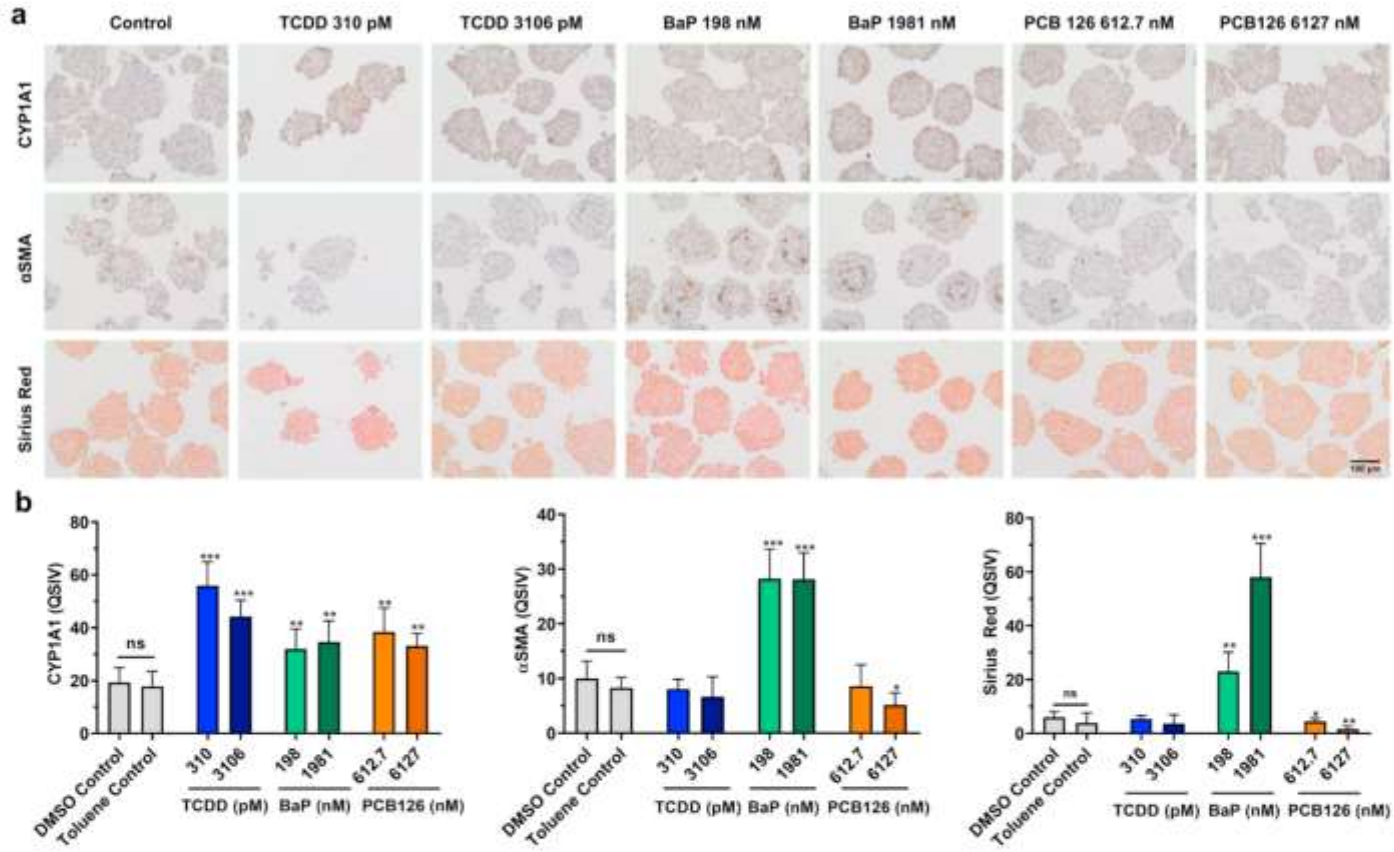


**Fig. 6. Immunostaining of liver microtissues for CYP1A1, αSMA and Sirius Red.** After 14 days the liver microtissues were collected and fixed in 4% PFA and processed via paraffin embedding for IHC analysis. Liver microtissues were stained using anti-CYP1A1 and anti-SMA antibodies and Sirius Red, scale bar is 100 μm. Staining was quantified using QSIV methodology which is described in the methods section and data are expressed as QSIV ±SD. $^{*}p \leq 0.05$, $^{**}p \leq 0.01$, $^{***}p \leq 0.001$ determined using unpaired *t*-test. (For interpretation of the references to colour in this figure legend, the reader is referred to the Web version of this article.)

monoculture of HepaRG and HSC.

In contrast, MTs were more sensitive than any of the three 2D cell lines in identifying toxicity induced by TAA and BaP. TAA and BaP are known to require metabolic activation to elicit toxicity and MTs have an enhanced metabolism activity than the 2D monolayer systems (Ba Qian et al., 2015; Hajovsky et al., 2012). Interestingly, TCDD and PCB126 at

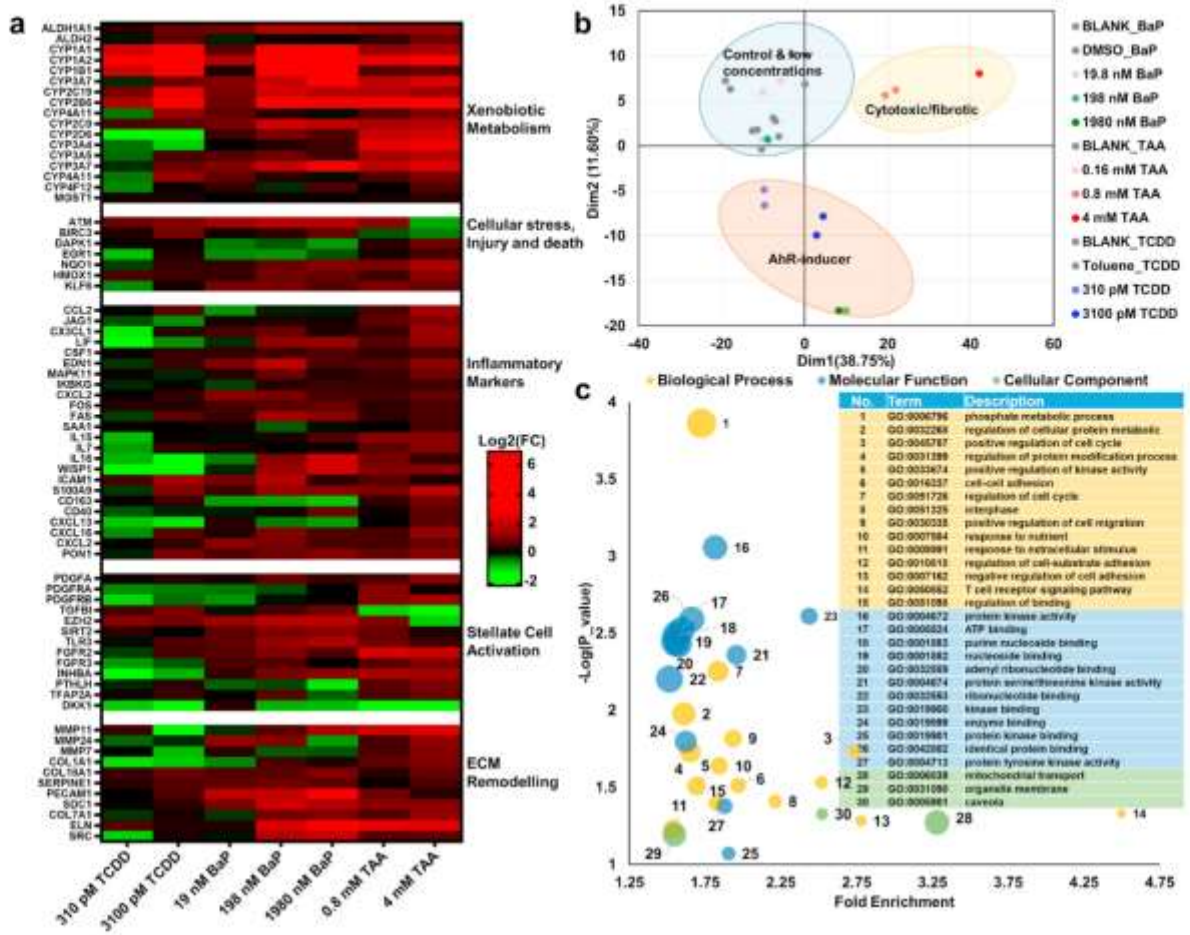


**Fig. 7. Transcriptomic analysis of liver microtissues samples exposed to TAA, TCDD and BaP.** After 14 days the liver microtissues were collected and RNA was extracted for further analysis using RNA-seq. (a) A heatmap was generated using genes related to xenobiotic metabolism and the key events of liver fibrosis: cellular stress, injury and death; inflammatory markers; stellate cell activation; ECM remodelling. Data are expressed as log2(FC). (b) Read counts of differentially expressed genes (DEGs) after normalization were used for principal component analysis (PCA). BaP (green), TAA (red) and TCDD (blue) were plotted based on the first two components and three groups were described: control & low concentrations, protein alkylation and AhR-inducer. (c) Significantly enriched Gene Ontology (GO) terms identified for common DEGs between TAA and BaP. Using the overlapping genes which were only identified in BaP and TAA groups, the relevant biological process, molecular function and cellular components were identified and corresponding information is displayed. The size of circles represents gene number involved in the term, and the bigger the size is, the more genes are involved. (For interpretation of the references to colour in this figure legend, the reader is referred to the Web version of this article.)

the given concentrations failed to induce toxicity in MTs, which highlights the differential sensitivities of different *in vitro* models. The lower sensitivity of MTs to TCDD and PCB126 might be due to the fact that the interaction of different cell lines in MTs protected the HepaRG cells from the damage induced by chemicals when adverse effects were minor.

Regarding specific liver fibrosis markers, BaP and TAA led to the transcriptional upregulation of the fibrosis markers αSMA and Col1α1 in a dose-response relationship. The other two substances, PCB126 and TCDD did not affect αSMA or Col1α1 levels (changes below the arbitrary threshold of 2-fold) (Fig. 5). Immunohistochemistry (IHC) analysis showed that CYP1A1, Col1α1 and αSMA protein expression increased in the group with BaP. Similarly, previous published and unpublished data also show that TAA increases αSMA and elicits the deposit of collagen in this model (Prestigiacomo et al., 2017). In contrast, at the highest concentration of TCDD, only CYP1A1 protein expression but not αSMA or Col1α1 was upregulated. 6127 nM PCB126 induced the upregulation of CYP1A1 protein expression, but downregulated the other two proteins (Fig. 6). Previous studies showed that BaP has the potential of inducing liver carcinogenesis that may be exacerbated by underlying steatosis, but no direct evidence has linked this substance with liver fibrosis (Table S3) (Bucher et al., 2018; Murawska-Ciałowicz et al., 2011). Our results suggested that BaP induced fibrotic pathways in human liver MT model, while the detailed molecular mechanism need to be further explored. In the human liver MT, PCB126 did not elicit any relevant transcriptional upregulation of αSMA and Col1α1, contrarily downregulated the expression of Col1α1(Fig. 5). However, several studies found that PCB126 induced a significant increase of hepatic steatosis, inflammation, and fibrosis in mice/rat. Lipid metabolism dysregulation were observed in PCB126-treated HepaRG cells by analyzing metabolome and transcriptome profiles (Gadupudi et al., 2016; Mesnage et al., 2018, p. 126; Su et al., 2020). The discrepancy between our studies and previous results may be due to the bioaccumulation properties of PCB126 in animals that cannot be compared to sub-chronic (14-days) *in vitro* exposures (Te et al., 2020; Warenik-Bany et al., 2016). On the other hand, dioxin is thought to exert its biological and toxicological effects primarily by binding to the aryl hydrocarbon receptor (AhR, dioxin receptor) (Beischlag et al., 2008; Xie et al., 2013). Different structural characteristics of the AhR were observed among mammalian species and it has been recognized that structural difference contributes to the species specificity of the dioxin effects (Farmahin et al., 2013; Okey, 2007). Thus, one of reasons why we did not observe liver fibrosis potential of PCB126 in human liver microtissues may be the species specificity. Furthermore, while the three chemicals in this study are known as ligands of the aryl hydrocarbon receptor (AhR), only BaP induced fibrotic

pathways in the human liver MTs model. These results suggested that activation of AhR is not sufficient to elicit fibrotic pathway and chemically-induced cytotoxicity is necessary to trigger the early events leading to fibrotic phenotype (Yan et al., 2019). Detailed mechanism on the role of AhR activation in development of liver fibrosis still need to be explored in the future.

### 3.3. Tested chemicals induced specific molecular events

TAA and BaP treatment resulted in a number of gene upregulation in the panel of genes associated with the biological pathway of liver fibrosis. There were five categories relevant to liver function and the fibrosis AOP, including xenobiotic metabolism, cellular stress injury and death, inflammatory markers, stellate cell activation, and ECM remodelling (Fig. 7a). Upregulated genes in MTs treated with TAA and BaP were associated with cytochromes, stress markers (e.g. NQO1 & HMOX1), inflammatory markers (e.g. IL15, IL7 & IL16), HSC activation markers (e.g. PDGFA, PDGFRA & FGFR2) and ECM remodelling (e.g. MMP11, COL1A1 & COL7A1) (Fig. 7a). On the other hand, TCDD only significantly induced upregulation of genes associated with xenobiotic metabolism in MTs model. *In vivo*, TCDD has been reported that it can cause liver fibrosis in mice (Table S3), but the fibrotic effect might have been secondary to TCDD-induced hepatotoxicity and inflammation (Jin et al., 2020; Li et al., 2020; Yan et al., 2019). This may lead to the speculation that higher concentrations of TCDD may cause cytotoxicity and potentially ensuing fibrosis in this *in vitro* system.

The transcriptomic effect of TAA at high concentration on MTs is similar to the high dose treatment of BaP and TCDD. A total of 381 and 363 DEGs were identified for MTs exposed to TAA and BaP, respectively. TCDD had a less marked effect on gene expression and only 60 DEGs were identified, including 45 upregulated and 15 downregulated genes (Figure S2). The DEGs (n = 574) from the three treatment profiles were combined for PCA analysis, leading to contributions of the first two principal components of 38.75% (Dim1) and 11.60% (Dim2), respectively. PCA analysis showed that the first principal component separated compounds based on their cytotoxic/fibrotic potential, with the effect from TAA as the strongest, followed by BaP and last by TCDD. The second principal component seems to separate groups based on their AhR-activation potential, with no effect for TAA (Fig. 7 b). Additionally, the detailed information of common DEGs among the three treatments were listed in Figure S2.

TAA and BaP affected the signaling pathways involved in the development of liver fibrosis. There were 30 GO entries with P-values $<0.05$ and fold enrichment $>1.5$ enriched by the 154 common DEGs between BaP and TAA (69 up-regulated and 85 down-regulated genes) (Fig. 7c, S2). GO enrichment analysis further revealed that the overlapping genes only identified in the BaP and TAA treatment groups were relevant to cell metabolism, cell cycle, cell adhesion, immunity and response to stimulus, which are key responses when liver fibrosis occurs (Zhan et al., 2019). In addition, phosphate metabolic process, protein kinase activity, protein serine/threonine kinase activity and kinase binding were related to AMP-activated protein kinase (AMPK) signaling which is a critical player in the pathogenesis of cholestatic liver injury and the regulation of hepatic inflammation and fibrosis (Li et al., 2017). The enriched KEGG pathways mainly belonged to metabolism, immune and chemical carcinogenesis (Figure S3). It is worth noting that adhesion junctions and adhesion spots were enriched in TAA and BaP treatment group. This is consistent with the described participation of a variety of adhesion molecules in liver fibrosis (Hintermann and Christen, 2019).

In summary, the responses in 3D MTs exposed to the four tested chemicals demonstrated different responses from that in 2D monoculture. Similar to TAA, the BaP at the measured concentrations induced fibrotic pathways in human originated 3D multicellular MT. Moreover, our study indicates that 3D multicellular MT is more sensitive to identifying liver toxicity of chemicals which need metabolism to elicit their toxicity. Thus, 3D multicellular MT provides a novel test system to assess liver fibrotic pathway by environmental chemicals.

## Declaration of competing interest

The authors declare that they have no known competing financial interests or personal relationships that could have appeared to influence the work reported in this paper.

## Acknowledgments

We would like to acknowledge the financial support of the Sino Swiss Science and Technology Cooperation Programme (BG02-12207, EG–CN–05-042018) and National Natural Science Foundation of China (Grant No. 21677072). This work is also supported by the China Scholarship Council (CSC), by the School of Life Sciences (FHNW, Switzerland) and by the School of Environmental Sciences (Nanjing University, China). We would also like to thank Dr. V. Prestigiacomo for the confocal image of the human liver MT used in the TOC. Finally, we would like to thank Dr B. Schnabl for making the hTERT-HSC available for our research.

## Appendix A. Supplementary data

Supplementary data to this article can be found online at https://doi.org/10.1016/j.envres.2020.110679.

## References

Anzenbacher, P., Anzenbacherová, E., 2001. Cytochromes P450 and metabolism of xenobiotics: CMLS, Cell. Mol. Life Sci. 58, 737–747. https://doi.org/10.1007/PL00000897.

Beischlag, T.V., Morales, J.L., Hollingshead, B.D., Perdew, G.H., 2008. The aryl hydrocarbon receptor complex and the control of gene expression. Crit. Rev. Eukaryot. Gene Expr. 18, 207–250. https://doi.org/10.1615/CritRevEukarGeneExpr.v18.i3.20.

Borkham-Kamphorst, E., Meurer, S.K., Van de Leur, E., Haas, U., Tihaa, L., Weiskirchen, R., 2015. PDGF-D signaling in portal myofibroblasts and hepatic stellate cells proves identical to PDGF-B via both PDGF receptor type α and β. Cell. Signal. 27, 1305–1314. https://doi.org/10.1016/j.cellsig.2015.03.012.

Bucher, S., Tête, A., Podechard, N., Liamin, M., Guillou, D.L., Chevanne, M., Coulouarn, C., Imran, M., Gallais, I., Fernier, M., Hamdaoui, Q., Robin, M.-A., Sergent, O., Fromenty, B., Lagadic-Gossmann, D., 2018. Co-exposure to benzo[a] pyrene and ethanol induces a pathological progression of liver steatosis in vitro and in vivo. Sci. Rep. 8, 1–18. https://doi.org/10.1038/s41598-018-24403-1.

Carvalho, J.R., Machado, M.V., 2018. New insights about albumin and liver disease. Ann. Hepatol. 17, 547–560. https://doi.org/10.5604/01.3001.0012.0916.

Crespo Yanguas, S., Cogliati, B., Willebrords, J., Maes, M., Colle, I., van den Bossche, B., de Oliveira, C.P.M.S., Andraus, W., Alves, V.A., Leclercq, I., Vinken, M., 2016. Experimental models of liver fibrosis. Arch. Toxicol. 90, 1025–1048. https://doi.org/10.1007/s00204-015-1543-4.

Deierlein, A.L., Rock, S., Park, S., 2017. Persistent endocrine-disrupting chemicals and fatty liver disease. Curr. Envir. Health Rep. 4, 439–449. https://doi.org/10.1007/s40572-017-0166-8.

Dere, E., Lee, A.W., Burgoon, L.D., Zacharewski, T.R., 2011. Differences in TCDD-elicited gene expression profiles in human HepG2, mouse Hepa1c1c7 and rat H4IIE hepatoma cells. BMC Genom. 12, 193. https://doi.org/10.1186/1471-2164-12-193.

Farmahin, R., Manning, G.E., Crump, D., Wu, D., Mundy, L.J., Jones, S.P., Hahn, M.E., Karchner, S.I., Giesy, J.P., Bursian, S.J., Zwiernik, M.J., Fredricks, T.B., Kennedy, S. W., 2013. Amino acid sequence of the ligand-binding domain of the aryl hydrocarbon receptor 1 predicts sensitivity of wild birds to effects of dioxin-like compounds. Toxicol. Sci. 131, 139–152. https://doi.org/10.1093/toxsci/kfs259.

Friedman, S.L., 2008. Hepatic fibrosis—overview. Toxicology, highlights of the 2008. Annual Congress of The British Toxicology Society 254, 120–129. https://doi.org/10.1016/j.tox.2008.06.013.

Gadupudi, G.S., Klaren, W.D., Olivier, A.K., Klingelhutz, A.J., Robertson, L.W., 2016. PCB126-Induced disruption in gluconeogenesis and fatty acid oxidation precedes fatty liver in male rats. Toxicol. Sci. 149, 98–110. https://doi.org/10.1093/toxsci/kfv215.

Hajovsky, H., Hu, G., Koen, Y., Sarma, D., Cui, W., Moore, D.S., Staudinger, J.L., Hanzlik, R.P., 2012. Metabolism and toxicity of thioacetamide and thioacetamide S-oxide in rat hepatocytes. Chem. Res. Toxicol. 25, 1955–1963. https://doi.org/10.1021/tx3002719.

Harrad, S., Wemken, N., Drage, D.S., Abdallah, M.A.-E., Coggins, A.-M., 2019. Perfluoroalkyl substances in drinking water, indoor air and dust from Ireland: implications for human exposure. Environ. Sci. Technol. 53, 13449–13457. https://doi.org/10.1021/acs.est.9b04604.

Hintermann, E., Christen, U., 2019. The many roles of cell adhesion molecules in hepatic fibrosis. Cells 8, 1503. https://doi.org/10.3390/cells8121503.

Horvat, T., Landesmann, B., Lostia, A., Vinken, M., Munn, S., Whelan, M., 2017. Adverse outcome pathway development from protein alkylation to liver fibrosis. Arch. Toxicol. 91, 1523–1543. https://doi.org/10.1007/s00204-016-1814-8.

Ivanova, O.N., Snezhkina, A.V., Krasnov, G.S., Valuev-Elliston, V.T., Khomich, O.A., Khomutov, A.R., Keinanen, T.A., Alhonen, L., Bartosch, B., Kudryavtseva, A.V., Kochetkov, S.N., Ivanov, A.V., 2018. Activation of polyamine catabolism by N1,N11-diethylnorspermine in hepatic HepaRG cells induces dedifferentiation and mesenchymal-like phenotype. Cells 7, 275. https://doi.org/10.3390/cells7120275.

Jennen, D.G.J., Magkoufopoulou, C., Ketelslegers, H.B., van Herwijnen, M.H.M., Kleinjans, J.C.S., van Delft, J.H.M., 2010. Comparison of HepG2 and HepaRG by whole-genome gene expression analysis for the purpose of chemical hazard identification. Toxicol. Sci. 115, 66–79. https://doi.org/10.1093/toxsci/kfq026.

Jetten, M.J.A., Kleinjans, J.C.S., Claessen, S.M., Chesné, C., van Delft, J.H.M., 2013. Baseline and genotoxic compound induced gene expression profiles in HepG2 and HepaRG compared to primary human hepatocytes. Toxicol. Vitro 27, 2031–2040. https://doi.org/10.1016/j.tiv.2013.07.010.

Jiang, J., Messner, S., Kelm, J.M., van Herwijnen, M., Jennen, D.G.J., Kleinjans, J.C., de Kok, T.M., 2019. Human 3D multicellular microtissues: an upgraded model for the in vitro mechanistic investigation of inflammation-associated drug toxicity. Toxicol. Lett. 312, 34–44. https://doi.org/10.1016/j.toxlet.2019.05.004.

Jin, J., Wahlang, B., Shi, H., Hardesty, J.E., Falkner, K.C., Head, K.Z., Srivastava, S., Merchant, M.L., Rai, S.N., Cave, M.C., Prough, R.A., 2020. Dioxin-like and non-dioxin-like PCBs differentially regulate the hepatic proteome and modify diet-induced nonalcoholic fatty liver disease severity. Med. Chem. Res. 29, 1247–1263. https://doi.org/10.1007/s00044-020-02581-w.

Kostadinova, R., Boess, F., Applegate, D., Suter, L., Weiser, T., Singer, T., Naughton, B., Roth, A., 2013. A long-term three dimensional liver co-culture system for improved prediction of clinically relevant drug-induced hepatotoxicity. Toxicol. Appl. Pharmacol. 268, 1–16. https://doi.org/10.1016/j.taap.2013.01.012.

Lauschke, V.M., Hendriks, D.F.G., Bell, C.C., Andersson, T.B., Ingelman-Sundberg, M., 2016. Novel 3D culture systems for studies of human liver function and assessments of the hepatotoxicity of drugs and drug candidates. Chem. Res. Toxicol. 29, 1936–1955. https://doi.org/10.1021/acs.chemrestox.6b00150.

Leite, S.B., Roosens, T., El Taghdouini, A., Mannaerts, I., Smout, A.J., Najimi, M., Sokal, E., Noor, F., Chesne, C., van Grunsven, L.A., 2016. Novel human hepatic organoid model enables testing of drug-induced liver fibrosis in vitro. Biomaterials 78, 1–10. https://doi.org/10.1016/j.biomaterials.2015.11.026.

Li, X., Liu, R., Zhang, L., Jiang, Z., 2017. The emerging role of AMP-activated protein kinase in cholestatic liver diseases. Pharmacol. Res. 125, 105–113. https://doi.org/10.1016/j.phrs.2017.09.002.

Li, C., Liu, Y., Dong, Z., Xu, M., Gao, M., Cong, M., Liu, S., 2020. TCDD promotes liver fibrosis through disordering systemic and hepatic iron homeostasis. J. Hazard Mater. 395, 122588. https://doi.org/10.1016/j.jhazmat.2020.122588.

Magliano, D.J., Loh, V.H.Y., Harding, J.L., Botton, J., Shaw, J.E., 2014. Persistent organic pollutants and diabetes: a review of the epidemiological evidence. Diabetes Metab. 40, 1–14. https://doi.org/10.1016/j.diabet.2013.09.006.

Mesnage, R., Biserni, M., Balu, S., Frainay, C., Poupin, N., Jourdan, F., Wozniak, E., Xenakis, T., Mein, C.A., Antoniou, M.N., 2018. Integrated transcriptomics and metabolomics reveal signatures of lipid metabolism dysregulation in HepaRG liver cells exposed to PCB 126. Arch. Toxicol. 92, 2533–2547. https://doi.org/10.1007/s00204-018-2235-7.

Messner, C.J., Mauch, L., Suter-Dick, L., 2019. Bile salts regulate CYP7A1 expression and elicit a fibrotic response and abnormal lipid production in 3D liver microtissues. Toxicol. Vitro 60, 261–271. https://doi.org/10.1016/j.tiv.2019.06.002.

Murawska-Ciałowicz, E., Jethon, Z., Magdalan, J., Januszewska, L., Podhorska-Okołów, M., Zawadzki, M., Sozański, T., Dziegiel, P., 2011. Effects of melatonin on lipid peroxidation and antioxidative enzyme activities in the liver, kidneys and brain of rats administered with benzo(a)pyrene. Exp. Toxicol. Pathol. 63, 97–103. https://doi.org/10.1016/j.etp.2009.10.002.

Nault, R., Fader, K.A., Kopec, A.K., Harkema, J.R., Zacharewski, T.R., Luyendyk, J.P., 2016. From the cover: coagulation-driven hepatic fibrosis requires protease activated receptor-1 (PAR-1) in a mouse model of TCDD-elicited steatohepatitis. Toxicol. Sci. 154, 381–391. https://doi.org/10.1093/toxsci/kfw175.

Okey, A.B., 2007. An aryl hydrocarbon receptor odyssey to the shores of toxicology: the deichmann lecture, international congress of toxicology-XI. Toxicol. Sci. 98, 5–38. https://doi.org/10.1093/toxsci/kfm096.

Prestigiacomo, V., Weston, A., Messner, S., Lampart, F., Suter-Dick, L., 2017. Pro-fibrotic compounds induce stellate cell activation, ECM-remodelling and Nrf2 activation in a human 3D-multicellular model of liver fibrosis. PloS One 12, e0179995. https://doi.org/10.1371/journal.pone.0179995.

Qian, Ba, Li, Junyang, Huang, Chao, Qiu, Hongling, Li, Jingquan, Chu, Ruiai, Zhang, Wei, Xie, Dong, Wu, Yongning, Wang, Hui, 2015. Effects of benzo[a]pyrene exposure on human hepatocellular carcinoma cell angiogenesis, metastasis, and NF-κB signaling. Environ. Health Perspect. 123, 246–254. https://doi.org/10.1289/ehp.1408524.

Ramaiahgari, S.C., Waidyanatha, S., Dixon, D., DeVito, M.J., Paules, R.S., Ferguson, S.S., 2017. From the cover: three-dimensional (3D) HepaRG spheroid model with physiologically relevant xenobiotic metabolism competence and hepatocyte functionality for liver toxicity screening. Toxicol. Sci. 159, 124–136. https://doi.org/10.1093/toxsci/kfx122.

Su, H., Liu, Jiangzheng, Wu, G., Long, Z., Fan, J., Xu, Z., Jiawei, Liu, Yu, Z., Cao, M., Liao, N., Peng, J., Yu, W., Li, W., Wu, H., Wang, X., 2020. Homeostasis of gut microbiota protects against polychlorinated biphenyl 126-induced metabolic dysfunction in liver of mice. Sci. Total Environ. 720, 137597. https://doi.org/10.1016/j.scitotenv.2020.137597.

Sutherst, R.W., 2004. Global change and human vulnerability to vector-borne diseases. Clin. Microbiol. Rev. 17, 136–173. https://doi.org/10.1128/CMR.17.1.136-173.2004.

Takaaki, H., Scott, L.F., Yujin, H., 2017. Hepatic stellate cells as key target in liver fibrosis. Adv. Drug Deliv. Rev. 121, 27–42. https://doi.org/10.1016/j.addr.2017.05.007.

Te, B., Yiming, L., Tianwei, L., Huiting, W., Pengyuan, Z., Wenming, C., Jun, J., 2020. Polychlorinated biphenyls in a grassland food network: concentrations, biomagnification, and transmission of toxicity. Sci. Total Environ. 709, 135781. https://doi.org/10.1016/j.scitotenv.2019.135781.

van Grunsven, L.A., 2017. 3D in vitro models of liver fibrosis. Adv. Drug Deliv. Rev. 121, 133–146. https://doi.org/10.1016/j.addr.2017.07.004.

Warenik-Bany, M., Strucinski, P., Piskorska-Pliszczynska, J., 2016. Dioxins and PCBs in game animals: interspecies comparison and related consumer exposure. Environ. Int. 89–90, 21–29. https://doi.org/10.1016/j.envint.2016.01.007.

Xia, P., Zhang, X., Zhang, H., Wang, P., Tian, M., Yu, H., 2017. Benchmarking water quality from wastewater to drinking waters using reduced transcriptome of human cells. Environ. Sci. Technol. 51, 9318–9326. https://doi.org/10.1021/acs.est.7b02648.

Xia, P., Zhang, H., Peng, Y., Shi, W., Zhang, X., 2020. Pathway-based assessment of single chemicals and mixtures by a high-throughput transcriptomics approach. Environ. Int. 136, 105455. https://doi.org/10.1016/j.envint.2019.105455.

Xie, Heidi Qunhui, Hai-Ming, Xu, Fu, Hua-Ling, Hu, Qin, Tian, Wen-Jing, Xin-Hui, Pei, Zhao, Bin, 2013. AhR-mediated effects of dioxin on neuronal acetylcholinesterase expression in vitro. Environ. Health Perspect. 121, 613–618. https://doi.org/10.1289/ehp.1206066.

Yan, J., Tung, H.-C., Li, S., Niu, Y., Garbacz, W.G., Lu, P., Bi, Y., Li, Y., He, J., Xu, M., Ren, S., Monga, S.P., Schwabe, R.F., Yang, D., Xie, W., 2019. Aryl hydrocarbon receptor signaling prevents activation of hepatic stellate cells and liver fibrogenesis in mice. Gastroenterology 157, 793–806. https://doi.org/10.1053/j.gastro.2019.05.066 e14.

Zhan, Z., Chen, Y., Duan, Y., Li, L., Mew, K., Hu, P., Ren, H., Peng, M., 2019. Identification of key genes, pathways and potential therapeutic agents for liver fibrosis using an integrated bioinformatics analysis. PeerJ 7, e6645. https://doi.org/10.7717/peerj.6645.

Zhang, X., Hu, M.-G., Pan, K., Li, C.-H., Liu, R., 2016. 3D spheroid culture enhances the expression of antifibrotic factors in human adipose-derived MSCs and improves their therapeutic effects on hepatic fibrosis. Stem Cell. Int. https://doi.org/10.1155/2016/4626073, 2016.

Zhu, X.-Y., Xia, H.-G., Wang, Z.-H., Li, B., Jiang, H.-Y., Li, D.-L., Jin, R., Jin, Y., 2020. In vitro and in vivo approaches for identifying the role of aryl hydrocarbon receptor in the development of nonalcoholic fatty liver disease. Toxicol. Lett. 319, 85–94. https://doi.org/10.1016/j.toxlet.2019.10.010.

## 5.6 Conclusion

The research goal addressed in project 2 was to assess the effects of additional compounds on the 3D human liver MTs to investigate the potential adverse outcomes they may cause.

In the first paper (Messner *at al. In vitro* Toxicology, 2019) the MTs were exposed to high concentrations of bile salts (CA & DCA) to investigate the link between cholestatic injury (characterised by bile accumulation) and fibrosis. Using 3D multicellular MTs in comparison to 2D culture systems, we see increased sensitivity to bile salts, closer to the physiological concentrations. Recently, the median concentration of bile salts in subjects with fibrosis has been identified to be approximately 1.3 µg/ml (≈2.9 µM) [347], demonstrating the toxicity we see at 30 µg/ml is only 20 times higher, as opposed to previous studies investigating bile salt induced HSC activation that used concentrations as high as 205 µg/ml (≈500 µM) [273].

We demonstrate that the multicellular MTs contain bile canaliculi and bile salts treatment decreased CYP7A1 expression, thereby regulating bile salt production through the negative feedback loop, demonstrating the suitability of this *in vitro* MT model to investigate cholestasis. Clinically bile accumulation leads to hepatotoxicity, inflammation, fibrosis and dysregulation of hepatic functions such as lipid production, which we were also able to recapitulate using bile salts and our 3D culture system. These data are in support of the 3D human liver MTs as being a useful *in vitro* tool for investigating the hepatotoxicity of bile salts and the link to fibrosis, which could contribute to further understanding and therapy development.

In the second paper (Yan and Messner *et al.* under review) the MTs were exposed to three environmental pollutants TCDD, PCB126, B[a]P to assess the adverse outcomes these toxins could cause. Human relevant *in vitro* models are required, as a large number of dioxin studies use rodent models, despite known species differences in AhR signalling [338]. All three compounds are known to activate AhR leading to increased expression of CYP1A1, CYP1A2 and CYP1B1, which the MTs were able to recapitulate. Interestingly, we saw a strong CYP1A1 induction by PCB 126 even at the lowest concentration of 60 pM, which is a concentration seen environmentally [342]. This response shows that the MTs are presenting a compound-specific response to dioxin and dioxin-like compounds.

Only B[a]P elicited hepatotoxicity and fibrosis in the MTs at the concentrations tested, despite all three compounds eliciting AhR signalling. This suggests that activation of AhR signalling alone does not promote a fibrotic response. This is also supported by the response to PBC126, which stimulated the highest expression of CYP1A1 and CYP1A2 but did not cause toxicity or fibrosis. Our finding that AhR signalling is not directly linked to fibrosis is in agreement with a previous finding that demonstrated AhR stimulation by a non-toxic compound resulted in decreased HSC activation [312]. These data demonstrate that the MTs are a promising *in vitro* tool for

assessing the safety of environmental toxins and could provide a more human-relevant model for extrapolating human risk.

In conclusion, the MTs demonstrate the capacity to respond to a variety of different compounds and display the expected phenotypic response: toxic bile salt concentrations elicit CYP7A1 downregulation and cholestatic injury; environmental pollutants activate AhR signalling. This demonstrates the versatility of the MTs as an *in vitro* tool for understanding the biological response to many different compounds.

# 6 Project 3: Incorporation of endothelial cells to the multicellular MT model

## 6.1 Aims

The aim of this project was to increase the structural complexity of the MTs through the addition of an endothelial cell type. The endothelial cell type chosen are HUVECs, which are readily available and a commonly used surrogate in *in vitro* models for a wide range of endothelial cells.

We also aimed to investigate whether the 4-cell model containing HepaRG, THP-1, hTERT-HSC and HUVECs was viable and stable overtime. Furthermore, the MTs were exposed to pro-fibrotic stimuli (TGF-β1, MTX and TAA) in order to assess whether the incorporation of the additional cell type would result in a different response or affect the capacity of the MTs to recapitulate fibrosis.

## 6.2 Introduction

### 6.2.1 LSECs in healthy and fibrotic liver

LSECs are differentiated during embryogenesis at gestational weeks 5-12 in humans and ultimately make up 15-20 % of total liver cells [2]. It has been shown that during differentiation the endothelial cells destined to become LSECs lose classic endothelial cell markers such as platelet endothelial adhesion molecule-1 (PECAM-1) also known as cluster of differentiation (CD31), CD34 and 1F10 antigen. They also gain expression of markers of adult sinusoidal cells such as CD4, CD32 and intracellular adhesion molecule-1 (ICAM-1) [19].

Three cell types contribute to LSEC renewal: mature LSECs, intrahepatic or resident sinusoidal endothelial cell progenitors, and bone marrow derived sinusoidal endothelial cell progenitors [20]. Mature LSECs can proliferate in normal conditions when stimulated with growth factors including vascular endothelial growth factor (VEGF) and fibroblast growth factor (FGF) [20,348]. Resident sinusoidal endothelial cell progenitors most likely contribute to LSEC regeneration. Bone marrow derived sinusoidal endothelial cell progenitors do not elicit LSEC turnover in a normal liver. However, it is important to remember that LSEC renewal differs between physiological and pathological conditions and after liver injury, the bone marrow derived sinusoidal endothelial cell progenitors have been shown to be a main driver in liver regeneration [20].

The liver sinusoid has a dual blood supply and receives blood from the portal vein (70%) and the hepatic artery (30%) [19]. Intrahepatic shear stress is recognised as a main driver of hepatic blood flow regulation and is known as the frictional force applied by blood flow on the endothelial surface [349]. It has been previously demonstrated that LSECs are the main source of NO in the normal liver through endothelial nitric oxide synthase (eNOS) activation by shear stress. Kruppel-like factor 2 (KLF2) elicits the downregulation of vasoconstrictive molecules such as endothelin-1. LSECs also release other molecules capable of regulating blood flow including vasodilating agent carbon monoxide (CO) and the metabolites of the cyclooxygenase (COX) pathway (thromboxane A2, Prostacyclin) [19]. All these molecules act in a paracrine manner on hepatic stellate cells localized in the space of Disse. Healthy LSECs maintain hepatic stellate cell quiescence, thereby inhibiting their vasoconstrictive effect [350]. LSECs form highly permeable structures due to their fenestrae and absence of basement membrane [19]. The fenestrae are 50-150 nm in diameter, organised in clusters termed sieve plates. The periportal region contains larger but fewer fenestrae per sieve plate whereas the centrilobular region has smaller but more numerous fenestrae per sieve plate [351]. It was also been shown that the cytoskeleton is of great importance for the structure of the fenestrae which appear surrounded by actin filaments [352]. LSECs retain blood cells in the vessels while other molecules such as metabolites, plasma proteins, pharmaceutical drugs, lipoproteins, small chylomicron remnants, viruses and exosomes can access the space of Disse to be taken up by hepatocytes and hepatic stellate cells [352,353].

LSECs have one of the highest endocytic capacities in humans. This in combination with a strong lysosomal activity give the LSECs the ability to clear waste from the blood. LSECs clear soluble macromolecules and small particles through endocytic receptors. LSECs also endocytose molecules into the space of Disse, which is a process called transcytosis. LSECs express multiple endocytosis receptors such as scavenger receptors (SR-A, SR-B and SR-H), vascular cell adhesion molecule-1 (VCAM-1), ICAM-1, selectins, mannose receptor and FC gamma-receptor IIb2 [354]. The SRs mediate endocytosis of polyanionic molecules such as oxidised and acetylated low-density lipoproteins, advanced glycation end points and waste products (hyaluronan, chondroitin sulfate or N-terminal propeptides of procollagen (I, III)) [22]. The mannose receptors are not specific to LSECs and bind a wide range of glycoproteins and microbial glycans, such as collagen alpha chains (I, II, III, IV, V, XI), tissue plasminogen activator regulating fibrinolytic activity, and lysosomal enzymes that are recruited for further use in LSEC [354]. The Fc gamma-receptor IIb2 is the only Fc gamma-receptor expressed by LSECs and mediates the clearance of small circulating immune complexes; LSECs play a role in vascular immunity through this receptor [354].

LSECs are strongly involved in initiation and progression of chronic liver disease. Four processes mark their contribution: sinusoid capillarisation (dedifferentiation), angiogenesis, angiocrine signals and vasoconstriction (Figure 19) [19]. Capillarisation in the context of liver injury corresponds to the loss the unique phenotype of LSECs to become ordinary non-specialised endothelial cells [19,355]. Capilliarisation precedes HSC activation and KC activation, making it an early event in liver fibrosis progression [19]. The crosstalk between LSECs and hepatic stellate cells underlines that LSECs contribute to the maintenance of HSC quiescence [350]. Two major pathways, *i.e.* capillarisation of the LSECs and the release of soluble factors affecting the phenotype of neighbouring cells initiate the onset of fibrogenesis. In parallel, other key events mentioned previously are occurring such as hepatocellular injury and KC activation [19].

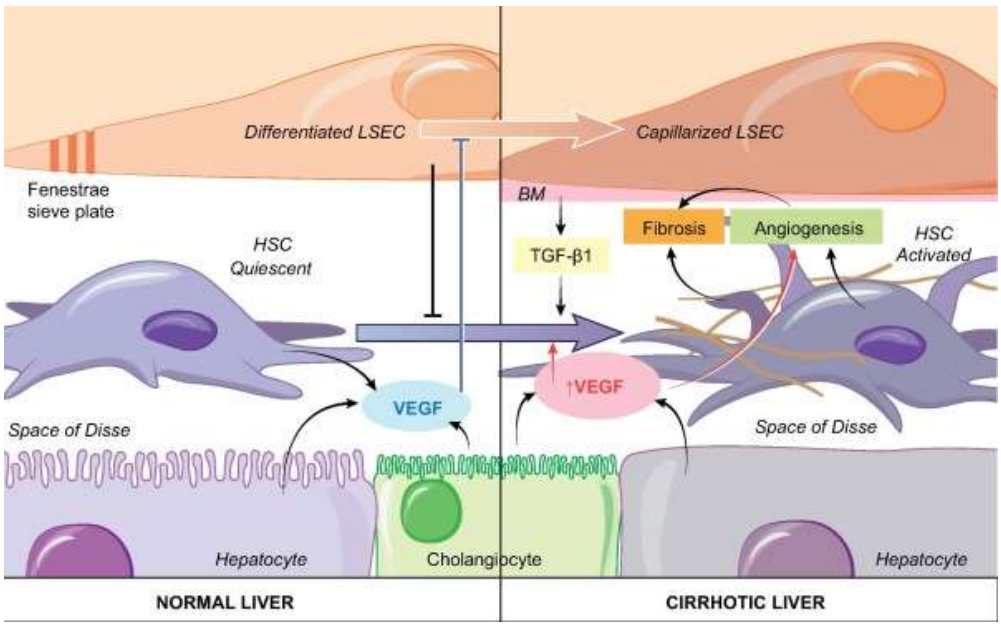


***Figure 19. Role of LSECs in liver fibrosis & cirrhosis.***

In the healthy liver, liver sinusoidal endothelial cells (LSECs) maintain hepatic stellate cell (HSC) quiescence via a NO-dependent pathway. Physiological stress activates the transcription factor Kruppel-like factor 2 (KLF2), which results in the release of vasodilating agents such as nitric oxide (NO). It also causes downregulation of vasoconstrictive molecules including endothelin-1. LSECs also undergo capillarisation, which promotes HSC activation, the production of collagen and fibrosis progression. Cirrhotic livers have shown that endothelial cells lose their fenestrae and develop a basement membrane. *Image taken from Poisson et al.* [19].

### 6.2.2 Current *in vitro* liver models containing endothelial cells

Successful extraction and culture of LSECS (human and rodent) using 2D culture techniques has been reported. Experiments using 2D LSECs have demonstrated it is possible to assess multiple characteristics such as fenestrae, expression of Von Willebrand (vWF) and acetylated low density lipoprotein (acLDL) uptake [357]. Short-term experiments can also be carried out such as transcriptional characterisation and identification of new markers/transcriptional regulators for LSECs such as GATA binding protein 4 and Meis homeobox 2 [358].

However, using LSECs in 2D has drawbacks as it was shown that the LSEC morphology and growth rate is only maintained for ≤ 3 passages, when the cells become flattened, granular fenestrae are lost and irregular cytoplasmic projections appear [350,359]. Therefore, long-term cultures required for assessing certain diseases such as liver fibrosis are not possible using this system. LSECs have also been successfully immortalised using both rodent and human primary cells. Examples of immortalised LSECs include TRP3, SK Hep1, TMNK-1, TSEC and NP11 [19]. The different immortalised cell lines display different benefits and drawbacks. Of the human cell lines, TRP3 and SK Hep1 demonstrate a more successful maintenance of fenestrae, are capable

of forming tubes, taking up acLDL and express vWF [360,361]. Whereas, the human LSEC cell line TMNK1 is capable of taking up acLDL, forming tubes and expresses vWF on an mRNA level but no organised fenestrae were maintained [362]. The rodent models TSEC and NP11 showed a few and no organised fenestrae, respectively. However, similar to the TMNK1 human cell line they were capable of taking up acLDL and forming tubes [363,364]. The use of immortalised LSECs provides us with the ability to maintain typical LSEC characteristics for longer (≤ 11 passages) but even immortalisation does not provide us with the capacity to carry out long-term culture experiments. Micropatterned sandwich culture techniques have also been used which involved co-cultures directly together and separated cultures using Matrigel, in an attempt to prolong characteristic maintenance. However, co-cultures with and without Matrigel did not significantly improve the model or allow for long experiments.

Interestingly, despite the benefits of 3D cell culture mentioned above in section 3.5 no publications were found using LSECs in 3D alone, as they are typically only used in combination with other cell types. There are both human and rodent 3D culture models published that incorporate different variations of hepatocytes, LSECs, KCs and HSCS [97,101,106,365–367]. Hepatocytes and NPCs have been successfully extracted from rats and mice, characterised and cultured long-term [365,367]. However, as described above (section 3.5) rodent *in vivo* and *in vitro* models have issues when extrapolating findings to humans dependent on the research question. Therefore, human *in vitro* models are the primary focus.

Successful incorporation of the PHH and NPC mixture into 3D microtissues has been carried out demonstrating the spheroids express both PHH and NPC markers [97,101,106,368]. In addition to the incorporation and characterisation, drug toxicity studies have been carried out on the multicellular MTs demonstrating successful results with APAP, Diclofenac, Trovafloxacin and fialuridine [93,106]. PHH and NPC microtissues were also assessed for CYP induction using Phenobarbital, Omeprazole, Rifampicin, phenacetin, diclofenac, S-mephenytoin, bufuralol and midazolam [106,368]. However, of these publications only Baze *et al.* showed data demonstrating the successful incorporation of endothelial cells by LYVE1, PECAM1 expression [101]. Messner *et al.* demonstrated that no positive staining was visible for endothelial markers, thereby demonstrating a lack of efficient LSEC incorporation [93].

Two studies have successfully used iPSCs to generate LSEC-like cells [81,369]. Koui *et al.* obtained mature LSECs by using an established protocol to induce IPSC differentiation into mesoderm and then endothelial cell progenitors, which are CD34 positive. The cells were further matured using a TGFβ inhibitor and hypoxic conditions that promote the acquisition of mature endothelial morphology [81]. Gage *et al.* used a similar method as they first produced venous and arterial angioblasts, which was followed by hypoxia, cyclic AMP (cAMP) agonism, and TGF-βinhibition resulting in LSEC-like cells. They also concluded that using venous angioblasts was a more effi-

cient method to produce LSEC-like cells with increased LSEC markers over the arterial angioblasts [369]. These have not yet been incorporated into a 3D model. iPSC derived hepatocyte-like cells have been cultured with human adipose microvascular endothelial cells (HAMEC) to generate 3D models containing endothelial cells. Co-culture of iPSC-derived hepatocytes and HAMEC, demonstrated enhanced hepatocyte characteristics through the co-culture based model [370]. iPSC-derived hepatocytes have also been co-cultured with human umbilical vein endothelial cells (HUVECs) and mesenchymal stem cells (MSCs), which self-assembled to create clusters that resembled liver buds [371].

HUVECs are a commonly used endothelial cell surrogate in a variety of different models as umbilical veins are more readily available and are isolated and maintained with relatively minimal effort [372,373]. HUVECs have been incorporated into a handful of *in vitro* liver models [371,374–376]. Suurmond *et al.* generated a co-culture model of hepG2, mouse KCs and HUVECs to establish a NASH liver model. However, this model is lacking HSCs and contains mouse KCs so it is not optimal for reflecting human physiology [374]. Jung *et al.* also used a hepatoma cell line Huh7 in combination with HUVECs to investigate HCC *in vitro*. As mentioned previously in section 3.5 HepG2 and Huh7 are not the most relevant cell lines for assessing hepatocyte function, additionally this model is lacking essential HSCs and KCs. HUVECs have also been incorporated into collagen/fibronectin matrix composites by Takebe *et al.* and co-cultured with human fetal liver cells and MSCs to generate hepatic tissue [377]. Co-culture has also been performed by Nelson *et al.* with hepatocyte-like C3A cells and HUVECs to assess APAP toxicity [376]. Similar to the other models mentioned these models successfully incorporate HUVECS, but are lacking other essential cell types that play important roles in liver function and injury. All the models were lacking HSCs, which as mentioned previously plays an important role in liver injury and wound healing. The majority of them are also missing KCs, which provide an inflammatory response, which is another essential contributor to liver injury and disease.

A 3D *in vitro* model that efficiently and consistently contains endothelial cells co-cultured with other essential liver cells (HSCs, hepatocytes, KCs) is required to investigate the role endothelial cells play in liver injury.

## 6.3 Materials and Methods

### 6.3.1 Cell culture

HepaRG cells were obtained from Biopredic International (Rennes, France). The cells were seeded at 1 x $10^5$ undifferentiated cells/$cm^2$ in medium with growth supplements ADD710 (Biopredic). The cells were cultured at 37°C in 5% $CO_2$ for 14 days before differentiation. After 14 days of culture, cell differentiation was induced with medium with differentiation supplements ADD720 (Biopredic) for 14 days. Then the cells were maintained in differentiation medium for up to 4 weeks. HepaRG were passaged using Trypsin-EDTA (Invitrogen, Cat. 25300).

hTERT-HSC were kindly provided by Dr. Bernd Schnabl (UC San Diego, USA) and were cultured in DMEM High Glucose (Invitrogen, Cat. 41965) supplemented with 10% fetal bovine serum (FBS) (Invitrogen, Cat. 10270) and 1% P/S (Gibco, Cat.15070063). The cells were maintained in the humidified incubator at 37°C in 5% CO2. hTERT-HSC were passaged using Trypsin-EDTA.

THP-1 monocytic cells (Cell Line Service) were cultured at 2–10 x $10^5$ cells/mL in RPMI 1640 containing (Bioconcept, Cat. 1-41F50-I) 10% FBS, 1% P/S and maintained at 37°C in 5% $CO_2$. THP-1 cells were differentiated into macrophages over 48 hours in RPMI 1640 medium containing 10 ng/mL Phorbol 12-myristate 12-acetate (PMA) (Sigma, Cat. 79346) as described in previous literature [92] . The media containing PMA was removed and the differentiated THP-1 were washed with fresh medium and maintained in DMEM High Glucose supplemented with 10% FBS and 1% P/S. Differentiated THP-1 were detached using Accutase (Sigma, SCR005).

Human umbilical vein endothelial cells (ThermoFischer, Cat. C0035C) were cultured in Endothelial Cell Growth Medium (Promocell, Cat. C-22110) and maintained at 37°C in 5% $CO_2$. T75 flasks were precoated with 10 ml EmbryoMax® 0.1% Gelatin Solution (Sigma, Cat. ES-006-B) for 15 minutes at RT and then 15 minutes at 37°C in 5% $CO_2$. Excess gelatin solution was aspirated and HUVECs were seeded. HUVECs were passaged using Accutase (Sigma, SCR005).

### 6.3.2 Human liver microtissue generation

All HLMTs were generated using the microtissue 3D Petri Dish system from Sigma-Aldrich (Cat. Z764051-6EA) using UltraPure Agarose (ThermoFischer, Cat. 16500100). Cells were counted and resuspended in AM (Table 3). After 72 hours of aggregation the HLMTs were maintained/treated in MM (Table 3). Human liver HLMTs were generated using 2400 cells per MT containing differentiated HepaRG, HUVECs, hTERT-HSC and differentiated THP-1 at a cell-ratio of 2:2:1:1, respectively.

***Table 3. Medium composition for HLMT generation***

| Medium Name | Abbreviation | Composition |
|---|---|---|
| Hepatocyte Medium | HCM | William's E Medium + GlutaMAX (Invitrogen, Cat. 32551), 2mM L-Glutamine (Sigma, Cat. G7513), 1X ITS (Sigma, Cat. 11074547001), 100nM Dexamethasone (Sigma, Cat. D1756) and 1% P/S |
| Endothelial Cell Growth Medium | ECGM | Promocell, Cat. C-22110) |
| Aggregation Medium | AM | 40% ECGM + 40% HCM + 20% FBS |
| Maintenance medium | MM | 50 % ECGM & 50 % HCM |

### 6.3.3 CellTracker™ staining

All four cell types were collected using passaging reagents described for each cell type in methods 6.3.1 and then centrifuged at 300 x g for 5 minutes. The cells were resuspended in CellTracker™ diluted in HCM medium (no FBS) to obtain the correct final concentration (Table. 4). Cells were incubated for 20 min at 37°C in 5% $CO_2$ then washed with PBS prior to MT generation (methods 6.2.2).

***Table 4. CellTracker™ information and concentration***

| Cell type | CellTracker™ | Stock | Final concentration |
|---|---|---|---|
| HUVECs | CellTracker™ Red CMTPX Dye (ThermoFischer, C34552) | 10 mM | 12.5 µM |
| HepaRG | CellTracker™ Green CMFDA Dye (ThermoFischer, C7025) | 10 mM | 20 µM |
| THP-1 and hTERT-HSC | CellTracker™ Violet BMQC Dye (ThermoFischer, C10094) | 10 mM | 25 µM |

### 6.3.4 Cell treatments

3D HLMTs were formed as described above (methods 6.3.2) and treatment was carried out using MM (Table 3). All three cell types and the HLMTs were exposed to a variety of pro-fibrotic treatments (Table 5) for 10 days, with medium exchange every 2-3 days.

***Table 5. Pro-fibrotic treatment information***

| Treatment | Cat. Nr | Solvent | Final Concentration | Remark |
|---|---|---|---|---|
| Transforming growth factor beta 1 (TGF-β1) | Sigma, T5050-1UG | 1 mg/ml BSA & 4 mM HCl | 1 ng/ml | Pro-fibrotic cytokine is key event in fibrosis AOP [263]. |
| Platelet-derived growth factor ( PDGF) | Sigma, P8147-1VL | 0.1 % BSA | 5 ng/ml | PDGF promotes HSC proliferation and fibrosis [378]. |
| Methotrexate (MTX) | Sigma, M8407 | Initial 100 mM stock in DMSO. | 30 µM | Common treatment for psoriasis and arthritis and can elicit fibrosis [207,379]. |
| Thioacetamide (TAA) | Sigma, 163678 | $H_2O$ | 10 mM | Commonly used for *in vivo* and *in vitro* liver fibrosis models [92,380]. |

### 6.3.5 Cell viability assay

Cell viability was assessed using the Cell Counting Kit-8/WST-8 Assay (Sigma, Cat. 96992) and the CellTiter-Glo® Luminescent Cell Viability Assay (Promega, Cat. G7570). Both were carried out as described in the manufacturer's protocols and adjusted to quantities necessary for the HLMTs.

### 6.3.6 Gene expression analysis

mRNA was isolated following standard TRIzol extraction procedure. RNA was reverse transcribed using a M-MLV Reverse transcriptase (Promega, Cat. M1705) and oligo dT (Qiagen, 79237) and real time PCR was performed using FastStart TaqMan® Probe Master (Roche, Cat. 04673417001) and TaqMan probes from Invitrogen. Real time, TaqMan PCR was performed on selected genes (see Table 6). The q-RT-PCR Program used: 10 minutes denaturation at 95°C, followed by 40 cycles of 15 seconds at 95°C and 1 minute at 60°C. The Ct values were generated using the Corbett Rotorgene Analysis Software 6000 and processed on GraphPad Prism. Data are expressed as fold change and Beta-2-Microglobulin was used as an internal standard for normalisation.

***Table 6. q-RT-PCR probes for gene expression analysis***

| Gene of Interest | Abbreviation | Invitrogen REF. Nr |
|---|---|---|
| Beta-2-Microglobulin | B2M | Hs00187842_m1 |
| Actin, alpha 2, smooth muscle | ACTA2 (αSMA) | Hs00426835_g1 |
| Collagen 1 alpha 1 | COL1α1 | Hs00164004_m1 |
| Collagen 4 alpha 1 | COL4α1 | Hs00266237_m1 |

### 6.3.7 Immunohistochemistry

HLMTs were fixed with 4% PFA 1h in PBS containing calcium and magnesium. Fixed HLMTs were either embedded in 2% agarose in PBS or stained whole using the protocol described by Ravenscroft et al [381] using primary and secondary antibodies listed below (Table 7). Images were taken using an Olympus Fluoview FV1000 Confocal Microscope.

HLMTs were also subjected to paraffin embedding, cut, stained for αSMA, Col I, vimentin and H&E by Sophistolab. The staining was then imaged on an Olympus CKX41. Quantification was carried out using the IHC Toolbox on the image analysis software NIH ImageJ (version 2.0.0-rc-56/1.51h).

***Table 7. Antibodies used for whole MT immunostaining***

| Protein of Interest | Primary Antibody | Secondary Antibody |
|---|---|---|
| αSMA | Mouse polyclonal antibody (Sigma A5228)/ 1:200 | Goat anti mouse Alexafluor 488 LOT: 1858259/ 1:1000 |
| CD68 | Mouse monoclonal antibody (Abcam, ab955)/ 1:200 | Goat anti mouse Alexafluor 488 LOT: 1858259/ 1:1000 |
| Albumin | Rabbit monoclonal Anti-Albumin antibody (Abcam, ab207327)/ 1:800 | Goat anti rabbit Alexafluor 546 LOT: 1896381/ 1:1000 |
| Vimentin | Rabbit monoclonal antibody (Abcam, ab92547) / 1:100 | Goat anti rabbit Alexafluor 546 LOT: 1896381/ 1:1000 |

### 6.3.8 Statistical Analysis

Data were analysed using GraphPad Prism 8 (GraphPad Software, Version 8.0.2) and expressed as mean values ± SD. The unpaired Student *t* test was used for comparison between two groups and $P < 0.05$ was considered to be significant: * , $P \leq 0.05$; ** , $P \leq 0.01$; ***, $P \leq 0.001$.

## 6.4 Results

HLMTs were generated (methods 6.3.2) using differentiated HepaRG, HUVECs, hTERT-HSC and differentiated THP-1 stained with Celltracker™ (methods 6.3.3). At 48 hrs of maintenance the HepaRG appeared to be located on the outer layers of the HLMTs. Both the THP-1 and hTERT-HSC were stained with violet Celltracker™ so we can conclude that these two cell types are also located on the outer layers but a few cells are more central. HUVECS which were stained using red Celltracker™ can be seen in the centre of the HLMTs (Figure 20A).

Following this, the HLMTs were cultured for longer periods. The ATP content of the HLMTs were measured over 28 days and the relative content is shown in comparison to day one demonstrated there was no significant change in HLMT viability (Figure 20B). Following the aggregation phase the diameter of the HLMTs was also measured over 21 days, which also demonstrated that there was no significant difference in size during the maintenance phase (Figure 20C). Expression of CD31 was assessed using q-RT-PCR to confirm the incorporation of HUVECs over the 28 day culture period. Results demonstrate that CD31 is stably expressed over time in the HLMTS (Figure 20D).

HLMTs were fixed at day 7, day 10 and day 14 and stained to identify the incorporation of the four cells types: CD31 positive HUVECs and THP-1; Vimentin positive hTERT-HSC, HUVECs and THP-1; Albumin positive HepaRG; CD68 positive THP-1 (Figure 21). As the THP-1 stained positive for CD31 additional staining was carried out using vWF, which is specific to HUVECs, to confirm incorporation and investigate localisation. The HUVECs were located in the central area of the 14 day old MTs (Figure 22), which is consistent with the results using CellTracker™ (Figure 20A).

In order to identify whether the HLMTs were capable of recapitulating liver fibrosis they were exposed to pro-fibrotic treatments 1 ng/ml TGF-β1, 1 ng/ml TGF-β1 with 5 ng/ml PDGF, 30 μM MTX and 10 mM TAA for 10 days. Relative ATP content (% of untreated) was measured and demonstrated that 1 ng/ml TGF-β1 and the co-exposure of 1 ng/ml TGF-β1 and 5 ng/ml PDGF significantly increased relative ATP content, whereas 30 μM MTX and 10 mM TAA elicited a significant decrease in relative ATP content (Figure 23A). RNA was extracted from day 10 treated HLMTs and fibrosis markers αSMA, Col I and Col IV were measured using q-RT-PCR. Gene expression results show that all the treatment conditions elicited an increase in fibrotic marker expression (Figure 23B).

Treated day 10 HLMTs were fixed and stained to investigate the quantity/ changes in αSMA protein. Immunostaining results show that 1 ng/ml TGF-β1, 30 μM MTX and 10 mM TAA elicited an increase in HSC activation demonstrated by the increase in αSMA staining (Figure 24).

In conclusion, all four cell types were successfully incorporated into the HLMTs and successfully cultured for up to 28 days without a change in size or viability. Exposure to pro-fibrotic compounds resulted in increased fibrotic marker expression and increased αSMA protein.

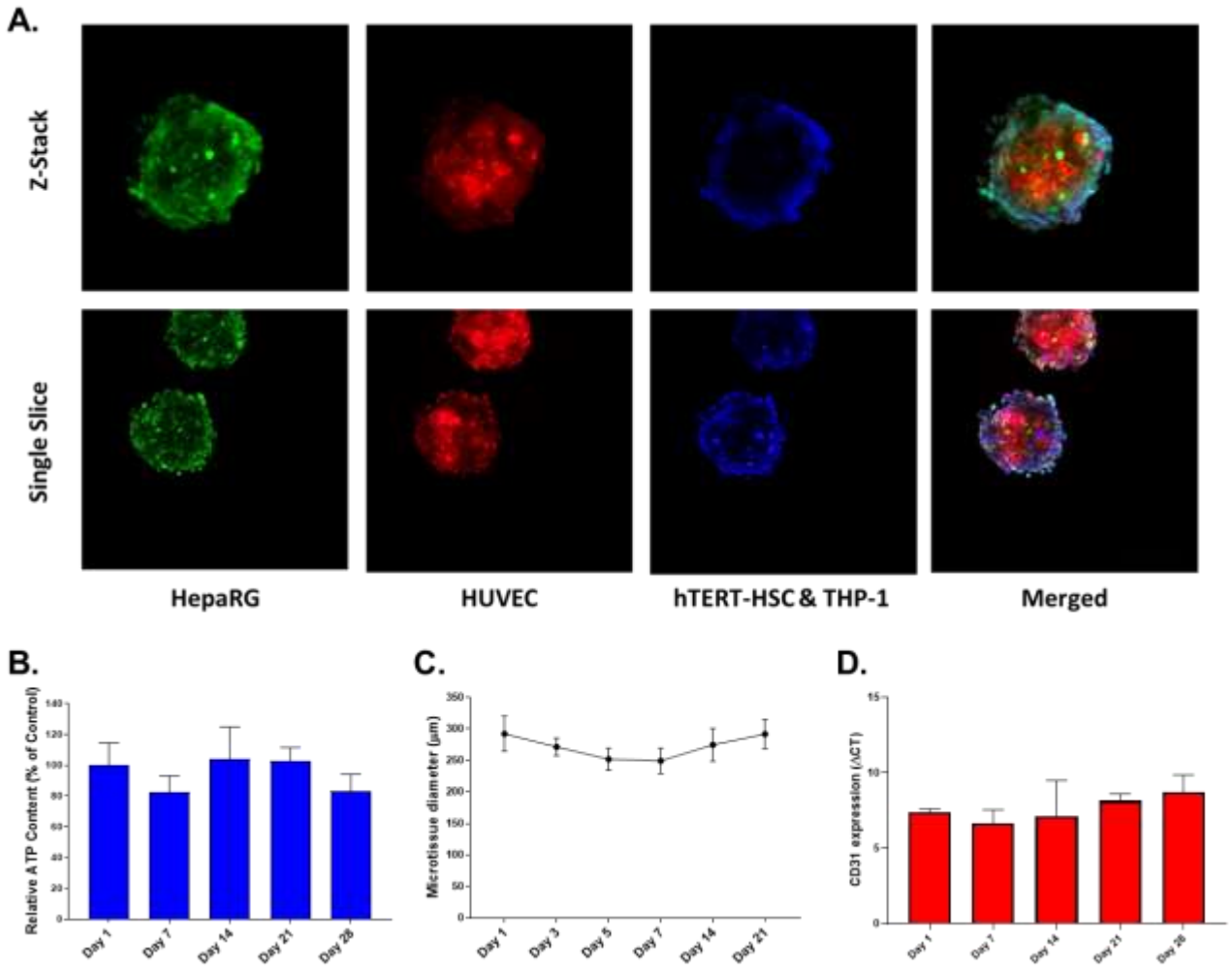


***Figure 20. Long-term culture of four cell HLMTs.***

*HLMTs were generated using CellTracker™ stained differentiated HepaRG (green), HUVEC (red), hTERT-HSC (blue) and differentiated THP-1 (blue). Following aggregation, medium was refreshed using MM and maintained for a further 48 hrs prior to fixation using 4% PFA. Both Z-stack and single slice confocal images were taken to identify the location of the 4 cell types in the HLMTs, scale bar is 100 um (A). HLMTs were generated as described in methods 6.3.2. Following aggregation MM was added and HLMTs were maintained for up to 28 days. Relative ATP was measured using the CellTiter-Glo® Luminescent Cell Viability assay and data are expressed as a percentage with day 1 HLMTs as 100%, N= 2 biological and 2 technical replicates (B). The diameter of the HLMTs was measured over 21 days and the size change is expressed as um, N= 2 biological and 3 technical replicates (C). q-RT-PCR was carried out to identify CD31 expression overtime and expressed as ΔCT, N= 1 biological and 2 technical replicates (D).*

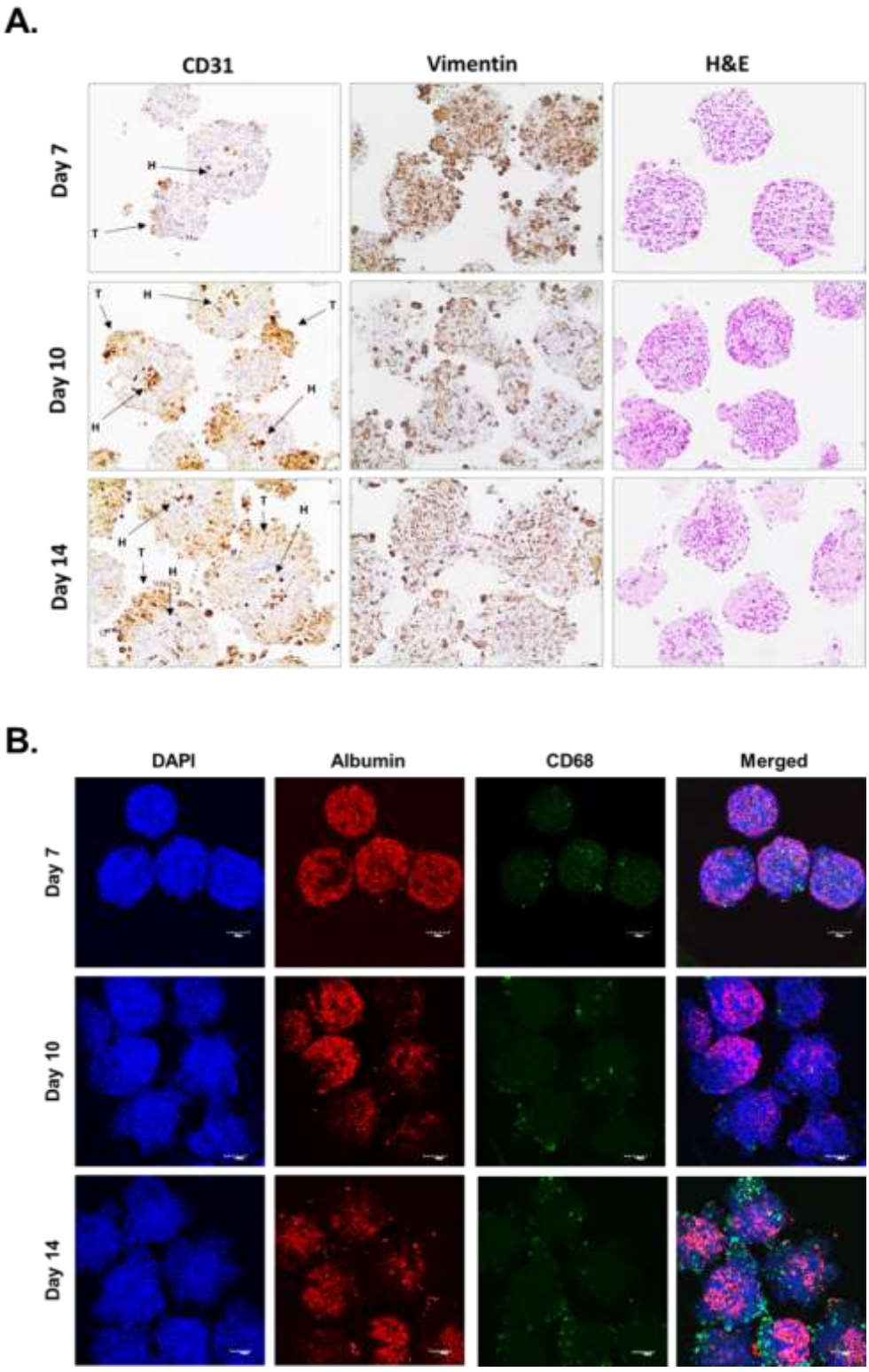


***Figure 21. Immunostaining confirmation of four cell HLMTs.***

*HLMTs were generated as described in methods 6.3.2. Following aggregation, MM medium was added and HLMTs were maintained for up to 14 days. HLMTs were fixed using 4% PFA at day 7, 10 and 14 and then either embedded in paraffin then processed for immunostaining using antibodies for CD31, albumin and vimentin (Both THP-1, T and HUVECS, H) (A), or they were stained using method 6.3.7 (B).*

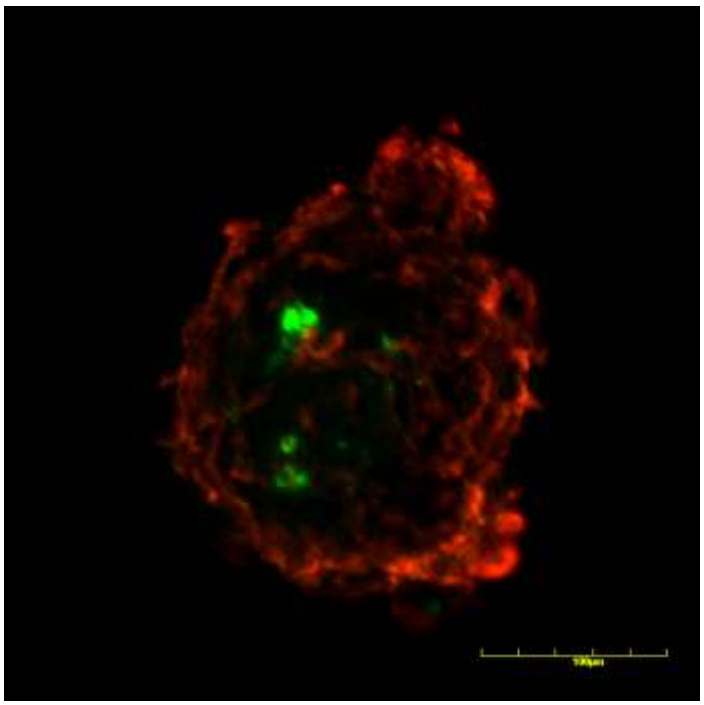

***Figure 22. vWF and vimentin staining of HLMTs.***

*HLMTs were generated as described in methods 6.3.2. Following aggregation, MM medium was added and HLMTs were maintained for up to 14 days and fixed using 4% PFA. vWF is stained green and vimentin is stained red demonstrating the location of the HUVECs.*

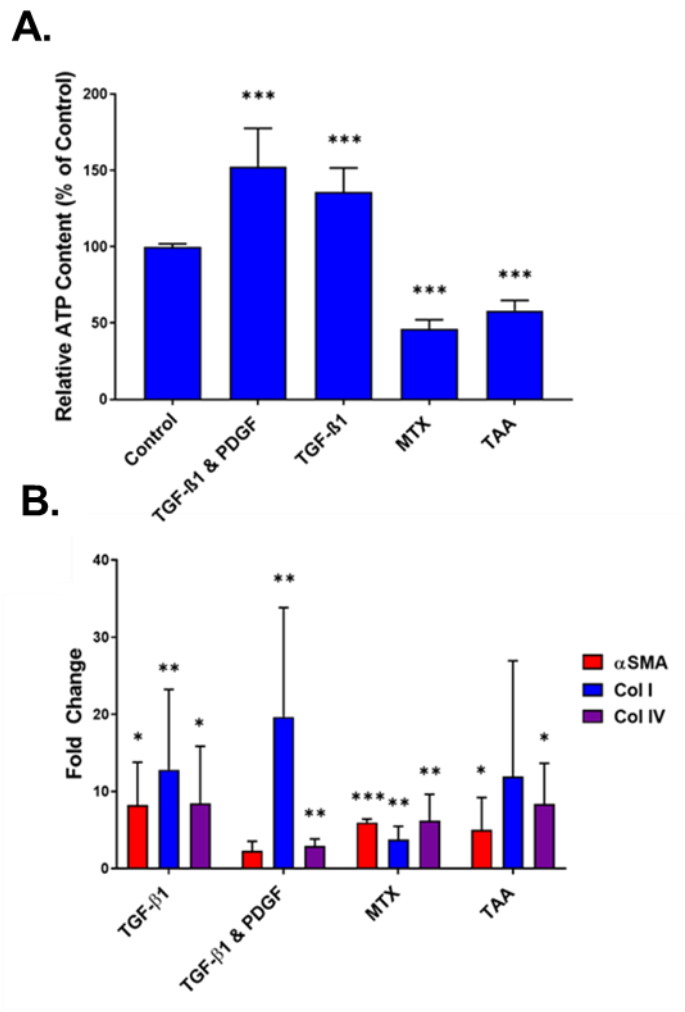


***Figure 23. Exposure of HLMTs to pro-fibrotic compounds.***

*HLMTs were generated as described in methods 6.3.2. Following aggregation pro-fibrotic treatments (Table 5) were added and HLMTs were treated for 10 days with 1 ng/ml TGF-β1, 1 ng/ml TGF-β1 with 5 ng/ml PDGF, 30 µM MTX and 10 mM TAA. Relative ATP was measured using the CellTiter-Glo® Luminescent Cell Viability assay and data are expressed as a percentage of untreated HLMTs (A). q-RT-PCR was carried out to assess gene expression with respect to control (1) of fibrosis markers αSMA, Col I and Col IV (B) N= 1 biological and 3 technical replicates.*

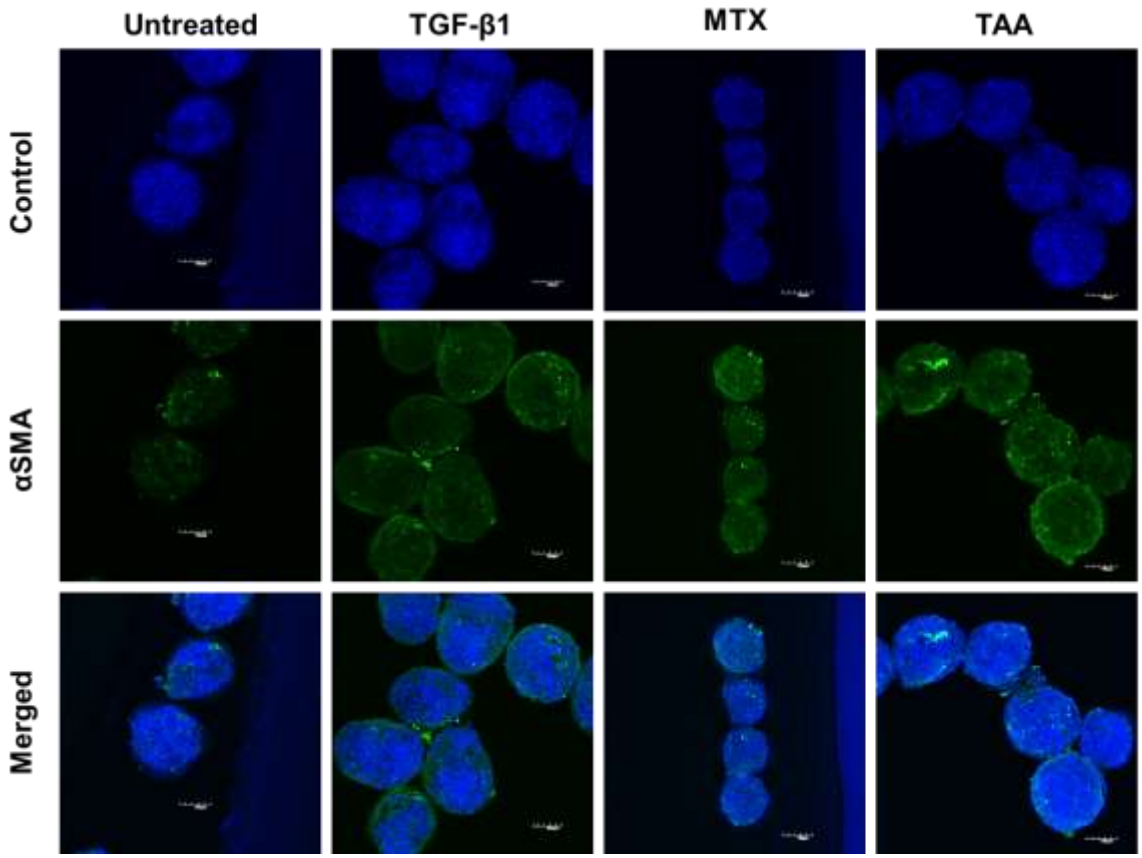


***Figure 24. Pro-fibrotic compounds result in increased quantities of αSMA.***

*HLMTs were generated as described in methods 6.3.2. Following aggregation pro-fibrotic treatments (Table 5) were added and HLMTs were treated for 10 days with 1 ng/ml TGF-β1, 30 µM MTX and 10 mM TAA. Microtissues were fixed using 4% PFA at day 7, 10 and 14 and stained for αSMA.*

## 6.5 Discussion

We successfully produced MTs which contain HepaRG, hTERT-HSC, THP-1 and HUVECs as surrogates for hepatocytes, HSCs, KCs and LSECS, respectively. The MT with the four cell types could be maintained in culture for up to 28 days. Additionally, pro-fibrotic treatments TGF-β1, TGF-β1 with PDGF, MTX and TAA resulted in increased gene expression of fibrotic markers αSMA, Col I and Col IV and increased staining for αSMA.

HepaRG have been shown to be an excellent surrogate for primary hepatocytes as they display many characteristics of PHHs and retain metabolic activity [86]. Additionally, the co-culture of HepaRG, hTERT-HSC and THP-1 has been demonstrated to be capable of recapitulating liver fibrosis upon exposure to pro-fibrotic compounds including hepatocellular damage, HSC activation, inflammation and ECM deposition [92]. Using this established liver fibrosis, we aimed to increase complexity and physiological relevance through the addition of an endothelial cell type. HUVECs were successfully co-cultured with HepaRG, hTERT-HSC and THP-1, which was demonstrated using cell tracker, IHC and q-RT-PCR.

Co-culture of the HLMTs was successful for 28 days as demonstrated by the unchanged ATP content and MT size. CD31 expression was maintained up to 28 days. CD31 is an endothelial cell marker, yet the THP-1 were also stained positive for CD31 in our HLMTs. Monocytes such as THP-1 have been shown to stain positive for CD31 under angiogenic conditions [382]**.** The medium included endothelial growth factors, which could have promoted the THP-1 to express CD31. Therefore, further investigation needs to be carried out including alterations in medium to improve the maintenance of the macrophage phenotype. Although the THP-1 and HUVECs stained positive for CD31, we can infer based on the CellTracker™ localisation that the CD31 positive cells in the centre of the HLMT are HUVECs and those further to the exterior are the THP-1. This was confirmed by staining the MTs with vWF, a marker of endothelial cells [383], which stained strongly in the centre of the HLMTs.

MTX and TAA are two substances that have been shown to elicit toxicity and liver fibrosis *in vitro* [92,98]. TGF-β1 and PDGF are cellular factors involved in HSC activation and migration [263]. Additionally, TGF-β1 expression is a key event in the liver fibrosis AOP [263]. These four compounds were used to assess whether the HLMTs would respond to pro-fibrotic stimuli. We demonstrate that exposure of the HLMTs to TGF-β1 and PDGF we resulted in increased expression of fibrotic markers Col I and Col IV. TGF-β1 also elicited increased HSC activation shown using immunostaining and gene expression. MTX and TAA elicited a toxicity in the HLMTs as expected based on previous findings [92]. HSC activation is a key event of the liver fibrosis AOP [263], which our HLMTs recapitulated as demonstrated by increased αSMA expression and staining. This suggests that the addition of the fourth cell type (HUVECs) did not affect the susceptibility of HSCs towards exposure to pro-fibrotic treatments. The activated HSC led to increased Col I and Col IV

expression, suggesting increased ECM production, a key event in fibrosis progression [263]. Further experiments are required to confirm ECM deposition on a protein-level and other key events including hepatocellular damage and pro-inflammatory response through KC activation [263].

Although HUVECs phenotypically differ from LSECs, they are endothelial cells capable of expressing VCAM-1 and ICAM-1 [384]. These proteins are involved in antigen presentation, thereby playing an important role in inflammation and immune responses in the liver [19]. Additionally, capillarisation is involved in the progression of liver fibrosis and it has been shown that HUVECs have the potential to form capillaries [385]. Therefore, HUVECs do possess relevant endothelial characteristics that could be useful when investigating liver fibrosis *in vitro*.

Additional experiments are required to assess whether the HUVECs are capable of recapitulating LSEC-specific changes during fibrosis progression. Further investigation could involve assessing the capillarisation capacity of HUVECs upon exposure to pro-fibrotic compounds, as this is an important step during liver damage [19]. Finally, it would also be of interest to optimise a 3D *in vitro* model using PHHs, HSCs, KCs and LSECs and to compare the cell line based model to the primary model to identify benefits and limitations of each model.

## 6.6 Conclusion

We successfully produced HLMTs comprising HepaRG, THP-1, hTERT-HSC and HUVECS, which were able to be cultured for 28 days with no effect in viability and composition. We also demonstrate that the cells self-aggregate and localise into specific positions, which were maintained overtime.

We also demonstrate that the HLMTs recapitulate the final sequence of events leading to fibrosis, including HSC activation and increased collagen expression. In conclusion, we suggest that, after additional optimisation, our HLMTs are a suitable *in vitro* model for investigating liver fibrosis.

# 7 Scientific impact, limitations and future perspectives

The research hypothesis on which this work was based was that multicellular, 3D, human *in vitro* models could recapitulate clinically relevant cellular processes leading to fibrosis. Thus, a model based on three hepatic cell lines was employed to mimic events leading to liver fibrosis, to evaluate responses to a variety of chemicals and to identify miRNAs that could serve as translational biomarkers of liver fibrosis. The results presented in this thesis confirm that the 3D model is able to recapitulate physiologically relevant, compound-specific effects related with liver fibrosis and that released miRNAs are promising biomarkers *in vitro* and potentially *in vivo*. The presented model represents thus a contribution towards the replacement of animal models and the advancement of the 3Rs.

We could establish that the 3D-HepaRG cell line (a surrogate for primary hepatocytes) differentially released miRNAs into the cell culture supernatant when exposed to MTX and APAP. Further evaluation of the release of miRNA-122 from HepaRG-cells undergoing toxic insult confirmed the suitability of extracellular miRNAs, in particular released via exosomes, as early biomarkers in this *in vitro* system. Experiments using a multicellular model and NGS to identify novel miRNAs as putative specific biomarkers of fibrosis resulted in a selection of four extracellular miRNAs (miR-199a-5p, miR-214-3p, miR-99b-5p and miR-125a-5p). Mechanistic investigations showed that three of these miRNAs were associated with stellate cell activation, providing phenotypic anchoring to these putative biomarkers. In addition, comparable results were also obtained using 3D cell cultures generated with primary human hepatic cells exposed to profibrotic stimuli.

Regarding the transferability of the results to the clinical situation, the miRNAs identified using the MTs still require confirmation for use as biomarkers by assessing miRNAs in human serum/plasma and tissue samples. The obtained data however demonstrate that the cell-based models are capable of recapitulating clinically proven APAP-induced miR-122 release. We can thus infer that there is a potential for *in vitro-in vivo* translation of the results, but future investigations should be performed to substantiate that claim. Furthermore, three of the four investigated miRNAs led to decreased expression of known target proteins and to HSC activation. These findings also support the potential of these selected extracellular miRNAs as relevant fibrosis biomarkers. Additional research is required to identify which cell types are releasing each specific miRNAs and how potential intercellular interactions take place. Applying *in situ* hybridisation for miRNA-detection on fibrotic tissue and immunostaining for detection of suspected protein targets, we may be able to enhance our understanding of the role of the miRNAs and their targets in fibrosis progression.

The results presented here with different chemicals make evident that the MTs display great versatility and broad applicability as an *in vitro* tool for assessing adverse outcomes. The

system was able to reproduce the toxic effects of compounds causing different types of DILI (MTX and APAP eliciting fibrosis and acute hepatotoxicity, respectively); of bile salts causing decreased CYP7A1 and cholestatic injury; of dioxins and dioxin-like compounds stimulating AhR signalling. These physiologically relevant results provide us with further confirmation that the MTs are a suitable *in vitro* tool, which could contribute towards the replacement of animal models and advance the 3Rs.

Despite the demonstrated good performance, the MT model could be optimised further in terms of physiological likeness by including endothelial cells, as the LSECs play an important role in the liver. To this end, we introduced HUVECs into the multicellular model to enhance its relevance and more faithfully recapitulate liver physiology. The generated four-cell model was also able to develop a fibrotic phenotype upon exposure to pro-fibrotic stimuli including TGF-β1, MTX and TAA. These are promising results, but due to the unique nature of LSECs (fenestrae and lack of basement membrane) a more appropriate endothelial cell line should be considered for future developments and investigation of specific endothelial cell responses such as capillarisation.

In summary, in this thesis we clearly demonstrated the versatility and potential of a multicellular, 3D, *in vitro* model based on human cell lines for the investigation of hepatic fibrosis and the identification of novel biomarkers. The presented results contribute to the understanding of cellular events in the progression of liver fibrosis, to the discovery of potential non-invasive biomarkers and to the 3Rs, as the model represents a sound alternative to animal studies.

# 8 Acknowledgements

I would like to express my appreciation and gratitude for the support that a large number of people have provided me throughout my PhD studies.

Firstly, I would like to express my endless thanks and gratitude to my professor and supervisor at the Fachhochschule Nordwestschweiz Prof. Dr. Laura Suter-Dick for her support over the past 3.5 years. As a supervisor throughout my studies, she has always been excited to discuss and hear my ideas, which raised my confidence massively. With her guidance and advice, I have reached my research goals and grown professionally and personally. I would also like to thank her for giving me, the chance to travel and present my work as being allowed to network and share my results greatly enhanced my experience as a student.

I would like to thank my faculty representative at the University of Basel Prof. Dr. Stephan Krähenbühl for the interesting discussions and critical evaluation of my work. I would also like to thank my co-referee from the University of Liverpool Prof. Dr. Christopher Goldring for his critical assessment of my work. I would like to thank Prof. Dr. Bernd Schnabl from UC San Diego for kindly providing the hTERT-HSC used in this research. Thanks also to the Fachhochschule Nordwestschweiz and the Swiss Centre for Applied Human for their financial support during this research.

To all the amazing co-workers I have had during my PhD, I would like to thank them sincerely for their support and making such an enjoyable and friendly work environment. Thank you to Dr Vincenzo Prestigiacomo for providing me with a great start and supporting me even after he left the group. I would particularly like to thank Dilek Özkul and Saskia Schmidt for not only being great friends but also for contributing towards my research. Thanks to Michaela Caj and Floriana Burgio for the encouragement they provided me. Special thanks to Dr. Carine Gaiser, who has been a great co-worker and friend and supported me every step of the way both professionally and personally.

Thank you to my amazing friends Joëlle, Linda, Gaia, Federica, Clara, Francesco, Andrea, Lmar and Annika who have supported me and made Basel feel like home. It would not have been the same without you all. A very special thanks to Gabriele, we have laughed and cried together and he has cheered me on at the end when I needed it the most.

I would like to thank my family for the huge amount of support they have given me throughout my whole life and during all my studies. Thanks to my sisters for being there for me. I am deeply grateful to my parents for being my personal cheerleaders and for providing me with immeasurable amounts of emotional support. I would also like to thank my husband's family for their support, especially Kalle Opa who is probably my biggest fan. Finally, yet importantly, I would like to thank my amazing husband Nils, who has believed in me and supported me every single day during the highs and lows. His love has encouraged me to face everything life and my PhD has thrown at me and I cannot thank him enough.

# 9 Abbreviations

| | |
|---|---|
| 5-$CH_3$-THF | 5-methyltetrahydrofolate |
| ABC | ATP-binding cassette |
| acLDL | acetylated low density lipoprotein |
| AGO | Argonaute |
| AHRR | AhR repressor |
| AICAR | 5-aminoimidazole-4-carboxamide ribonucleotide |
| AIP | AhR-interacting protein |
| ALD | Alcoholic liver disease |
| Alix | ALG2-interacting protein X |
| ALP | Alkaline phosphatase |
| ALT | Alanine aminotransferase |
| a-MCA | a-muricholic acid |
| AOP | Adverse outcome pathway |
| APAP | Acetaminophen |
| ApoE−/−mice | Atherosclerosis-prone apolipoprotein E-deficient mice |
| APRI | Serum aspartate aminotransferase/platelet ratio index |
| ARFI | Acoustic radiation force impulse |
| AST | Aspartate aminotransferase |
| ATIC | inhibits bifunctional purine biosynthesis protein |
| BDL | bile duct ligation |
| bHLH | basic Helix–Loop–Helix |
| BSEP | Bile salt export pump |
| CA | Cholic acid |
| cAMP | cyclic AMP |
| $CCL_4$ | Carbon tetrachloride |
| CD31 | cluster of differentiation |
| CDCA | Chenodeoxycholic acid |
| CFTR | cystic fibrosis transmembrane conductase regulator |
| Con A | Concanavalin A |
| COX | cyclooxygenase |
| COX-2 | cyclooxygenase 2 |
| CPZ | Chlorpromazine |
| CT | Computed tomography |
| CTGF | Connective growth factor |
| CYP | Cytochrome p450 enzymes |
| CYP27A1 | Mitochondrial steroid 27-hydroxylase |
| CYP7A1 | cholesterol 7α-hydrolase |
| CYP7B1 | oxysterol 7a-hydroxyla |
| CYP8B1 | sterol 12a-hydroxylase |
| DAMPs | damage-associated molecular pattern molecules |
| DCA | Deoxycholic acid |
| DGCR8 | DiGeorge Syndrome Critical Region 8 |
| DHFR | dihydrofolate reductase |
| DILI | Drug-induced liver injury |
| ECM | Extracellular matrix |
| EGF | Epidermal growth factor |
| eIF4F | eukaryotic initiation factor 4f |
| eNOS | endothelial nitric oxide synthase |
| ER | Endoplasmic reticulum |
| EVs | extracellular vesicles |
| FGF | fibroblast growth factor |
| FIB-4 | Fibrosis-4 |
| FPGS | folylpolyglutamate synthase |
| FS | FibroSpect II |
| GGH | gamma-glutamyl hydrolase |
| GGT | Gamma-glutamyl transpeptidase |
| GSH | Glutathione |

| | |
|---|---|
| GSSG | glutathionine disulphide |
| GST | glutathione S-transferase |
| HAMEC | human adipose microvascular endothelial cells |
| HBV | Hepatitis B virus |
| HCC | Hepatocellular carcinoma |
| HCV | Hepatitis C virus |
| HDL | high-density lipoprotein |
| HLMT | Human liver microtissue |
| HMEC-1 | Human microvascular endothelial cell line |
| HSC | Hepatic stellate cell |
| hTERT-HSC | Immortalised hepatic stellate cells |
| HUVECs | human umbilical vein endothelial cells |
| I/R | ischemia and reperfusion |
| ICAM-1 | intercellular adhesion molecule-1 |
| IL-17 | Interleukin-17 |
| IL-1β | Interleukin-1beta |
| IL-6 | Interleukin-6 |
| iPSC | Induced pluripotent stem cell |
| KC | Kupffer cell |
| KLF2 | Kruppel-like factor 2 |
| LCA | Lithocholic acid |
| LDLR | Low-density lipoprotein receptor |
| LSEC | Liver sinusoidal endothelial cell |
| LYVE1 | Lymphatic Vessel Endothelial Hyaluronan Receptor 1) |
| $m^7G$ | 7-methylguanosine |
| MDR1 | Multidrug resistance protein 1 |
| MHC | Major histocompatibility complex |
| miRISC | miRNA-induced silencing complex |
| miRNA | MicroRNA |
| MMPs | Matrix metallopeptidase |
| MRE | Magnetic resonance elastography |
| MSCs | Mesenchymal stem cells |
| MTX | Methotrexate |
| MTXPG | rheumatoid arthritis |
| MVs | microvesicles |
| NAC | N-acetylcysteine |
| NAFLD | Non alcoholic fatty liver disease |
| NAPQI | N-acetyl-p-benzoquinone imine |
| NAT | N-acetyltransferases |
| NF-κB | nuclear factor kappa-light-chain-enhancer of activated B cells |
| NSAIDs | non-steroidal anti-inflammatory drugs |
| OAT | Organic anion transporter |
| OATP | Organic anion transporting polypeptide |
| OCT | Organic cation transporter |
| OSTa/b | organic solute transporter |
| PABPC | poly(A)-binding protein C |
| PAH | polycyclic aromatic hydrocarbons |
| PAS | Per-ARNT-Sim |
| PCBs | polychlorinated biphenyls |
| PCDD | polychlorinated dibenzo-dioxins |
| PCDFs | polychlorinated dibenzofurans |
| PDGF | Platelet derived growth factor |
| PDGF- βR | Platelet derived growth factor  beta receptor |
| PE | Phosphatidylethanolamine |
| PE | phosphatidylethanolamine |
| PHH | Primary human hepatocytes |
| Pre-miRNAs | Precursor miRNA |
| Pri-miRNA | Primary miRNA |
| PTGES3 | prostaglandin E synthase 3 |
| RA | rheumatoid arthritis |
| ROS | Reactive oxygen species |
| shRNA | short hairpin RNA |

| | |
|---|---|
| SLC | Solute carrier |
| SLC19A1 | Folate transporter 1 |
| SR | scavenger receptors |
| SULT | sulfotransferase |
| TAA | Thioacetamide |
| TBL | Total bilirubin |
| TE | Transient elastography |
| TfR | Transferrin receptor |
| TGF-β1 | Transforming growth factor beta 1 |
| THF | tetrahydrofolate |
| TIMPs | Tissue inhibitor of metalloproteinases-1 |
| TLRs | toll-like receptors |
| TNF-α | Tumour necrosis factor alpha |
| Tsg101 | tumor susceptibility gene 101 protein |
| TYMS | thymidylate synthase |
| UDCA | a-MCA |
| UGT | UDP-glucuronosyltransferase |
| VCAM-1 | vascular cell adhesion molecule-1 |
| VEGF | vascular endothelial growth factor |
| vWF | Von Willebrand factor |
| XPO5 | Exportin-5 |
| XRE | xenobiotic-response elements |
| XRN1 | exoribonuclease 1 |

# 10 References


1. Anthony L. Mescher. *Junqueira's Basic Histology Text and Atlas, 14th Edition*. (2016).
2. Couvelard, A. *et al.* Structural and functional differentiation of sinusoidal endothelial cells during liver organogenesis in humans. *Blood* **87**, 4568–4580 (1996).
3. Kmieć, Z. Hepatocytes. in *Cooperation of Liver Cells in Health and Disease* (ed. Kmieć, Z.) 9–12 (Springer, 2001). doi:10.1007/978-3-642-56553-3_2.
4. Ryan J. Schulze, Micah B Schott, Carol A. Casey, Pamela L. Tuma & Mark A. McNiven. The cell biology of the hepatocyte: A membrane trafficking machine. *J. Cell Biol.* **218**, 2096–2112 (2019).
5. Wang, L. & Boyer, J. L. The maintenance and generation of membrane polarity in hepatocytes. *Hepatology* **39**, 892–899 (2004).
6. Boyer, J. L. Bile Formation and Secretion. *Compr Physiol* **3**, 1035–1078 (2013).
7. Gissen, P. & Arias, I. M. Structural and functional hepatocyte polarity and liver disease. *J Hepatol* **63**, 1023–1037 (2015).
8. Kietzmann, T. Metabolic zonation of the liver: The oxygen gradient revisited. *Redox Biology* **11**, 622–630 (2017).
9. Tabibian, J. H., Masyuk, A. I., Masyuk, T. V., O'Hara, S. P. & LaRusso, N. F. Physiology of Cholangiocytes. *Compr Physiol* **3**, (2013).
10. Sasse, D., Spornitz, U. M. & Maly, I. P. Liver architecture. *Enzyme* **46**, 8–32 (1992).
11. Braet, F. & Wisse, E. Structural and functional aspects of liver sinusoidal endothelial cell fenestrae: a review. *Comparative Hepatology* **1**, 1 (2002).
12. Levitt, D. G. & Levitt, M. D. Human serum albumin homeostasis: a new look at the roles of synthesis, catabolism, renal and gastrointestinal excretion, and the clinical value of serum albumin measurements. *Int J Gen Med* **9**, 229–255 (2016).
13. Luo, J., Yang, H. & Song, B.-L. Mechanisms and regulation of cholesterol homeostasis. *Nature Reviews Molecular Cell Biology* 1–21 (2019) doi:10.1038/s41580-019-0190-7.
14. Trapani, L., Segatto, M. & Pallottini, V. Regulation and deregulation of cholesterol homeostasis: The liver as a metabolic "power station". *World J Hepatol* **4**, 184–190 (2012).
15. Corsini, A. & Bortolini, M. Drug-Induced Liver Injury: The Role of Drug Metabolism and Transport. *The Journal of Clinical Pharmacology* **53**, 463–474 (2013).
16. Yoo, K.-S., Lim, W. T. & Choi, H. S. Biology of Cholangiocytes: From Bench to Bedside. *Gut Liver* **10**, 687–698 (2016).
17. Banales, J. M. *et al.* Cholangiocyte pathobiology. *Nature Reviews Gastroenterology & Hepatology* **16**, 269–281 (2019).
18. Masyuk, A. I., Masyuk, T. V. & LaRusso, N. F. Cholangiocyte primary cilia in liver health and disease. *Dev. Dyn.* **237**, 2007–2012 (2008).
19. Poisson, J. *et al.* Liver sinusoidal endothelial cells: Physiology and role in liver diseases. *J. Hepatol.* **66**, 212–227 (2017).
20. DeLeve, L. D. Liver sinusoidal endothelial cells and liver regeneration. *Journal of Clinical Investigation* **123**, 1861–1866 (2013).
21. Svistounov, D. *et al.* The Relationship between Fenestrations, Sieve Plates and Rafts in Liver Sinusoidal Endothelial Cells. *PLOS ONE* **7**, e46134 (2012).
22. Sørensen, K. K., Simon-Santamaria, J., McCuskey, R. S. & Smedsrød, B. Liver Sinusoidal Endothelial Cells. in *Comprehensive Physiology* 1751–1774 (American Cancer Society, 2015). doi:10.1002/cphy.c140078.

23. Smedsrod, B. Scavenger function of liver sinusoidal endothelial cells. *The FASEB Journal* **23**, 66.1-66.1 (2009).
24. Sherman, M. H. Stellate Cells in Tissue Repair, Inflammation, and Cancer. *Annual Review of Cell and Developmental Biology* **34**, 333–355 (2018).
25. Puche, J. E., Saiman, Y. & Friedman, S. L. Hepatic Stellate Cells and Liver Fibrosis. in *Comprehensive Physiology* 1473–1492 (American Cancer Society, 2013). doi:10.1002/cphy.c120035.
26. Senoo, H., Mezaki, Y. & Fujiwara, M. The stellate cell system (vitamin A-storing cell system). *Anat Sci Int* **92**, 387–455 (2017).
27. Hou, W. & Syn, W.-K. Role of Metabolism in Hepatic Stellate Cell Activation and Fibrogenesis. *Front. Cell Dev. Biol.* **6**, (2018).
28. Dixon, L. J., Barnes, M., Tang, H., Pritchard, M. T. & Nagy, L. E. Kupffer Cells in the Liver. *Compr Physiol* **3**, 785–797 (2013).
29. Sun, Y.-Y. *et al.* Macrophage Phenotype in Liver Injury and Repair. *Scandinavian Journal of Immunology* **85**, 166–174 (2017).
30. *Drug Transporters*. (Springer-Verlag, 2011). doi:10.1007/978-3-642-14541-4.
31. Kadlubar, S. & Kadlubar, F. F. Enzymatic Basis of Phase I and Phase II Drug Metabolism. in *Enzyme- and Transporter-Based Drug-Drug Interactions: Progress and Future Challenges* (eds. Pang, K. S., Rodrigues, A. D. & Peter, R. M.) 3–25 (Springer, 2010). doi:10.1007/978-1-4419-0840-7_1.
32. Andrade, R. J. *et al.* Drug-induced liver injury. *Nature Reviews Disease Primers* **5**, 1–22 (2019).
33. David, S. & Hamilton, J. P. Drug-induced Liver Injury. *US Gastroenterol Hepatol Rev* **6**, 73–80 (2010).
34. Mano, Y., Usui, T. & Kamimura, H. Effects of bosentan, an endothelin receptor antagonist, on bile salt export pump and multidrug resistance–associated protein 2. *Biopharmaceutics & Drug Disposition* **28**, 13–18 (2007).
35. Andrade, R. J. *et al.* EASL Clinical Practice Guidelines: Drug-induced liver injury. *Journal of Hepatology* **70**, 1222–1261 (2019).
36. Björnsson, E. S. Global Epidemiology of Drug-Induced Liver Injury (DILI). *Curr Hepatology Rep* **18**, 274–279 (2019).
37. O'Grady, J. G., Alexander, G. J., Hayllar, K. M. & Williams, R. Early indicators of prognosis in fulminant hepatic failure. *Gastroenterology* **97**, 439–445 (1989).
38. Bataller, R. & Brenner, D. A. Liver fibrosis. *J Clin Invest* **115**, 209–218 (2005).
39. BENYON, R. & IREDALE, J. Is liver fibrosis reversible? *Gut* **46**, 443–446 (2000).
40. Horvat, T. *et al.* Adverse outcome pathway development from protein alkylation to liver fibrosis. *Archives of Toxicology* **91**, 1523–1543 (2017).
41. Iredale, J. P. Models of liver fibrosis: exploring the dynamic nature of inflammation and repair in a solid organ. *J Clin Invest* **117**, 539–548 (2007).
42. Liu, C. *et al.* Kupffer cells are associated with apoptosis, inflammation and fibrotic effects in hepatic fibrosis in rats. *Laboratory Investigation* **90**, 1805–1816 (2010).
43. Guo, J. & Friedman, S. L. Toll-like receptor 4 signaling in liver injury and hepatic fibrogenesis. *Fibrogenesis Tissue Repair* **3**, 21 (2010).
44. Jaeschke, H. Reactive oxygen and mechanisms of inflammatory liver injury: Present concepts. *J. Gastroenterol. Hepatol.* **26 Suppl 1**, 173–179 (2011).
45. Yoshida, K. & Matsuzaki, K. Differential Regulation of TGF-β/Smad Signaling in Hepatic Stellate Cells between Acute and Chronic Liver Injuries. *Front. Physiol.* **3**, (2012).
46. Koyama, Y. & Brenner, D. A. Liver inflammation and fibrosis. *J Clin Invest* **127**, 55–64 (2017).

47. Sebastiani, G. & Alberti, A. Non invasive fibrosis biomarkers reduce but not substitute the need for liver biopsy. *World J Gastroenterol* **12**, 3682–3694 (2006).
48. Standish, R. A., Cholongitas, E., Dhillon, A., Burroughs, A. K. & Dhillon, A. P. An appraisal of the histopathological assessment of liver fibrosis. *Gut* **55**, 569–578 (2006).
49. Nallagangula, K. S., Nagaraj, S. K., Venkataswamy, L. & Chandrappa, M. Liver fibrosis: a compilation on the biomarkers status and their significance during disease progression. *Future Sci OA* **4**, (2017).
50. Hall, P. & Cash, J. What is the Real Function of the Liver 'Function' Tests? *Ulster Med J* **81**, 30–36 (2012).
51. Loaeza-del-Castillo, A., Paz-Pineda, F., Oviedo-Cárdenas, E., Sánchez-Ávila, F. & Vargas-Voráckova, F. AST to platelet ratio index (APRI) for the noninvasive evaluation of liver fibrosis: Original Article. *Annals of Hepatology* **7**, 350–357 (2008).
52. Shaheen, A. A. M. & Myers, R. P. Diagnostic accuracy of the aspartate aminotransferase-to-platelet ratio index for the prediction of hepatitis C–related fibrosis: A systematic review. *Hepatology* **46**, 912–921 (2007).
53. Vallet-Pichard, A. *et al.* FIB-4: An inexpensive and accurate marker of fibrosis in HCV infection. comparison with liver biopsy and fibrotest. *Hepatology* **46**, 32–36 (2007).
54. Yakoob, R. *et al.* Noninvasive biomarkers FibroTest and ActiTest versus liver biopsy in chronic hepatitis C patients: the Middle East experience. *Ann Gastroenterol* **28**, 265–270 (2015).
55. Christensen, C. *et al.* Diagnostic accuracy of a fibrosis serum panel (FIBROSpect II) compared with Knodell and Ishak liver biopsy scores in chronic hepatitis C patients. *Journal of Viral Hepatitis* **13**, 652–658 (2006).
56. Koda, M. *et al.* FibroIndex, a practical index for predicting significant fibrosis in patients with chronic hepatitis C. *Hepatology* **45**, 297–306 (2007).
57. Adams, L. A. *et al.* Hepascore: an accurate validated predictor of liver fibrosis in chronic hepatitis C infection. *Clin. Chem.* **51**, 1867–1873 (2005).
58. Lurie, Y., Webb, M., Cytter-Kuint, R., Shteingart, S. & Lederkremer, G. Z. Non-invasive diagnosis of liver fibrosis and cirrhosis. *World J Gastroenterol* **21**, 11567–11583 (2015).
59. Allan, R., Thoirs, K. & Phillips, M. Accuracy of ultrasound to identify chronic liver disease. *World J. Gastroenterol.* **16**, 3510–3520 (2010).
60. Arena, U. *et al.* Acute viral hepatitis increases liver stiffness values measured by transient elastography. *Hepatology* **47**, 380–384 (2008).
61. Jung, K. S. & Kim, S. U. Clinical applications of transient elastography. *Clin Mol Hepatol* **18**, 163–173 (2012).
62. Son, J. H. *et al.* Assessment of liver fibrosis severity using computed tomography–based liver and spleen volumetric indices in patients with chronic liver disease. *Eur Radiol* **30**, 3486–3496 (2020).
63. Venkatesh, S. K., Yin, M. & Ehman, R. L. Magnetic Resonance Elastography of Liver: Technique, Analysis and Clinical Applications. *J Magn Reson Imaging* **37**, 544–555 (2013).
64. Yin, M. *et al.* Assessment of hepatic fibrosis with magnetic resonance elastography. *Clin. Gastroenterol. Hepatol.* **5**, 1207-1213.e2 (2007).
65. Bellan, M., Castello, L. M. & Pirisi, M. Candidate Biomarkers of Liver Fibrosis: A Concise, Pathophysiology-oriented Review. *J Clin Transl Hepatol* **6**, 317–325 (2018).
66. Thakkar, S. *et al.* Drug-induced liver injury severity and toxicity (DILIst): binary classification of 1279 drugs by human hepatotoxicity. *Drug Discovery Today* **25**, 201–208 (2020).
67. Delire, B., Stärkel, P. & Leclercq, I. Animal Models for Fibrotic Liver Diseases: What We Have, What We Need, and What Is under Development. *J Clin Transl Hepatol* **3**, 53–66 (2015).

68. Gómez-Lechón, M. J., Tolosa, L., Conde, I. & Donato, M. T. Competency of different cell models to predict human hepatotoxic drugs. *Expert Opinion on Drug Metabolism & Toxicology* **10**, 1553–1568 (2014).
69. Hubrecht, R. C. & Carter, E. The 3Rs and Humane Experimental Technique: Implementing Change. *Animals (Basel)* **9**, (2019).
70. Gómez-Lechón, M. J., Castell, J. V. & Donato, M. T. An update on metabolism studies using human hepatocytes in primary culture. *null* **4**, 837–854 (2008).
71. Godoy, P. *et al.* Recent advances in 2D and 3D *in vitro* systems using primary hepatocytes, alternative hepatocyte sources and non-parenchymal liver cells and their use in investigating mechanisms of hepatotoxicity, cell signaling and ADME. *Arch Toxicol* **87**, 1315–1530 (2013).
72. Yin, C., Evason, K. J., Asahina, K. & Stainier, D. Y. R. Hepatic stellate cells in liver development, regeneration, and cancer. *J Clin Invest* **123**, 1902–1910 (2013).
73. Si-Tayeb, K. *et al.* Highly Efficient Generation of Human Hepatocyte–like Cells from Induced Pluripotent Stem Cells. *Hepatology* **51**, 297–305 (2010).
74. Hannan, N. R. F., Segeritz, C.-P., Touboul, T. & Vallier, L. Production of hepatocyte like cells from human pluripotent stem cells. *Nat Protoc* **8**, 430–437 (2013).
75. Ghodsizadeh, A. *et al.* Generation of liver disease-specific induced pluripotent stem cells along with efficient differentiation to functional hepatocyte-like cells. *Stem Cell Reviews and Reports* **6**, 622–632 (2010).
76. Song, Z. *et al.* Efficient generation of hepatocyte-like cells from human induced pluripotent stem cells. *Cell Res.* **19**, 1233–1242 (2009).
77. De Assuncao, T. M. *et al.* Development and Characterization of Human Induced Pluripotent Stem Cell-Derived Cholangiocytes. *Lab Invest* **95**, 684–696 (2015).
78. Sampaziotis, F. *et al.* Cholangiocytes derived from human induced pluripotent stem cells for disease modeling and drug validation. *Nat Biotechnol* **33**, 845–852 (2015).
79. Shan, J. *et al.* Identification of small molecules for human hepatocyte expansion and iPS differentiation. *Nat Chem Biol* **9**, 514–520 (2013).
80. Ogawa, M. *et al.* Directed differentiation of cholangiocytes from human pluripotent stem cells. *Nature Biotechnology* **33**, 853–861 (2015).
81. Koui, Y. *et al.* An *In vitro* Human Liver Model by iPSC-Derived Parenchymal and Non-parenchymal Cells. *Stem Cell Reports* **9**, 490–498 (2017).
82. Coll, M. *et al.* Generation of Hepatic Stellate Cells from Human Pluripotent Stem Cells Enables *In vitro* Modeling of Liver Fibrosis. *Cell Stem Cell* **23**, 101-113.e7 (2018).
83. Tasnim, F. *et al.* Generation of mature kupffer cells from human induced pluripotent stem cells. *Biomaterials* **192**, 377–391 (2019).
84. Shah, U.-K. *et al.* A three-dimensional *in vitro* HepG2 cells liver spheroid model for genotoxicity studies. *Mutation Research/Genetic Toxicology and Environmental Mutagenesis* **825**, 51–58 (2018).
85. Donato, M. T., Tolosa, L. & Gómez-Lechón, M. J. Culture and Functional Characterization of Human Hepatoma HepG2 Cells. in *Protocols in In vitro Hepatocyte Research* (eds. Vinken, M. & Rogiers, V.) 77–93 (Springer, 2015). doi:10.1007/978-1-4939-2074-7_5.
86. Gerets, H. H. J. *et al.* Characterization of primary human hepatocytes, HepG2 cells, and HepaRG cells at the mRNA level and CYP activity in response to inducers and their predictivity for the detection of human hepatotoxins. *Cell Biol Toxicol* **28**, 69–87 (2012).
87. Xu, L. *et al.* Human hepatic stellate cell lines, LX-1 and LX-2: new tools for analysis of hepatic fibrosis. *Gut* **54**, 142–151 (2005).

88. Schnabl, B., Choi, Y. H., Olsen, J. C., Hagedorn, C. H. & Brenner, D. A. Immortal Activated Human Hepatic Stellate Cells Generated by Ectopic Telomerase Expression. *Laboratory Investigation* **82**, 323–333 (2002).
89. Gupta, P. *et al.* TGF-β induces liver fibrosis via miRNA-181a-mediated down regulation of augmenter of liver regeneration in hepatic stellate cells. *PLOS ONE* **14**, e0214534 (2019).
90. Prestigiacomo, V. & Suter-Dick, L. Nrf2 protects stellate cells from Smad-dependent cell activation. *PLOS ONE* **13**, e0201044 (2018).
91. Shang, L., Hosseini, M., Liu, X., Kisseleva, T. & Brenner, D. A. Human hepatic stellate cell isolation and characterization. *J Gastroenterol* **53**, 6–17 (2018).
92. Prestigiacomo, V., Weston, A., Messner, S., Lampart, F. & Suter-Dick, L. Pro-fibrotic compounds induce stellate cell activation, ECM-remodelling and Nrf2 activation in a human 3D-multicellular model of liver fibrosis. *PLOS ONE* **12**, e0179995 (2017).
93. Messner, S., Agarkova, I., Moritz, W. & Kelm, J. M. Multi-cell type human liver microtissues for hepatotoxicity testing. *Arch Toxicol* **87**, 209–213 (2013).
94. Tibbitt, M. W. & Anseth, K. S. Hydrogels as Extracellular Matrix Mimics for 3D Cell Culture. *Biotechnol Bioeng* **103**, 655–663 (2009).
95. De Kock, J. *et al.* Simple and quick method for whole-liver decellularization: a novel *in vitro* three-dimensional bioengineering tool? *Arch. Toxicol.* **85**, 607–612 (2011).
96. Hosseini, V. *et al.* Current progress in hepatic tissue regeneration by tissue engineering. *Journal of Translational Medicine* **17**, 383 (2019).
97. Bell, C. C. *et al.* Characterization of primary human hepatocyte spheroids as a model system for drug-induced liver injury, liver function and disease. *Scientific Reports* **6**, 25187 (2016).
98. Leite, S. B. *et al.* Novel human hepatic organoid model enables testing of drug-induced liver fibrosis *in vitro*. *Biomaterials* **78**, 1–10 (2016).
99. Langhans, S. A. Three-Dimensional *in vitro* Cell Culture Models in Drug Discovery and Drug Repositioning. *Front Pharmacol* **9**, (2018).
100. Proctor, W. R. *et al.* Utility of spherical human liver microtissues for prediction of clinical drug-induced liver injury. *Archives of Toxicology* **91**, 2849–2863 (2017).
101. Baze, A. *et al.* Three-Dimensional Spheroid Primary Human Hepatocytes in Monoculture and Coculture with Nonparenchymal Cells. *Tissue Eng Part C Methods* **24**, 534–545 (2018).
102. Mandon, M., Huet, S., Dubreil, E., Fessard, V. & Hégarat, L. L. Three-dimensional HepaRG spheroids as a liver model to study human genotoxicity *in vitro* with the single cell gel electrophoresis assay. *Sci Rep* **9**, 1–9 (2019).
103. Li, J., Settivari, R. S., LeBaron, M. J. & Marty, M. S. Functional Comparison of HepaRG Cells and Primary Human Hepatocytes in Sandwich and Spheroid Culture as Repeated-Exposure Models for Hepatotoxicity. *Applied In vitro Toxicology* **5**, 187–195 (2019).
104. Hendriks, D. F. G., Fredriksson Puigvert, L., Messner, S., Mortiz, W. & Ingelman-Sundberg, M. Hepatic 3D spheroid models for the detection and study of compounds with cholestatic liability. *Scientific Reports* **6**, 35434 (2016).
105. Li, F., Cao, L., Parikh, S. & Zuo, R. Three-Dimensional Spheroids With Primary Human Liver Cells and Differential Roles of Kupffer Cells in Drug-Induced Liver Injury. *Journal of Pharmaceutical Sciences* **109**, 1912–1923 (2020).
106. Foster, A. J. *et al.* Integrated *in vitro* models for hepatic safety and metabolism: evaluation of a human Liver-Chip and liver spheroid. *Arch Toxicol* **93**, 1021–1037 (2019).
107. Meier, F. *et al.* Hepatic differentiation of human iPSCs in different 3D models: A comparative study. *Int J Mol Med* **40**, 1759–1771 (2017).
108. Mukherjee, S. *et al.* Development and validation of an *in vitro* 3D model of NASH with severe fibrotic phenotype. *Am J Transl Res* **11**, 1531–1540 (2019).

109. O'Brien, J., Hayder, H., Zayed, Y. & Peng, C. Overview of MicroRNA Biogenesis, Mechanisms of Actions, and Circulation. *Front Endocrinol (Lausanne)* **9**, (2018).
110. de Rie, D. *et al.* An integrated expression atlas of miRNAs and their promoters in human and mouse. *Nature Biotechnology* **35**, 872–878 (2017).
111. Denli, A. M., Tops, B. B. J., Plasterk, R. H. A., Ketting, R. F. & Hannon, G. J. Processing of primary microRNAs by the Microprocessor complex. *Nature* **432**, 231–235 (2004).
112. Zhang, H., Kolb, F. A., Jaskiewicz, L., Westhof, E. & Filipowicz, W. Single Processing Center Models for Human Dicer and Bacterial RNase III. *Cell* **118**, 57–68 (2004).
113. Yoda, M. *et al.* ATP-dependent human RISC assembly pathways. *Nature Structural & Molecular Biology* **17**, 17–23 (2010).
114. Meijer, H. A., Smith, E. M. & Bushell, M. Regulation of miRNA strand selection: follow the leader? *Biochem Soc Trans* **42**, 1135–1140 (2014).
115. Jo, M. H. *et al.* Human Argonaute 2 Has Diverse Reaction Pathways on Target RNAs. *Mol. Cell* **59**, 117–124 (2015).
116. Ameres, S. L. *et al.* Target RNA–Directed Trimming and Tailing of Small Silencing RNAs. *Science* **328**, 1534–1539 (2010).
117. Jonas, S. & Izaurralde, E. Towards a molecular understanding of microRNA-mediated gene silencing. *Nature Reviews Genetics* **16**, 421–433 (2015).
118. Xu, W., San Lucas, A., Wang, Z. & Liu, Y. Identifying microRNA targets in different gene regions. *BMC Bioinformatics* **15**, S4 (2014).
119. Broughton, J. P., Lovci, M. T., Huang, J. L., Yeo, G. W. & Pasquinelli, A. E. Pairing beyond the Seed Supports MicroRNA Targeting Specificity. *Molecular Cell* **64**, 320–333 (2016).
120. Benhamed, M., Herbig, U., Ye, T., Dejean, A. & Bischof, O. Senescence is an endogenous trigger for microRNA-directed transcriptional gene silencing in human cells. *Nature Cell Biology* **14**, 266–275 (2012).
121. Nishi, K., Nishi, A., Nagasawa, T. & Ui-Tei, K. Human TNRC6A is an Argonaute-navigator protein for microRNA-mediated gene silencing in the nucleus. *RNA* **19**, 17–35 (2013).
122. Sohel, M. H. Extracellular/Circulating MicroRNAs: Release Mechanisms, Functions and Challenges. *Achievements in the Life Sciences* **10**, 175–186 (2016).
123. Zhang, Y., Liu, Y., Liu, H. & Tang, W. H. Exosomes: biogenesis, biologic function and clinical potential. *Cell Biosci* **9**, (2019).
124. Raposo, G. & Stoorvogel, W. Extracellular vesicles: Exosomes, microvesicles, and friends. *J Cell Biol* **200**, 373–383 (2013).
125. Lee, Y., El Andaloussi, S. & Wood, M. J. A. Exosomes and microvesicles: extracellular vesicles for genetic information transfer and gene therapy. *Human Molecular Genetics* **21**, R125-134 (2012).
126. Rayner, K. J. & Hennessy, E. J. Extracellular communication via microRNA: lipid particles have a new message. *J Lipid Res* **54**, 1174–1181 (2013).
127. Zernecke, A. *et al.* Delivery of microRNA-126 by apoptotic bodies induces CXCL12-dependent vascular protection. *Science Signaling* **2**, ra81 (2009).
128. Hergenreider, E. *et al.* Atheroprotective communication between endothelial cells and smooth muscle cells through miRNAs. *Nature Cell Biology* **14**, 249–256 (2012).
129. Gidlöf, O. *et al.* Platelets activated during myocardial infarction release functional miRNA, which can be taken up by endothelial cells and regulate ICAM1 expression. *Blood* **121**, 3908–3917, S1-26 (2013).
130. Mosedale, M. *et al.* miR-122 Release in Exosomes Precedes Overt Tolvaptan-Induced Necrosis in a Primary Human Hepatocyte Micropatterned Coculture Model. *Toxicol. Sci.* **161**, 149–158 (2018).

131. Arroyo, J. D. *et al.* Argonaute2 complexes carry a population of circulating microRNAs independent of vesicles in human plasma. *PNAS* **108**, 5003–5008 (2011).
132. Vickers, K. C., Palmisano, B. T., Shoucri, B. M., Shamburek, R. D. & Remaley, A. T. MicroRNAs are transported in plasma and delivered to recipient cells by high-density lipoproteins. *Nature Cell Biology* **13**, 423–433 (2011).
133. Turchinovich, A., Weiz, L., Langheinz, A. & Burwinkel, B. Characterization of extracellular circulating microRNA. *Nucleic Acids Res* **39**, 7223–7233 (2011).
134. Norona, L. M. *et al.* Bioprinted liver provides early insight into the role of Kupffer cells in TGF-β1 and methotrexate-induced fibrogenesis. *PLOS ONE* **14**, e0208958 (2019).
135. Condrat, C. E. *et al.* miRNAs as Biomarkers in Disease: Latest Findings Regarding Their Role in Diagnosis and Prognosis. *Cells* **9**, (2020).
136. Gamazon, E. R. *et al.* A genome-wide integrative study of microRNAs in human liver. *BMC Genomics* **14**, 395 (2013).
137. Bandiera, S., Pfeffer, S., Baumert, T. F. & Zeisel, M. B. miR-122 – A key factor and therapeutic target in liver disease. *Journal of Hepatology* **62**, 448–457 (2015).
138. Bala, S. *et al.* Circulating microRNAs in exosomes indicate hepatocyte injury and inflammation in alcoholic, drug-induced and inflammatory liver diseases. *Hepatology* **56**, 1946–1957 (2012).
139. Holman, N. S., Mosedale, M., Wolf, K. K., LeCluyse, E. L. & Watkins, P. B. Subtoxic Alterations in Hepatocyte-Derived Exosomes: An Early Step in Drug-Induced Liver Injury? *Toxicol Sci* **151**, 365–375 (2016).
140. Howell, L. S., Ireland, L., Park, B. K. & Goldring, C. E. MiR-122 and other microRNAs as potential circulating biomarkers of drug-induced liver injury. *Expert Review of Molecular Diagnostics* **18**, 47–54 (2018).
141. Starkey Lewis, P. J. *et al.* Serum microRNA biomarkers for drug-induced liver injury. *Clin. Pharmacol. Ther.* **92**, 291–293 (2012).
142. Afonso, M. B., Rodrigues, P. M., Simão, A. L. & Castro, R. E. Circulating microRNAs as Potential Biomarkers in Non-Alcoholic Fatty Liver Disease and Hepatocellular Carcinoma. *J Clin Med* **5**, (2016).
143. Krauskopf, J. *et al.* Serum microRNA signatures as 'liquid biopsies' for interrogating hepatotoxic mechanisms and liver pathogenesis in human. *PLoS One* **12**, (2017).
144. Starkey Lewis, P. J. *et al.* Circulating microRNAs as potential markers of human drug-induced liver injury. *Hepatology* **54**, 1767–1776 (2011).
145. Krauskopf, J. *et al.* Application of High-Throughput Sequencing to Circulating microRNAs Reveals Novel Biomarkers for Drug-Induced Liver Injury. *Toxicol Sci* **143**, 268–276 (2015).
146. Schueller, F. *et al.* The Role of miRNAs in the Pathophysiology of Liver Diseases and Toxicity. *Int J Mol Sci* **19**, (2018).
147. Brunetto, M. R. *et al.* A Serum MicroRNA Signature Is Associated with the Immune Control of Chronic Hepatitis B Virus Infection. *PLoS ONE* **9**, (2014).
148. Schueller, F. *et al.* miR-223 represents a biomarker in acute and chronic liver injury. *Clin. Sci.* **131**, 1971–1987 (2017).
149. Cisilotto, J. *et al.* MicroRNA profiles in serum samples from Acute-On-Chronic Liver Failure patients and miR-25-3p as a potential biomarker for survival prediction. *Scientific Reports* **10**, 100 (2020).
150. Bala, S. *et al.* The pro-inflammatory effects of miR-155 promote liver fibrosis and alcohol-induced steatohepatitis. *J. Hepatol.* **64**, 1378–1387 (2016).

151. Dolganiuc, A. *et al.* MicroRNA expression profile in Lieber-DeCarli diet-induced alcoholic and methionine choline deficient diet-induced nonalcoholic steatohepatitis models in mice. *Alcohol. Clin. Exp. Res.* **33**, 1704–1710 (2009).
152. Dippold, R. P., Vadigepalli, R., Gonye, G. E., Patra, B. & Hoek, J. B. Chronic ethanol feeding alters miRNA expression dynamics during liver regeneration. *Alcohol. Clin. Exp. Res.* **37 Suppl 1**, E59-69 (2013).
153. Hartmann, P. & Tacke, F. Tiny RNA with great effects: miR-155 in alcoholic liver disease. *Journal of Hepatology* **64**, 1214–1216 (2016).
154. M, W., R, M., X, L. & L, Y. Involvement of miR-30c in hepatic stellate cell activation through the repression of plasminogen activator inhibitor-1. *Life sciences* https://pubmed.ncbi.nlm.nih.gov/27142827/ (2016) doi:10.1016/j.lfs.2016.04.034.
155. S, R. *et al.* miR-30c and miR-193 are a part of the TGF-β-dependent regulatory network controlling extracellular matrix genes in liver fibrosis. *Journal of digestive diseases* https://pubmed.ncbi.nlm.nih.gov/26120970/ (2015) doi:10.1111/1751-2980.12266.
156. Coppola, N. *et al.* Correlation Between the Hepatic Expression of Human MicroRNA hsa-miR-125a-5p and the Progression of Fibrosis in Patients With Overt and Occult HBV Infection. *Front Immunol* **9**, 1334 (2018).
157. Li, G. *et al.* MicroRNA-125a-5p Contributes to Hepatic Stellate Cell Activation through Targeting FIH1. *Cellular physiology and biochemistry : international journal of experimental cellular physiology, biochemistry, and pharmacology* **38**, 1544–1552 (2016).
158. Am, L. *et al.* Inhibitory effects of microRNA 19b in hepatic stellate cell-mediated fibrogenesis. *Hepatology (Baltimore, Md.)* https://pubmed.ncbi.nlm.nih.gov/22278637/ (2012) doi:10.1002/hep.25613.
159. Y, Z. *et al.* MiR-146a attenuates liver fibrosis by inhibiting transforming growth factor-β1 mediated epithelial-mesenchymal transition in hepatocytes. *Cellular signalling* https://pubmed.ncbi.nlm.nih.gov/30711634/ (2019) doi:10.1016/j.cellsig.2019.01.012.
160. Yang, Z., Peng, Y. & Yang, S. MicroRNA-146a regulates the transformation from liver fibrosis to cirrhosis in patients with hepatitis B via interleukin-6. *Experimental and Therapeutic Medicine* **17**, 4670 (2019).
161. Zou, Y. *et al.* MicroRNA-146a-5p attenuates liver fibrosis by suppressing profibrogenic effects of TGFβ1 and lipopolysaccharide. *Cellular Signalling* **39**, 1–8 (2017).
162. Ge, S. *et al.* MicroRNA-146b regulates hepatic stellate cell activation via targeting of KLF4. *Annals of Hepatology* **15**, 918–928 (2016).
163. Murakami, Y. *et al.* The Progression of Liver Fibrosis Is Related with Overexpression of the miR-199 and 200 Families. *PLoS ONE* **6**, e16081 (2011).
164. Cf, H., Cc, S., F, Z., Yd, Z. & Dj, L. miR-33a levels in hepatic and serum after chronic HBV-induced fibrosis. *Journal of gastroenterology* https://pubmed.ncbi.nlm.nih.gov/25155445/ (2015) doi:10.1007/s00535-014-0986-3.
165. Lendvai, G. *et al.* Elevated miR-33a and miR-224 in steatotic chronic hepatitis C liver biopsies. *World J Gastroenterol* **20**, 15343–15350 (2014).
166. Zhang, H. *et al.* MiR-27a as a predictor for the activation of hepatic stellate cells and hepatitis B virus-induced liver cirrhosis. *Oncotarget* **9**, 1075 (2018).
167. Sun, J., Zhang, H., Li, L., Yu, L. & Fu, L. MicroRNA-9 limits hepatic fibrosis by suppressing the activation and proliferation of hepatic stellate cells by directly targeting MRP1/ABCC1. *Oncology Reports* **37**, 1698–1706 (2017).
168. Yu, F. *et al.* Epigenetically-Regulated MicroRNA-9-5p Suppresses the Activation of Hepatic Stellate Cells via TGFBR1 and TGFBR2. *CPB* **43**, 2242–2252 (2017).
169. Hall, C. *et al.* Inhibition of microRNA-24 increases liver fibrosis by enhanced menin expression in Mdr2−/− mice. *Journal of Surgical Research* **217**, 160–169 (2017).

170. Iizuka, M. *et al.* Induction of microRNA-214-5p in human and rodent liver fibrosis. *Fibrogenesis Tissue Repair* **5**, 12 (2012).
171. Ma, L. *et al.* MicroRNA-214 promotes hepatic stellate cell activation and liver fibrosis by suppressing Sufu expression. *Cell Death & Disease* **9**, 1–13 (2018).
172. Ezaz, G. *et al.* Differential Associations of Circulating MicroRNAs With Pathogenic Factors in NAFLD. *Hepatology Communications* **4**, 670–680 (2020).
173. Feili, X., Wu, S., Ye, W., Tu, J. & Lou, L. MicroRNA-34a-5p inhibits liver fibrosis by regulating TGF-β1/Smad3 pathway in hepatic stellate cells. *Cell Biol. Int.* **42**, 1370–1376 (2018).
174. Li, X., Zhang, W., Xu, K. & Lu, J. miR-34a promotes liver fibrosis in patients with chronic hepatitis via mediating Sirt1/p53 signaling pathway. *Pathology - Research and Practice* **216**, 152876 (2020).
175. Chen, W. *et al.* miRNA-150-5p promotes hepatic stellate cell proliferation and sensitizes hepatocyte apoptosis during liver fibrosis. *Epigenomics* **12**, 53–67 (2019).
176. Venugopal, S. K. *et al.* Liver fibrosis causes downregulation of miRNA-150 and miRNA-194 in hepatic stellate cells, and their overexpression causes decreased stellate cell activation. *Am J Physiol Gastrointest Liver Physiol* **298**, G101–G106 (2010).
177. Wasik, U., Kempinska-Podhorodecka, A., Bogdanos, D. P., Milkiewicz, P. & Milkiewicz, M. Enhanced expression of miR-21 and miR-150 is a feature of anti-mitochondrial antibody-negative primary biliary cholangitis. *Molecular Medicine* **26**, 8 (2020).
178. Zheng, J. *et al.* Activation of hepatic stellate cells is suppressed by microRNA-150. *International Journal of Molecular Medicine* **32**, 17–24 (2013).
179. Ma, T. *et al.* miR-200c Accelerates Hepatic Stellate Cell-Induced Liver Fibrosis via Targeting the FOG2/PI3K Pathway. *Biomed Res Int* **2017**, (2017).
180. Chandel, R., Saxena, R., Das, A. & Kaur, J. Association of rno-miR-183-96-182 cluster with diethyinitrosamine induced liver fibrosis in Wistar rats. *Journal of Cellular Biochemistry* **119**, 4072–4084 (2018).
181. Keuren-Jensen, K. R. V. *et al.* microRNA changes in liver tissue associated with fibrosis progression in patients with hepatitis C. *Liver International* **36**, 334–343 (2016).
182. Leti, F. *et al.* High-throughput sequencing reveals altered expression of hepatic microRNAs in nonalcoholic fatty liver disease–related fibrosis. *Translational Research* **166**, 304–314 (2015).
183. Yang, X. *et al.* Twist1-induced miR-199a-3p promotes liver fibrosis by suppressing caveolin-2 and activating TGF-β pathway. *Signal Transduction and Targeted Therapy* **5**, 1–12 (2020).
184. Markovic, J., Sharma, A. D. & Balakrishnan, A. MicroRNA-221: A Fine Tuner and Potential Biomarker of Chronic Liver Injury. *Cells* **9**, (2020).
185. Ogawa, T. *et al.* MicroRNA-221/222 upregulation indicates the activation of stellate cells and the progression of liver fibrosis. *Gut* **61**, 1600–1609 (2012).
186. Yang, X. *et al.* MiR-142-3p blocks TGF-β-induced activation of hepatic stellate cells through targeting TGFβRI. *Life Sci.* **187**, 22–30 (2017).
187. Roderburg, C. *et al.* Micro-RNA profiling reveals a role for miR-29 in human and murine liver fibrosis. *Hepatology* **53**, 209–218 (2011).
188. Wei, J., Feng, L., Li, Z., Xu, G. & Fan, X. MicroRNA-21 activates hepatic stellate cells via PTEN/Akt signaling. *Biomedicine & Pharmacotherapy* **67**, 387–392 (2013).
189. Zhao, J. *et al.* MiR-21 Simultaneously Regulates ERK1 Signaling in HSC Activation and Hepatocyte EMT in Hepatic Fibrosis. *PLOS ONE* **9**, e108005 (2014).
190. Tu, X. *et al.* MicroRNA-101 suppresses liver fibrosis by targeting the TGFβ signalling pathway. *The Journal of Pathology* **234**, 46–59 (2014).

191. Xie, Y. *et al.* Expression profiling of serum microRNA-101 in HBV-associated chronic hepatitis, liver cirrhosis, and hepatocellular carcinoma. *Cancer Biology & Therapy* **15**, 1248–1255 (2014).
192. Wang, B. *et al.* miR-181b Promotes hepatic stellate cells proliferation by targeting p27 and is elevated in the serum of cirrhosis patients. *Biochemical and Biophysical Research Communications* **421**, 4–8 (2012).
193. Zheng, J. *et al.* Hepatic stellate cell is activated by microRNA-181b via PTEN/Akt pathway. *Mol Cell Biochem* **398**, 1–9 (2015).
194. Yu, F., Guo, Y., Chen, B., Dong, P. & Zheng, J. MicroRNA-17-5p activates hepatic stellate cells through targeting of Smad7. *Laboratory Investigation* **95**, 781–789 (2015).
195. Hu, J. *et al.* The role of the miR-31/FIH1 pathway in TGF-β-induced liver fibrosis. *Clin Sci (Lond)* **129**, 305–317 (2015).
196. Halász, T. *et al.* miR-122 negatively correlates with liver fibrosis as detected by histology and FibroScan. *World J Gastroenterol* **21**, 7814–7823 (2015).
197. Hyun, J. *et al.* MicroRNA-378 limits activation of hepatic stellate cells and liver fibrosis by suppressing Gli3 expression. *Nature Communications* **7**, 10993 (2016).
198. Schmeling, H., Horneff, G., Benseler, S. M. & Fritzler, M. J. Pharmacogenetics: can genes determine treatment efficacy and safety in JIA? *Nature Reviews Rheumatology* **10**, 682–690 (2014).
199. Lima, A. *et al.* Genetic polymorphisms in low-dose methotrexate transporters: current relevance as methotrexate therapeutic outcome biomarkers. *Pharmacogenomics* **15**, 1611–1635 (2014).
200. Mikkelsen, T. S. *et al.* PharmGKB summary: methotrexate pathway. *Pharmacogenet Genomics* **21**, 679–686 (2011).
201. Berdis, A. J. Inhibiting DNA Polymerases as a Therapeutic Intervention against Cancer. *Front Mol Biosci* **4**, (2017).
202. Bywater, M. J. *et al.* Inhibition of RNA Polymerase I as a Therapeutic Strategy to Promote Cancer-Specific Activation of p53. *Cancer Cell* **22**, 51–65 (2012).
203. Morgan, S. L. & Baggott, J. E. Folate supplementation during methotrexate therapy for rheumatoid arthritis. *Clin. Exp. Rheumatol.* **28**, S102-109 (2010).
204. Alarcón, G. S., Tracy, I. C. & Blackburn, W. D. Methotrexate in rheumatoid arthritis. Toxic effects as the major factor in limiting long-term treatment. *Arthritis Rheum.* **32**, 671–676 (1989).
205. Tang, K.-T., Hung, W.-T., Chen, Y.-H., Lin, C.-H. & Chen, D.-Y. Methotrexate is not associated with increased liver cirrhosis in a population-based cohort of rheumatoid arthritis patients with chronic hepatitis B. *Scientific Reports* **6**, 1–7 (2016).
206. Lertnawapan, R., Chonprasertsuk, S. & Siramolpiwat, S. Association between cumulative methotrexate dose, non-invasive scoring system and hepatic fibrosis detected by Fibroscan in rheumatoid arthritis patients receiving methotrexate. *International Journal of Rheumatic Diseases* **22**, 214–221 (2019).
207. Aithal, G. P. *et al.* Monitoring methotrexate-induced hepatic fibrosis in patients with psoriasis: are serial liver biopsies justified? *Alimentary Pharmacology & Therapeutics* **19**, 391–399 (2004).
208. Berends, M. A. M. *et al.* Reliability of the Roenigk Classification of Liver Damage After Methotrexate Treatment for Psoriasis: A Clinicopathologic Study of 160 Liver Biopsy Specimens. *Arch Dermatol* **143**, 1515–1519 (2007).
209. Cobb, J. *et al.* Genome-wide data reveal novel genes for methotrexate response in a large cohort of juvenile idiopathic arthritis cases. *The Pharmacogenomics Journal* **14**, 356–364 (2014).

210. Moncrieffe, H. *et al.* Generation of novel pharmacogenomic candidates in the response to methotrexate in juvenile idiopathic arthritis: correlation between gene expression and genotype. *Pharmacogenet Genomics* **20**, 665–676 (2010).
211. Graham, G. G., Davies, M. J., Day, R. O., Mohamudally, A. & Scott, K. F. The modern pharmacology of paracetamol: therapeutic actions, mechanism of action, metabolism, toxicity and recent pharmacological findings. *Inflammopharmacology* **21**, 201–232 (2013).
212. Mazaleuskaya, L. L. *et al.* PharmGKB summary: Pathways of acetaminophen metabolism at the therapeutic versus toxic doses. *Pharmacogenet Genomics* **25**, 416–426 (2015).
213. Reiter, C. & Weinshilboum, R. M. Acetaminophen and phenol: substrates for both a thermostable and a thermolabile form of human platelet phenol sulfotransferase. *J. Pharmacol. Exp. Ther.* **221**, 43–51 (1982).
214. Prescott, L. F. Paracetamol overdosage. Pharmacological considerations and clinical management. *Drugs* **25**, 290–314 (1983).
215. Manyike, P. T., Kharasch, E. D., Kalhorn, T. F. & Slattery, J. T. Contribution of CYP2E1 and CYP3A to acetaminophen reactive metabolite formation. *Clin. Pharmacol. Ther.* **67**, 275–282 (2000).
216. Chen, W. *et al.* Oxidation of acetaminophen to its toxic quinone imine and nontoxic catechol metabolites by baculovirus-expressed and purified human cytochromes P450 2E1 and 2A6. *Chem. Res. Toxicol.* **11**, 295–301 (1998).
217. Dong, H., Haining, R. L., Thummel, K. E., Rettie, A. E. & Nelson, S. D. Involvement of human cytochrome P450 2D6 in the bioactivation of acetaminophen. *Drug Metab. Dispos.* **28**, 1397–1400 (2000).
218. Laine, J. E., Auriola, S., Pasanen, M. & Juvonen, R. O. Acetaminophen bioactivation by human cytochrome P450 enzymes and animal microsomes. *Xenobiotica* **39**, 11–21 (2009).
219. Board, P. G. & Menon, D. Glutathione transferases, regulators of cellular metabolism and physiology. *Biochim. Biophys. Acta* **1830**, 3267–3288 (2013).
220. Beckett, G. J., Donovan, J. W., Hussey, A. J., Proudfoot, A. T. & Prescott, L. F. Intravenous N-acetylcysteine, hepatotoxicity and plasma glutathione S-transferase in patients with paracetamol overdosage. *Hum Exp Toxicol* **9**, 183–186 (1990).
221. Beckett, G. J., Chapman, B. J., Dyson, E. H. & Hayes, J. D. Plasma glutathione S-transferase measurements after paracetamol overdose: evidence for early hepatocellular damage. *Gut* **26**, 26–31 (1985).
222. James, L. P., Mayeux, P. R. & Hinson, J. A. Acetaminophen-induced hepatotoxicity. *Drug Metab. Dispos.* **31**, 1499–1506 (2003).
223. Fickert, P. & Wagner, M. Biliary bile acids in hepatobiliary injury – What is the link? *Journal of Hepatology* **67**, 619–631 (2017).
224. Shiffman, M. L., Sugerman, H. J. & Moore, E. W. Human gallbladder mucosal function: Effect of concentration and acidification of bile on cholesterol and calcium solubility. *Gastroenterology* **99**, 1452–1459 (1990).
225. Hofmann, A. F. & Eckmann, L. How bile acids confer gut mucosal protection against bacteria. *Proceedings of the National Academy of Sciences of the United States of America* **103**, 4333–4334 (2006).
226. Hofmann, A. F. Overview: Enterohepatic Circulation of Bile Acids — a Topic in Molecular Physiology. in *Bile Acids in Health and Disease: Update on Cholesterol Gallstones and Bile Acid Diarrhoea* (eds. Northfield, T., Jazrawi, R. & Zentler-Munro, P.) 1–18 (Springer Netherlands, 1988). doi:10.1007/978-94-009-1249-6_1.
227. Chiang, J. Y. L. Bile acids: regulation of synthesis. *J Lipid Res* **50**, 1955–1966 (2009).
228. Woolbright, B. L. & Jaeschke, H. Critical Factors in the Assessment of Cholestatic Liver Injury *In vitro*. *Methods Mol Biol* **1250**, 363–376 (2015).

229. Li, T. & Apte, U. Bile acid metabolism and signaling in cholestasis, inflammation and cancer. *Adv Pharmacol* **74**, 263–302 (2015).
230. Chiang, J. Y. L. Bile acid metabolism and signaling in liver disease and therapy. *Liver Research* **1**, 3–9 (2017).
231. Li, M., Cai, S.-Y. & Boyer, J. L. Mechanisms of bile acid mediated Inflammation in the Liver. *Mol Aspects Med* **56**, 45–53 (2017).
232. Kullak-Ublick, G. A., Stieger, B., Hagenbuch, B. & Meier, P. J. Hepatic transport of bile salts. *Semin. Liver Dis.* **20**, 273–292 (2000).
233. Trauner, M. & Boyer, J. L. Bile Salt Transporters: Molecular Characterization, Function, and Regulation. *Physiological Reviews* **83**, 633–671 (2003).
234. Müller, M. & Jansen, P. L. The secretory function of the liver: new aspects of hepatobiliary transport. *J. Hepatol.* **28**, 344–354 (1998).
235. Kullak-Ublick, G. A., Beuers, U. & Paumgartner, G. Hepatobiliary transport. *Journal of Hepatology* **32**, 3–18 (2000).
236. Smit, J. J. M. *et al.* Homozygous disruption of the murine MDR2 P-glycoprotein gene leads to a complete absence of phospholipid from bile and to liver disease. *Cell* **75**, 451–462 (1993).
237. Estill, M. & Zakko, S. F. Extrahepatic Cholestasis. in *Diseases of the Liver and Bile Ducts: A Practical Guide to Diagnosis and Treatment* (eds. Wu, G. Y. & Israel, J.) 217–228 (Humana Press, 1998). doi:10.1007/978-1-4612-1808-1_16.
238. Samant, H. *et al.* Cholestatic liver diseases: An era of emerging therapies. *World Journal of Clinical Cases* **7**, 1571–1581 (2019).
239. Azzi, P. B.-E. *et al.* Impact of Inflammation on Chlorpromazine-Induced Cytotoxicity and Cholestatic Features in HepaRG Cells. *Drug Metab Dispos* **42**, 1556–1566 (2014).
240. Anthérieu, S. *et al.* Oxidative stress plays a major role in chlorpromazine-induced cholestasis in human HepaRG cells. *Hepatology* **57**, 1518–1529 (2013).
241. Gandhi, A., Guo, T. & Ghose, R. Role of c-Jun N-terminal kinase (JNK) in regulating tumor necrosis factor-alpha (TNF-alpha) mediated increase of acetaminophen (APAP) and chlorpromazine (CPZ) toxicity in murine hepatocytes. *The Journal of Toxicological Sciences* **35**, 163–173 (2010).
242. Kullak-Ublick, G. A. *Drug-Induced Cholestatic Liver Disease*. (Landes Bioscience, 2013).
243. Tag, C. G. *et al.* Bile Duct Ligation in Mice: Induction of Inflammatory Liver Injury and Fibrosis by Obstructive Cholestasis. *J Vis Exp* (2015) doi:10.3791/52438.
244. Fickert, P. *et al.* Lithocholic acid feeding induces segmental bile duct obstruction and destructive cholangitis in mice. *Am. J. Pathol.* **168**, 410–422 (2006).
245. Joshi, N., Ray, J. L., Kopec, A. K. & Luyendyk, J. P. Dose-Dependent Effects of Alpha-Naphthylisothiocyanate Disconnect Biliary Fibrosis from Hepatocellular Necrosis. *J Biochem Mol Toxicol* **31**, 1–7 (2017).
246. Fickert, P. *et al.* Ursodeoxycholic acid aggravates bile infarcts in bile duct-ligated and Mdr2 knockout mice via disruption of cholangioles. *Gastroenterology* **123**, 1238–1251 (2002).
247. Rodrigues, A. D. *et al.* Drug-induced perturbations of the bile acid pool, cholestasis, and hepatotoxicity: mechanistic considerations beyond the direct inhibition of the bile salt export pump. *Drug Metab. Dispos.* **42**, 566–574 (2014).
248. Zhang, Y. *et al.* EFFECT OF BILE DUCT LIGATION ON BILE ACID COMPOSITION IN MOUSE SERUM AND LIVER. *Liver Int* **32**, 58–69 (2012).
249. Woolbright, B. L. *et al.* LITHOCHOLIC ACID FEEDING RESULTS IN DIRECT HEPATOTOXICITY INDEPENDENT OF NEUTROPHIL FUNCTION IN MICE. *Toxicol Lett* **228**, 56–66 (2014).

250. Malhi, H., Guicciardi, M. E. & Gores, G. J. Hepatocyte death: a clear and present danger. *Physiol. Rev.* **90**, 1165–1194 (2010).
251. Allen, K., Jaeschke, H. & Copple, B. L. Bile Acids Induce Inflammatory Genes in Hepatocytes. *Am J Pathol* **178**, 175–186 (2011).
252. Jackson, J. P., Freeman, K. M., St. Claire, R. L., Black, C. B. & Brouwer, K. R. Cholestatic Drug Induced Liver Injury: A Function of Bile Salt Export Pump Inhibition and Farnesoid X Receptor Antagonism. *Applied In vitro Toxicology* **4**, 265–279 (2018).
253. Szabo, M., Veres, Z., Baranyai, Z., Jakab, F. & Jemnitz, K. Comparison of human hepatoma HepaRG cells with human and rat hepatocytes in uptake transport assays in order to predict a risk of drug induced hepatotoxicity. *PLoS ONE* **8**, e59432 (2013).
254. Mühlfeld, S. *et al.* Short-term feedback regulation of bile salt uptake by bile salts in rodent liver. *Hepatology* **56**, 2387–2397 (2012).
255. Denk, G. U. *et al.* Tauro-β-muricholic acid restricts bile acid-induced hepatocellular apoptosis by preserving the mitochondrial membrane potential. *Biochem. Biophys. Res. Commun.* **424**, 758–764 (2012).
256. Denk, G. U. *et al.* Conjugation is essential for the anticholestatic effect of NorUrsodeoxycholic acid in taurolithocholic acid-induced cholestasis in rat liver. *Hepatology* **52**, 1758–1768 (2010).
257. Decaens, C., Durand, M., Grosse, B. & Cassio, D. Which *in vitro* models could be best used to study hepatocyte polarity? *Biology of the Cell* **100**, 387–398 (2008).
258. Le Vee, M. *et al.* Functional expression of sinusoidal and canalicular hepatic drug transporters in the differentiated human hepatoma HepaRG cell line. *Eur J Pharm Sci* **28**, 109–117 (2006).
259. Sharanek, A. *et al.* Different Dose-Dependent Mechanisms Are Involved in Early Cyclosporine A-Induced Cholestatic Effects in HepaRG Cells. *Toxicol Sci* **141**, 244–253 (2014).
260. Woolbright, B. L., McGill, M. R., Yan, H. & Jaeschke, H. Bile Acid-Induced Toxicity in HepaRG Cells Recapitulates the Response in Primary Human Hepatocytes. *Basic Clin Pharmacol Toxicol* **118**, 160–167 (2016).
261. Seki, E. & Brenner, D. A. Recent advancement of molecular mechanisms of liver fibrosis. *Journal of Hepato-Biliary-Pancreatic Sciences* **22**, 512–518 (2015).
262. Pollock, G. & Minuk, G. Y. Diagnostic considerations for cholestatic liver disease. *Journal of Gastroenterology and Hepatology* **32**, 1303–1309 (2017).
263. Horvat, T. *et al.* Adverse outcome pathway development from protein alkylation to liver fibrosis. *Arch Toxicol* **91**, 1523–1543 (2017).
264. Gujral, J. S., Liu, J., Farhood, A., Hinson, J. A. & Jaeschke, H. Functional importance of ICAM-1 in the mechanism of neutrophil-induced liver injury in bile duct-ligated mice. *American Journal of Physiology. Gastrointestinal and Liver Physiology* **286**, G499-507 (2004).
265. Gujral, J. S., Farhood, A., Bajt, M. L. & Jaeschke, H. Neutrophils aggravate acute liver injury during obstructive cholestasis in bile duct-ligated mice. *Hepatology (Baltimore, Md.)* **38**, 355–363 (2003).
266. Gulubova, M. V. Intercellular adhesion molecule-1 (ICAM-1) expression in the liver of patients with extrahepatic cholestasis. *Acta Histochemica* **100**, 59–74 (1998).
267. O'Brien, K. M. *et al.* IL-17A Synergistically Enhances Bile Acid–Induced Inflammation during Obstructive Cholestasis. *Am J Pathol* **183**, 1498–1507 (2013).
268. Meng, F. *et al.* IL-17 signaling in inflammatory cells, Kupffer cells and Hepatic Stellate cells exacerbates liver fibrosis. *Gastroenterology* **143**, 765-76.e1–3 (2012).
269. Alpini, G. *et al.* Bile acid feeding induces cholangiocyte proliferation and secretion: evidence for bile acid-regulated ductal secretion. *Gastroenterology* **116**, 179–186 (1999).

270. Baghdasaryan, A. *et al.* Dual farnesoid X receptor/TGR5 agonist INT-767 reduces liver injury in the Mdr2−/− (Abcb4−/−) mouse cholangiopathy model by promoting biliary HCO output. *Hepatology* **54**, 1303–1312 (2011).
271. Péan, N. *et al.* The receptor TGR5 protects the liver from bile acid overload during liver regeneration in mice. *Hepatology* **58**, 1451–1460 (2013).
272. Sato, K., Meng, F., Giang, T., Glaser, S. & Alpini, G. Mechanisms of cholangiocyte responses to injury. *Biochimica et Biophysica Acta (BBA) - Molecular Basis of Disease* **1864**, 1262–1269 (2018).
273. Saga, K. *et al.* Secondary Unconjugated Bile Acids Induce Hepatic Stellate Cell Activation. *Int J Mol Sci* **19**, (2018).
274. Yarde, S. S. & Cheng, X. Primary and Secondary Bile Acids Activate Hepatic Stellate Cells. *The FASEB Journal* **34**, 1–1 (2020).
275. Svegliati-Baroni, G. *et al.* Bile acids induce hepatic stellate cell proliferation via activation of the epidermal growth factor receptor. *Gastroenterology* **128**, 1042–1055 (2005).
276. Wasi, S., Tabrez, S. & Ahmad, M. Toxicological effects of major environmental pollutants: an overview. *Environ Monit Assess* **185**, 2585–2593 (2013).
277. Srogi, K. Levels and congener distributions of PCDDs, PCDFs and dioxin-like PCBs in environmental and human samples: a review. *Environ Chem Lett* **6**, 1–28 (2008).
278. Marinković, N., Pašalić, D., Ferenčak, G., Gršković, B. & Rukavina, A. Dioxins and Human Toxicity. *Archives of Industrial Hygiene and Toxicology* **61**, (2010).
279. Zhou, Y. & Liu, J. Emissions, environmental levels, sources, formation pathways, and analysis of polybrominated dibenzo-p-dioxins and dibenzofurans: a review. *Environ Sci Pollut Res* **25**, 33082–33102 (2018).
280. Zhang, W. *et al.* PCB 126 and Other Dioxin-Like PCBs Specifically Suppress Hepatic PEPCK Expression via the Aryl Hydrocarbon Receptor. *PLoS One* **7**, (2012).
281. Dioxins and their effects on human health. https://www.who.int/news-room/fact-sheets/detail/dioxins-and-their-effects-on-human-health.
282. Malisch, R. & Kotz, A. Dioxins and PCBs in feed and food — Review from European perspective. *Science of The Total Environment* **491–492**, 2–10 (2014).
283. Larebeke, N. V., Covaci, A., Schepens, P. & Hens, L. Food contamination with polychlorinated biphenyls and dioxins in Belgium. Effects on the body burden. *Journal of Epidemiology & Community Health* **56**, 828–830 (2002).
284. White, S. S. & Birnbaum, L. S. An Overview of the Effects of Dioxins and Dioxin-like Compounds on Vertebrates, as Documented in Human and Ecological Epidemiology. *J Environ Sci Health C Environ Carcinog Ecotoxicol Rev* **27**, 197–211 (2009).
285. Sorg, O. AhR signalling and dioxin toxicity. *Toxicol. Lett.* **230**, 225–233 (2014).
286. Ma, C., Marlowe, J. L. & Puga, A. The aryl hydrocarbon receptor at the crossroads of multiple signaling pathways. in *Molecular, Clinical and Environmental Toxicology: Volume 1: Molecular Toxicology* (ed. Luch, A.) 231–257 (Birkhäuser, 2009). doi:10.1007/978-3-7643-8336-7_9.
287. Boverhof, D. R., Kwekel, J. C., Humes, D. G., Burgoon, L. D. & Zacharewski, T. R. Dioxin Induces an Estrogen-Like, Estrogen Receptor-Dependent Gene Expression Response in the Murine Uterus. *Mol Pharmacol* **69**, 1599–1606 (2006).
288. Tian, Y. Ah receptor and NF-κB interplay on the stage of epigenome. *Biochemical Pharmacology* **77**, 670–680 (2009).
289. Guyot, E., Chevallier, A., Barouki, R. & Coumoul, X. The AhR twist: ligand-dependent AhR signaling and pharmaco-toxicological implications. *Drug Discovery Today* **18**, 479–486 (2013).

290. Quintana, F. J. The aryl hydrocarbon receptor: a molecular pathway for the environmental control of the immune response. *Immunology* **138**, 183–189 (2013).
291. Fingerhut, M. A. *et al.* Cancer Mortality in Workers Exposed to 2,3,7,8-Tetrachlorodibenzo-P-Dioxin. *New England Journal of Medicine* **324**, 212–218 (1991).
292. Marshall, N. B. & Kerkvliet, N. I. Dioxin and immune regulation: emerging role of aryl hydrocarbon receptor in the generation of regulatory T cells. *Ann. N. Y. Acad. Sci.* **1183**, 25–37 (2010).
293. Lauretta, R., Sansone, A., Sansone, M., Romanelli, F. & Appetecchia, M. Endocrine Disrupting Chemicals: Effects on Endocrine Glands. *Front. Endocrinol.* **10**, (2019).
294. Patrizi, B. & Siciliani de Cumis, M. TCDD Toxicity Mediated by Epigenetic Mechanisms. *Int J Mol Sci* **19**, (2018).
295. Brunnberg, S. *et al.* The constitutively active Ah receptor (CA-AhR) mouse as a potential model for dioxin exposure—Effects in vital organs. *Toxicology* **224**, 191–201 (2006).
296. Boutros, P. C., Yan, R., Moffat, I. D., Pohjanvirta, R. & Okey, A. B. Transcriptomic responses to 2,3,7,8-tetrachlorodibenzo-p-dioxin (TCDD) in liver: Comparison of rat and mouse. *BMC Genomics* **9**, 419 (2008).
297. Becker, R. A., Patlewicz, G., Simon, T. W., Rowlands, J. C. & Budinsky, R. A. The adverse outcome pathway for rodent liver tumor promotion by sustained activation of the aryl hydrocarbon receptor. *Regulatory Toxicology and Pharmacology* **73**, 172–190 (2015).
298. Lin, P. P., Chang, L. W., Wang, Y. J. & Ho, Y. S. The Possible Mechanism of TCDD-Mediated Tumor Promotion in NNK-Initiated Lung Tumorigenesis in Female A/J Mice. *Epidemiology* **17**, S319 (2006).
299. Chapados, N. A. & Boucher, M.-P. Liver metabolic disruption induced after a single exposure to PCB126 in rats. *Environ Sci Pollut Res Int* **24**, 1854–1861 (2017).
300. Gadupudi, G. S., Klaren, W. D., Olivier, A. K., Klingelhutz, A. J. & Robertson, L. W. PCB126-Induced Disruption in Gluconeogenesis and Fatty Acid Oxidation Precedes Fatty Liver in Male Rats. *Toxicol. Sci.* **149**, 98–110 (2016).
301. Jin, J. *et al.* Dioxin-like and non-dioxin-like PCBs differentially regulate the hepatic proteome and modify diet-induced nonalcoholic fatty liver disease severity. *Med Chem Res* **29**, 1247–1263 (2020).
302. Shi, Z. *et al.* Oral benzo[a]pyrene-induced cancer: two distinct types in different target organs depend on the mouse Cyp1 genotype. *Int J Cancer* **127**, 2334–2350 (2010).
303. Beal, M. A. *et al.* Paternal exposure to benzo(a)pyrene induces genome-wide mutations in mouse offspring. *Communications Biology* **2**, 1–10 (2019).
304. Silkworth, J. B. *et al.* Comparison of TCDD and PCB CYP1A Induction Sensitivities in Fresh Hepatocytes from Human Donors, Sprague-Dawley Rats, and Rhesus Monkeys and HepG2 Cells. *Toxicol Sci* **87**, 508–519 (2005).
305. Soldatow, V. Y., LeCluyse, E. L., Griffith, L. G. & Rusyn, I. *In vitro* models for liver toxicity testing. *Toxicol Res (Camb)* **2**, 23–39 (2013).
306. Le Vee, M., Jouan, E. & Fardel, O. Involvement of aryl hydrocarbon receptor in basal and 2,3,7,8-tetrachlorodibenzo-p-dioxin-induced expression of target genes in primary human hepatocytes. *Toxicol In vitro* **24**, 1775–1781 (2010).
307. Gierthy, J. F., Bennett, J. A., Bradley, L. M. & Cutler, D. S. Correlation of *in vitro* and *in vivo* growth suppression of MCF-7 human breast cancer by 2,3,7,8-tetrachlorodibenzo-p-dioxin. *Cancer Res.* **53**, 3149–3153 (1993).
308. Xie, H. Q. *et al.* AhR-mediated effects of dioxin on neuronal acetylcholinesterase expression *in vitro*. *Environ. Health Perspect.* **121**, 613–618 (2013).
309. Strapáčová, S. *et al.* Relative effective potencies of dioxin-like compounds in rodent and human lung cell models. *Toxicology* **404–405**, 33–41 (2018).

310. Leblanc, A. F. *et al.* A dual mixture of persistent organic pollutants modifies carbohydrate metabolism in the human hepatic cell line HepaRG. *Environ. Res.* **178**, 108628 (2019).
311. Natsume, Y., Satsu, H., Kitamura, K., Okamoto, N. & Shimizu, M. Assessment system for dioxin absorption in the small intestine and prevention of its absorption by food factors. *Biofactors* **21**, 375–377 (2004).
312. Yan, J. *et al.* Aryl Hydrocarbon Receptor Signaling Prevents Activation of Hepatic Stellate Cells and Liver Fibrogenesis in Mice. *Gastroenterology* **157**, 793-806.e14 (2019).
313. Sweeney, M. H. & Mocarelli, P. Human health effects after exposure to 2,3,7,8-TCDD. *Food Additives and Contaminants* **17**, 303–316 (2000).
314. Mukerjee, D. Health Impact of Polychlorinated Dibenzo-p-dioxins: A Critical Review. *Journal of the Air & Waste Management Association* **48**, 157–165 (1998).
315. Duval Caroline *et al.* Chronic Exposure to Low Doses of Dioxin Promotes Liver Fibrosis Development in the C57BL/6J Diet-Induced Obesity Mouse Model. *Environmental Health Perspectives* **125**, 428–436 (2017).
316. Pierre, S. *et al.* Aryl hydrocarbon receptor-dependent induction of liver fibrosis by dioxin. *Toxicol. Sci.* **137**, 114–124 (2014).
317. Han, M. *et al.* 2,3,7,8-Tetrachlorodibenzo-p-dioxin (TCDD) induces hepatic stellate cell (HSC) activation and liver fibrosis in C57BL6 mouse via activating Akt and NF-κB signaling pathways. *Toxicol. Lett.* **273**, 10–19 (2017).
318. Li, C. *et al.* TCDD promotes liver fibrosis through disordering systemic and hepatic iron homeostasis. *Journal of Hazardous Materials* **395**, 122588 (2020).
319. Lamb, C. L. *et al.* Aryl Hydrocarbon Receptor Activation by TCDD Modulates Expression of Extracellular Matrix Remodeling Genes during Experimental Liver Fibrosis. *Biomed Res Int* **2016**, 5309328 (2016).
320. Nault, R. *et al.* Dose-Dependent Metabolic Reprogramming and Differential Gene Expression in TCDD-Elicited Hepatic Fibrosis. *Toxicol. Sci.* **154**, 253–266 (2016).
321. Chang, H., Wang, Y.-J., Chang, L. W. & Lin, P. A histochemical and pathological study on the interrelationship between TCDD-induced AhR expression, AhR activation, and hepatotoxicity in mice. *Journal of Toxicology and Environmental Health. Part A* **68**, 1567–1579 (2005).
322. Ohbayashi, H. *et al.* Dose- and time-dependent effects of 2,3,7,8-tetrabromodibenzo-p-dioxin on rat liver. *The Journal of Toxicological Sciences* **32**, 47–56 (2007).
323. Lamb, C. L. *et al.* 2,3,7,8-Tetrachlorodibenzo-p-dioxin (TCDD) increases necroinflammation and hepatic stellate cell activation but does not exacerbate experimental liver fibrosis in mice. *Toxicol. Appl. Pharmacol.* **311**, 42–51 (2016).
324. Ozeki, J. *et al.* Aryl hydrocarbon receptor ligand 2,3,7,8-tetrachlorodibenzo-p-dioxin enhances liver damage in bile duct-ligated mice. *Toxicology* **280**, 10–17 (2011).
325. Fling, R. R., Doskey, C. M., Fader, K. A., Nault, R. & Zacharewski, T. R. 2,3,7,8-Tetrachlorodibenzo- p -dioxin (TCDD) dysregulates hepatic one carbon metabolism during the progression of steatosis to steatohepatitis with fibrosis in mice. *Scientific Reports* **10**, 14831 (2020).
326. Shan, Q., Huang, F., Wang, J. & Du, Y. Effects of co-exposure to 2,3,7,8-tetrachlorodibenzo-p-dioxin and polychlorinated biphenyls on nonalcoholic fatty liver disease in mice. *Environmental Toxicology* **30**, 1364–1374 (2015).
327. Wahlang, B. *et al.* A compromised liver alters polychlorinated biphenyl-mediated toxicity. *Toxicology* **380**, 11–22 (2017).
328. Yuan, L., Liu, J., Deng, H. & Gao, C. Benzo[a]pyrene Induces Autophagic and Pyroptotic Death Simultaneously in HL-7702 Human Normal Liver Cells. *Journal of Agricultural and Food Chemistry* **65**, 9763–9773 (2017).

329. Cui, H. *et al.* Pregnane X receptor regulates the AhR/Cyp1A1 pathway and protects liver cells from benzo-[α]-pyrene-induced DNA damage. *Toxicology Letters* **275**, 67–76 (2017).
330. Regnault, C. *et al.* Impaired liver function in Xenopus tropicalis exposed to benzo[a]pyrene: transcriptomic and metabolic evidence. *BMC genomics* **15**, 666 (2014).
331. Michurina, S. V., Arkhipov, S. A. & Kolesnikov, S. I. Hepatocyte apoptosis in rats exposed to benzo(a)pyrene. *Bull. Exp. Biol. Med.* **158**, 150–152 (2014).
332. Li, F. *et al.* Hepatotoxic effects of inhalation exposure to polycyclic aromatic hydrocarbons on lipid metabolism of C57BL/6 mice. *Environment International* **134**, 105000 (2020).
333. Harvey, W. A. *et al.* Exposure to 2,3,7,8-tetrachlorodibenzo-p-dioxin (TCDD) increases human hepatic stellate cell activation. *Toxicology* **344–346**, 26–33 (2016).
334. Ibrahim, M. *et al.* Functional cytochrome P450 1A enzymes are induced in mouse and human islets following pollutant exposure. *Diabetologia* **63**, 162–178 (2020).
335. Puga, A., Maier, A. & Medvedovic, M. The transcriptional signature of dioxin in human hepatoma HepG2 cells. *Biochem. Pharmacol.* **60**, 1129–1142 (2000).
336. Ruiz-Aracama, A. *et al.* An untargeted multi-technique metabolomics approach to studying intracellular metabolites of HepG2 cells exposed to 2,3,7,8-tetrachlorodibenzo-p-dioxin. *BMC Genomics* **12**, 251 (2011).
337. Yamaguchi, M. & Hankinson, O. 2,3,7,8-Tetrachlorodibenzo-p-dioxin suppresses the growth of human liver cancer HepG2 cells *in vitro*: Involvement of cell signaling factors. *Int. J. Oncol.* **53**, 1657–1666 (2018).
338. Dere, E., Lee, A. W., Burgoon, L. D. & Zacharewski, T. R. Differences in TCDD-elicited gene expression profiles in human HepG2, mouse Hepa1c1c7 and rat H4IIE hepatoma cells. *BMC Genomics* **12**, 193 (2011).
339. Vrzal, R., Vrzalova, A., Grycova, A. & Dvorak, Z. Activated thyroid hormone receptor modulates dioxin-inducible aryl hydrocarbon receptor-mediated CYP1A1 induction in human hepatocytes but not in human hepatocarcinoma HepG2 cells. *Toxicol. Lett.* **275**, 77–82 (2017).
340. Xuan, J., Chen, S., Ning, B., Tolleson, W. H. & Guo, L. Development of HepG2-derived cells expressing cytochrome P450s for assessing metabolism-associated drug-induced liver toxicity. *Chem Biol Interact* **255**, 63–73 (2016).
341. Jennen, D. G. J. *et al.* Comparison of HepG2 and HepaRG by Whole-Genome Gene Expression Analysis for the Purpose of Chemical Hazard Identification. *Toxicol Sci* **115**, 66–79 (2010).
342. Mesnage, R. *et al.* Integrated transcriptomics and metabolomics reveal signatures of lipid metabolism dysregulation in HepaRG liver cells exposed to PCB 126. *Arch. Toxicol.* **92**, 2533–2547 (2018).
343. Rasmussen, M. K., Daujat-Chavanieu, M. & Gerbal-Chaloin, S. Activation of the aryl hydrocarbon receptor decreases rifampicin-induced CYP3A4 expression in primary human hepatocytes and HepaRG. *Toxicol. Lett.* **277**, 1–8 (2017).
344. Vrzal, R. *et al.* Dexamethasone controls aryl hydrocarbon receptor (AhR)-mediated CYP1A1 and CYP1A2 expression and activity in primary cultures of human hepatocytes. *Chem. Biol. Interact.* **179**, 288–296 (2009).
345. Bachleda, P., Vrzal, R. & Dvorák, Z. Activation of MAPKs influences the expression of drug-metabolizing enzymes in primary human hepatocytes. *Gen. Physiol. Biophys.* **28**, 316–320 (2009).
346. Beníšek, M. *et al.* Dioxins and dioxin-like compounds in composts and digestates from European countries as determined by the *in vitro* bioassay and chemical analysis. *Chemosphere* **122**, 168–175 (2015).

347. Kwan, S. Y. *et al.* Bile Acid Changes Associated With Liver Fibrosis and Steatosis in the Mexican-American Population of South Texas. *Hepatology Communications* **4**, 555–568 (2020).
348. Leeuw, A. M. D., Brouwer, A. & Knook, D. L. Sinusoidal endothelial cells of the liver: Fine structure and function in relation to age. *Journal of Electron Microscopy Technique* **14**, 218–236 (1990).
349. Davies, P. F. Flow-mediated endothelial mechanotransduction. *Physiological Reviews* **75**, 519–560 (1995).
350. DeLeve, L. D., Wang, X. & Guo, Y. Sinusoidal endothelial cells prevent rat stellate cell activation and promote reversion to quiescence. *Hepatology* **48**, 920–930 (2008).
351. Xie, G., Wang, L., Wang, X., Wang, L. & DeLeve, L. D. Isolation of periportal, midlobular, and centrilobular rat liver sinusoidal endothelial cells enables study of zonated drug toxicity. *American Journal of Physiology-Gastrointestinal and Liver Physiology* **299**, G1204–G1210 (2010).
352. Mönkemöller, V., Øie, C., Hübner, W., Huser, T. & McCourt, P. Multimodal super-resolution optical microscopy visualizes the close connection between membrane and the cytoskeleton in liver sinusoidal endothelial cell fenestrations. *Scientific Reports* **5**, 1–10 (2015).
353. Géraud, C. *et al.* Unique Cell Type-Specific Junctional Complexes in Vascular Endothelium of Human and Rat Liver Sinusoids. *PLoS One* **7**, (2012).
354. Pandey, E., Nour, A. S. & Harris, E. N. Prominent Receptors of Liver Sinusoidal Endothelial Cells in Liver Homeostasis and Disease. *Front Physiol* **11**, (2020).
355. Lalor, P. F., Lai, W. K., Curbishley, S. M., Shetty, S. & Adams, D. H. Human hepatic sinusoidal endothelial cells can be distinguished by expression of phenotypic markers related to their specialised functions *in vivo*. *World Journal of Gastroenterology* **12**, 5429–5439 (2006).
356. Miyao, M. *et al.* Pivotal role of liver sinusoidal endothelial cells in NAFLD/NASH progression. *Laboratory Investigation* **95**, 1130–1144 (2015).
357. Daneker, G. W. *et al.* Culture and characterization of sinusoidal endothelial cells isolated from human liver. *In vitro Cell.Dev.Biol.-Animal* **34**, 370–377 (1998).
358. de Haan, W. *et al.* Unraveling the transcriptional determinants of liver sinusoidal endothelial cell specialization. *American Journal of Physiology-Gastrointestinal and Liver Physiology* **318**, G803–G815 (2020).
359. DeLeve, L. D., Wang, X., McCuskey, M. K. & McCuskey, R. S. Rat liver endothelial cells isolated by anti-CD31 immunomagnetic separation lack fenestrae and sieve plates. *American Journal of Physiology-Gastrointestinal and Liver Physiology* **291**, G1187–G1189 (2006).
360. Parent, R. *et al.* An immortalized human liver endothelial sinusoidal cell line for the study of the pathobiology of the liver endothelium. *Biochemical and Biophysical Research Communications* **450**, 7–12 (2014).
361. Cogger, V. C. *et al.* The response of fenestrations, actin, and caveolin-1 to vascular endothelial growth factor in SK Hep1 cells. *American Journal of Physiology-Gastrointestinal and Liver Physiology* **295**, G137–G145 (2008).
362. Matsumura, T. *et al.* Establishment of an immortalized human-liver endothelial cell line with SV40T and hTERT. *Transplantation* **77**, 1357–1365 (2004).
363. Huebert, R. C. *et al.* Immortalized Liver Endothelial Cells: A Cell Culture Model for Studies of Motility and Angiogenesis. *Lab Invest* **90**, 1770–1781 (2010).
364. Maru, Y., Yamaguchi, S., Takahashi, T., Ueno, H. & Shibuya, M. Virally activated Ras cooperates with integrin to induce tubulogenesis in sinusoidal endothelial cell lines. *Journal of Cellular Physiology* **176**, 223–234 (1998).

365. Kim, Y. & Rajagopalan, P. 3D Hepatic Cultures Simultaneously Maintain Primary Hepatocyte and Liver Sinusoidal Endothelial Cell Phenotypes. *PLOS ONE* **5**, e15456 (2010).
366. Nudischer, R., Renggli, K., Hierlemann, A., Roth, A. B. & Bertinetti-Lapatki, C. Characterization of a long-term mouse primary liver 3D tissue model recapitulating innate-immune responses and drug-induced liver toxicity. *PLOS ONE* **15**, e0235745 (2020).
367. Tegge, A. N. *et al.* Transcriptomic Analysis of Hepatic Cells in Multicellular Organotypic Liver Models. *Scientific Reports* **8**, 11306 (2018).
368. Messner, S. *et al.* Transcriptomic, Proteomic, and Functional Long-Term Characterization of Multicellular Three-Dimensional Human Liver Microtissues. *Applied In vitro Toxicology* **4**, 1–12 (2017).
369. Gage, B. K. *et al.* Generation of Functional Liver Sinusoidal Endothelial Cells from Human Pluripotent Stem-Cell-Derived Venous Angioblasts. *Cell Stem Cell* **27**, 254-269.e9 (2020).
370. Pettinato, G. *et al.* Generation of fully functional hepatocyte-like organoids from human induced pluripotent stem cells mixed with Endothelial Cells. *Scientific Reports* **9**, 8920 (2019).
371. Takebe, T. *et al.* Vascularized and functional human liver from an iPSC-derived organ bud transplant. *Nature* **499**, 481–484 (2013).
372. Marin, V., Kaplanski, G., Grès, S., Farnarier, C. & Bongrand, P. Endothelial cell culture: protocol to obtain and cultivate human umbilical endothelial cells. *J. Immunol. Methods* **254**, 183–190 (2001).
373. Baudin, B., Bruneel, A., Bosselut, N. & Vaubourdolle, M. A protocol for isolation and culture of human umbilical vein endothelial cells. *Nature Protocols* **2**, 481–485 (2007).
374. Suurmond, C.-A. E. *et al. In vitro* Human Liver Model of Nonalcoholic Steatohepatitis by Coculturing Hepatocytes, Endothelial Cells, and Kupffer Cells. *Advanced Healthcare Materials* **8**, 1901379 (2019).
375. Jung, H.-R. *et al.* Cell Spheroids with Enhanced Aggressiveness to Mimic Human Liver Cancer *In vitro* and *In vivo*. *Scientific Reports* **7**, 10499 (2017).
376. Nelson, L. J. *et al.* Acetaminophen cytotoxicity is ameliorated in a human liver organotypic co-culture model. *Scientific Reports* **5**, 17455 (2015).
377. Takebe, T. *et al.* Engineering of human hepatic tissue with functional vascular networks. *Organogenesis* **10**, 260–267 (2014).
378. Borkham-Kamphorst, E. & Weiskirchen, R. The PDGF system and its antagonists in liver fibrosis. *Cytokine & Growth Factor Reviews* **28**, 53–61 (2016).
379. Brown, P. M., Pratt, A. G. & Isaacs, J. D. Mechanism of action of methotrexate in rheumatoid arthritis, and the search for biomarkers. *Nat Rev Rheumatol* **12**, 731–742 (2016).
380. Liedtke, C. *et al.* Experimental liver fibrosis research: update on animal models, legal issues and translational aspects. *Fibrogenesis Tissue Repair* **6**, 19 (2013).
381. Ravenscroft, S. M., Pointon, A., Williams, A. W., Cross, M. J. & Sidaway, J. E. Cardiac Non-myocyte Cells Show Enhanced Pharmacological Function Suggestive of Contractile Maturity in Stem Cell Derived Cardiomyocyte Microtissues. *Toxicol Sci* **152**, 99–112 (2016).
382. Schmeisser, A. *et al.* Monocytes coexpress endothelial and macrophagocytic lineage markers and form cord-like structures in Matrigel® under angiogenic conditions. *Cardiovasc Res* **49**, 671–680 (2001).
383. Müller, A. M. *et al.* Expression of the Endothelial Markers PECAM-1, vWf, and CD34 *in vivo* and *in vitro*. *Experimental and Molecular Pathology* **72**, 221–229 (2002).

384. Xu, B. *et al.* Capillarization of Hepatic Sinusoid by Liver Endothelial Cell-Reactive Autoantibodies in Patients with Cirrhosis and Chronic Hepatitis. *Am J Pathol* **163**, 1275–1289 (2003).
385. Du, P., Subbiah, R., Park, J.-H. & Park, K. Vascular Morphogenesis of Human Umbilical Vein Endothelial Cells on Cell-Derived Macromolecular Matrix Microenvironment. *Tissue Eng Part A* **20**, 2365–2377 (2014).

# 11 Curriculum vitae


## MEßNER, CATHERINE JANE

| 01516 4654349 |
catherine.messner@fhnw.ch


## EDUCATION

**University of Applied Sciences Northwestern Switzerland**
**Postdoctoral Researcher** — **2020 - Ongoing**
Group: Molecular toxicology

**University of Basel & University of Applied Sciences Northwestern Switzerland**
**Doctor of Philosophy** — **2017 - 2020**
Topic: Biomarkers of liver fibrosis

**University of York**
**MSc by Research in Cell Biology** — **2014 - 2016**
Thesis: Conversion of human fibroblasts to endothelial-like cells via dedifferentiation to mesodermal progenitors in 3D condensates.

**University of York**
**BSc (Hons) of Biochemistry** — **2011 - 2014**
Thesis: Extraction and analysis of nucleosomes from *Fragaria ananassa*

## AWARDS

First place poster prize at Swiss Society of Toxicology Annual Meeting — **2019**
Third place poster prize at Swiss Society of Toxicology Annual Meeting — **2018**

## TEACHING EXPERIENCE

**University of Applied Sciences Northwestern Switzerland**
**Lecturer** — **2019 – 2020**
Literature Seminar
Cell biology

**Practical Course Assistant** — **2020 – 2021**
Practical cell biology course 1 and 2 for bachelor students

**Summer School Teacher** — **2018**
Taught advanced cell biology techniques

**Supervisor of Bachelor, Masters and PhD Students** — **2018 - ongoing**
Supervised and supported a large number of students with practical work, experimental planning and scientific writing skills.

**University of York**
**Practical Course Assistant** — **2014 - 2015**
aided Dr Setareh Chong in teaching laboratories by explaining biological principles and demonstrating how specific techniques work.

## CONFERENCES AND MEETINGS

### Poster Presentations

1. 3D human liver microtissues as an in vitro tool for testing fibrogenic compounds. Swiss Society of Toxicology Annual Meeting (2017).
2. 3D human liver microtissues vs. 2D monolayer culture as an in vitro tool for compound testing. European Society of Toxicology In Vitro 2018.
3. The role of bile salts in cholestatic injury and fibrosis using a human 3D in vitro model. Eurotox (2019).
4. Assessment of fibrotic pathways induced by environmental chemicals using 3D-human liver microtissue model. Swiss Society of Toxicology Annual Meeting (2019).
5. miR-122 is selectively secreted via exosomes by HepaRG exposed to methotrexate or acetaminophen. Swiss Society of Toxicology Annual Meeting (2021).

### Presentations

1. The role of bile salts in cholestatic injury and fibrosis using a human 3D in vitro model. Swiss Society of Toxicology Annual Meeting (2018).
2. Investigating the link between cholestasis and fibrosis. Opentox Annual Meeting (2019).
3. 3D Human liver microtissues as an in vitro model for cholestasis and fibrosis. Seminar at The University of Nanjing (2019).
4. Presentation at 10$^{th}$ anniversary Swiss Centre for Human Toxicology event in 2019.
5. Annual update meetings at Swiss Centre for Human Toxicology 2018-2020.

## PUBLICATIONS

1. Messner C. J., Mauch L. & Suter-Dick L. Bile salts regulate CYP7A1 expression and elicit a fibrotic response and abnormal lipid production in 3D liver microtissues. Toxicol. In Vitro 60, 261–271 (2019).
2. Messner C. J., Premand C., Gaiser C., Kluser, T. Kübler E. Suter-Dick L. Exosomal miRNA release as a sensitive marker for drug-induced liver injury *in vitro*. Appl In Vitro Toxicol. (2020).
3. Yan L., Messner C. J., Zhang, X., Suter-Dick, L. Assessment of fibrotic pathways induced by environmental chemicals using 3D-human liver microtissue model. Environ. Res. (2021).
4. Messner C. J., Babrak L., Titolo G., Caj M. & Suter-Dick L. Single cell gene expression analysis in a 3D microtissue liver model reveals cell type-specific responses to pro-fibrotic TGF-β1 stimulation. Int. J. Mol. Sci. (2021).

## LANGUAGES

English (native language) and German (speak fluently and read/write with proficiency).